technische universität
dortmund

Functional Porous Polymer Beads Nanostructured by Imprinting, Layer by Layer Grafting and Templated Synthesis

Mahadeo R. Halhalli

Functional Porous Polymer Beads Nanostructured by Imprinting, Layer by Layer Grafting and Templated Synthesis

A thesis presented to
the Faculty of Chemistry
at the Technical University of Dortmund

for the degree of
Doctor of Philosophy in Chemistry
(Ph.D. – Dr. rer. nat.)

by

Mahadeo R. Halhalli

born on the 1st June of 1983 in Binjager, Solapur district, India

Supervisors:

Priv. Doz. Dr. Börje Sellergren

Prof. Dr. Jörg C. Tiller

November 2012

Declaration

The work presented in this thesis was carried out in the Institute of Environmental Research of the Faculty of Chemistry, at Technical University of Dortmund (Germany) and is a result of the original work of the author, except where acknowledged in the text. The thesis was composed by the author and was not submitted to any other degree or professional qualification.

Mahadeo R. Halhalli

Marie Curie Fellow
Institute of Environmental Research of the
Faculty of Chemistry,
Technical University of Dortmund
Germany

Functional Porous Polymer Beads Nanostructured by Imprinting, Layer by Layer Grafting and Templated Synthesis

Dissertation

zur Erlangung des akademischen Grades

Doktor der Naturwissenschaften

(Dr. rer. nat.)

der Technischen Universität Dortmund

vorgelegt von

M.Sc. Mahadeo R. Halhalli

geboren am 01.06.1983
in Binjager,Solapur district, Indien

November 2012

Die vorliegende Doktorarbeit wurde am Institut für Umweltforschung angefertigt und eingereicht an der Fakultät für Chemie der Technischen Universität Dortmund.

Gutachter der Dissertation:

1. Gutachter: Priv. Doz. Dr. Börje Sellergren

2. Gutachter: Prof. Dr. Jörg C. Tiller

Tag des öffentlichen Promotionskolloquiums:

Erklärung

Hiermit erkläre ich, dass ich die vorliegende Dissertation selbständig und nur mit den angegebenen Hilfsmitteln angefertigt habe. Die Arbeit wurde bisher in gleicher oder ähnlicher Form keiner anderen Prüfungskommission vorgelegt und auch nicht veröffentlicht.

Dortmund, den date

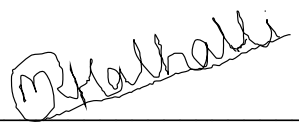

Mahadeo Ramchandra Halhalli

Dedicated To

MY Family

Acknowledgments

First and foremost, I would like to express my deep sense of gratitude to my supervisor Prof. Dr. Börje Sellergren for giving me an opportunity to pursue a doctoral study in his group. I am very thankful to him for his, inspiring guidance, numerous discussions, creative ideas and constant support during these years.

I would like to thank Prof. Dr. Jörg Tiller for accepting me as a second supervisor and for some key suggestion at initial stage of the project. I acknowledge to Prof. Dr. Michael Spiteller for providing the opportunity to work in the INFU.

My special thanks goes to former and present members of AK Sellergren group Dr. Eric Schillinger, Dr. Carla Aureliano, Dr. Javier Urraca, Dr. Wei Sun and Dr. Ali Nematollahzadeh, Dr. Robert Sulc as well as present members Sudhir, Abed, Ricarda, Emelie, Annabell, Reza, Farid, Melanie, Porkodi, Wasim, Deepak, Raj, Adam, Patrick, Zhiqi, Raquel, Malak, and Celina Love you all for making my life so easy and enjoyable in and out of working premises.

I am grateful to Dr.Francesca lanza-Sellergren, Karl, Maria, and Neil for welcoming us at home and for barbeque parties and enjoyable evenings.

I would like to thank Dr. Eric Shillinger who helped at the beginning of the project and for his valuable suggestion during the project and for home made French wine. Also, thanks to Carla and Ali for their fruitful discussion about work and critical suggestion and for film thickness calculations.

Thanks to Dr. Javier Urraca who made my life so easy in analytical lab and for his useful suggestions during the rebinding study.

I am very thankful to Farid, Ricarda, Emelie, Annabell, and Abed for reviewing this thesis and for being always nice colleagues. Special thanks to Annabell and Ricarda for solving so many bureaucratic issues and also translating the summary in German language. I also like to thank my project partner Emelie for her friendship and for all the great moments shared in Dortmund and in our trips around Europe during the NEMOPUR meetings. Thanks to Reza for helping me in the lab while writing and also thanks to Melanie and Patrick for their software skill which saved my lot of time during writing.

It’s my pleasure to thank Sudhir and Kirti (Raje) for being good friends and for support, help advice during the initial journey in Germany and fun moments we shared.

I would like to thank all the INFU co-workers specially Dr. Lamshöft, Dr. Zühlke, Dr. Kusari Mrs. Apitius, Jana, Uli for always being kind and helpful .and also thanks to our IT expert Jurgen for providing me more space on group server. Further I would like to thank all colleagues of NEMOPUR EU project team for sharing ideas and mutual interactions, especially Prof. Dr. Andrew Livingston (Imperial College London) and Dr. Ecevit Yilmaz (Biotage, Sweden) and I also thanks to Gyuri, Rustem and Samuel for more enjoyable evenings after project meetings.

I would like to thank Dr. Magda Titirici (MPI, Postdam, Berlin) and Mrs. Monika Meuris (TU Dortmund) for recording the SEM and TEM micrographs, and also thanks to Brigitte Muller at the University of Mainz for the elemental analysis measurements. Thanks to all NMR faculty staff for recording NMR.

I express my sincere thanks to Dr.P.P Wadgaonkar, Dr. Abbas Shaikh, Prof. Dr. N. N. Maldar, Dr. Ashish lele, and Prof. Dr. S.V. Lonikar for their encouragement and constant guidance during the initial stage of my career as project assistant in National Chemical Laboratory Pune and GE global research centre (Bangalore). It is pleasure to thank Dr. C.V. Avdhani, Dr. Gautam Chatterjee, Dr. Sanjay Charati, Dr. Veera, and Dr. Anil Ghanwat for their affection and valuable suggestion they offered during my stay at NCL and GE.

I extended my thanks to all PPW group members Anjana, Sony, Bapu, Prakash, Pandu, Nana, Arun, Arvind, Nagesh, Mahesh, Savita, for being a friends and making more memorable days during my stay at NCL. Special thanks to Sony and Prakash for encouraging me to apply abroad. I also thank to Ram Kandre for his personal guidance and helping me at initial for searching a PhD position at abroad.

I thank my friends Shivkumar, Nagesh, Jijeesh, Vijay, Gajanan (Bandu), Vish, Sanjay and Parmeshwar for their support and fun moments we shared during our visits.

I would like to thank my entire school teacher, especially Guru Devidas Maharaj who inspired me to go for higher study and for their valuable philosophical thoughts which are essential to become a good human being.

Last but not least, I would like to express my sincere gratitude to my father Shri Ramchandra Halhalli and my mother Sau Nagbai Halhalli for their immense love, moral support, and patience beyond limits as well as their great efforts and pains to educate me. I am very grateful to my brother Shankar, his wife Renuka and their three kids Shivkumar, Mahesh and Nilesh, who made my life so enjoyable with full of fun. I also thank to my sister Vitabai, her husband Vittal and their kids Gajanan, Daya, and Varsha for their support and enjoyable conversation during these years. I would like to thank my fiancee Suvidha for her love and patience.

Financial support from European Commission under FP7-Marie Curie Action, contract PITN-GA-2008-214226 (NEMOPUR) and from the Deutsche Forschungsgemeinschaft DFG (Se777/5-2) is gratefully acknowledged.

Table of Contents

LIST OF ABBREVIATIONS ix
LIST OF TABLES xii
LIST OF FIGURES xiv
LIST OF SCHEMES xxi
1 Summary and Zusammenfassung 1
1.1 Summary 1
1.2 Zusammenfassung 3
2 Background and State of the Art 6
2.1 Molecular Imprinting technology 6
2.2 Imprinting Approaches 7
2.2.1 Covalent Imprinting 7
2.2.2 Noncovalent imprinting 8
2.2.3 Semi-covalent Imprinting Approach 10
2.3 MIPs synthesized by Free radical Polymerization 12
2.3.1.1 Initiation 12
2.3.1.2 Propagation 12
2.3.1.3 Termination: 13
2.4 Limitation of FRP-MIPs 14
2.5 Improvement in binding capacity by reducing the binding site heterogeneity 15
2.5.1 Stoichiometric Imprinting 16
2.5.2 Post imprinting modification 17
2.5.3 Thermodynamically controlled polymerization 18
2.5.4 Single particle imprinting (Dendrimer Imprinting) 19
2.5.5 Synthetic polymer nanoparticles for affinity sorting 20
2.5.6 Controlled radical/Living polymerization 21
2.5.6.1 Iniferter Polymerization 23
2.5.6.2 Nitroxide Mediated Polymerization 24
2.5.6.3 Atom Transfer Radical Polymerization 26
2.5.6.4 Reversible Addition Fragmentation chain Transfer Polymerization (RAFT) . 28

2.6 Surface Initiated Polymerization 31
2.6.1 Covalent attachment via “Grafting to Approach” 33
2.6.2 Covalent attachment via ‘grafting from approach’ 34
2.6.2.1 Surface imprinting via conventional FRP 35
2.6.2.2 Surface imprinting via CRP 36
2.6.2.2.1 Surface initiated iniferter polymerization 36
2.6.2.2.2 Surface initiated ATRP 38
2.6.2.2.3 Surface initiated RAFT polymerization 39
2.7 Template synthesis of materials 44
3 Investigation of influence of RAFT agent on the performance of LPA imprinted polymers 46
3.1 Introduction 46
3.2 Results and discussion (I): 48
3.2.1 Polymerization onset: Effect of the CTA to initiator ratio 49
3.2.2 Double bond conversion: 51
3.2.3 Swelling and Pore analysis: 57
3.2.4 Thermoporometry 62
3.2.5 Inverse size exclusion chromatography (ISEC) 64
3.2.6 Thermal stability 65
3.2.7 Chromatography evaluation 67
3.2.8 Determination of binding capacity of the MIPs 70
3.3 Conclusions 74
4 Thin film MIP composite beads 76
4.1 Introduction 76
4.2 Results and discussion (IIA) 79
4.2.1 Grafting of molecularly imprinted polymers via azo initiator modified silica support 79
4.2.2 Silica surface activation 79
4.2.3 Functionalisation of silica surface with APS 80
4.2.4 End capped amino modified silica 81
4.2.5 Surface attachment of free radical initiator - 4,4’ azobis (4-cyanopentanoic acid) .. 81

4.2.6 Characterization of the resulting intermediates 82
4.2.7 Composites prepared by grafting from techniques 85
4.2.8 Characterization of grafted polymer layers 86
4.2.9 Characterisation of composite beads in chromatographic mode 93
4.2.10 Fluorescence labeling 97
4.2.11 Grafting of molecularly imprinted polymers via RAFT modified silica support 98
4.2.12 Synthesis and characterization of RAFT modified silica particles 99
4.2.13 Polymer Grafting and composite characterization 101
4.2.14 Chromatographic evaluation 104
4.3 Conclusion and outlook 105
5 Template synthesis of thin walled materials 107
5.1 Introduction 107
5.2 Results and discussion (IIB) 109
5.2.1 Thin walled imprinted polymer beads generated from azoinitiator or RAFT composite MIPs. 109
5.2.2 Characterization of Thin walled materials by chromatographic mode 117
5.2.3 Thinwalled imprinted polymer beads generated from RAFT modified support 120
5.2.4 Evaluation of RAFT thinwalled beads in liquid chromatography mode 126
5.2.5 Saturation binding experiments 129
5.2.6 Kinetic binding experiment 137
5.2.7 Engelhardt test: Surface acidity and hydrophobicity 138
5.3 Conclusions and Outlook 142
6 Results and discussion (IIC): Layer by layer grafting of thinfilm MIP via SIRAFT 144
6.1 Synthesis and characterization of RAFT modified support 145
6.1.1 Layer by layer grafting and characterisation 146
6.1.2 Chromatographic Evaluation 151
6.2 Conclusions 154
7 Experimental Section 156
7.1 Investigation of influence of RAFT agent on performance of L-PA MIPs 156
7.1.1 Odourless RAFT agent synthesis 156

7.1.1.1 Synthesis of α-bromobenzene acetonitrile 156
7.1.1.2 Synthesis of α-Cyanobenzyl Dithibenzoate 157
7.1.2 Template Synthesis 158
7.1.2.1 Synthesis of BOC-L/D-Phenylalanine anilide 158
7.1.2.2 Synthesis of L/D-Phenylalanine anylide 158
7.1.3 General Polymerization Procedure 159
7.2 Thin film composite beads and generated thinwalled beads 160
7.2.1 Silica Surface Activation 160
7.2.2 Silanisation of silica surface with Aminopropyl triethoxysilane 160
7.2.3 End-Capping using Hexamethyldisilazane (HMDS) 161
7.2.4 Azo-initiator immobilization 161
7.2.5 Immobilization of RAFT agent 162
7.2.6 Grafting of polymer from azo-modified silica 162
7.2.7 Grafting of polymer from RAFT-modified silica 163
7.2.8 Coupling of the fluorescence label 163
7.2.9 Generation of thinwalled MIPs 164
7.2.10 Dithoester RAFT group survival test 164
7.3 Layer by layer grafting of thinfilm MIP via SIRAFT 164
7.3.1 Immobilization of RAFT agent 164
7.3.2 Grafting of Layer by layer MIP films via RAFT-modified silica 165
7.3.3 Silica removal 165
7.4 Characterization techniques 166
7.4.1 Thermogravimetric analysis 166
7.4.2 Differential scanning colorimeter (DSC) 167
7.4.3 Thermoporometry 168
7.4.3.1 Pore diameter[151] 168
7.4.3.2 Pore volume measurement[152] 169
7.4.3.3 Surface area 169
7.4.4 Swelling tests 170
7.4.5 Infrared spectroscopy 170
7.4.6 Solution NMR 170

7.4.7 Elemental analysis 171
7.4.8 Optical microscopy 172
7.4.9 Scanning electron microscopy 173
7.4.10 Energy Dispersive X-ray analysis 173
7.4.11 Nitrogen adsorption 173
7.4.12 Chromatography 174
7.4.12.1 Evaluation of binding affinity and selectivity in the chromatographic mode 174
7.4.13 Binding experiments 177
7.4.13.1 Evaluation of binding affinity and selectivity in the static mode 177
7.4.13.2 Kinetic Experiments 178
7.4.14 Engelhardt test of hydrophobicity and acidity 178
7.4.15 Inverse size exclusion chromatography (ISEC) 179
8 CHEMICALS 180
9 REFERENCES 184
APPENDIX 191
CURRICULUM VITAE 192

LIST OF ABBREVIATIONS

3-AQ	3-aminoquinoline
ABDV	Azo-bis-dimethylvaleronitrile
ACN	Acetonitrile
ACPA	4,4'Azobis cyanopentanoic acid
AIBN	Azo-bis isobutyronitrile
APS	3- Aminopropyltriethoxysilane
ATRP	Atom transfer radical polymerization
BET	Brunauer-Emmett-Teller
BJH	Barrett - Joyner – Halenda
CRP	Controlled radical polymerization
CTA	Chain transfer agent
DCC	Dicyclohexylcarbodiimide
DCM	Dichloromethane
DMAP	Dimethylamino pyridine
DMF	Dimethylformamide
DMSO	Dimethylsulphoxide
D_p	Pore diameter
D-PA	D-Phenylalanine aniline
DSC	Differential Scanning Colorimeter
D_s	Surface density
EA	Elemental analysis
EDC	1-ethyl-3-(3-dimethylaminopropyl) carbodiimide hydrochloride
EDMA	Ethylene glycol dimethacrylate
EDX	Energy -dispersive X-ray spectroscopy
FRP	Free radical polymerization
FT-IR	Fourier transform infrared spectroscopy

HMDS	Hexamethyldisilazane
HOBt	1-Hydroxybenzotriazole
HPLC	High performance liquid chromatography
Iniferter	Initiator-transfer agent-terminator
L-PA	L- Phenylalanine anilide
MAA	Methacrylic acid
MeOH	Methanol
MeCN	Acetonitrile
MIP	Molecularly imprinted polymer
MISPE	Molecularly imprinted solid phase extraction
NIP	Non-imprinted polymer
NMP	Nitroxide mediated polymerization
PMMA	Polymethylmethacrylate
PS	Polystyrene
RP-HPLC	Reversed phase HPLC
RT	Room temperature
RAFT	Reversible Addition Fragmentation chain Transfer polymerization
S_A	Surface area
SEM	Scanning electron microscopy
SPE	Solid phase extraction
TEA	Triethylamine
TEM	Transmission electron microscopy
TFA	Trifluoroacetic acid
TGA	Thermogravimetric analysis
THF	Tetrahydrofuran
TLC	Thin layer chromatography
TMS	Trimethylsilyl

TW-MIP	Thin walled molecularly imprinted polymer
V_p	Pore volume

LIST OF TABLES

Table 2.1 Surface-imprinted materials prepared by the controlled/living radical polymerization (CRP) method. 37
Table 3.1Polymer feed composition and Pore analysis parameters for the Imprinted and non imprinted polymers measured by BET and Thermoporometry (value in bracket) 49
Table 3.2 Unreacted double bonds in crude polymer determined by DSC. 55
Table 3.3 Comparison of pore analysis in dry state and swollen state. 65
Table 3.4 Temperature at %Weight loss of imprinted and non imprinted polymers. 67
Table 3.5 Comparison of chromatographic performance between conventional MIPs and RAFT MIPs. 69
Table 3.6 Freundlich isotherms fitting parameters obtained by nonlinear regression of data shown in Figure 3.18 as described in the experimental section. 73
Table 3.7 Mono-Langmuir Isotherm fitting parameters obtained by nonlinear regression of data shown in Figure 3.18 as described in the experimental section. 73
Table 3.8 Bi-Langmuir Isotherm fitting parameters obtained by nonlinear regression of data shown in Figure 3.18 as described in the experimental section. 74
Table 4.1 Characterisation of azoinitiator modified silica supports used for grafting. 83
Table 4.2 Characteristics of molecularly imprinted polymer composites prepared by photoinitiated grafting to full monomer conversion from silica modified with azoinitiator. 87
Table 4.3 Characterisation of the materials in chromatographic mode using sodium acetate buffer/acetonitrile as mobile phase (30/70, v/v). 93
Table 4.4 Coupling of Fluorescent Label for high dilution system (20mL) composites 97
Table 4.5 Characterisation of the RAFT modified silica supports used for grafting. 99
Table 4.6 Characteristics of molecularly imprinted polymer composites prepared by thermally initiated grafting to high monomer conversion from silica modified with RAFT agent. 101
Table 5.1 Characteristics of molecularly imprinted polymer composites and corresponding thinwalled imprinted beads prepared by photoinitiated grafting from silica modified with azoinitiator. 111
Table 5.2 Characteristics of molecularly imprinted polymer composites prepared by thermally initiated grafting to full monomer conversion from silica modified with RAFT agent. 121

Table 5.3 Mono-Langmuir Isotherm fitting parameters obtained by nonlinear regression of data shown in Figure 5.22 and Figure 5.23 as described in the experimental section. 132
Table 5.4 Bi-Langmuir Isotherm fitting parameters obtained by nonlinear regression of data shown in Figure 5.22 and Figure 5.23 as described in the experimental section. 133
Table 5.5 Freundlich Isotherm fitting parameters obtained by nonlinear regression of data shown in Figure 5.22 and Figure 5.23 as described in the experimental section. 134
Table 5.6 Properties of stationary phases and columns used in the Engelhardt test. 138
Table 6.1 Characterization of the RAFT modified silica supports used for grafting. 146
Table 6.2 Polymer feed composition with respect to nominal film thickness. 147
Table 6.3 Characteristics of Layer-by-Layer molecularly imprinted polymer composites prepared by SI RAFT polymerization..... 148

LIST OF FIGURES

Figure 2.1 Schematic representation of the molecular imprinting process 7
Figure 2.2 Covalent Imprinting of 4-nitrophenyl-a-d-mannopyranoside-2,3:4,6-di-O-(4vinylphenylboronate). 8
Figure 2.3 Model of L-PA binding site based on NMR and chromatographic data 10
Figure 2.4 Imprinting of cholesterol by the sacrificial spacer (semi-covalent) method. Adapted from ref.[11] 11
Figure 2.5 Schematic representation of Free radical polymerization 13
Figure 2.6 Irregularly shaped particles resulting from mechanical grinding of a "traditional" molecularly imprinted polymer (MIP-FRP). 15
Figure 2.7 (a) Schematic representation of a diazepam MIP containing heterogeneous binding sites: high affinity site in macropore (A) and micropore (F) and lower affinity sites(B) in macropore,(C) trapped template,(E) embedded site, (D) highest affinity site with site with shape selectivity from polymer.(b) chart showing the dissociation constant of three classes of binding sites needed to fit binding isotherm. Adapted from ref.[29] 16
Figure 2.8 Schematic representation of site selective chemical modification strategy[38] 18
Figure 2.9 Synthesis of MIPs via ROMP[39] 19
Figure 2.10 Monomolecular imprinting inside dendrimer; A dendrimer with crosslinkable double bonds at out shell, and the covalently attached porphyrin template in the core.[40] 20
Figure 2.11 General mechanism for iniferter kinetics proposed by Otsu and Yoshida.R_2 is usually sulphur radical.R_1 may be either a sulphur radical or a carbon radical.[57] 23
Figure 2.12 The activation-deactivation equilibrium in nitroxide mediated polymerization. 25
Figure 2.13 Transition Metal-catalyzed ATRP[69] 26
Figure 2.14 Reverse ATRP using AIBN as a initiator.[69] 27
Figure 2.15 Schematic representation of RAFT polymerization using a dithioester.[75] 30
Figure 2.16 Synthetic strategies for the preparation of polymer brushes. 33
Figure 2.17 The grafting of L-phenylalanine anilide (L-PA) imprinted polymer films from porous silica supports controlled by addition of RAFT agent.[94] 40
Figure 2.18 R-group and Z-group approaches for Surface-initiated RAFT polymerizations..... 41
Figure 2.19 Templated synthesis material by endo and exo-templating. Adapated from ref.[129] .. 45
Figure 3.1 Preparation of L-PA imprinted polymer using RAFT polymerization. 47

Figure 3.2 DSC dynamic scanning curves for prepolymerization mixtures of imprinted (A) and non imprinted (B) polymers at heating rate 10 ^{o}C/min. 50
Figure 3.3 vinyl double bond conversion of poly (MAA-co-EGDMA) recognitive netwroks: RAFT agent wt% effect upon the double bond conversion. 52
Figure 3.4 Temperature influence on vinyl double bond conversion of poly(MAA-co-EDMA) recognitive network templated for L-PA. 53
Figure 3.5 Isothermal DSC scanning curves at three different temperatures for traditional MIP (MIPA) and RAFTMIP (MIPD). 53
Figure 3.6 Crude polymer DSC curves before soxhlet (A) and after soxhlet (B). 55
Figure 3.7 Influence of RAFT agent on imprinted (A) and nonimprinted (B) particles images. . 56
Figure 3.8 Infrared spectra (KBr) of L-PA imprinted polymer with increasing RAFT content... 56
Figure 3.9 Swelling study of imprinted and non imprinted polymers in pure acetonitrile. 57
Figure 3.10 Nitrogen adsorption – desorption isotherms of L-PA imprinted polymer with increasing RAFT content (A) and pore size distribution (B). 58
Figure 3.11 Influence of CRP on imprinted network structure. (A) In linear polymerization, the use of RAFT agent yields a lower polydispersity of kinetic chains and decreased average chain length. (B) Within crosslinked networks, addition of RAFT agent leads to a more uniform and higher population of appropriately sized imprinted macromolecular cavities for the template. .. 60
Figure 3.12 SEM images of conventional imprinted and nonimprinted polymers (MIPA and NIPA) and RAFT polymers with varying the RAFT/ABDV ratio (MIPB to MIPF and NIPB to NIPF)..... 61
Figure 3.13 DSC curves for the melting of acetonitrile in the L-PA imprinted polymers. The sample was frozen by rapidly quenching to -60 ^{0}C. The heating curves shows pore melt and excess melt. 63
Figure 3.14 Pore size distribution obtained from ISEC measurements. 64
Figure 3.15 TGA curves of L-PA imprinted polymer (A) and DTG curves (B). 66
Figure 3.16 The graph shows Capacity factor (kL) and separation factor (α) for L-PA. Mobile phase: MeCN-0.01M sodium acetate buffer, pH 4.8 (9:1); 0.5mM racemate D- and L-PA enantiomer; injected voume 10µL, flow rate 0.5mL/min. DAD= 260nm, column 35mm X 4.6 mm. 68

Figure 3.17 Elution profiles obtained for different concentration of racemic mixtures (D, L-PA) on MIPA and MIPD using as mobile phase: MeCN-0.01M sodium acetate buffer, pH 4.8 (9:1) at flow rate of 0.5mL/min, DAD = 260 nm and column size = 35 mm X 4.6 mm. 70
Figure 3.18 Adsorption isotherms of D/L-PA on MIPA (A) and MIPD (B) with corresponding non imprinted polymer, as solutions in pure acetonitrile..... 72
Figure 3.19 Fischer values obtained by fitting the L/D-PA binding curves in Figure 14 to mono-Langmuir (LI 1 site), bi-Langmuir (LI 2 sites) or Freundlich isotherm models (FI) (see Tables 3.6 to Table 3.8). 74
Figure 4.1 Grafting of L-phenylalanine anilide (L-PA) imprinted polymer films from an porous silica support modified with azoinitiator (A), or RAFT agent (R). The grafting was performed using a common prepolymerization mixture to reach near full conversions under five different dilution (0-20mL) for Azo-system and using different RAFT/initiator ratio in RAFT system.... 78
Figure 4.2 FT-IR spectra of Si-ACPA initiator and corresponding intermediate step such as bare silica SiO_2- before (SiO_2) and after rehydroxylation (Si-OH), and after modification with APTS (Si-NH2). 84
Figure 4.3 Protocol for grafting of imprinted polymer layers on support materials with recycling of monomer solution. 86
Figure 4.4 Elemental composition of the imprinted composite beads tuned to 1 (blue bars), 2 (red bars) or 3 (green bars) nm film thickness, prepared under different dilutions with toluene..... 89
Figure 4.5 FT-IR transmission spectra (KBr) of imprinted composites prepared using azoinitiator modified silicas (A) $SiPA_{20}^{1}$, (B) $SiPA_{20}^{2}$, (C) $SiPA_{20}^{3}$, (D) $SiPA_{5}^{1}$, (E) $SiPA_{5}^{2}$ and (F) $SiPA_{5}^{3}$ 90
Figure 4.6 Thickness of grafted polymer films calculated based on the mass loss obtained by TGA. for composites with film thickness adjusted to 1, 2 or 3 nm thickness prepared under different dilutions with toluene. 90
Figure 4.7 Pore system parameters from BET for the composites with films adjusted to 1 nm, 2 nm and 3 nm thickness prepared under different dilutions with toluene. 91
Figure 4.8 Scanning electron micrographs of imprinted composites (A) $SiPA_{10}^{1}$, (B) $SiPA_{10}^{2}$, (C) $SiPA_{10}^{3}$, (D) $SiPA_{20}^{1}$, (E) $SiPA_{20}^{2}$ and (F) $SiPA_{20}^{3}$ 92
Figure 4.9 Plot of retention factors (k) for L-PA (A) or enantiomer separation factors (B) for composites with films adjusted to 1, 2 or 3 nm thickness prepared under different dilutions with toluene. Mobile phase: MeCN/ acetate buffer pH 4.8:70/30 (v/v). 94

Figure 4.10 Plot of retention factors (k) for L-PA (solid symbols) and D-PA (open symbols) versus carbon content (%C) for $SiPA_{20}$ (blue circles) and the $SiPA_5$ (red triangles) series composites. Mobile phase: MeCN/ acetate buffer pH 4.8:70/30 (v/v). 94
Figure 4.11 Chromatogramms obtained by separate injection of(10µL of 0.5mM) D-PA (red traces) and L-PA (blue traces) on columns (35mm X 4.6 mm) packed with the indicated materials. Mobile phase: MeCN/sodium acetate buffer 0.01M pH 4.8: 70/30 (v/v). 96
Figure 4.12 Fluorescence micrographs (20 X magnification) of (A) SiPA201 ,(C) SiPA203 before coupling with 3-aminoquinoline and (B) SiPA201 ,(D) SiPA203 after coupling with 3-aminoquinoline. 98
Figure 4.13 Picture of imprinted composite RAFT (A) Si-500 RAFT agent (B) $SiPR^{500}$ (C) $SiPR_E^{500}$ (D) SiPR (E) PR (after etching). 102
Figure 4.14 Scanning electron micrographs of imprinted composites (A) SiPR, (B) $SiPR_E$, (C) $SiPR^{500}$ and (D) $SiPR_E^{500}$ (E) $SiPR_{EE}^{500}$ at two magnifications. 103
Figure 4.15 Nitrogen sorption isotherm (A), and pore size distribution (B) of respective imprinted RAFT composites beads. 104
Figure 4.16 Plot of retention factors (k) for L-PA (A) and associated separation factors (α) (B) at three different sample loads for L-PA imprinted composites prepared by grafting from different RAFT modified supports. Mobile phase: MeCN. 105
Figure 5.1 Generation of thinwalled beads from composite MIPs.[80] 109
Figure 5.2 Carbon content of the composites (blue bars) and the corresponding polymers obtained after fluoride etching (red bars) listed in Table 5.1. 110
Figure 5.3 FT-IR of the composite $SiPA_{20}^3$ (A)and the corresponding thin-walled MIP PA_{20}^3 (B) and bulk polymer(C). 112
Figure 5.4 TGA of the composites $SiPA_{20}^1$ (blue),$SIPA_{20}^2$(red),$SiPA_{20}^3$(green) and the corresponding thin-walled imprinted polymers. 113
Figure 5.5 Scanning electron micrographs of imprinted composites beads (A) $SiPA_{10}^1$, (B) $SiPA_{10}^2$, (C) $SiPA_{10}^3$, (D) $SiPA_{20}^1$, (E) $SiPA_{20}^2$ and (F) $SiPA_{20}^3$ 114
Figure 5.6 Scanning electron micrographs of the polymers resulting from etching of the composites –thinwalled imprinted polymer beads. (A) PA_{10}^1, (B) PA_{10}^2, (C) PA_{10}^3, (D) PA_{20}^1, (E) PA_{20}^2 and (F) PA_{20}^3 115
Figure 5.7 Volume swelling ratio of thinwalled beads in pure acetonitrile. 116

Figure 5.8 Surface area in the dry state of composites (blue bars) and corresponding polymers (red bars) resulting after fluoride catalyzed etching. 116
Figure 5.9 Plot of retention factors (k) (A-C) and enantiomer separation factors (D-F) versus sample load per column cross section area (n/A) for L-PA (filled symbols) and D-PA (open symbols) on columns packed with composite beads (blue triangles) and beads after etching (red squares) for $SiPA_{15}^{1}$ and PA_{15}^{1} (A and D); $SiPA_{15}^{2}$ and PA_{15}^{2} (B and E) and $SiPA_{15}^{3}$ and PA_{15}^{3} (C and F). Mobile phase: MeCN. The nominal film thickness (d) has been indicated. 118
Figure 5.10 Chromatogramms obtained by separate injection of D-PA (red traces) and L-PA (blue traces) on columns packed with the indicated materials. The sample load per column cross section area was 30nmol/cm2. Mobile phase: MeCN/sodium acetate buffer 0.01M pH 4.8: 70/30 (v/v)..... 119
Figure 5.11 Number of theoretical plates (A) and peak asymmetry factors (B) at comparable sample loads (30nmol/cm2) on columns packed with the indicated materials. Mobile phase: MeCN/sodium acetate buffer (0.01M), pH 4.8: 70/30 (v/v)..... 120
Figure 5.12 TGA curves of Si100RAFT-agent (a), L-PA imprinted composite SiPRE (b), and the thin-walled imprinted polymer PRE (c)..... 122
Figure 5.13 FTIR of the thinwalled PR_E (A), composite $SiPR_E$(B), and RAFT agent si100RAFT (c). 123
Figure 5.14 Scanning electron microscopy of composites and corresponding thinwalled bead of PR^{500} in two magnification. 123
Figure 5.15 Scanning electron micrographs of the polymers resulting from etching of the composites (A) PR, (B) PR_E, (C) PR^{500}, (D) PR_E^{500} and (E) PR_{EE}^{500} at two magnifications. 124
Figure 5.16 SEM-EDX spectrum of $SiPR^{500}$ composite (A), and corresponding thinwalled material, PR^{500} (B). 125
Figure 5.17 Plot of retention factors (k) for L-PA (A) and associated separation factors (α) (B) at four different sample loads for L-PA imprinted TW material prepared by grafting from different RAFT modified supports. The RAFT/ABDV ratio and type of silica support has been indicated in above table. Mobile phase; MeCN. 126
Figure 5.18 Elution profiles of D,L-PA injected (10 mL of a 0.1 mM solution) separately into columns (20X2mm) packed with the indicated L-PA imprinted RE100- TW material. The RAFT/ABDV ratio is 2. Mobile phase: MeCN. 127

Figure 5.19 Plot of retention factors (k) for L-PA (A) and associated separation factors (α) (B) at three different sample loads for L-PA imprinted PR_E^{100} TW material. The RAFT/ABDV ratio is 2. Mobile phase: Sodium acetate buffer (pH 5) with increasing amount of acetonitrile. 127
Figure 5.20 Plot of retention factors (k) for L-PA (A) and associated separation factors (α) (B) at three different sample loads for L-PA imprinted $SiPR_E^{100}$ composite material. The RAFT/ABDV ratio is 2. Mobile phase: Sodium acetate buffer (pH 5) with increasing amount of acetonitrile. 128
Figure 5.21 Retention factors (k) for L-PA (A) and enantiomer separation factors (B) obtained in the chromatographic mode at comparable sample loads (300 nmol/cm2) on columns packed with the indicated composite beads(red bar) or polymer beads(blue bar). Mobile phase; MeCN. 128
Figure 5.22 Equilibrium binding isotherms of D- (open symbols) and L-PA (solid symbols) (A) for composite beads SiPA203 (red triangles) and the resulting beads after etching PA203 (blue squares); (B) a bulk reference polymer PA_{ref}; (C) composite beads SiPR (red triangles), the resulting beads after etching PR (blue squares) and PRE (green circles); (D) a bulk RAFT reference polymer $PR_{ref.}$ Solvent: MeCN. 130
Figure 5.23 Equilibrium binding isotherms of D- (open symbols) and L-PA (solid symbols) for (A) composite beads $SiPA_{20}^2$ (red triangles) and the resulting beads after etching PA_{20}^2 (blue squares), (B) PA_{10}^2 and (C) PA_{10}^3 131
Figure 5.24 Fisher values obtained by fitting the L-PA binding curves in Figure 5.22 and Figure 5.23 to mono-Langmuir (mono-LI), bi-Langmuir (bi-LI) or Freundlich isotherm models (FI) (see Table 5.3 to Table 5.5) 131
Figure 5.25 Adsorption saturation capacities (q) for D-PA (red bars), L-PA (blue bars) obtained for the materials in Tables 5-3 to table 5-5 estimated from mono-Langmuir curve fitting (PA_{20}^2, PA_{20}^3), bi-Langmuir curve fitting (PAref) or estimated as the q-value at the highest concentration of L-PA (PR, PR_E and PR_{ref}). The dashed line represents the theoretical saturation capacity assuming a quantitative yield of imprinted sites. 136
Figure 5.26 Kinetics of the binding data for PA_{10}^2 shown in Figure 5.23B 137
Figure 5.27 Hydrophobicity index, estimated as the ratio of retention factors of ethylbenzene to toluene, of columns packed with the indicated materials. Mobile phase: MeOH/H20: 55/45 (v/v). 139

Figure 5.28 Retention factors (k) on columns packed with the indicated materials, for compounds used to probe surface acidic groups and hydrophobicity. 139
Figure 5.29 Photographs of imprinted composites prepared by RAFT mediated grafting corresponding to SiPRE (B) and PRE(A) after removal of silica by etching. 141
Figure 5.30 Photograph of a solution of RAFT agent in DMSO-d6, after treatment with aqueous HF solution (NH4HF2, 3M) (A) and before treatment (B). 141
Figure 5.31 ^{13}C-NMR of RAFT agent dissolved in DMSO-d6, after treatment with aqueous HF solution (A), and before treatment (B). 142
Figure 6.1 Schematic representation of layer by layer grafting procedure 145
Figure 6.2 TGA curves of (a) aminosilica (b)RAFT modified silica (c) SiP_L(Layer1), (d) SiP_LP_D (Layer2), (e) $SiP_LP_DP_N$ (Layer3), (f) $P_LP_DP_N$, after removal of silica by etching. 149
Figure 6.3 Pore size distribution of consecutive grafted layer and RAFT modified silica support. 149
Figure 6.4 Scanning electron micrographs of imprinted polymer composite prepared by RAFT mediated consecutive grafting corresponding to SiP_L(Layer1), SiP_LP_D(Layer2), $SiP_LP_DP_N$(Layer3), and $P_LP_DP_N$ after removal of silica by etching. 150
Figure 6.5 Retention factors (kL) for L-PA (A,C) and enantiomer separation factors (α) (B,D) obtained in the chromatographic mode after separate injection of stock solutions of D- and L-PA at four different sample loads for corresponding imprinted composites beads prepared by consecutive grafting from RAFT modified support. Mobile phase: for (A,B); pure acetonitrile, for (C,D);MeCN/Sodium acetate buffer pH 4.8(70/30,v/v). 151
Figure 6.6 Elution profiles of D(red), L(blue)-PA injected (10µL of 1mM solution) separately on columns (35mm x 4.6 mm) packed with indicated material. Mobile phase; pure MeCN, flow rate 0.5mL/min, DAD=260 nm. 152
Figure 6.7 Retention factors (k) for L-PA(kL) and D-PA (kD) (A) and enantiomer separation factors (α) (B) at 30 nmol/cm^2 sample loads for corresponding imprinted composites beads and thinwalled material after removal of third layer. Mobile phase: pure Acetonitrile. 153

LIST OF SCHEMES

Scheme 1 17
Scheme 2 Rehydroxylation of siloxane groups. 80
Scheme 3 Functionalisation of silica surface with APS. 80
Scheme 4 Consecutive synthesis of amino silica and end-capping of remaining silanol groups. 81
Scheme 5 Covalent immobilization of Azo- initiator on silica surface. 82
Scheme 6 Labelling of COOH groups with 3-aminoquinoline 97
Scheme 7 Immobilization of RAFT agent on silica surface. 100
Scheme 8 140
Scheme 9 Synthesis of α-bromobenzene acetonitrile 156
Scheme 10 Synthesis of α-Cyanobenzyl Dithibenzoate 157
Scheme 11 Synthesis of BOC-L/D phenylalanine aniline 158
Scheme 12 Synthesis of L/D- Phenylalanine anilide. 159

1 Summary and Zusammenfassung

1.1 Summary

This thesis describes the development of new methods for producing molecularly imprinted polymeric materials with improved properties for analytical and preparative applications.

This thesis is divided into two parts. The first part of the thesis describes the influence of chain transfer agent on the performance of imprinted polymers synthesized using the bulk polymerization method. Reversible Addition Fragmentation chain Transfer polymerization (RAFT) controlled by α-cyanobenzyldithiobenzoate was employed during the synthesis of a poly (methacrylic acid-co-ethylene glycol dimethacrylate) conventional MIPs for L-phenylalanine anilide. In this system, the major synthetic conditions were studied including the ratio of RAFT/ABDV and the prepolymerization complex by differential scanning colorimetry (DSC). The polymer was analysed by FTIR, elemental analysis, and scanning electron microscopy. The pore size analysis in swollen state versus dry state was measured by inverse size exclusion chromatography (ISEC), thermoporometry and nitrogen adsorption technique. The RAFT polymers demonstrated a higher swelling ratio than the non-RAFT polymers, which may be the result of their smaller pore size and narrow size distribution. This was accompanied by an enhanced thermal stability of up to 100°C.

The RAFT polymers were then tested for their ability to resolve the racemate of the template using HPLC. An optimum RAFT agent level (1.56 wt %) during polymerization was found to result in markedly enhanced selectivity, column efficiency and resolution accompanied by a considerably higher sample load capacity. Equilibrium binding test showed 30% increase in binding capacity for RAFT MIP compared to conventionally prepared MIP.

The second part of the thesis describes a novel approach addressing the classical deficiencies of molecularly imprinted polymers (MIPs) i.e. low binding capacity and nonuniform binding sites, poor efficiency and accessibility in chromatography. It also describes the advantages of living polymerization. The thin walled beads were produced in two steps by first grafting thin MIP films, under controlled (RAFT) or noncontrolled conditions, from porous silica beads. The resulting composites were compared in terms of film thickness, the grafted layer homogeneity,

effect of different support morphologies and their chromatographic performance regarding enantioselectivity, and efficiency. Film thickness was stoichiometrically controlled. Thus, L-Phenylalanine anilide (L-PA) imprinted poly (MAA-co-EDMA) silica composites were prepared using the azo or RAFT modified supports. All the materials were characterized using elemental microanalysis, FT-IR, nitrogen sorption, fluorescence microscopy, TGA, SEM, and EDX. The layer thicknesses of the grafted polymers were estimated from two different experimental methods and the materials were applied in HPLC. The azo- composites showed a pronounced enantioselectivity which was strongly dependent on the film thickness, monomer dilution, the RAFT/initiator ratio and the method of grafting. Hence, composites prepared by exhaustive polymerization under dilute conditions using high RAFT/initiator ratios displayed strongly enhanced chromatographic performance in terms of retentivity and enantioselectivity.

In the second step, removing the silica supports from the above composites by etching led to nanometer thin walled beads with structure, morphology and recognition properties strongly depending on grafting chemistry (RAFT or nonRAFT) and on the film thickness of the original composite. Thus whereas the thicker walled materials retained their mesoporous morphology and displayed enhanced enantioselectivity, load capacity and a higher surface areas compared to their composite precursors. The thin walled beads showed lower surface areas indicating network collaps. The thin walled beads prepared in absence of RAFT displayed a perfectly uniform binding site distribution and a saturation capacity exceeding that of a conventional monolithic MIPs. The beads prepared by RAFT control showed a further enhanced saturation capacity significantly exceeding that of the reference material. Finally, the reduced hydrophobic character of the thin walled materials indicated the existence of two separate pore systems with different pore wettabilities.

This approach was further verified in an attempt to demonstrate the layered nature of grafted MIPs. The first layer was grafted with poly (MAA-co-EDMA) thin film with an average thickness 5nm in presence of L-PA as template molecule. The resulting composite preferentially retained the L-enantiomer when tested as a chromatographic stationary phase. Consecutively, a D-PA imprinted film (d=5 nm) was grafted on top of the L-PA imprinted film. The stationary phase now displayed D-selectivity indicating a switch of the chiral preference. In order to block the D-selective sites, a nonimprinted layer occupying the remaining pore system was then grafted

on top of the D-selective layer. This resulting composite showed no chiral discrimination. The layered nature of the composites was finally demonstrated by removing the underlying silica support. The resulting composite preferentially retained the L-enantiomer as the previously covered L-selective sites had been uncovered.

1.2 Zusammenfassung

Die vorliegende Arbeit beschreibt die Entwicklung neuer Methoden zur Herstellung molekular geprägter Polymermaterialien mit verbesserten Eigenschaften für analytischen und präparative Anwendungen.

Die Arbeit ist in zwei Teile gegliedert. Der erste Teil der Arbeit beschreibt den Einfluß von Chain-transfer agents auf die Performanz von geprägten Polymeren, die mit Hilfe der Bulk-Polymerization hergestellt wurden. Die Reversible Additions-Fragmentierungs-Kettenübertragungspolymerization (RAFT), kontrolliert durch α-cyanobenzyldithiobenzoate wurde eingesetzt in der Synthese eines konventionellen MIPs für L-Phenylalanin Anilid bestehend aus Polymethacrylsäure-coethylenglycol-dimethacrylat. Anhand dieses Systems wurden die grundlegenden Synthesebedingungen einschließlich des Verhältnisses von RAFT/ABDV und des Pre-Polymerizationskomplexes mit Hilfe von dynamischer Differenzkalorimetrie studiert. Das Polymer wurde mit FTIR, Elementaranalyse und Rasterelektronenmikroskopie analysiert. Die Porengröße in geschwollenem Zustand wurde im Vergleich zum trockenen Zustand gemessen mit Hilfe von inverser Größenexklusionschromatographie (ISEC), Thermoporosität und Stickstoffadsorption. Die RAFT Polymere zeigten ein größeres Schwellverhältnis als die Nicht-RAFT Polymere. Die kann auf ihrer kleineren Porengröße und ihrer engeren Größenverteilung basieren. Diese Beobachtung wurde begleitet von einer erhöhten Thermostabilität bis zu 100°C.

Die RAFT Polymere wurden im Hinblick auf ihre Fähigkeit getestet, ein Racemat des Templates in einer HPLC Analyse aufzutrennen. Als optimaler Gehalt an RAFT Agent während der Polymerization wurden 1,56 w % ermittelt. Dieser Gehalt resultierte in wesentlich stärkerer Selektivität, Säuleneffizienz und Auflösung, begleitet von einer wesentlich höheren

Probenbeladungskapazität. Gleichgewichtsbindungsexperimente zeigten eine 30 % höhere Bindungskapazität der RAFT MIPs im Vergleich zu konventionell hergestellten MIPs.

Der zweite Teil der Arbeit beschreibt einen neuen Ansatz im Hinblick auf die klassischen Schwachpunkte molekular geprägter Polymere (MIPs). Hier wären z.B. zu nennen die geringe Bindungskapazität und inhomogene Bindungsstellen, geringe Effizienz und Nutzbarkeit in chromatographischen Anwendungen. Darüber hinaus werden die Vorteile der lebenden Polymerization beschrieben. Dünnwandige Beads wurden in einer Zweistufen-Synthese hergestellt. Im ersten Schritt wurden dünne MIP Filme unter kontrollierten (RAFT) und nichtkontrollierten Bedingungen von porösen Silica-Partikeln gebildet. Die entstehenden Komposite wurden im Hinblick auf Filmdicke, Homogenität der entstehenden Schichten, dem Effekt verschiedener Trägermaterialien und ihre Performanz in chromatographischen Experimenten bezüglich Effizienz und Enantioselektivität untersucht. Die Filmdicke wurde stöchiometrisch kontrolliert. Auf L-Phenylalanin Anilid (L-PA) geprägte poly (MAA-co-EDMA) Silica-Komposite wurden unter Verwendung von Azo- oder RAFT modifizierten Trägermaterialien hergestellt. Alle materialien wurden mit Hilfe von Mikroanalyse, FT-IR, Stickstoffsorption, Fluoreszenzmikroskopie, TGA, SEM und EDX charakterisiert. Die Schichtdicke der entstehenden Polymere wurde mit Hilfe von zwei unabhängigen experimentellen Methoden ermittelt und die Materialien wurden in HPLC Experimenten verwendet. Die Azokomposite zeigten eine starke Enantioselektivität, die stark von der Filmdicke, der Monomerverdünnung, dem RAFT/Initiatorverhältnis und der Grafting-Methode abhing. Bei Kompositen, die durch vollständige Polymerization unter verdünnten Bedingungen hergestellt wurden zeigten hohe RAFT/Initiator Verhältnisse stark verbessertes chromatographisches Verhalten im Hinblick auf Retentionszeit und Enantioselektivität.

Im zweiten Schritt wurde das Silica-Trägermaterial mit Hilfe von Etching aus den Kompositmaterialien entfernt. Hierbei entstanden dünnwändige Partikel mit nanometer-Stärke, deren Struktur, Morphologie und Erkennungseigenschaften stark von der Herstellungsmethode (RAFT oder nicht RAFT) und der Filmdicke des Originalpartikels abhing. Es wurde beobachtet, daß die Materialen mit dickeren Wänden ihre mesopore Morphologie erhalten. Sie zeigten verbesserte Enantioselektivität, Beladungskapazität und größere Oberflächen im Vergleich zu ihren Komposit-Vorstufen. Die dünneren Beads zeigten eine geringere Oberfläche. Dies deutet

auf einen Zusammenbruch des Netzwerkes hin. Die dünnwandigen Beads, die in Abwesenheit des RAFT agents hergestellt wurden zeigten eine perfekt uniforme Bindungsstellenverteilung und eine Sättigungskapazität größer als für ein konventionelles monolithisches MIP. Die Partikel die RAFT-kontrolliert hergestellt wurden zeigten eine abermals erhöhte Sättigungskapazität, die signifikant höher war als die des Referenzmaterials. Durch den verringerten hydrophoben Charakter der dünnwändigen Materialien wurde die Existenz zweier separater Porensysteme mit unterschiedlicher Benetzbarkeit indiziert.

Dieser Ansatz wurde weiterhin verifiziert in dem Versuch, den Schichtaufbau gegrafteter MIPs zu demonstrieren. Die erste Schicht wurde mit einem poly (MAA-co-EDMA) dünnen Film mit einer durchschnittlichen Dicke von 5 nm in Anwesenheit von L-PA als Templatmolekül hergestellt. Die enstehenden Komposite banden in chromatographischen Tests vorzugsweise das L-Enantiomer. Nachfolgend wurde ein auf D-PA geprägter Film (d=5nm) auf den ersten Film aufgetragen. Die stationäre Phase zeigte nun D-Selektivität und somit eine Änderung in der chiralen Präferenz. Um die D-selektiven Bindungsstellen zu blockieren wurde eine nicht-geprägte Schicht auf die obere Sicht aufgetragen. Das entstehende Kompositmaterial zeigte nun keine chirale Diskriminierung. Das Schichtsystem der Komposite wurde bewiesen durch die Entfernung des zugrundeliegenden Silica-Trägermaterials. Das erhaltene Kompositmaterial band vorzugsweise das L-Enantiomer, da die zuvor bedeckten L-selektiven Bindungsstellen freigelegt wurden.

2 Background and State of the Art

2.1 Molecular Imprinting technology

In recent years, nanostructured materials have generated a great deal of interest in research and development around the world. Realization of such a, structurally ordered materials on nanoscale might have far-reaching implication for biomimetic engineering. Thus design, synthesis and investigation of complex molecular structures and assemblies would lead to new generation of sensing, separation, catalysis, ion exchange, medical diagnostics and other biomedical and biotechnological applications mimicking biological functions.[1,2] Since molecular recognition is central to the development of these systems, there has always been great interest designing the molecular recognition materials with high degree of affinity and selectivity. Several strategies involving template mediated chemical synthesis and molecular self assembly process have been developed for preparing these molecular and supramolecular systems with functional group arrays on the scale of nanometers.[1-3]

Molecular Imprinting technology is a well known method to prepare polymer based synthetic receptors.[1,3-6] It is a process whereby functional and cross-linking monomers are co-polymerized in the presence of template molecules, which may be small molecules, biological macromolecules, micro-organisms or whole crystals.[4] The functional monomers initially form a complex with the template molecule and following polymerization with crosslinker, their functional groups are held in position by the highly cross-linked polymeric structure. Subsequent removal of the imprint molecule reveals binding sites that are complementary in size and shape to the template or to an analogous structure (Figure 2.1). The association between the template molecule and the monomers can be based on different type of interaction such as reversible covalent bond(s), electrostatic, hydrogen bonds, hydrophobic or van der Waals or co-ordination with a metal centre. Molecularly imprinted polymers have been used in many different applications such as affinity separation, immunoassays, biosensors, solid phase extraction media, and controlled drug release.[1,6] Recently the group of Shea has shown that MIP neutralizes the toxic melittin peptides and inhibits its haemolytic activity in complex biological media.[7]

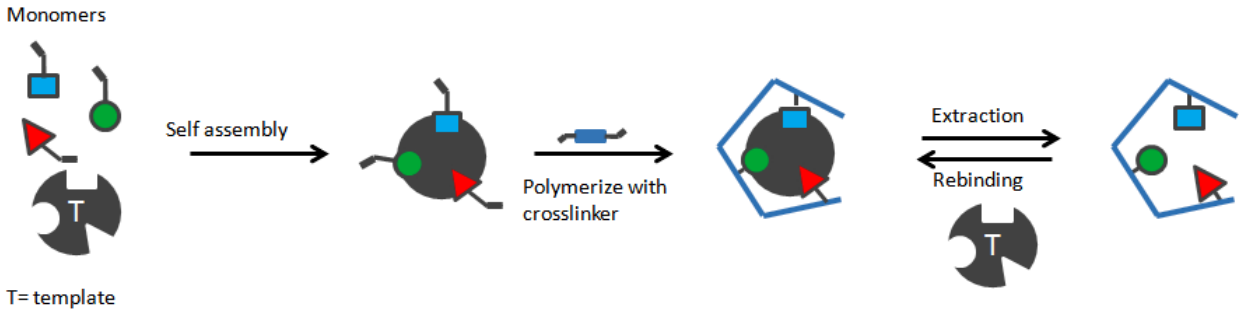

Figure 2.1 Schematic representation of the molecular imprinting process

2.2 Imprinting Approaches

In order to introduce functionality into these recognition sites three main approaches can be taken into account, the covalent and the non-covalent and semi-covalent imprinting.

2.2.1 Covalent Imprinting

Covalent imprinting, developed by the group of Wulff [8,9], is defined by the use of covalently bound templates (Figure 2.1). In this approach, prior to polymerization, functional monomer and template are bound to each other by reversible bond. After polymerization, the covalent linkage is cleaved and the template is removed from the polymer. Upon the guest binding by the imprinted polymers, the same covalent linkage is formed. Following this principle, Shea et al. formed a ketal conjugate between the carbonyl group of a template and the 1,3-diol group in a functional monomer, and used this covalent conjugate for molecular imprinting.[10] For example covalent imprinting of 4-nitrophenyl-a-d-mannopyranoside is shown in Figure 2.2. The template monomer (4-nitrophenyl-a-d-mannopyranoside-2,3:4,6-di-O-(4 vinylphenylboronate)) was prepared by condensation of 4-vinylbenzeneboronic acid with 4-nitrophenyl-a-d-mannopyranoside and the MIP was prepared via copolymerization of divinylbenzene or ethyleneglycol dimethacrylate. [11]

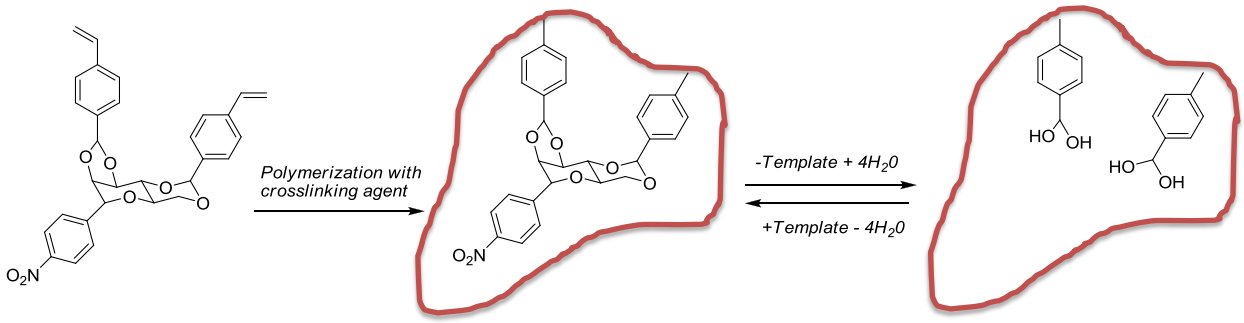

Figure 2.2 Covalent Imprinting of 4-nitrophenyl-a-d-mannopyranoside-2,3:4,6-di-O-(4vinylphenylboronate).

2.2.2 Noncovalent imprinting

This method was first introduced in organic polymers by the group of Mosbach [12]. In non-covalent imprinting the interactions between functional monomer and template during polymerization are the same as those between polymer and template in the rebinding step. The interactions between functional monomer and template are based on interactions such as H–bonding or ion–pairing (Figure 2.1). This method is most widely applied until now to generate molecularly imprinted polymers because of its simplicity and it is more straightforward than covalent imprinting. Here monomer and template is dissolved in a suitable solvent and self association occurs to give template-monomer complexes, followed by the polymerization in presences of excess crosslinker forms an insoluble 3D polymer matrix. Subsequent removal of template by simple solvent extraction leaves behind the cavities whose size, shape complimentary to the template molecule. The template, or analogues, may then be selectively rebound by the polymer.

To date the most successful non-covalent imprinting systems using commercially available monomers are those based on acrylic or methacrylic monomers, such as methacrylic acid (MAA), cross-linked with ethyleneglycol dimethacrylate (EDMA). The reason for MAA as functional monomer can be related to the greater versatility of non covalent interaction with respect to the available modes of interaction and the more favorable kinetics properties of the recognition process. In the assembly phase MAA can act as hydrogen bond donor or acceptor, enabling ionic interactions to amines and hydogen bonds to amides, carbamate or carboxyls. The first endeavours based on this approach for enantiomer separations were made by Sellergren et

al.[13] With derivatives of aminoacids enantiomers as the template a series of highly selective chiral stationary phases were prepared.[13-16]

Firstly, the template L-phenylalanine anilide, MAA and EDMA are dissolved in to a low polar medium. The polymerization is then carried out in glass ampoule using free radical polymerization followed by grinding and extracting the template. The resultant particles were sieved to suitable size for chromatographic (25-36 μm) and batch (150-250 μm) applications. The results showed that the prepared polymers can present a high distinguished to the enantiomers.[13,16]

Many studies have been performed using L-PA imprinted monolith polymers as a model system. These involved the study of chromatographic band broadening, effect of the porogen ion exchange retention model, protonation states photo-*versus*-thermal polymerization, effect of thermal annealing, factors affecting the chromatographic response, monomer-template interaction and model of a binding site study of the adsorption isotherms *etc.*[15,17-19 20,21]

^{1}H-NMR spectroscopy and chromatography were used to study the association between MAA and L-PA in solution as a mimic of the pre-polymerization mixture. [19] The ^{1}H-NMR chemical shifts of either the template or the monomer versus the amount of added MAA, as well as the chromatographic retention of L/D-PA versus the amount of acid in the mobile phase, varied in accordance with the formation of multimolecular complexes between the template and the monomer in the mobile phase. A 1:2 template-monomer complex was proposed to exist prior to polymerization. Based on these results, hydrogen bond theory and the assumption that the solution structure was preserved after polymerization, a structure for the polymeric binding was proposed (Figure 2.3).

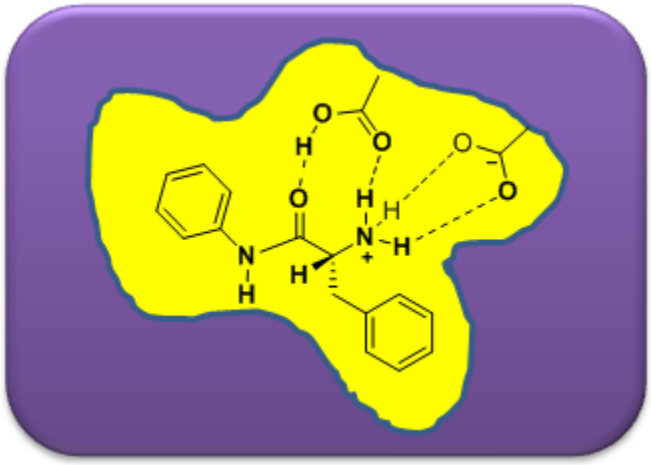

Figure 2.3 Model of L-PA binding site based on NMR and chromatographic data

MIPs with an enhanced capacity can also be obtained via non-covalent imprinting by taking advantage of elements from supramolecular chemistry thus, novel functional monomers that will interact more strongly with a given target molecule than the commonly used monomer.

2.2.3 Semi-covalent Imprinting Approach

The semi-covalent approach is a hybrid between the two main approaches, where covalently attached polymerizable binding groups are activated for non-covalent interaction by template cleavage. Semi-covalent approach can be distinguished in to two types (1) the template and the monomer are connected directly or (2) the template and the monomer are connected using a spacer group [3]. In 1990, Sellergren and Andersson first reported the semicovalent approach for the imprinting of p-aminophenylalanine ethyl ester. A structural analogue was used which possessed two polymerizable groups attached via ester linkages. After hydrolysis the carboxylic acid groups left in the polymer binding site rebind the amino acid through mixture of hydrogen bonding and electrostatic interactions.[22]

In order to avoid crowding in the binding site and to allow unhindered non covalent rebinding to occur, Whitcombe et al. introduced the sacrificial spacer approach. [23] In the first example (Figure 2.4) the template, cholesterol, was attached via carbonyl spacer to 4-vinyl phenol giving cholesteryl 4-vinyl phenyl carbonate as the template monomer (a); the template monomer,

cholesteryl (4-vinyl) phenyl carbonate is polymerized with ethyleneglycol dimethacrylate (EDMA) in a porogenic solvent (b); the template remains attached covalently to the resultant polymer. After polymerization the cholesterol was cleaved from the polymer by base hydrolysis and loss of the spacer (CO2), leaving a phenolic hydroxyl group(c) in the binding site. (d) non-covalent rebinding of the template, by hydrogen-bonding with the phenol, is possible with the cholesterol molecule re-occupying its original position in the site.[3,11]

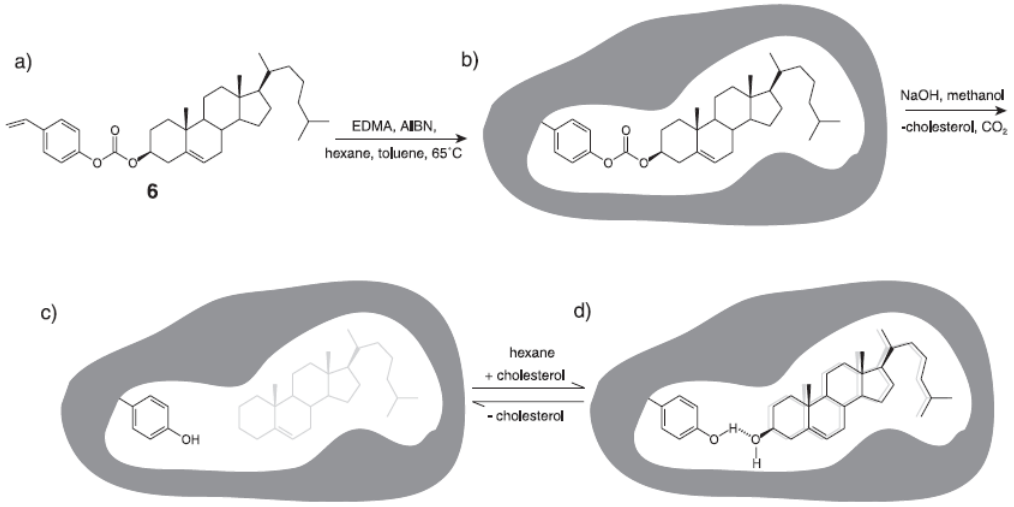

Figure 2.4 Imprinting of cholesterol by the sacrificial spacer (semi-covalent) method. Adapted from ref.[11]

A variety of other combinations can be used for the preparation of imprinted polymers, such as metal-ion mediated imprinting.[3]

The advantages of molecularly imprinted polymers, as compared to biological receptors, include their mechanical and chemical stability, low cost of preparation and wide range of operating conditions. However, they suffer from some drawbacks in certain applications, such as the heterogeneous distribution of binding sites, low capacity and selectivity and poor site accessibility. [21] The development of suitable methods for overcoming these problems will open the door to considerably more diverse application opportunities than are available right now. This thesis is focused on the development of such new methodologies for producing imprinted materials exhibiting uniform structures, homogeneous binding sites and high affinity to the target molecules.

2.3 MIPs synthesized by Free radical Polymerization

Free radical polymerization (FRP) is one of the most simple and straight forward technique to prepare a polymers in large industrial scale. In fact most of vinyl polymers are produced in this way because this technique is more flexible in terms of reagent purity, experimental conditions.[24,25] In the context of molecular imprinting this method is very attaractive since it is compatible with a wide range of monomers carrying different functinal groups, and because it usually tolerates the presence of additional chemicals, most importantly the imprint molecule. It is therefore not surprising that this polymeization method has been widely adopted by molecular imprinting.[1] Free radical polymerization is a chain reaction and involves three fundamental steps (Figure 2.5).[26]

2.3.1.1 Initiation

The polymerization is initiated by generating free radicals using an initiator, a molecule that homolytically decomposes under thermal or UV irradiation. A radical attacks the double bond of a monomer, resulting in the formation of intermediate radical.

The rate of initiator decomposition can be written as

$\upsilon_i = d[RM^*]/dt = 2k_d f [I]$

Where 2 relates to the two radicals generated per initiator molecule, f is the initiator efficiency of the radicals to propagate chains, [I] is the initiator concentration and [RM] is the concentration of propagating species

2.3.1.2 Propagation

A chain carrier is formed from the reaction of a free radical and new monomer unit and propagation occurs rapidly by addition of new monomers to produce primary linear polymer chains.

$RM_n^* + M \rightarrow RM_{n+1}^*$

With the rate of propagation given by:

$\upsilon_p = k_p [M][M^*]$

Where [M*] represents the concentration of growing reactive ends. The reaction can be followed by the disappearance of monomer.

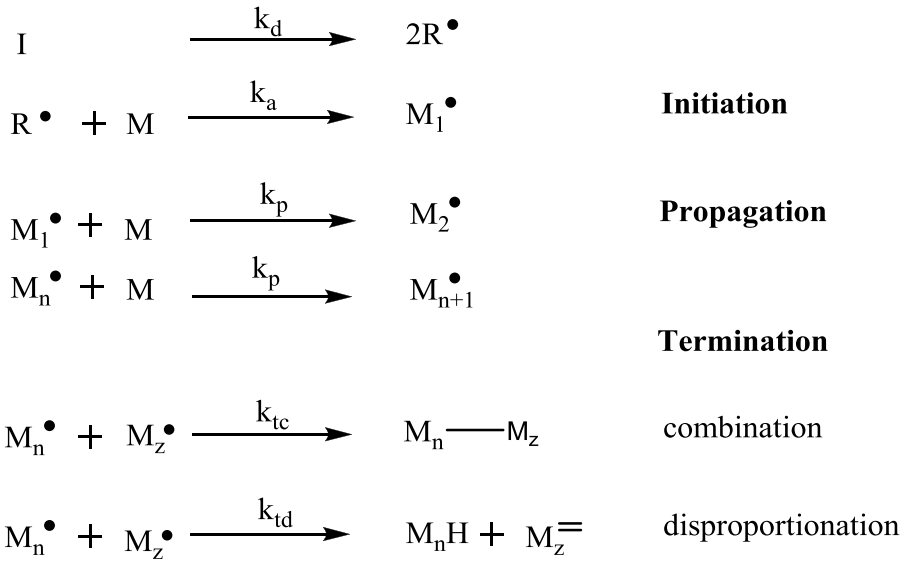

Figure 2.5 Schematic representation of Free radical polymerization

2.3.1.3 Termination:

Propagation continues until the free radical reacts to form an inactive covalent bond. This can occur when the concentration of free radicals is high or when chain transfer agents are present. Termination of the reaction can take place in two ways: recombination of two macroradicals forming a macrochain or disproportionation yielding a double bond and C-H bond at the chain terminus.

In addition, termination can occur in many ways: i) interaction of two active chain ends; ii) the reaction of an active chain end with an initiator radical; iii) termination by transfer of the active centre to another molecule, which may be solvent, initiator , monomer or template; or iv) interaction with impurities e.g.oxygen or inhibitors.

The rate of termination is given by:

$\upsilon_t = 2k_t[M^*][M^*]$

Steady state:

At steady state, the rate of production of free radical equals the rate of consumption i.e.

$2k_t [M^*]^2 = 2k_d f [I]$

This can be put into equation above giving the rate of polymerization:

$\upsilon_p = k_p [M](f k_d [I]/k_t)^{1/2}$

2.4 Limitation of FRP-MIPs

Free radical polymerization has some major draw backs. It does not allow one to control the size, architecture and number of the macromolecules synthesized, due to the high reactivity of alkyl radical produced constantly during the polymerization process, which favor irreversible termination reactions by recombination and disproportionation.(Figure 2.5) Thus, the molecular weight of the polymer cannot be controlled or predicted, and block copolymers and other polymers of complex architecture are totally inaccessible. The MIPs produced using FRP technique has some advantages such as a high affinity and selectivity towards the target molecules. However these *MIPs are suffering from slow mass transfer, non uniform binding sites, template bleeding, low saturation capacity, poor site accessibility, low yield, high amount of template consumption.* It is an impractical manufacturing process, because the resulting MIPs have to be crushed, sieved using motor and pestle. During the crushing and sieving polymer will be lost which will yield less imprinting sites and irregular shape of particles formed (Figure 2.6). Due to flow disturbances and diffusion limitations, this causes a poor efficiency in chromatography, making these particles unsuitable for such applications.[16,27] Some of these limitations have been addressed by surface initiated controlled radical polymerization, graft polymerization and template techniques.

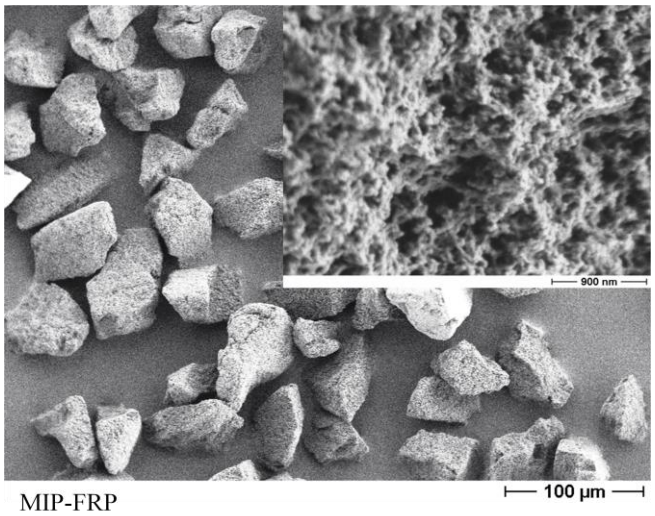

Figure 2.6 Irregularly shaped particles resulting from mechanical grinding of a "traditional" molecularly imprinted polymer (MIP-FRP).

2.5 Improvement in binding capacity by reducing the binding site heterogeneity

The classic bulk imprinting of diazepam (1) MIPs reported by Mosbach[28] illustrates the degree of heterogeneity possible as well as its origin. As seen in Figure 2.7 the hydrogen bonding interaction between the template (1) and functional monomer (2) is weak in solution. To make a strong complex as such (3) there is need to add an excess amount of functional monomer to make a maximum complexation between monomer and template. Thus excess added monomer is unassociated with template molecules in prepolymerization mixture so the resultant polymer produces a larger number of low affinity binding sites (e.g. binding sites B in figure 2.7). Only a small fraction of monomer make a strong complexation, produces the tight binding sites which have high affinity and selectivity.[29]

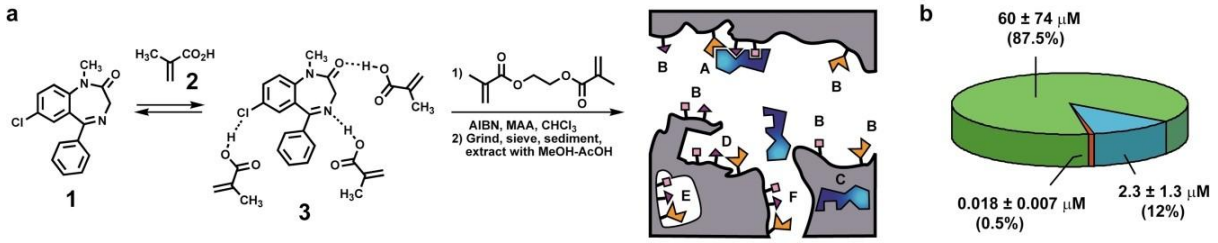

Figure 2.7 (a) Schematic representation of a diazepam MIP containing heterogeneous binding sites: high affinity site in macropore (A) and micropore (F) and lower affinity sites(B) in macropore,(C) trapped template,(E) embedded site, (D) highest affinity site with site with shape selectivity from polymer.(b) chart showing the dissociation constant of three classes of binding sites needed to fit binding isotherm. Adapted from ref.[29]

The heterogeneity property can limit the use of MIPs in chromatography where it gives poor resolution and peak asymmetry. The accurate assessment of binding affinity is measured by applying the discrete or continuous binding model to the experimental binding isotherm which is generated by either batch rebinding or frontal chromatography experiments.[21,30] The discrete binding model can only discriminate the two types of binding affinity and is more likely to the homogeneous system for monitoring the binding behavior i.e. Langmuir isotherm and bi-Langmuir.[21,31] The continuous binding model can be applied to the heterogeneous systems for accurate monitoring the binding behavior. For example the typical model is Freundlich isotherm.[32-35] These isotherm models were used for characterizing the binding affinity of MIPs throughout this thesis.

A number of strategies examined for reducing the binding site heterogeneity and they are explained below.

2.5.1 Stoichiometric Imprinting

In stoichiometric imprinting the complex between template and functional monomer is strong enough to ensure that the equilibrium lies well to the side of the complex; this can be achieved only when the association constant (Ka) of monomer and template interaction is $Ka \geq 10^3\ M^{-1}$. The group of Wulff [36] designed and synthesized polymerizable amidine based monomer(1) and the group of Sellergren [37] designed urea-based monomers(2) for imprinting of oxyanions

template. These specially designed monomers forms a strong 1:1 complex with oxyanions and form the tight binding sites with high affinity (Scheme 1).

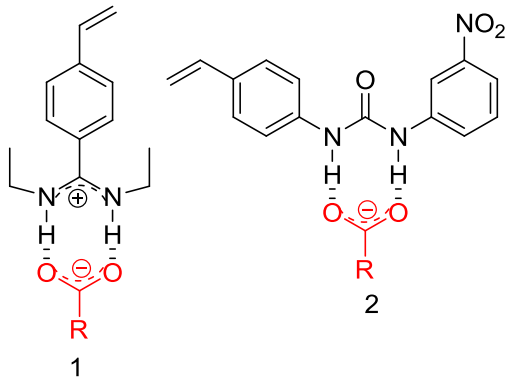

Scheme 1

2.5.2 Post imprinting modification

In post imprinting modification, where template is not involved, only the resultant MIP is treated either chemically or thermally to reduce the binding site heterogeneity. For example Chen et al[20] annealed a MIP prepared for L-PA. The authors have shown that the thermally treated MIP increased the saturation capacity by one third to one-half in comparison to non annealed MIP. It also decreases the separation factors of two enantiomers but slightly improved the mass transfer rate.

Shimizu and co-workers[38] demonstrated the site selective chemical modification strategy for 9-ethyladenine acetate MIP. In this strategy, MIPs were selectively chemically modified to improve the ratio high affinity to low affinity binding sites. The low affinity sites were eliminated by estrification with diazomethane. In this reaction the guest molecule plays a role as protecting group in situ that preferentially shields high affinity sites and leave the low affinity sites so estrification is selectively taken place only at low affinity sites (Figure 2.8). Then the population of high and low affinity sites were quantified using affinity distribution analysis, which quantitatively measures the heterogeneous distribution of binding sites in MIPs as the number of binding sites with respect to binding affinity. The chemically modified MIP was

shown to improved percentage of high affinity binding sites. The authors claim that this strategy can be applied to improve the binding properties of MIPs.

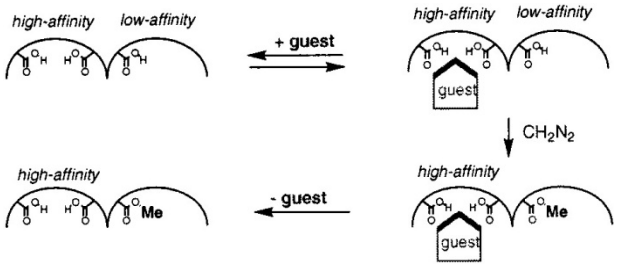

Figure 2.8 Schematic representation of site selective chemical modification strategy[38]

2.5.3 Thermodynamically controlled polymerization

Steinke and coworkers[39] claimed that statistical, kinetically driven nature of the network forming process of conventional radical polymerization makes it impossible to achieve monoclonality or homogeneous distribution of binding sites in MIPs. As a remedy they suggest a thermodynamically controlled process via ring-opening metathesis polymerization (ROMP) (Figure 2.9). In this approach the template (L-menthol) was covalently bond to polymerizable (ROMP) monomer and polymerized with dicyclopentadiene, in presence of Grubbs catalyst and after polymerization the template was cleared by hydrolysis so the covalent interaction is replaced to reversible non covalent ones, an approach pioneered by Whitcombe.[23] The authors have shown that a MIP has high selectivity and enantioselectivity towards L-menthol over D-menthol. So this approach could be useful for improving the binding properties of MIPs.

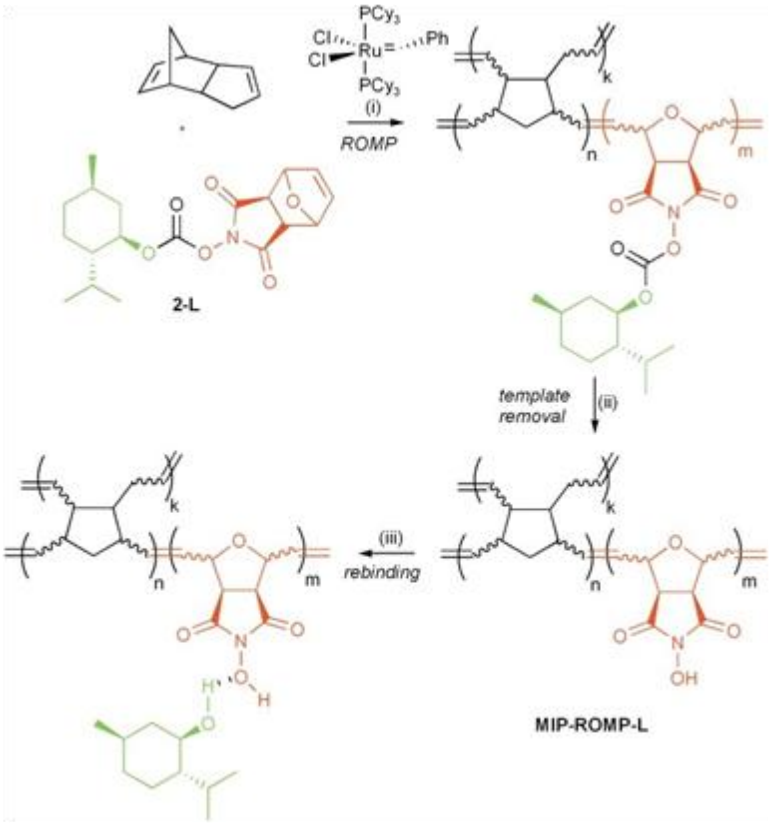

Figure 2.9 Synthesis of MIPs via ROMP[39]

2.5.4 Single particle imprinting (Dendrimer Imprinting)

Zimmermann and coworkers[40,41] reported a first time imprinting inside dendrimers (Figure 2.10). The process involves the covalent attachment of dendrons to a porphyrin core, cross-linking of end groups of the dendrons, and removal of porphyrin template by hydrolysis. This technique yields homogeneous binding sites and quantitative template removal. Moreover, the hosts are soluble in common organic solvents. The drawback of this approach is that it requires multistep organic synthesis and tedious purification. This technique can be applied only to high molecular symmetry templates. To avoid this issue recently Shea and co workers developed the simple and straight forward method to generate synthetic nanoparticles for affinity sorting and this is described in next section.

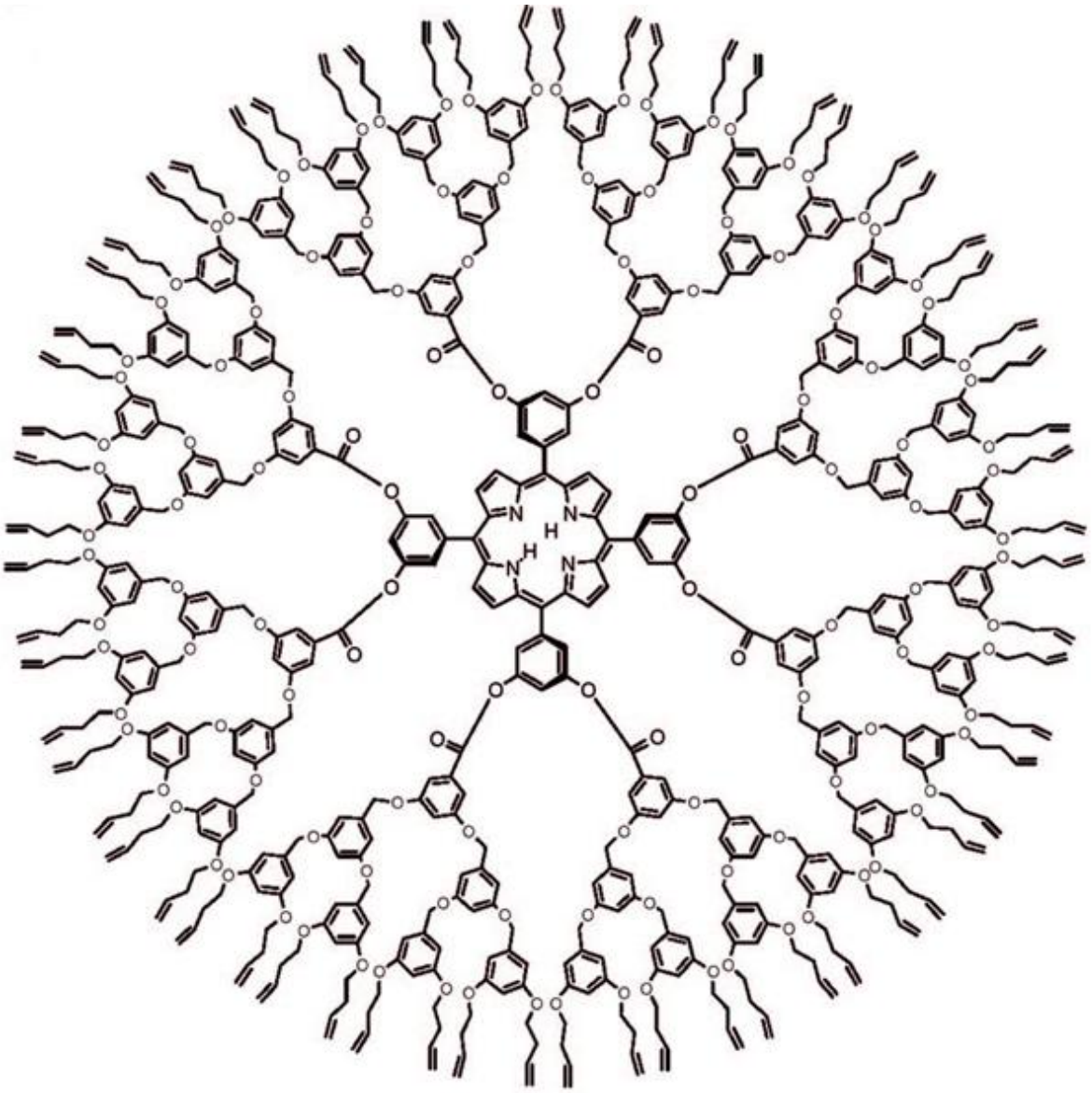

Figure 2.10 Monomolecular imprinting inside dendrimer; A dendrimer with crosslinkable double bonds at out shell, and the covalently attached porphyrin template in the core.[40]

2.5.5 Synthetic polymer nanoparticles for affinity sorting

The polymeric nanoparticle approach can offer a unique solution to the problems frequently encountered in molecular recognition associated with the presence of low affinity binding sites. These low affinity sites can be removed by affinity chromatography with immobilized template to capture nanoparticles containing a greater number of relatively high affinity sites. Recently an exciting contribution was made by Shea and coworkers in polymeric nanoparticles for molecular

recognition.[7,42-46] The authors created an imprinted cavity in synthetic polymer nanoparticles for peptide melittin.[44] The resulting plastic antibody can be used in vivo capture and neutralization of melittin.[7,42] Melittin is a toxic due to its cytolytic acitivity. Melittin is a 26 aminoacid peptide, it has six positive charges of which four are localized in a hydrophilic 6 amino acid sequence on the C-terminus. The remaining 20 amino acids have a high proportion of apolar residues. They also showed that the binding affinity and size of the MIP nanoparticles are similar to natural antibodies. The same groups demonstrated a protocol to purify synthetic polymer nanoparticles with high affinity binding sites for a melittin peptide from a acrylamide based multifunctional polymeric nanoparticles.[43] These nanopartilces are approximately the size of a protein and are purified on the basis of peptide affinity as in the case of antibodies, using an affinity chromatography strategy. Each fraction isolated during the affinity sorting process shows a different affinity for the target peptide. The selected nanoparticles have a much stronger and narrower affinity distribution than the materials before purification. The authors claimed that this affinity purification can be useful for nanosize materials for molecular recognition and also useful for preparation of plastic antibodies with a near homogeneous and tailor made affinity for target molecules.

2.5.6 Controlled radical/Living polymerization

In 1956, M. Szwarc was the first discovered the living polymer in the anionic polymerization of styrene.[47,48] Who stated that for a polymrization to be considered "living" it should meet the following requirements?

"• The polymerization proceeds to full conversion; further addition of monomer leads to continued polymerization.

• The number average molar mass is linearly dependent on conversion.

• The number of polymer chains is constant during polymerization.

• The molar mass can be controlled by the reaction stoichiometry.

• The polydispersity of the polymer molar mass distribution is low.

• Chain-end functionalised polymers can be obtained quantitatively.

• In radical polymerization, the number of active end groups should be two; one for each chain end."

Therefore, by definition, living polymerizations offer the preparation of polymers in well controlled composition, architecture and narrow molecular weight distribution. They also provide routes to narrow dispersity end functional polymers, to high purity block copolymers and to stars and other more complex architecture. Thereafter, living polymerizations system have been developed in the cationic, ring opening, metathesis, co-ordination , group transfer and immortal polymerizations as well as the anionic polymerization of many kinds of monomers other than styrene.[25] Here I will discuss the various approaches that have been developed in moving towards controlled/living radical polymerization paying particular attention to the concept and mechanism of Iniferter, NMP, ATRP and RAFT. These techniques are more attractive in developing new formats of molecularly imprinted polymers.

Effect of CRP on imprinted network: CRPs have advantages over FRP in preparing homogeneous binding sites in imprinted polymer networks. (See in section 3.1). In CRP there is fast exchange of propagating radicals with the dormant species; the chain growth through propagation is slower, giving rise to sufficient time for chain relaxation and diffusion of reaction species. The chain relaxation and the uniform distribution of reaction species minimize microgel formation by facilitating intermolecular reactions and thus generate homogeneous polymer networks.[49]. CRP offers the ability to create more homogeneous polymer networks and as a result can lead to better binding parameters in imprinted polymers.[50-54]

Recently Byrne *et al*[51] have studied the effect of iniferter on imprinted polymer networks. In mono vinyl polymerization the use of iniferter yields a lower polydispersity of kinetic chains and decreased average chain length within the crosslinked networks, addition of iniferter leads to more uniform and higher population of appropriately sized imprinted macromolecular cavities for the template (Figure 3.11). This can be explained as due to shorter kinetic chain lengths and or more narrow dispersity of kinetics chains which leads to more homogeneous network and potentially a more uniform crosslink density.

It is rather surprising that modern methods of CRP/living radical polymerization are still very little used in the molecular imprinting as these methods should have a great potential for generation a controlled morphology. In addition they give access to thin films and nanostructures with controlled dimensions and complex architectures.[6] Indeed, all of the following CRP methods have been applied to MIPs.

2.5.6.1 Iniferter Polymerization

In 1982, Otsu discovered that the addition of certain compounds e.g. dithiocarbamates, disulfides to a radical polymerization resulted in a system that exhibited some living characteristics.[55] Later he introduced the term iniferter for this technique because the dithiocarbamates acted as initiators as well as transfer and termination agents [56] (initiator-transfer agent-terminator).

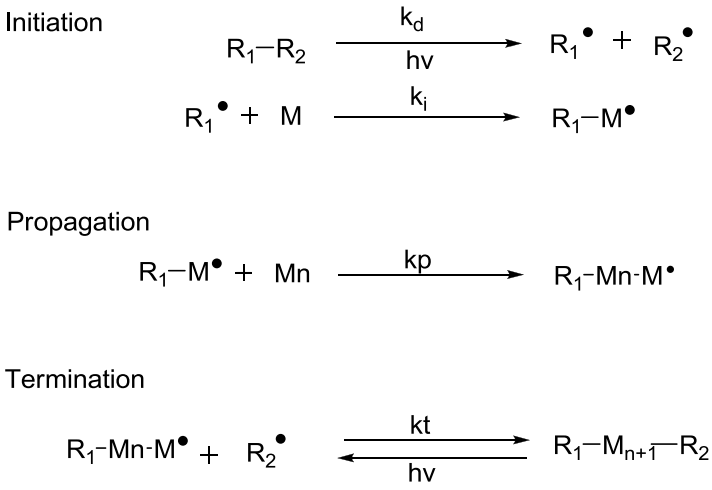

Figure 2.11 General mechanism for iniferter kinetics proposed by Otsu and Yoshida.R_2 is usually sulphur radical.R_1 may be either a sulphur radical or a carbon radical.[57]

The iniferter dissociates into two different radical species. One of these species is able to add to monomer and form a growing polymer chain. The other radical should be inactive in this respect and serves only to terminate the growing polymer chain. The species generated in this process is a dormant polymer chain, which can be reactivated photochemically or by thermal energy, allowing gradual growth through polymerization.

Byrne and coworkers[51] explored possible benefits of iniferter namely, gaining control over the polymerization reaction by altering the kinetic chain length and potentially increasing the homogeneity of the cross-linked architecture. This was hoped to be associated with better target binding properties of MIPs specific for ethyladenine-9-acetate, synthesized in a bulk format. The authors used an iniferter-type initiator, tetraethylthiuram disulfide, in addition to AIBN, apparently yielding a RAFT like system. The number of binding sites in a poly (methacrylic acid-co-ethylene glycol dimethacrylate) MIP was increased by 63% compared with a similar MIP synthesized by FRP using AIBN as a photoinitiator, the binding affinity remaining roughly the same. This was hypothesized by the authors to be due to a shorter kinetic chain length or a more narrowdispersity of kinetic chains, or both, and is supposed to lead to a more homogeneous network. The same authors later used iniferter polymerization for the synthesis of MIPs for controlled drug release. With CRP MIPs they observed a substantially increased drug load capacity and a delayed template release with respect to FRP MIPs.[52]

2.5.6.2 Nitroxide Mediated Polymerization

In 1985, NMP as CRP was first reported by Rizzardo *et al.*[58-60] These authors reported the application of stable nitroxide radicals as deactivators. The activation and deactivation rate constants resulted in rapid deactivation of propagating radicals and an equilibrium which was shifted strongly to the dormant side.

Once the initiator has been converted to dormant species equilibrium is established between the active chains and dormant species. Propagating species and deactivating persistent radicals (*i.e.* nitroxides) are generated in equimolar amounts. Propagating species are slowly taken out of this equilibrium via bimolecular termination resulting in an excess of nitroxide that shifts the equilibrium to the left, increasing the level of control over the reaction, but also decelerating polymerization (Figure 2.12).

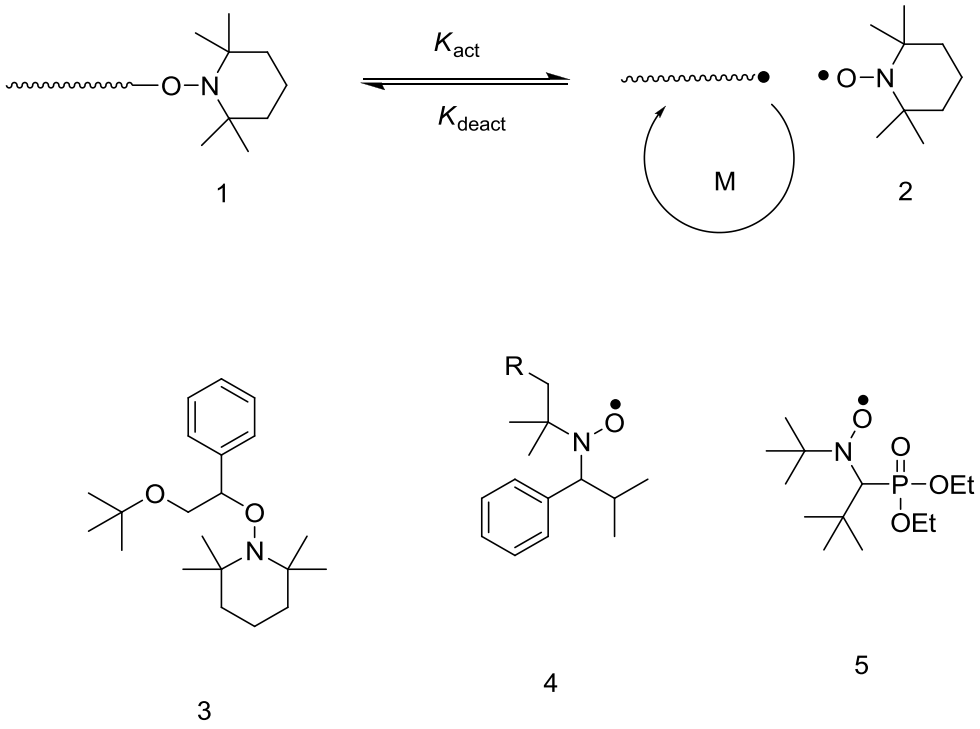

Figure 2.12 The activation-deactivation equilibrium in nitroxide mediated polymerization.

An alkoxyamine (1) dissociates reversibly to produce a radical, which can add monomer, and the persistent 2,2,6,6-tetramethylpiperidine-N-oxyl (2, TEMPO) radical. A typical example of an initial alkoxyamine structure (3) that is applied as initiator for *e.g.* polymerization of styrene-2,2,5-trimethyl-3-(1´-phenylethoxy)-4-phenyl-3-azahexane (4) and N-tert-butyl-N-[1-diethylphosphono-(2,2-dimethylpropyl) nitroxide (5), are two examples of more versatile nitroxides applicable to *e.g.* acrylates and conjugated dienes as well.

Boonpangrak *et al*[61] synthesized molecularly imprinted polymer for cholesterol using NMP in bulk format via covalent approach. They included a sacrificial spacer between the template and the functional monomer, and the binding of the target molecule to the MIP is via non covalent hydrogen bonding interactions. They found that the imprinted hydrolyzed MIP prepared by NMP displayed higher selective cholesterol binding than that prepared by FRP MIP, which can be attributed to the more ordered structure of the polymer network formed by NMP.

2.5.6.3 Atom Transfer Radical Polymerization

In 1995, Matyjaszewski [62-64] and Sawamoto[65] simultaneously reported ATRP. It is an extension of the Kharasch[66-68] addition reaction commonly referred to as atom transfer radical addition (ATRA). Since then it has been used as a useful tool for synthesis of different polymer architectures. The general mechanism for ATRP is shown in Figure 2.13.

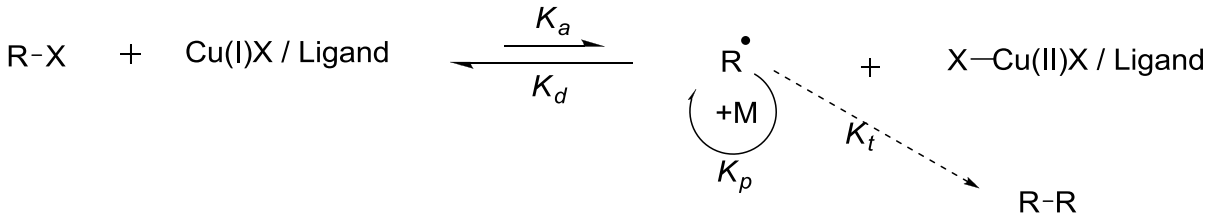

Figure 2.13 Transition Metal-catalyzed ATRP[69]

The radicals, or the active species, are generated through a reversible redox process catalyzed by a transition metal complex (Cu(I)X/Ligand) , which undergoes a one electron oxidation with concomitant abstraction of a (pseudo)halogen atom, X, from a dormant species, R-X. This process occurs with a rate constant of activation, *k*act, and deactivation *k*deact. Polymer chains grow by the addition of the intermediate radicals to monomers in a manner similar to a conventional radical polymerization, with the rate constant of propagation *k*p. Termination reactions (*k*t) also occur in ATRP, mainly through radical coupling and disproportionation; however, in a well-controlled ATRP, no more than a few percent of the polymer chains undergo termination. This process generates oxidized metal complexes, X-Cu(II)X/Ligand, as persistent radicals to reduce the stationary concentration of growing radicals and thereby minimize the contribution of termination. A successful ATRP will have not only a small contribution of terminated chains, but also a uniform growth of all the chains, which is accomplished through fast initiation and rapid reversible deactivation.

The process can be applied to a wide range of monomers and at mild reaction, though it must be said that traces of oxygen can have a much more dramatic effect on the reaction rate than in a conventional radical polymerization. A further drawback, restricting industrial application, is the

presence of considerable amounts of metal in the product. Nonetheless, numerous well-defined complex polymer architectures have been prepared with ATRP.[63,70]

Reverse ATRP

Reverse ATRP[69] is the polymerization using a traditional radical initiator, e.g. 2,2'-azobisisobutyronitrile (AIBN), in the presence of a copper/ligand complex (Figure 2.14). It differs from conventional ATRP in the initiation process. The primary radical abstracts a halogen atom from the catalyst/ligand complex and forms a dormant halide species and the reduced transition metal species activator. Equilibrium is established between propagating chains and dormant chains. The disadvantage with this technique is that the rate coefficient is relatively low (*e.g.* for 1-phenylethyliodide k_{tr}= 2400 dm ^{3} mol^{-1} s^{-1} for styrene at 80°C) such that starved conditions have to be used in order to obtain low polydispersities.

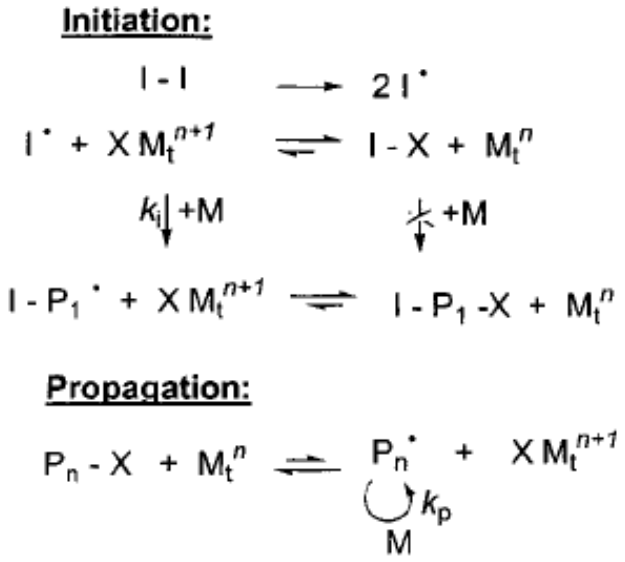

Figure 2.14 Reverse ATRP using AIBN as a initiator.[69]

Concerning the use of ATRP with MIPs, the major limitation for this technique is the small choice of monomers with suitable functional groups. Commonly used monomer in imprinting such as MAA which is incompatible in ATRP as they inhibit the metal-ligand complex and other

monomers like methacrylamide, vinylpyridine also have difficulty to achieve high monomer conversion.[54] Template molecules also often carry functional groups that may inhibit the catalyst. All this seems to make ATRP not the best choice for molecular imprinting.

Nevertheless it has been used on a number of occasions. For example, Zhang and co-workers[71] first used normal ATRP and reverse ATRP in radical bulk polymerization for Bisphenol-A and 2,4 dichlorophenoxyacetic acid imprinted polymers. The authors demonstrated that MIPs prepared by ATRP showed lower binding capacities and apparent maximum number Nmax for high affinity sites, as well as quite similar binding association constants ka and high affinity site densities in comparison with the MIP prepared via traditional bulk polymerization. This is tentatively ascribed to the occurrence of rather fast gelation process in ATRP bulk polymerization (ATRPBP) and resultant heavily interrupted equilibrium between the dortmant species and active radicals, thus leading to the total loss of controllability of ATRPBP. So the authors claimed that the appropriate choice of reaction conditions is crucial for the generation of MIPs with desired properties, which is of significant importance for rational use of CRPs in the synthesis of MIPs with improved binding properties.

Takeuchi's group[72] used reverse ATRP for the imprinting of bisphenol A through a covalent approach. They showed that swelling degrees of ATRP MIPs and non imprinted controls were approximately twice as high as those of FRP polymers, indicating lower crosslink density for the former. More template could be extracted compared to the FRP MIP, and capacity, selectivity, and imprinting factor were improved.

2.5.6.4 Reversible Addition Fragmentation chain Transfer Polymerization (RAFT)

RAFT polymerization was first reported by CSIRO scientists.[73-75] In RAFT polymerization, RAFT agents function by establishing a dynamic equilibrium between propagating radicals ($P_n^{\cdot}$) and dormant chains by a mechanism of reversible addition-fragmentation chain transfer, as shown in Figure 2.15. Initiation and radical–radical termination occur as in conventional radical polymerizations. Propagating radicals are generated as in a conventional radical polymerization, *i.e.* thermally, photo-chemically. The RAFT agent (1) is transformed into a polymeric RAFT

agent (3) through reaction with a propagating radical ($P_n^{\cdot}$) *via* an addition-fragmentation process. The radical liberated ($R^{\cdot}$) then reacts with monomer to form a new propagating radical ($P_m^{\cdot}$). Chain extension of the polymeric RAFT agent (3) involves essentially the same process. The reversible addition-fragmentation steps transfer the S=C(Z)S moiety between active and dormant chains and provide a mechanism for all chains to grow with similar rate and uniformity. At the end of the polymerization, most chains retains thiocarbonylthiolate end group. To achieve control, a delicate balance of the forward and reverse rates of addition (K_{add} and K_{-add}) and fragmentation ($K_ß$ and $K_{-ß}$), together with the rates of re-initiation (K_i) and propagation (K_p), is required.

RAFT agent (1) possesses two important areas of functionality, known as the R group and the Z group. Each group plays an important role in the RAFT process. The R group has two primary purposes; first it must be a good free radical leaving group, second, it must reinitiate polymerization readily. If the intermediate radical $R^{\cdot}$ is too stable relative to the propagating radicals P_n the RAFT agent will act as an inhibitor. Like the R group, the Z group also has two primary purposes, these are to activate the C=S bond for radical addition and (most importantly) to stabilize the intermediate radical adduct. RAFT polymerization requires selection of a suitable chain transfer agent, which has a very high transfer constant in radical polymerization of the desired monomers under appropriate reaction conditions.

Initiation/chain transfer

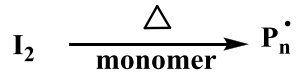

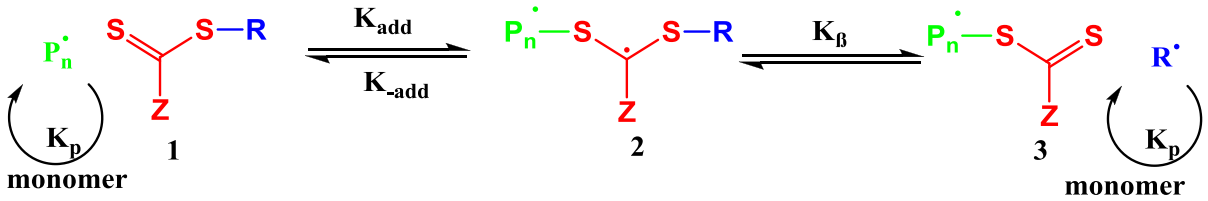

Reinitiation

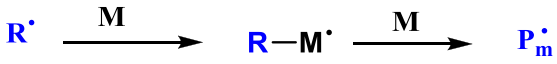

Chain equilibrium

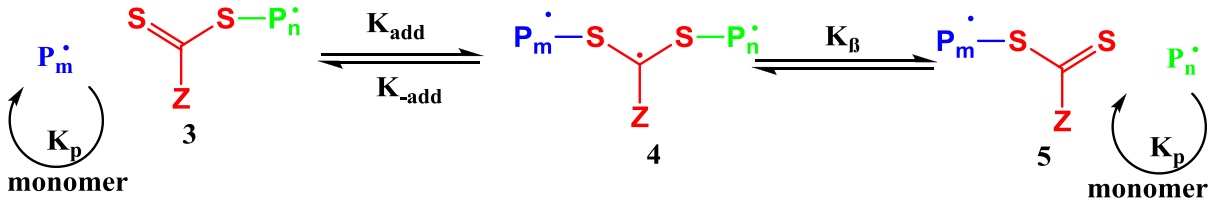

Dead polymer

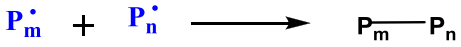

Figure 2.15 Schematic representation of RAFT polymerization using a dithioester.[75]

One of the more versatile RAFT agents is α-Cyanobenzyl dithioester and was used in my experiments (see chapter 3). This RAFT agent satisfies all the criteria mentioned above for functioning as an efficient CTA and has been used previously to make block copolymers [76,77] The polymers prepared by RAFT polymerization can be reactivated for chain extension or for use as precursors to produce block polymer, star polymers or polymers of more complex architectures. However, RAFT polymerization involves free radical intermediates. Thus, some

radical-radical termination, a complication in all forms of living radical polymerizations, cannot be avoided and an amount of dead polymer, determined by the number of chains initiated by initiator-derived radicals, will unfortunately be formed. In order to achieve a high degree of "livingness" in RAFT polymerization, it is clearly desirable to minimize the number of initiator-derived chains. Thus, RAFT polymerization could be used to graft several imprinted layers with different properties. The major benefit of the RAFT process over other forms of living radical polymerization is that the reaction conditions usually employed are typical of those used for conventional free radical polymerization. A possible disadvantage is the production of sulfur containing compounds due to the dithiocarbonyl end groups. But the color and the sulfur in the final products can be easily avoided by hydrolyzing end groups after polymerization with bases or by oxidants. In conclusion, RAFT is arguably the most promising among the CRP methods to employ in MIP systems. For example: our group was the first to report, 2-phenylprop-2-yl dithibenzoate was used as a free CTA in solution to control the film thickness of MIP on azo modified silica surface (see in next section 2.6.2.2.3.1). Latter the advantage of CTA in solution was used for bulk RAFT MIP. Liu *et al*[78] prepared the enrofloxacin imprinted monolithic columns and compared the separation efficiency with FRP MIP. The separation on the RAFT MIP was improved owing to an increased specific surface area and uniform pore size distribution. Pan et al [79] synthesized imprinted a MIP by RAFT precipitation polymerization. They observed a higher capacity, a better binding constant, and an increased density of high affinity sites compared to the FRP MIPs.

2.6 Surface Initiated Polymerization

The ability to control the structure and composition of materials at a nanometer scale is key to a number of advanced functions within diverse areas such as drug delivery, diagnostics and sensing, molecular electronics, catalysis, separations or as mimics of biological systems. Among the most promising approaches and techniques in nanomaterial design are on the one hand grafting and controlled radical polymerization (CRP) and on the other hand templated synthesis and molecular imprinting.[80,81]

Grafting can be performed on the solid surfaces either, chemically (covalent bonding) or physically (physiosorption). A drawback of physisorbed polymer is that they are thermally and solvolytically unstable due to the relatively weak van der waals forces or hydrogen bonding that anchors them to the surface. Covalent grafting techniques are preferred to maximize a stable interfacial compatibility between the two phases. Covalent grafting techniques involve either the "grafting to" or "grafting from" methods (Figure 2.16).[82] In the "grafting to" technique the polymer, bearing an appropriate functional group, reacts with the material surfaces to form chemically attached chains. However, due to the steric hindrance imposed by the already grafted chains it becomes increasingly difficult for the incoming polymer chains to diffuse to the surface which intrinsically results in low surface graft densities.

In the "grafting from" technique the initiators are initially anchored on the surface and then subsequently used to initiate the polymerization of monomer from the surface. Because the diffusion of monomer is not strongly hindered by the existing grafted polymer chains, this technique is more promising to achieve high graft densities. Using the right system and techniques, one can control the functionality, density and thickness of the polymer brushes. Preparation of MIP film on solid surfaces can be accomplished by conventional free radical, controlled free radical (CRP), cationic, anionic and ring-opening metathesis polymerization techniques, but I will focus here on the examples that combine polymer grafting with CRP and molecular imprinting.

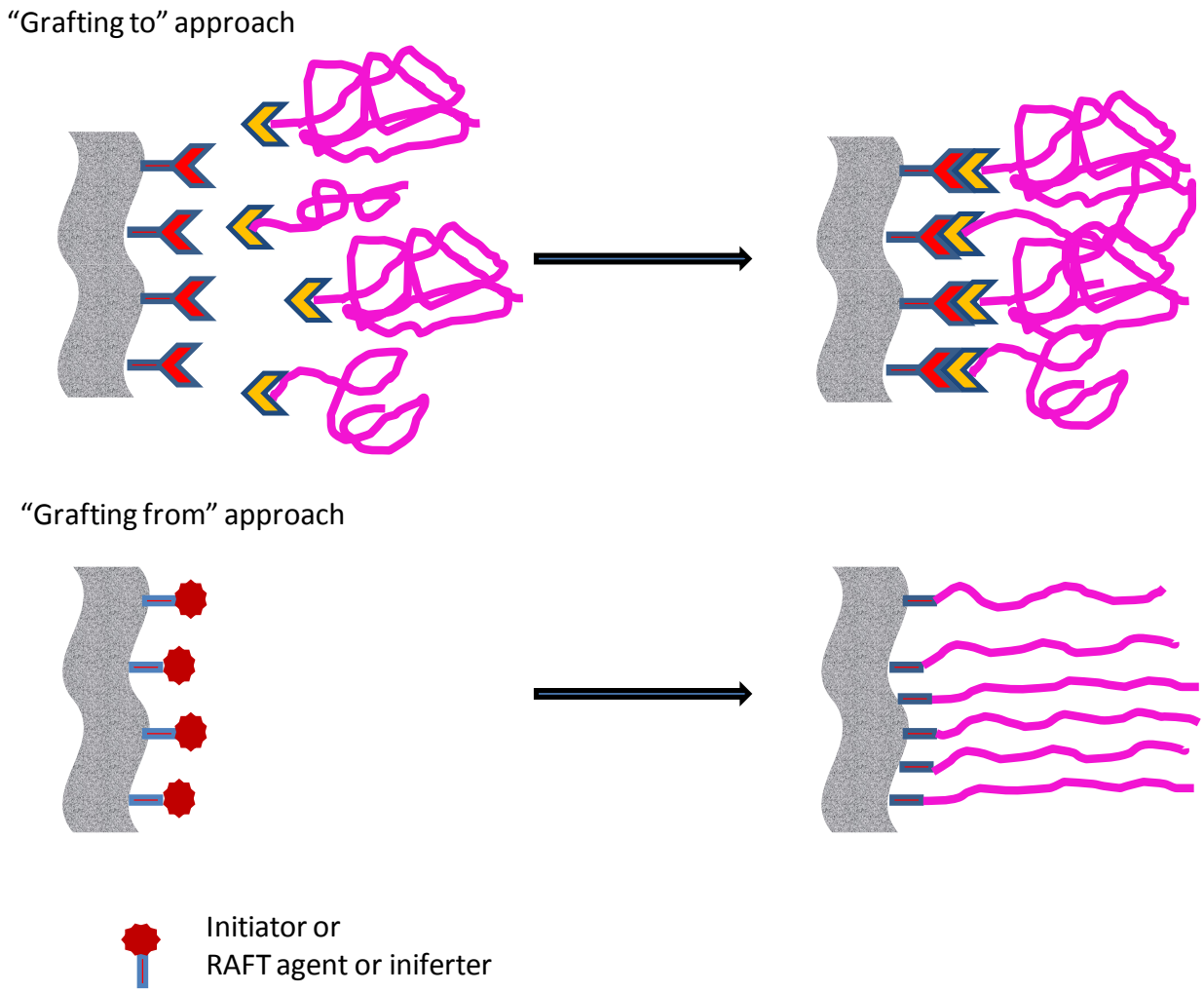

Figure 2.16 Synthetic strategies for the preparation of polymer brushes.

2.6.1 Covalent attachment via "Grafting to Approach"

In the "grafting to" method, pre-formed, end-functionalized polymer chains are reacted with a chemically activated substrate (Figure 2.16). The Mosbach group introduced the grafting to approach in the imprinting field. They prepared MIP film for dye (Safaranine O and rhodanine blue) on the porous silica micropartilces and tested in HPLC as a stationary phase. Interestingly they found silica MIP particles exhibited the same selectivity as bulk monolith particles but could be accomplished rapidly. In this approach the polymerisable acrylate groups were immobilized on porous silica support and coated the MIP film on surface of porous beads using

non covalent imprinting.[83] Further Wulff *et al* also reported the similar grafting approach but in covalent imprinting. The resulting materials were used in enantiomer separation.[84]

Minoura *et al*. reported the protein imprinting using grafting to technique. A polymer layer was grafted around silica beads containing vinyl groups. The layer was composed of acrylamide, acrylic acid and crosslinker using glucose oxidase as a template. The composite was able to recognize glucose oxidase in a mixture of proteins.[85]

One problem with the "grafting to" technique is the presence of initiator in solution requiring the monomer mixture to be applied as a liquid thin film on the surface prior to polymerization. Thus the exact amount of monomers that will coat the available surface with thin liquid film is dissolved together with the initiator in an excesss of solvent. Thereafter the modified support is added and the solvent evaporated to leave the monomer film and initiator on the surface. Polymerization is then usually carried out at elevated temperatures. With this procedure the thickness of the polymer layer is difficult to control and capillary forces upon evaporation of solvent may cause incomplete wetting of the surface. Moreover, the maximum density of grafted polymer chains is here limited due to kinetic and sterical factors. As an alternative, surface initiated polymerization has been employed using a variety of monomers in order to modify the surfaces of solid substrates.

2.6.2 Covalent attachment via 'grafting from approach'

The grafting from approach is the most frequently used technique in solid support modification due to simplicity and versatility. In 'grafting from' technique the initiator is immobilized on the silica surface (Figure 2.16) and polymerized with the monomer to make thick polymer brushes because the monomer can easily diffuse to the reactive sites of the growing polymer chains. In this method, the steric barrier to incoming polymers imposed by the in situ grafted chains does not limit the access of smaller monomer molecules to the active initiation sites. This polymerization technique is also commonly referred to as surface-initiated polymerization. Preparation of polymer brushes via the "grafting from" technique on silica particles can be accomplished by conventional free radical, controlled free radical, cationic, anionic and ring-

opening metathesis polymerization techniques.[86] Here I will discuss more on the combination of SIP with molecular imprinting via FRP and CRP.

2.6.2.1 Surface imprinting via conventional FRP

Conventional free radical polymerization (FRP) is one of the most studied systems. Radical processes are more tolerant of functional groups and impurities and are well suited for polar monomers. It is a leading industrial method to produce polymers.[86] The "grafting from" method has long been used for the preparation of covalently attached polymers by free radical techniques. This approach was first reported by Prucker and Rühe.[87,88] It consisted of grafting an azo initiator onto a particle or flat surface followed by polymerization. A self-assembled monolayer (SAM) of the azo initiator was grafted on the surface of silica and this was used for the radical chain polymerization of styrene.

The group of Sellergren was the first to report on the grafting of thin MIP layers on porous silica particles using immobilized initiators.[89] In the paper of Sulitzky *et al.*[89], an azo-initiator, 4,4´-azo-bis-(4-cyano pentanoic acid) (ACPA), was covalently immobilized on silica particles previously modified with epoxy or amino groups. Alternatively, a diamidine azo-initiator, 2,2´-azo-bis-(N, N´-dimethylene isobutyramidine), (AIDA) was physically adsorbed to similar silica particles.The grafting experiments were then performed using the chiral template L-phenyl alanine anilide (L-PA), EDMA as cross-linker and MAA as functional monomer, with dichloromethane or toluene serving as porogenic solvents.

The resulting materials prepared using covalently immobilized initiators proved to be superior to those prepared using physically adsorbed initiators, where the initiator or the polymer may be displaced by acids or bases competing with the initiator for the surface adsorption sites. The obtained materials were successfully applied as chiral stationary phases in HPLC[89] and CEC.[90] The use of azo initiator immobilized silica to produce molecularly imprinted composites and generate a new type of thin walled imprinted polymers will be described in this thesis.

2.6.2.2 Surface imprinting via CRP

In recent years, surface imprinting via CRP has been developed for preparing MIPs (Table 2.1). This technique grafts a thin film of imprinted polymer on the substrates. Using this strategy, homogeneously grafted thin layers of MIPs with reduced mass-transfer resistance can be created. In addition, desirable formats [e.g., particles, tubes or microchips with different characteristics (size, porosity, pore volume, and surface area)] can be obtained. Many research papers have been published on the preparation of surface-imprinted materials by CRP.[54,91]

2.6.2.2.1 Surface initiated iniferter polymerization

The iniferter method for surface grafting of MIPs has been used for imprinting different templates and for different applications e.g., solid-phase extraction (SPE) and chiral separation. Due to its compatibility to the majority of functional monomers commonly used, and seems to be the method best compatible with photopolymerization. Rückert *et al.* reported the use of an iniferter type initiator, covalently attached to silica particles or to Merrifield resins, for the grafting of thin MIP layers imprinted with D/L-PA for use in chiral chromatography.[92] The morphology and the properties of the materials were optimized by controlling the iniferter grafting density and use of different surface polarities. The composite materials obtained exhibited enantioselectivity in chromatography mode similar to the system based on immobilized azoinitiators. The use of such initiators prevents polymerization in solution, since one of the radicals formed upon decomposition is a very poor initiator. Taking advantage of the living properties of this system two consecutive polymer layers imprinted with two different templates or one imprinted and one non-imprinted layer in any order were grafted.[93]

Table 2.1 Surface-imprinted materials prepared by the controlled/living radical polymerization (CRP) method.

Support	Analyte	CRP method	Application	References
Polystyrene, silica gel	L/D-phenylalanine anilide	Iniferter, RAFT	Chiral separation	[81,92-94]
Silica gel	Propazine	Iniferter	HPLC	[95,96]
Polystyrene/DVB, MAA/EDMA	Propranolol	Iniferter	Radioligand binding assay	[97]
Chloromethylated polydivinyl benzene	Pyrimethanil	Iniferter	HPLC	[96]
Chloromethylated polystyrene	D-mandelic acid	Iniferter	Chiral separation	[98]
Poly(styrene-co-divinylbenzene)	(_)-Ephedrine	Iniferter	SPE	[99]
Chloromethylated polystyrene	Pyrimethanil	Iniferter	SPE	[100]
Silica gel	Sulfamethazine	Iniferter	SPE	[101]
Chloromethylated polystyrene	Lysozyme	Iniferter	HPLC	[102]
Poly(DVB-80), silica gel	Thiabendazole	Iniferter	SPE	[103]
Silica gel	Tributyltin	Iniferter	HPLC	[104]
Silica gel	Sulfonamides	Iniferter	HPLC	[105]
Silica gel	Boc-L-Trp, Boc-D-Trp	ATRP	Chiral separation	[106]
Gold	*N*,*N'*-didansyl-L-cystine *N*,*N*'-didansyl-L-lysine	ATRP	Detection of fluorescent labeled compound	[107]
Fe3O4	Lysozyme	ATRP	SPE	[108]
Carbon nanotube	Theophylline	ATRP		[109]
4vinylpyridine and ethylene glycol dimethacrylate beads	Propranolol, 2,4 dichlorophenoxy acetic acid	RAFT	Stimuli-responsive, water compatible MIPs	[110-113]
Silica gel	Theophylline	RAFT	HPLC	[114]
Silica gel	2,4 Dichlorophenol	RAFT	SPE	[115]
Silicon fiber	Sudan dyes	RAFT	SPE	[116]
Silica gel	Atrazine	RAFT	separation	[117]

Pérez-Moral and Mayes[97] used a dithiocarbamate iniferter to synthesize multilayer molecularly imprinted core-shell particles. Polystyrene nanoparticles obtained by emulsion polymerization were modified with the iniferter, and multiple shells of polymer were then sequentially added by UV-initiated polymerization in an organic solvent. The imprinted sites created in the first shell for propranolol, an ethylene glycol dimethacrylate– methacrylic acid copolymer of around 20 nm thickness, were still accessible and maintained their ability to bind the target specifically even after two more layers of approximate 20 nm each were added. Whereas the above examples demonstrate the usefulness of the iniferter based CRP for modifying solid support materials with thin MIP films by surface initiated polymerization.

2.6.2.2.2 Surface initiated ATRP

With ATRP, the major limitation for this technique in the context of MIP synthesis is the small choice of monomers with suitable functional groups. Typical monomers used for molecular imprinting such as methacrylic acid and trifluoromethyl acrylic acid are incompatible, and with methacrylamide and vinylpyridine, it is difficult to achieve high monomer conversion with the metal–ligand complex involved in ATRP. Template molecules also often carry functional groups that may inhibit the catalyst. Thus, the difficulty of obtaining high conversion in the presence of certain functional groups on monomer and template seems to make ATRP not the best choice for molecular imprinting.[54] However ATRP has also been used for the preparation of surface mprinted materials. Wei et al. used ATRP to functionalize silica gel with Boc-L-tryptophan/Boc-D-tryptophan (Boc-L-Trp/Boc-D-Trp)-imprinted polymer films (MIP-SG).[106] Compared with MIPs prepared by conventional bulk synthesis, MIP-SG had improved mass-transfer properties. An HPLC column packed with MIP-SG showed higher column efficiency and better resolution for enantiomers than that with MIP prepared using bulk polymerization. The same group also describes the use of surface-confined ATRP to create imprinted polymer films with controlled thickness on a gold substrate, using 2-vinylpyridine as the functional monomer, ethylene glycol dimethacrylate as the cross-linker, and the fluorescent template didansyl-l-lysine. A linear increase in thickness was observed over time, and 15-nm-thick polymer films were obtained in 20 h at room temperature. When the adsorption properties of these films were studied using fluorescence measurements,[107] an imprinting effect was observed, as the adsorption capacity and

the association constant of the didansyl-l-lysine template on the MIP film were approximately two times higher than those measured with the non-imprinted control polymer film. In addition, another amino acid derivative, didansyl-l-cystine, adsorbed less well to the didansyl-l-lysine-MIP compared with the original template.[107]

2.6.2.2.3 Surface initiated RAFT polymerization

Surface initiated RAFT polymerization has been widely explored as an approach to modify the material surface due to its ability to precisely control the structure of the grafted polymer chains with a low-to high range of grafting densities. In this approach there are two general routes to prepare surface grafted polymer chains.[118]

1. Surface anchored initiator with free CTA in solution
2. A surface anchored CTA with appropriate initiation method.

In both cases the polymer chains are able to grow from the surface of materials rather than diffuse to the surface against the concentration gradient of existing grafted polymers. Thus compared to the grafting to approach surface initiated RAFT polymerization is more promising approach to construct dense and thick polymer layers on the surface of materials.

2.6.2.2.3.1 Surface anchored initiator with free CTA in solution

The immobilization of initiators on the material surfaces can be achieved by various techniques, including chemical reaction, plasma discharge and high energy irradiation. The subsequent polymerization from these surface anchored initiators in the presence of free CTA can generate surface grafted polymer chains with uniform structure and adjustable length.

In the systems described so far in literature, azo compounds were mostly used as initiators for grafting using RAFT polymerization of various monomers.

Baum and Brittain,[119] synthesized the graft styrene, methaylmethacrylate, N N dimethylcryalamide and their copolymers from silica substrates using surface anchored azo initiator with free CTA in solution. A silane coupling agent was used to immobilize the azo initiator on the silicate surface. 2-phenylprop-2-yl dithibenzoate was used as a free CTA in solution to control the graft polymerization. The author observed that polymer film thickness was

increased with sequential addition of monomer, indicating the living characteristics of the grafted polymer chains prepared by SIP RAFT approach.

Based on this approach Titirici and Sellergren were first to introduce the surface grafted thinfilm MIP composite using RAFT polymerization from surface anchored azo initiator.[94]

In the reaction, MAA as monomer, EDMA as crosslinker and 2-phenylprop-2-yl-dithiobenzoate as the chain-transfer agent were used for imprinting L-phenylalanine aniline (Figure 2.17). The particles prepared via RAFT-mediated grafting appeared smooth with no agglomeration. The resulting materials could separate a racemate of phenylalanine anilide and some structural analogous within a few minutes. The materials exhibited superior mass transfer properties compared to the traditional imprinted bulk monoliths or materials prepared without the polymerization control through RAFT agents.

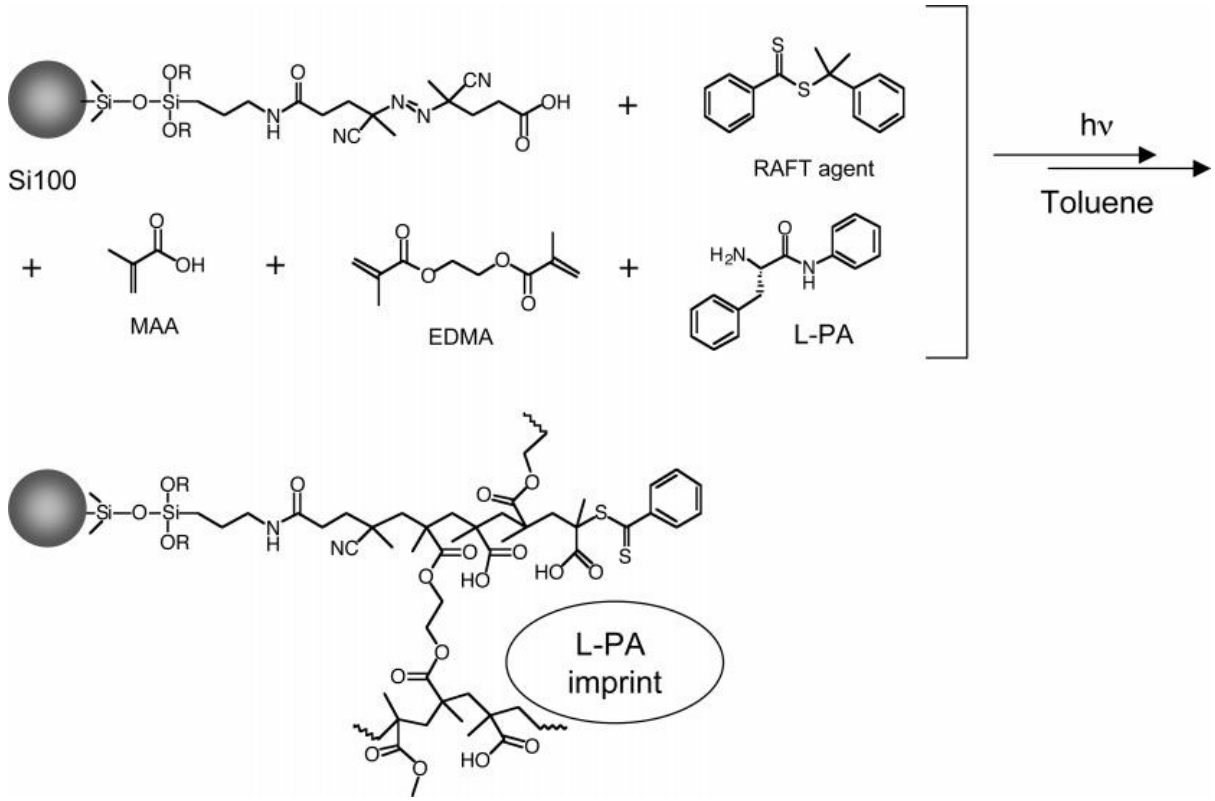

Figure 2.17 The grafting of L-phenylalanine anilide (L-PA) imprinted polymer films from porous silica supports controlled by addition of RAFT agent.[94]

2.6.2.2.3.2Grafting from surface anchored CTAs

An alternative way to modify the surface of materials via surface initiated RAFT polymerization is grafting from surface anchored CTA, which generally can be accomplished through either the R-group or Z-group approach.[118]

In the R-group approach (Figure 2.18), the RAFT agent is attached to the substrate surface via its leaving and reinitiating R group. The solid substrate acts as part of the leaving R group and thus the propagating radicals are located on the terminal end of the surface grafted polymer, which facilitates the growth of grafted polymer chains. This approach resembles a grafting from approach.

The Z-group approach (Figure 2.18) resembles a "grafting to" approach because the RAFT agent is attached to the surface via its stabilizing Z group. The polymeric radicals always propagate in solution before they attach to the surface of substrate via the chain transfer reactions with attached RAFT agents.

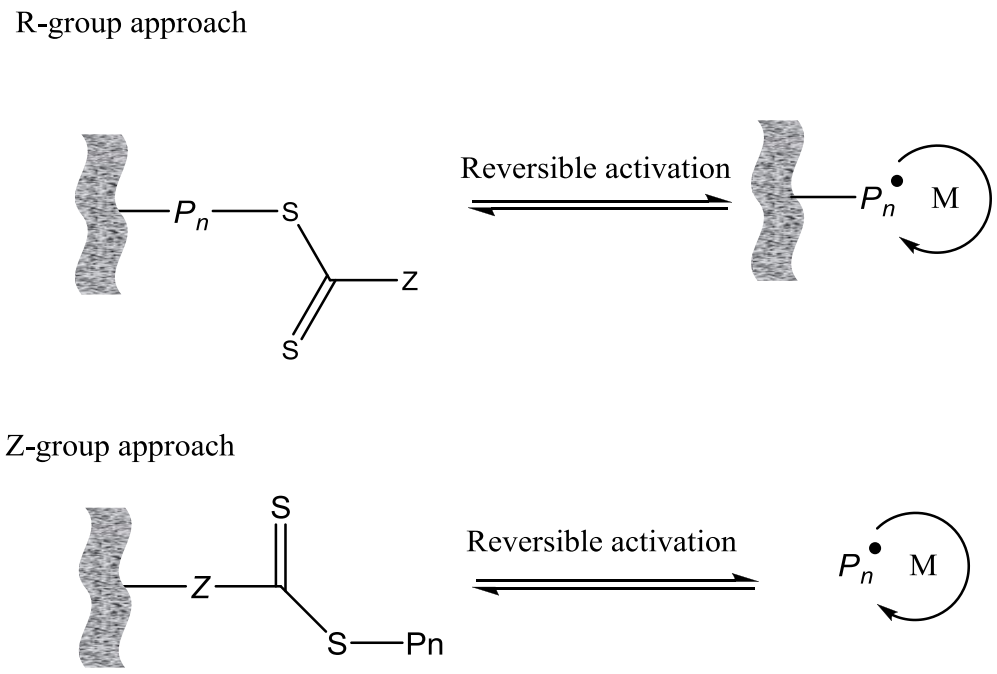

Figure 2.18 R-group and Z-group approaches for Surface-initiated RAFT polymerizations.

Here I will mainly focus on the R group approach with MIPs which is one part of my thesis work.

Fukuda and co-workers[120,121] reported the first application of surface-initiated RAFT polymerization in the modification of silica particles via an R-group approach. An ATRP macroinitiator was first prepared on the surface of silica particles, which was subsequently converted to a terminal RAFT moiety by reacting with 1-phenylethyl dithiobenzoate in the presence of CuBr via an atomtransfer addition (ATA) reaction. The conversion of this reaction was estimated to be 70% by UV–vis absorption spectroscopy. The surface-initiated RAFT polymerization of Styrene from the immobilized RAFT moiety was carried out at 110 oC with a free RAFT agent in solution. The addition of the free RAFT agent in solution could not only control the free polymerization in the bulk phase but also keep the graft polymerization under control at high conversions. Rowe-Konopacki and Boyes[122] used a similar strategy to prepare a series of diblock copolymer brushes, including PMMA-*b*-PDMAEMA, PMMA-*b*-PS and PS-*b*-PMMA on the surface of flat silicon substrates.

Although well-defined polymer brushes were successfully prepared on the surface of silicate substrates in the above studies, large amounts of free polymer were also produced in the final products due to the free RAFT agents required in the polymerization, which required laborious purification steps. To overcome this problem, Benicewicz et al. [123], reported a more versatile RAFT agent containing a 4-cyanopentanoic acid dithiobenzoate (CPDB) moiety, which was immobilized on the surface of silica nanoparticles and used to prepare both PS- and PMMA-grafted silica nanoparticles. Amino-group-functionalized silica nanoparticles were first prepared by reacting 3-aminopropyldimethylethoxysilane with silica particles. An initial attempt of directly reacting CPDB with amino-group-functionalized silica nanoparticles via condensation failed due to the aminolysis of the dithiobenzoate group of CPDB. Therefore, the carboxyl group of CPDB was first activated by reacting with 2-mercaptothiazoline. Due to the ability of mercaptothiazolineactivated amide bond to selectively consume the amino groups in the presence of dithiobenzoate groups, the subsequent reaction of activated CPDB with amino-group-functionalized silica nanoparticles successfully produced CPDB anchored silica nanoparticles with variable graft density. Surface-initiated RAFT polymerizations of methyl methacrylate (MMA) and styrene (St) were mediated by CPDB-anchored silica nanoparticles without the addition of free CTA in solution, producing surface-grafted polymers with narrow polydispersities and predictable molecular weights.

Based on this approach I immobilized the CPDB RAFT agent on porous silica particles by ethyl chloroformate catalyzed coupling of 4-cyanopentanoic acid dithiobenzoate (CPDB) to amino modified silica. This RAFT modified silica support was used for preparation of L-PA imprinted thinfilm MIP composites in presence of MAA and EDMA. The use of CPDB immobilized silica to produce molecularly imprinted composites. Taking the advantage of leaving end groups I grafted the layer by layer thinfilm MIPs and generated a new type of thin walled gel-like imprinted polymers that will be described throughout this thesis.

Li etal[114] also synthesized the theophylline imprinted composites using RAFT modified silica support. The authors observed that measured binding kinetics for theophylline to the MIP-silica and MIPs prepared by conventional bulk polymerization demonstrated that MIP silica had improved mass transfer properties. In addition the theophylline imprinted silica was used as the sorbent in SPE to determine theophylline in blood serum with satisfactory recovery higher than 90%.

Zhang and co-workers[79,110-113] synthesized a narrowly dispersed MIP by RAFT precipitation polymerization. They observed a higher capacity, a better binding constant, and an increased density of high affinity sites compared to FRP MIP. The same group recently reported multiple stimuli-responsive template binding MIPs by surface initiated RAFT polymerization.[111,112] First they prepared the living core particles by RAFT precipitation polymerization latter they polymerize the hydrophilic monomers such as HEMA, NIPAM, DMAEMA etc to form hydrophilic brushes and hydrogels for improved water compatibility.[111,113] Others have used the living character of RAFT in order to change the surface properties of MIP spheres.

Polymeric membranes with molecular imprint functionality have been also prepared using the "Grafting from" methodology. These materials are very attractive for efficient separations, including SPE. Kobayashi et al first time grafted theophylline MIPs on polyacrylonitrile membrane using living radical polymerization. It was found that MIPs on the surface can recognize with high efficiency the template theophylline, while the analogue caffeine could not be effectively recognised by the imprinted sites.[124]

Ulbricht et al explored the concept of heterogeneous photografting from membranes.[125-127] Here, polymer membranes are coated with a photoinitiator, for example benzophenone, which after selective UV excitation *via* a hydrogen abstraction reaction creates radicals on the membrane polymer surface. These radicals can be used as starters of a graft copolymerization of functional

monomers from the surface and thus creating a thin layer of covalently attached functional polymer covering the entire specific surface of the membrane.

Grafting methodologies allow the preparation of thin films of imprinted polymers on various support materials.[81,89,90,92-94] Since the morphology of the resulting composite materials is determined by the underlying support, this gives fast and facile access to monodisperse, spherical imprinted beads with immediate application in separation science. Furthermore, MIP grafting has the benefit of allowing the MIP films to be prepared using a variety of solvents and functional monomers, thus disregarding the effect of these parameters on polymer structure and morphology or the ability of these systems to yield stable suspensions. This allows the focus of the attention to be mainly on the search for conditions that result in high quality binding sites. The technique can be applied to different templates and exhibit distinct advantages over the conventional monolith procedure.

2.7 Template synthesis of materials

The templating is an attractive technique at molecular level to generate nano scale materials with tailored properties.[128,129] Mostly template synthesis is divided in to two methods one is endo template and another one is exo template. In endo template; the isolated template used as a single component and polymerization takes place around the template molecule afterwards removing the templates it forms nano porous polymer beads. In exo template; the template itself acts as a porous then polymerization is takes place inside the pores and it forms composites as endo template composites. The porous polymer can be obtained after removing the templates (Figure 2.19 and Figure 2.16).

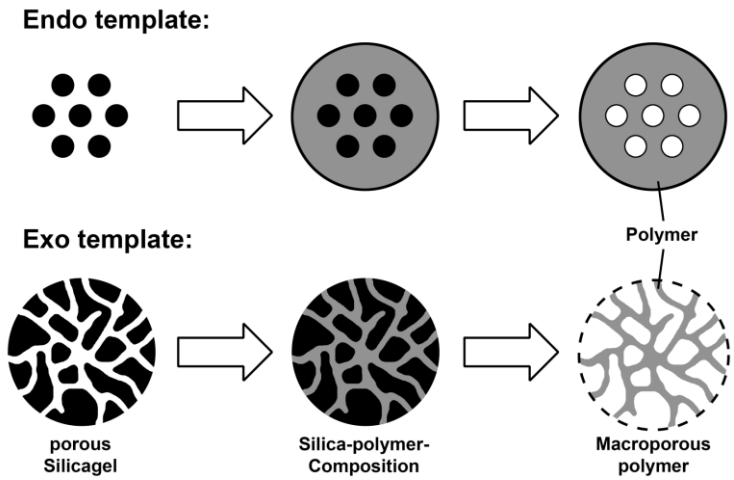

Figure 2.19 Templated synthesis material by endo and exo-templating. Adapated from ref.[129]

Both approaches have been used in this thesis for generating the porous materials with tailor made properties. The exo- template approach which is also called as *hierarchical imprinting.*[130-132] Especially in this thesis I used combination of surface initiated polymerization, controlled radical polymerization and exo-templating to generate thin walled beads. Which is one of the novel approaches to address the classical deficiencies of MIPs.

.

3 Investigation of influence of RAFT agent on the performance of LPA imprinted polymers

3.1 Introduction

MIPs are normally prepared by free radical polymerization mechanism because it is compatible with the wide range of functional monomers, porogens and template molecules as well as mild reaction conditions.[1] Free radical polymerization process was classified in three steps initiation, propagation and termination, (See in section 2.3).[24] In free radical polymerization it is difficult to control molecular architectures with regard to chain propagation and termination, which results in polymer networks with heterogeneous structures.[133] Due to the presence of heterogeneity within the network structures of the MIPs could have significant impact on the binding affinity, selectivity, and poor site accessibility. Therefore Controlled radical polymerization (CRP) has been demonstrated here to improve their properties in this regard. Free radical polymerization technique produce a heterogeneous network due to the monomer propagation is so quick that it gives no time to the polymer chain to relax so crosslink's will be formed mostly within the same molecule. As the polymerization reaction proceeds and the conversion increases, so the termination between two polymer chains is difficult due to diffusional limitations.[134] In contrast, CRP are thermodynamically controlled process with negligible chain termination and a more constant and much slower rate for the polymer chain growth, which results controlled molecular architectures, low polydispersity, predetermined molecular weight and homogenous network structures.[62-64,74,134] Several CRP techniques developed for making a homogenous polymer networks such as ATRP[69], RAFT[75], NMP[60], Iniferter chain polymerizatiton.[56,134]

Among the all CRP techniques RAFT polymerization is one of the most versatile systems because of its compatibility to the wide range of monomers and mild reaction condition. RAFT process involves reversible addition fragmentation sequences in which the transfer of a dithioester moiety between active and dormant chains serves to maintain the living character of the polymerization. Initiation of polymerization is by a classical free radical polymerization. In the early stages of the polymerization, addition of propagating radical to the CTA followed by fragmentation of the intermediate radical provides a macro-CTA and a new radical. Reaction of this new radical with new monomer forms a new propagating radical. There is a dynamic

equilibrium between the active propagating radical and the dormant macro-CTA provides equal probability of the all chains to grow and allows forming a narrow polydispersity polymers. Mostly the group of Sellergren is involved in making new formats of MIPs using surface initiated Iniferter and/or RAFT polymerization techniques.[80,81,92-95,135] So far, RAFT polymerization has shown great potential in preparing MIPs with superior mass transfer properties than the free radical polymerization.[94] However others also prepared the MIPs on solid surface using Iniferter[98,100], ATRP[106,107] and RAFT.[136] Only a few reports are available where CRP is used in preparation of MIPs in free radical polymerization techniques.[51,54,72,137-141] In this work the implication of controlling structural homogeneity and its influences associated binding parameters of a well known MIP system poly(MAA-Co-EDMA) for L-phenylalanine anilide and studied the double bond conversion, initiator to CTA ratio while keeping the other parameter constant.(Figure 3.1).

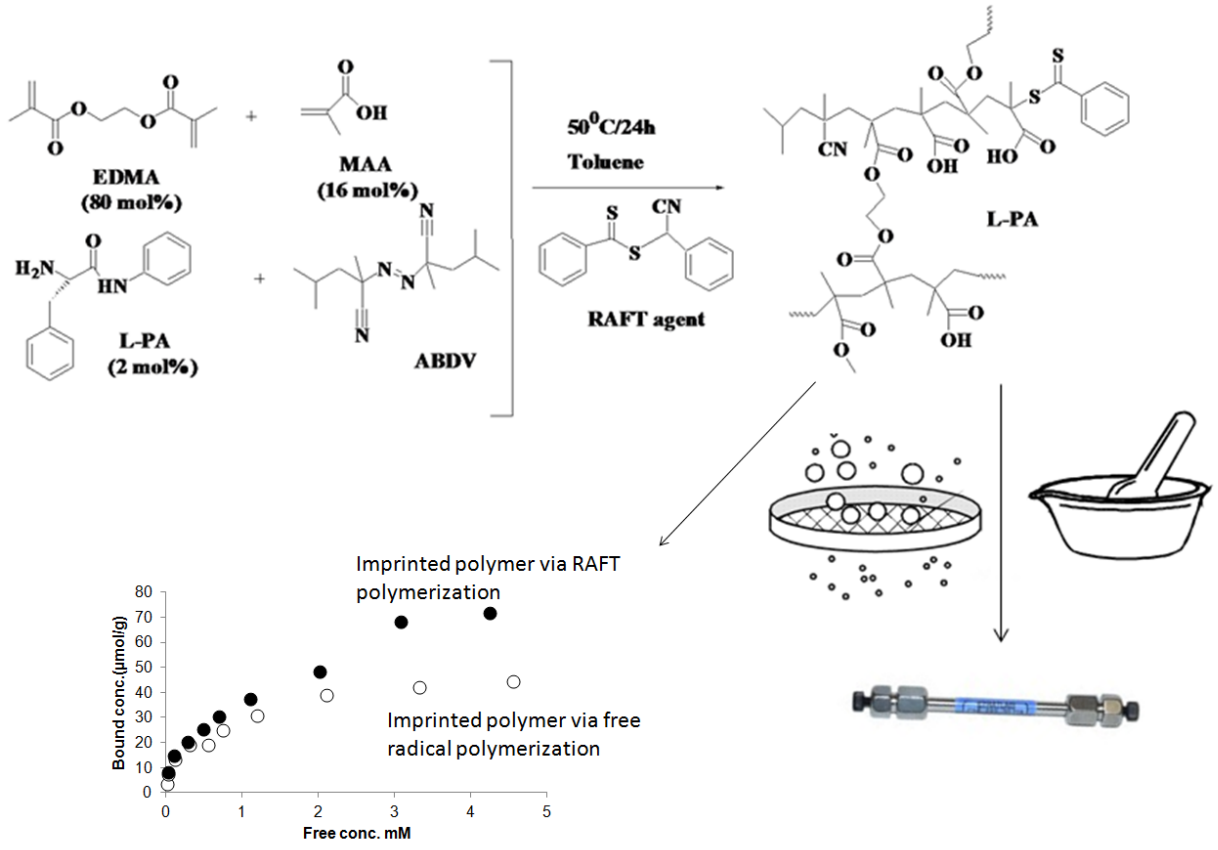

Figure 3.1 Preparation of L-PA imprinted polymer using RAFT polymerization.

3.2 Results and discussion (I):

The work presented here focuses on the preparation of L-PA imprinted polymers using controlled radical method RAFT. The aim of the RAFT technique is to produce homogenous network, narrow pore size distribution, and to improve the binding properties of MIPs. MAA and EDMA were chosen as functional monomer and corsslinker because during the polymerization template molecule and acrylic monomers are supposed to interact by formation of ion pairs between the positively charged amino groups of template molecules and negatively charged acrylic acid monomers (see in Figure 2.3 for the model binding sites for L-PA in polymer). The odor less RAFT agent α-Cyanobenzyl Dithibenzoate was synthesized according to literature protocol.[76] A well-known L-PA imprinted polymers were prepared as described elsewhere. A mixture of template molecule, monomer, crosslinkers and initiators in an inert organic solvent was allowed to polymerize in a sealed glass tube at 50 ^{o}C for 24h. After polymerization the template molecule can be removed by mild extraction of polymers with MeOH/formaic acid/water (v/v/v, 80/15/5) and finally with pure MeOH. The polymers obtained are presumed to have specific cavities, formed by the print molecules which contain carboxyl groups that can interact selectively with re-added substrate (Figure 3.1). In order to enhance the performance of resultant MIPs, different amount of CTA in the polymer was investigated (Table 3.1). The conditions under which a RAFT polymerization is performed may also have an effect on the characteristics of the final imprinted polymers. The rate of polymerization and control over the pore size distribution or molecular weight distribution (MWD), polydispersity index and morphology of the resultant polymer can be affected by the conditions of the reaction. For these reasons, the initiator concentration is chosen so that a balance is achieved between the rate of polymerization and control over molecular weight distribution.

In the current imprinting system, the major synthetic conditions were studied including the ratio of RAFT/ABDV and the prepolymerization complex by DSC. The polymer was analysed by FTIR, Elemental analysis, nitrogen adsorption and Scanning electron microscopy. The pore size analysis in wet condition was measured by Inverse size exclusion chromatography (ISEC) and thermoporometry technique. Finally polymers were tested as stationary phases in liquid chromatography and static binding test.

Table 3.1Polymer feed composition and Pore analysis parameters for the Imprinted and non imprinted polymers measured by BET and Thermoporometry (value in bracket)

Polymer Code	MAA:EDMA:LPA:ABDV:RAFT Mol (%)	Elemental analysis			Pore diameter nm	Pore volume cc/g	Surface area m^2/g
		%C	%N	%S			
MIPA	16 : 80 : 2 : 1 : 0	58.3	0.23		23.5(33)	0.69(0.83)	358(100)
MIPB	16 : 80 : 2 : 1 : 0.25	58.5	0.19	0.01	18.8(18.1)	0.8(0.71)	389(155)
MIPC	16 : 80 : 2 : 1 : 0.5	58.8	0.21	0.01	13.3(14.3)	0.76(0.86)	399(232)
MIPD	16 : 80 : 2 : 1 : 1	58.7	0.25	0.01	6.1(12.7)	0.43(0.69)	321(231)
MIPE	16 : 80 : 2 : 1 : 2	59.1	0.27	0.19	3.7(10.1)	0.36(0.52)	323(204)
MIPF	16 : 80 : 2 : 1 : 4	59.3	0.39	0.43	3.5(8.5)	0.23(0.55)	264(259)
NIPA	16 : 80 : 0 : 1 : 0	57.8	0.52		32.1	0.666	356
NIPB	16 : 80 : 0 : 1 : 0.25	57.9	0.44	0.01	23.7	0.821	386
NIPC	16 : 80 : 0 : 1 : 0.5	58.1	0.19	0.01	15.6	0.764	381
NIPD	16 : 80 : 0 : 1 : 1	58.7	0.22	0.03	7.6	0.509	354
NIPE	16 : 80 : 0 : 1 : 2	58.8	0.27	0.17	4.4	0.34	318
NIPF	16 : 80 : 0 : 1 : 4	59.1	0.41	0.43	3.729	0.199	274

3.2.1 Polymerization onset: Effect of the CTA to initiator ratio

RAFT polymerization is one of the leading research areas for the production of polymers with narrow molecular weight distributions and controlled polymeric architecture, the kinetics of the RAFT are still not fully understood in MIP. This is most apparent in the investigation of dithiobenzoate mediated RAFT polymerization where anomalous behaviour such as inhibition periods and rate retardation is commonly observed in linear polymers [142] However Titirici and

Sellergren studied the effect of RAFT on surface initiated polymerization. [94] They have shown that RAFT mediated MIP have high enantioselectivity and improved binding properties compared to conventional mediated MIP. For further continuation of this study the present work focused on the effect of RAFT in conventional mediated MIPs.

From Figure 3.2, shows that the RAFT effect on the polymerization onset displayed an increasing the onset temperature of polymerization(85 ^{o}C - 116 ^{o}C)and narrows the DSC curve with increasing the ratio RAFT /ABDV ratio (0, 0.25, 0.5, 1, 2), suggest that polymerization is delayed and chain transfer and radical termination reaction is suppressed. The higher ratio of RAFT/ABDV (4) display a higher polymerization onset temperature (116 ^{o}C) but broad DSC curve,(possibly broader molecular weight distribution) indicates that inhibition or termination reaction could be occurred due to more slower generation of radicals. The conventional polymer displays lower polymerization onset temperature and broad DSC curve compared to corresponding RAFT polymer (Figure 3.2) due to the presence of chain transfer and radical termination reaction. The same trend was observed for non imprinted polymers. The concentration of the radicals in the system will influence the rate of polymerization and the molecular weight distribution of the polymer. A higher concentration of radicals will increase the rate of polymerization but often yield a broad molecular weight distribution because of a higher probability of termination reactions occurring. For these reasons the initiator concentration is crucial in controlled radical polymerization.

A B

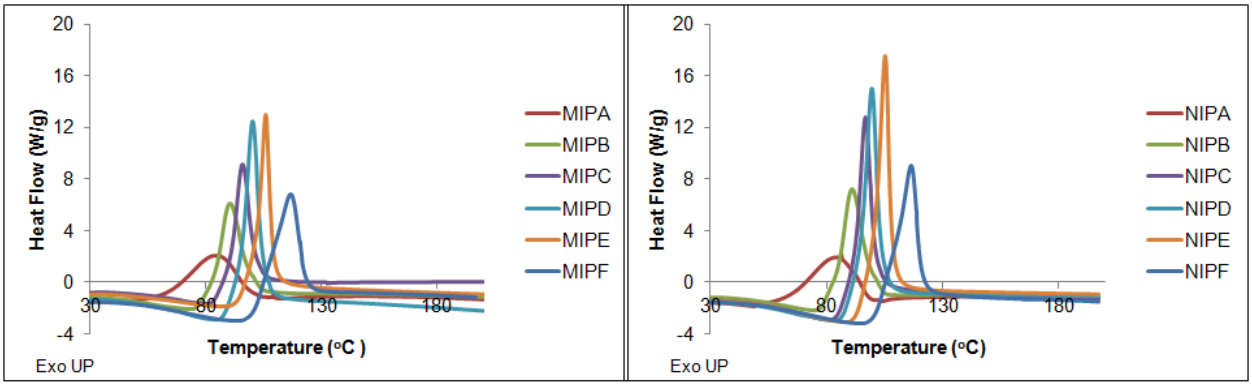

Figure 3.2 DSC dynamic scanning curves for prepolymerization mixtures of imprinted (A) and non imprinted (B) polymers at heating rate 10 ^{o}C/min.

3.2.2 Double bond conversion:

Dynamic and Isothermal scanning DSC method was used to study the influence of RAFT agent, and temperature on double bond conversion of poly(MAA-co-EDMA) prepolymerization complex. In dynamic DSC study, prepolymerization mixture of MIP and corresponding NIP was heated at heating rate 10 ^{o}C/min until 200 ^{o}C and measured the enthalpy of the reaction (Figure 3.2). Based on enthalpy the double bond conversion was calculated using X2 equation (see in experimental section). Analyses of reaction conversions versus RAFT concentration clearly indicates that an increase the RAFT concentration, while keeping the concentration of monomer constant, leads to an increase in the vinyl double bond conversion. The most significant increase in double bond conversion occurs between the systems of 0 to 1.6 wt% of RAFT (double bond conversion 45 to 60% for imprinted polymers and 47 to 70% for nonimprinted polymers), further increase in RAFT concentration displays less significant effect on double bond conversion (Figure 3.3).This suggest that the reduced or slower polymerization rate will not increase the monomer conversion The optimum concentration of RAFT displays higher double bonds conversion This can be explained as, an increase in RAFT agent concentration while keeping the concentration of the monomers constant leads to a decrease in the rate of polymerization (retardation effect) and longer induction period (the initiatlization effect). The PDI is expected to be lowered, as more CTA means a higher probability for degenerative chain transfer events. Reactions that yield low molecular weight polymers are therefore, slower than reactions that yield longer chains.[142]

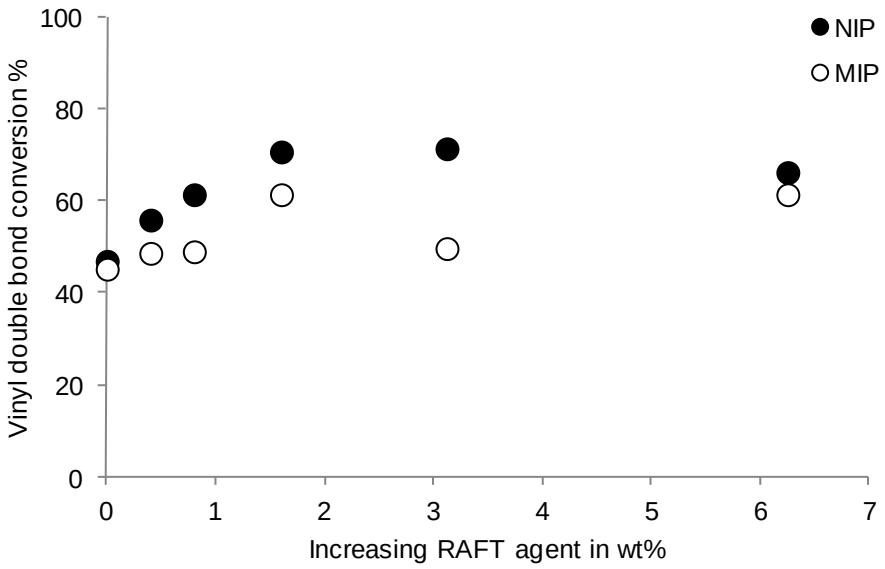

Figure 3.3 vinyl double bond conversion of poly (MAA-co-EGDMA) recognitive netwroks: RAFT agent wt% effect upon the double bond conversion.

For isothermal DSC scanning study was conducted for MIPA and MIPD by using a differential scanning colorimetry, temperature could be kept constant within ±1 ^{o}C during the course of the polymerization reaction. The temperature of reaction was set a 50 ^{o}C, 60 ^{o}C and 70 ^{o}C which resulted in enthalpy 88.5 J/g(30%), 123 J/g(42%), 118.1 J/g(41%) for conventional imprinted polymer (MIPA) and 113 J/g(40%), 127 J/g(44%), 100.5 J/g(35%) for RAFT polymer (MIPD) respectively (Figure 3.4 and Figure 3.5). This final double bond conversion for our imprinted system was calculated using X1 equation (See in experimental section).

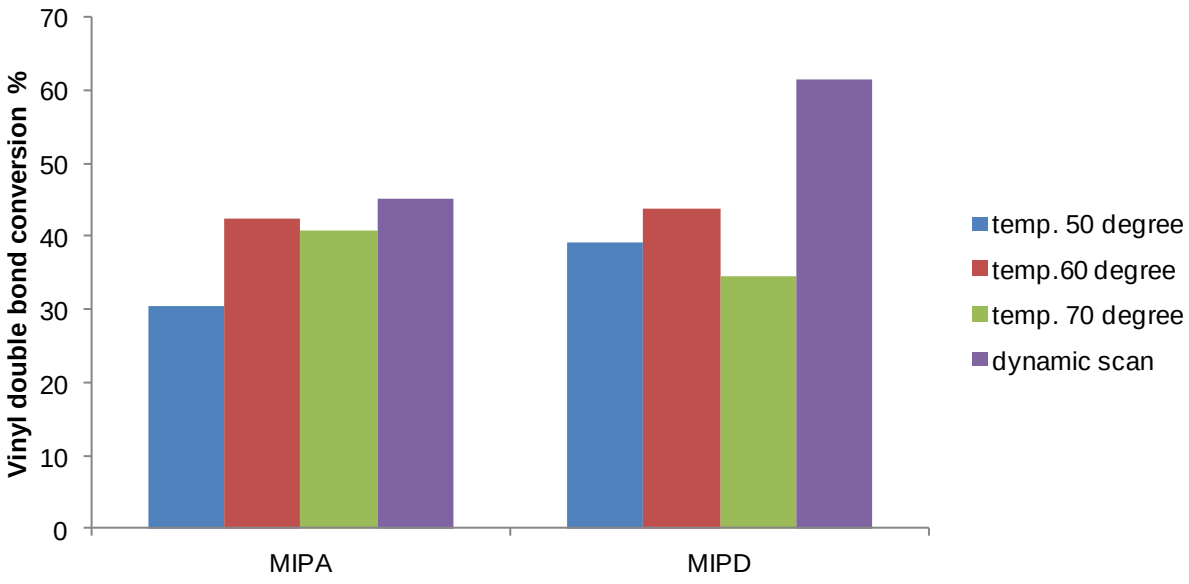

Figure 3.4 Temperature influence on vinyl double bond conversion of poly(MAA-co-EDMA) recognitive network templated for L-PA.

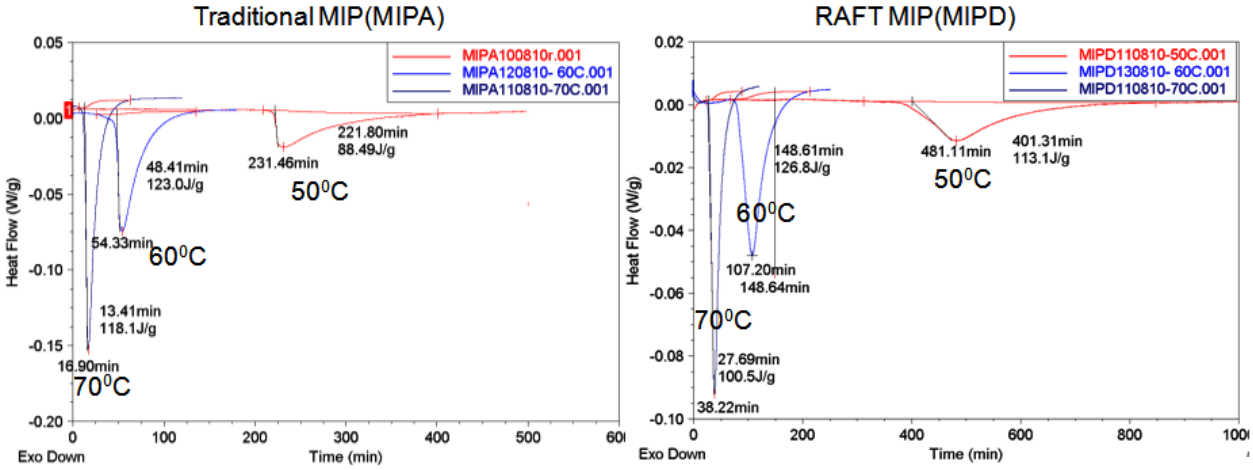

Figure 3.5 Isothermal DSC scanning curves at three different temperatures for traditional MIP (MIPA) and RAFTMIP (MIPD).

Figure 3.5 shows the Isothermal DSC curves at three different temperatures as 50, 60 and 70 ^{o}C of imprinted polymers via traditional method and CRP method. RAFT polymerization rate is two times slower than conventional free radical polymerization method. For example at 50 ^{o}C the traditional polymerization is finished at 232 minutes and a resulted 88.5 J/g enthalpy but the RAFT polymerization is finished at 481 minutes and resulted a 113 J/g enthalpy. The same trend was observed for 60 ^{o}C. At 70 ^{o}C both polymer displayed less amount of double bond conversion

compared to lower temperatures due to the generation of high radical concentration and faster polymerization rate. This led to uncontrolled polymerization reaction kinetics. In theory, the faster polymerizations rate higher the monomer conversion, but this is not the case. RAFT polymers have higher enthalpy compared to conventional polymers means RAFT polymers have higher amount of double bond conversion. Conventional polymer yield lower conversion because there is a decrease in the diffusional ability of pendent double bonds in the growing polymeric network to react or limited diffusion of radicals on the growing network.[51,72] This can be explained as propagation step in free radical polymerization is only controlled by the reactivity of radicals. As the reaction proceeds, the concentration of free monomer around propagating radicals in polymerization system decreases so the reaction is controlled by the diffusion of the free monomer and the propagating radicals. Thus, the concentration of free radicals is increases with respect to time so it results as radical radical termination reaction and finally end up with heterogeneous structures. In contrast, RAFT system is controlled by addition of the chain transfer agent to macroradicals and forms the dormant species. This process allows to forms a thermodynamically favourable network since it decreases the propagation rate and allows a more time to the growing radical to diffuse into the diffusion controlled phase. So the RAFT leads to a delayed transition from the reaction controlled phase to diffusion controlled phase. The extended propagation step in RAFT would result in polymer networks with fewer imperfections in the polymer network, such as pendant double bonds and, primary and secondary cycles, allowing for higher overall crosslinking, and more homogenous structure.[52,53,143]

For more evidence on the double bond conversion I decided to run the crude polymer DSC after the polymerization. The effect of RAFT content on crude polymer DSC is presented in Figure 3.6 and Table 3.2, before soxhlet and after soxhlet. In general two endothermic peaks could be observed for all samples in the first run. A second run performed directly after first run showed only a flat line indicating that the polymer is fully polymerised. The first endothermic peak (101-115 ^{o}C) can be assigned with double bonds which are more freely available where as the more isolated double bonds react at higher temperatures indicated by the second endothermic peak (155-173 ^{o}C).[144] In this system only one endothermic peak exhibits at 70-80 ^{o}C for all polymers (Figure 3.6) which could belongs to the freely available double bonds in the networks. Conventional polymer MIPA has showed higher amount of unreacted double bonds (9.5%) compared to RAFT polymer MIPF (4.5%). The obtained value for MIPA is comparable to

reported value. In the literature for the same system poly(MAA-co-EDMA) conventional imprinted polymers reported 17% final unreacted double bonds determined by ^{13}C CP-MAS NMR.[145] It suggests that RAFT polymer has higher conversion compared to conventional polymers (Vide supra).

A B

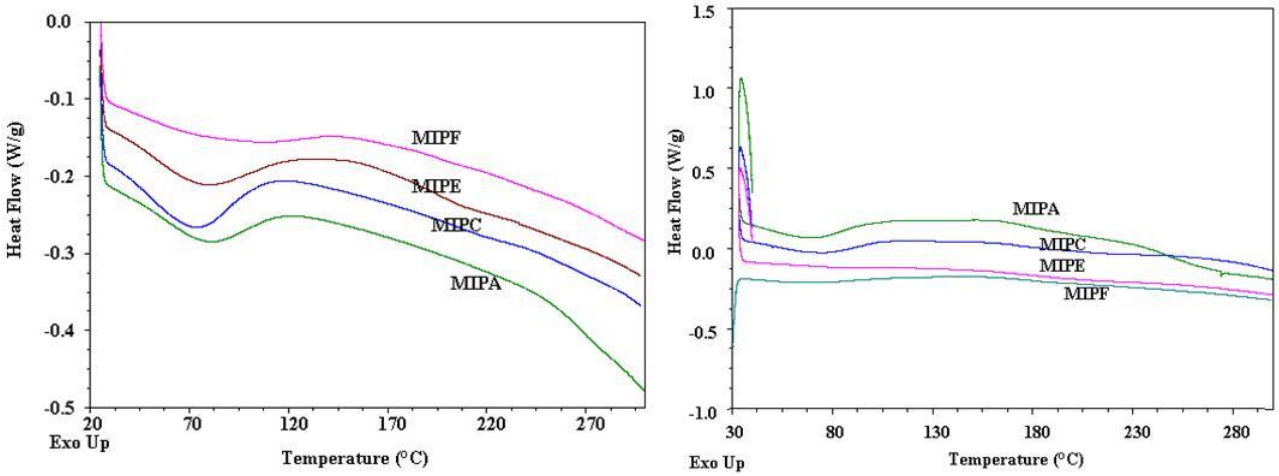

Figure 3.6 Crude polymer DSC curves before soxhlet (A) and after soxhlet (B).

Table 3.2 Unreacted double bonds in crude polymer determined by DSC.

Crude polymer	Enthalpy (J/g)	remaining unreacted double bonds (%)
MIPA	27.3(23.7)	9.4(8.2)
MIPC	20(16.5)	6.9(5.7)
MIPE	21.6(nd)	7.43(nd)
MIPF	13.1(7.4)	4.5(2.5)

The value in bracket showed after soxhlet extraction.

Where nd= not determined

Contrary to DSC results, the FT-IR spectra of all polymers were indistinguishable (Figure 3.8) indicating that they all contained same amount of unreacted double bonds and that no detectable difference in hydrogen bonding in the polymers is present.[146] The main difference between

RAFT and conventional polymer was the signal at 1068 cm^{-1}, which was assigned to the presence of C=S groups in the RAFT polymers. The signal 1068 cm^{-1} was not obvious due to the low content of CTA in the RAFT polymer and also evidence of elemental analysis(Table 3.1) shows poor content of sulphur compared to theoretical value.[147] Interestingly the resultant imprinted and non imprinted polymer particles displays reddish pink color with respect to added RAFT agent (Figure 3.7), which indicates the presence of RAFT in the final polymers with respect to added concentration.

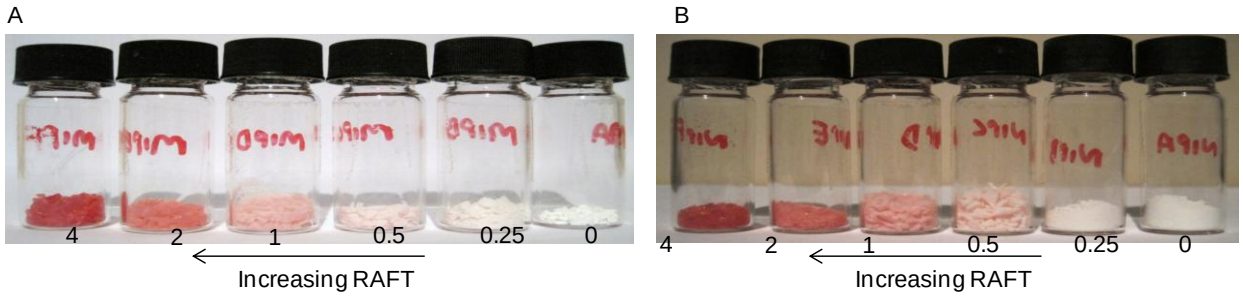

Figure 3.7 Influence of RAFT agent on imprinted (A) and nonimprinted (B) particles images.

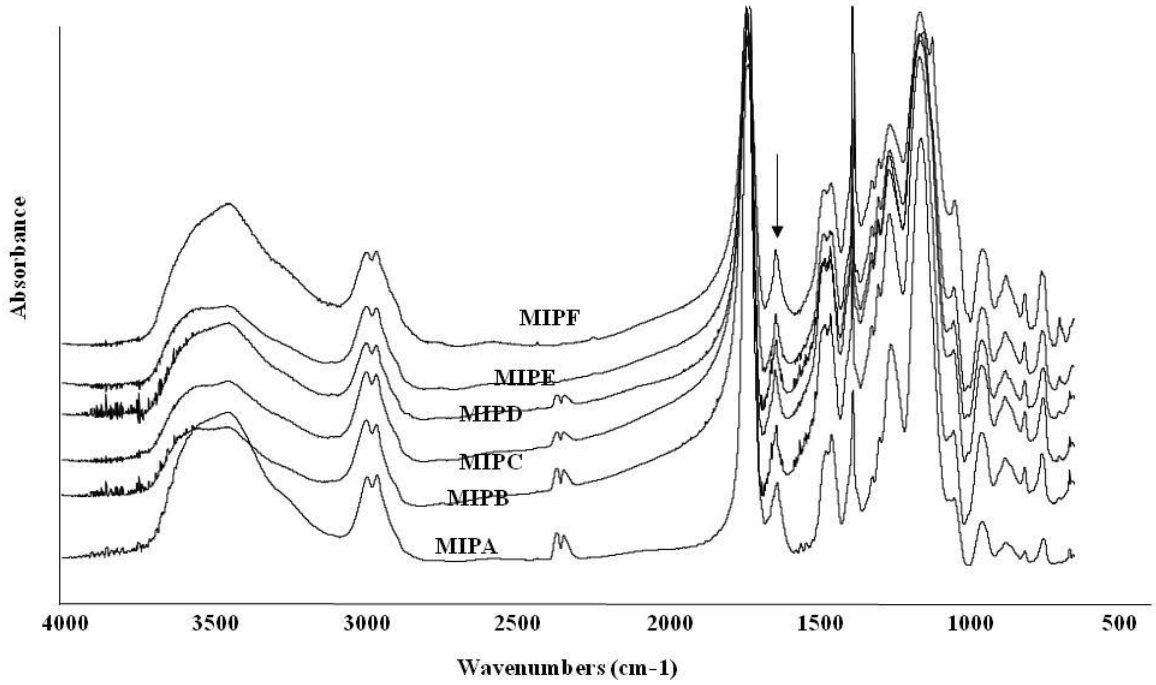

Figure 3.8 Infrared spectra (KBr) of L-PA imprinted polymer with increasing RAFT content.

3.2.3 Swelling and Pore analysis:

Figure 3.9 shows that the swelling ratio of imprinted and non imprinted polymers prepared via RAFT and conventional method. The RAFT polymer displays approximately two times higher swelling ratio compared to conventional polymer and corresponding non imprinted polymer also shows the same trend. In search for an explanation for this behavior the following effects should be considered. In RAFT polymerization the rate of polymerization decreases significantly when increasing the RAFT concentration, which might lead to different intrinsic structure between RAFT and conventional polymer.[61,72]

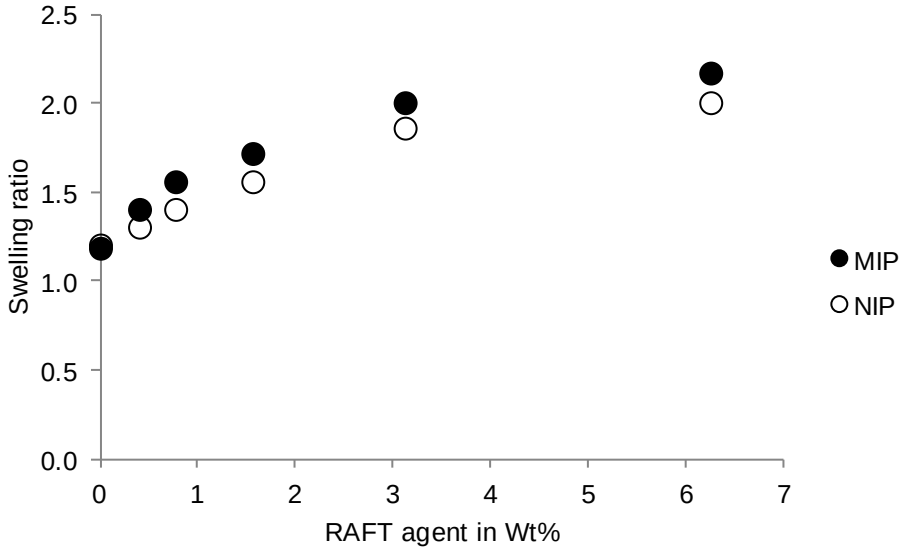

Figure 3.9 Swelling study of imprinted and non imprinted polymers in pure acetonitrile.

On the other hand the slow chain growth in the RAFT process allowed sufficient chain relaxation and uniform distribution of reacting species, which reduced intramolecular crosslinking and limited microgel formation. On the contrary in conventional polymerization the monomer propogation is so fast and there is no time to relax a polymer chains so crosslink reaction is happen between the same molecules and forms the early microgel formation.[147,148] These results suggest that the delayed crosslinking reaction under the RAFT conditions would proceed in a

fairly homogeneous manner, resulting in the construction of highly selective binding cavity with the lower density of crosslinking.[61]

From Table 3.1, clearly suggest that influence of CTA on pore size and surface area of polymers. As the concentration of RAFT increased, the average pore size and surface area decreased (Figure 3.10). Conventional polymer MIPA produced type IV hysteresis loop and the pore size is 24 nm but the higher RAFT/ABDV ratio polymers produced the type II hysteresis loop very similar to the adsorption isotherms observed for nonporous materials with three dimensionally connected porous networks and the pore sizes were 10-2 nm in the range with increasing RAFT concentration. In all the isotherms I observed that desorption branch was not connected to adsorption branch at low relative pressure i.e. the isotherms were open. This is normal in highly crosslinked polymer system. One possible explanation for this behaviour is that nitrogen remains dissolved within the polymer matrix at high relative pressure so the dissolved N_2 cannot be liberated easily at low relative pressure, and hence an open isotherms were observed.[149,150]

A **B**

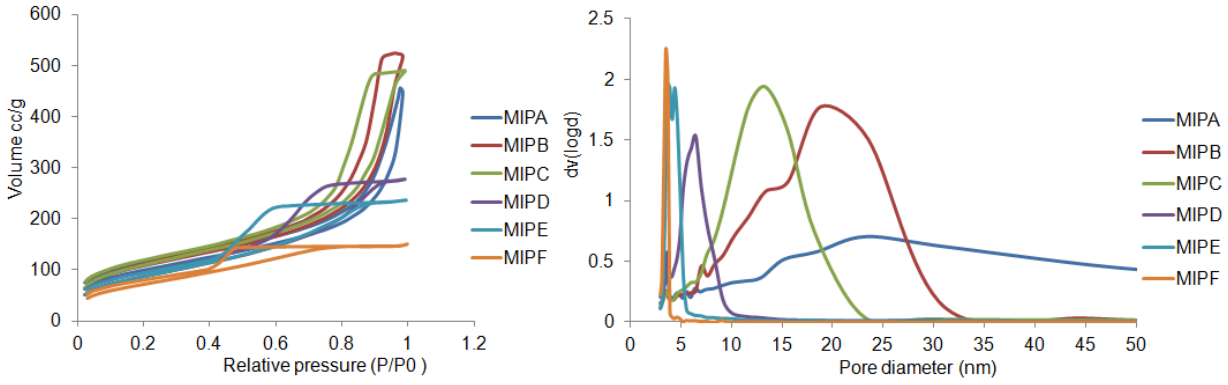

Figure 3.10 Nitrogen adsorption – desorption isotherms of L-PA imprinted polymer with increasing RAFT content (A) and pore size distribution (B).

The BJH (Barrett, Joyner and Halenda) [198] analysis of the desorption branch of the isotherms revealed that all samples display monomodal pore sizes varying between 23.5 and 3.5 nm (Figure 3.10B). The smallest pore sizes 3.5 nm were found for the high RAFT/ABDV ratio (MIPF), whereas conventional polymer (MIPA) displayed larger pore size 23.5 nm. The same

trend was observed for non imprinted polymer. Conventional polymer confirmed the macroporous morphology by BET (Brunauer-Emmett-Teller)[195,196] that's why it exhibits high surface area compared to RAFT polymer.[72] A similar observation has reported that MIPs prepared by Nitroxide mediated polymerization (NMP) shows smaller surface area compared to Conventional polymer.[61] It may be due to the change of surface morphology under the dry condition of BET measurement. It has been reported that shorter kinetic chain length forms more uniform crosslink density and narrow pore size distribution. Therefore Conventional polymerization results longer kinetic chains and forms more broad size distribution and heterogeneous crosslink network (Figure 3.11).[51]

Another evidence for change in surface morphology was studied by SEM. An SEM images revealed that the pore size decrease with increasing RAFT/ABDV ratio (Figure 3.12). This indicated that the pore diameter could be controlled by varying the concentration of RAFT agents. RAFT polymer displayed the interconnected smaller pores and they are evenly distributed through the surface where the conventional polymer displayed randomly distributed mesopores or macropores through the surface.

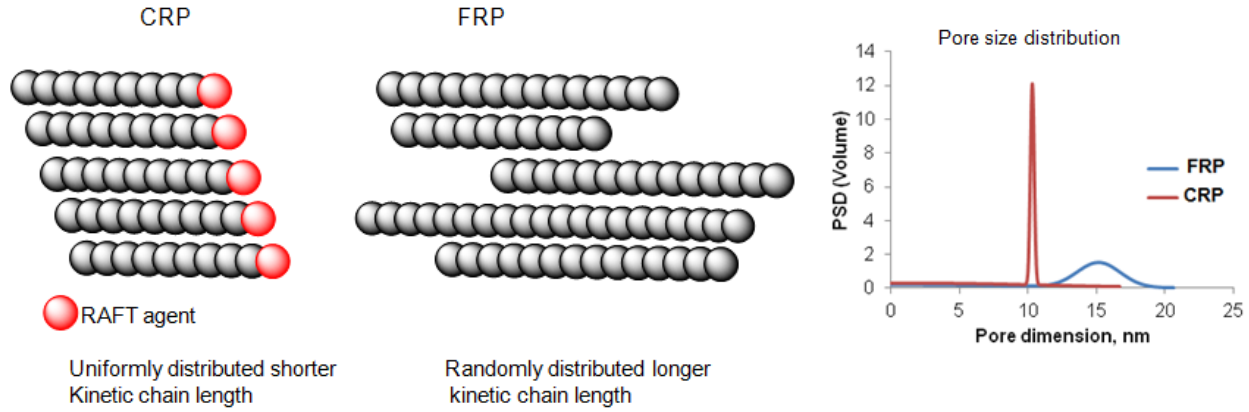

A

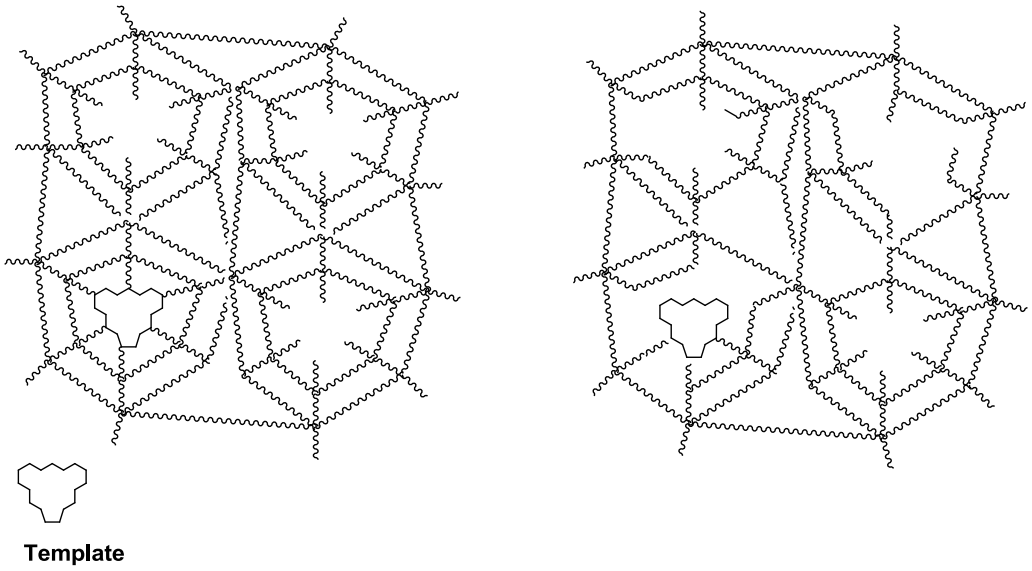

B

Figure 3.11 Influence of CRP on imprinted network structure. (A) In linear polymerization, the use of RAFT agent yields a lower polydispersity of kinetic chains and decreased average chain length. (B) Within crosslinked networks, addition of RAFT agent leads to a more uniform and higher population of appropriately sized imprinted macromolecular cavities for the template.

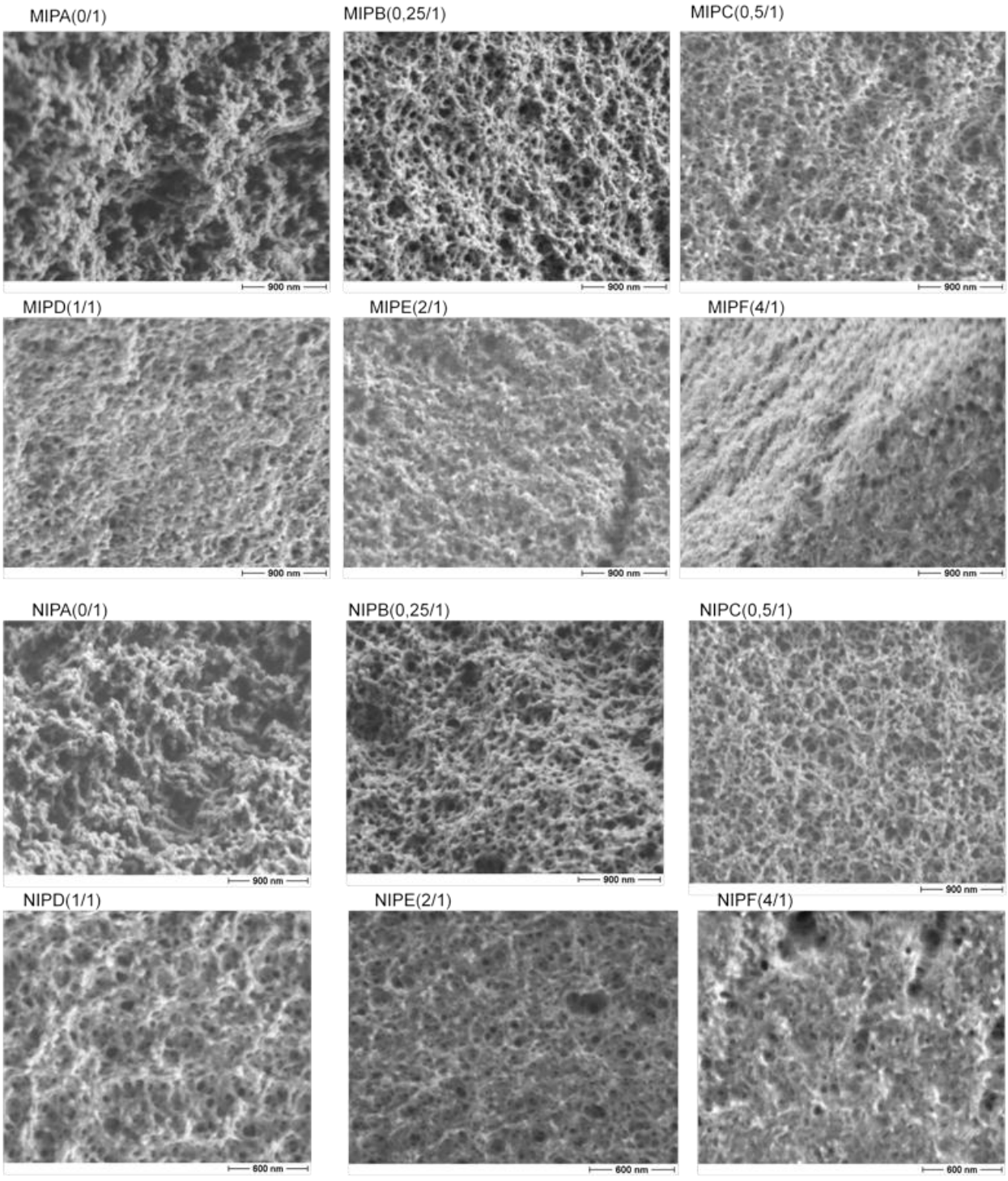

Figure 3.12 SEM images of conventional imprinted and nonimprinted polymers (MIPA and NIPA) and RAFT polymers with varying the RAFT/ABDV ratio (MIPB to MIPF and NIPB to NIPF).

3.2.4 Thermoporometry

Thermoporometry is a calorimetric method for characterising the pore structure of the material from melting or freezing point depression of liquid confined in a pore.[151,152] This technique was used in this study for further confirmation of narrower pore sizes in swollen state. From Figure 3.13 we observed that the DSC thermogram contains two melting peaks one at low temperature is due to the melting of the confined solvent while the second peak associated with the bulk solvent. The melting point in the pores was depressed with increasing RAFT content, and the magnitude of the shift increased with decreasing pore size.

From DSC curves $\Delta T = T - T0$ was calculated, To being the melting point of the pure acetonitrile = -46± 0.3 ^{0}C. Linear regression yields the following numerical expression for acetonitrile. The ΔT valued substituted in fallowing equation and calculated the radius of the pore (Table 3.1).

$Rp\ (Å) = -309/\Delta T + 13$

The value 13Å represents the thickness of the solvent layer remaining adsorbed on the internal pore surface (non-freezable solvent).

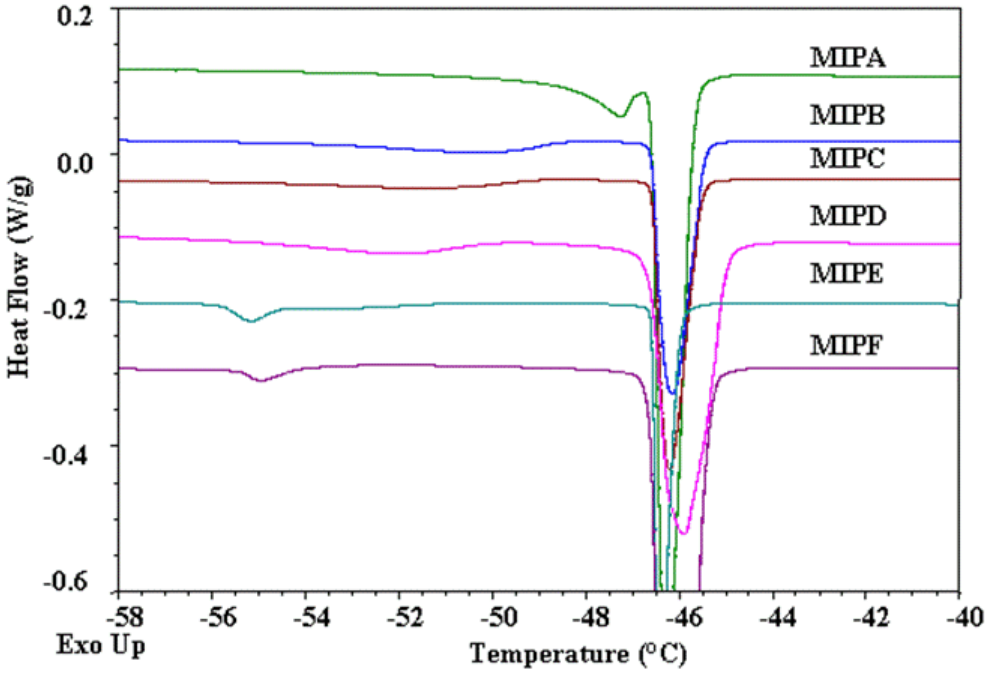

Figure 3.13 DSC curves for the melting of acetonitrile in the L-PA imprinted polymers. The sample was frozen by rapidly quenching to -60 ^{0}C. The heating curves shows pore melt and excess melt.

By using the above DSC curves one can calculate also the pore volume and surface area which is shown in Table 3.1.

From Table 3.1, showed that in swollen state polymer has a higher pore diameter and pore volume compared to dry state polymer but the surface area is less in swollen state for all polymers. This can be explained as in swollen state polymers were open their pores and accessible to the solvent so the pores becomes wider in size obviously larger the pore size smaller the surface area this is not the case in dry state where the pores are closed and also could be shrinking effect which makes pores smaller in size and results in high surface area. Conventional polymer (MIPA) in swollen state displayed higher pore diameter (33 nm), pore volume (0.83 cc/g) and two times less surface area (100 m^2/g) compared to dry state due to the macroporous structural arrangement of polymer network (vide supra). An increasing the RAFT concentration the pore diameter goes on decreases (33-8.5 nm) and surface area is increased (100-259 m^2/g). This clearly suggests that the influence of RAFT agent on polymer morphology which makes more uniform and narrow pore size distribution. Interestingly, RAFT polymer

showed higher surface area compared to conventional polymer in swollen state which is more useful for chromatography study.

3.2.5 Inverse size exclusion chromatography (ISEC)

For getting better understanding of these polymers morphology and porosity in swollen state then we turned to ISEC. It is an chromatographic technique widely used for measurements of the porosity of the polymers in swollen state.[153-161] ISEC is done by providing the exclusion volume for polystyrene standards of known molecular radii (see in experimental section 7.4.15). From the exclusion volumes, the accessible pore volume versus molecular radius can be modeled (see in Appendix). Figure 3.14 showed that the pore size distribution of MIPA (without RAFT) and MIPD (with RAFT). The RAFT polymer displayed the narrow pore size distribution compared to conventional polymer (MIPA) as expected. This proves that RAFT agent has pronounced effect on the polymer morphology. In swollen state RAFT polymers increased the pore diameter (12nm) double of the dry state measured diameter (6 nm) but the surface area is decreased compared to dry state. The values obtained in swollen state from thermoporometry and ISEC measurements are in good agreement (Table 3.3).

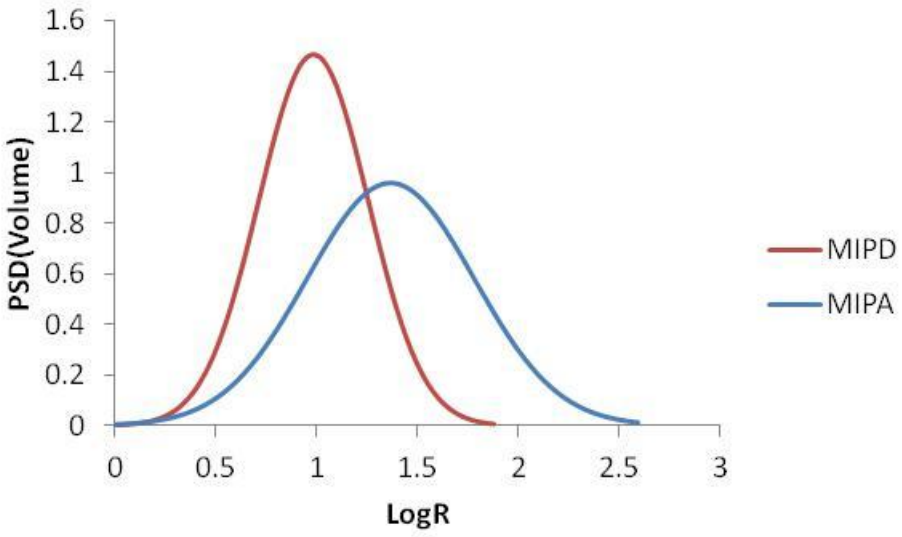

Figure 3.14 Pore size distribution obtained from ISEC measurements.

Table 3.3 Comparison of pore analysis in dry state and swollen state.

code	Dp^a nm	Dp^b Nm	Dp^c nm	$V_p{}^a$ cc/g	$V_p{}^b$	$V_p{}^c$	$S_A{}^a$ m^2/g	$S_A{}^b$ m^2/cm^3	$S_A{}^c$ m^2/cm^3
MIPA	23.02	33.2	36.8	0.69	0.83	0.495	358	100	135
MIPD	6.03	12.6	11.8	0.43	0.69	0.459	321	230	251

Where, Dp = pore diameter, V_p= pore volume, S_A= Specific surface area, a= dry state (BET), b= Swollen state (DSC), c= Swollen state (ISEC)

3.2.6 Thermal stability

The thermal stability of the polymers was measured by thermo-gravimetric analysis. The measurement was conducted at 30 ^{0}C to 800 ^{0}C at a constant heating rate 10 ^{0}C/min in N_2 atmosphere. Figure 3.15 demonstrates the thermo-gravimetric analysis (TGA) and corresponding differential thermogravimetry (DTG) curves of MIPs with the raise of temperature. As shown in Figure 3.15 the conventional polymer (MIPA) display initial degradation at 248 ^{o}C and also showed a two step degredation at peak maxima 300 ^{o}C and 420 ^{o}C from DTG curve. High RAFT/ABDV ratios polymer (MIPF) display initial degradation at 347 ^{o}C and interestingly showed single step degradation at peak maxima 420 ^{o}C from DTG curve. Temperature at initial, 25, 50 and 75 % mass loss values were given in the Table 3.4. At closer observation from TGA curves suggest that with increasing the RAFT concentration makes possibly more homogenous polymer network and higher thermal stability (up to 100 ^{o}C) compared to conventional polymer. This could be explained as in RAFT polymers the thermally weak links could be absent i.e. head to head bonds and chain end unsaturation and another reason is due to the most of the RAFT polymer chains end capped with CTA which containing the aromatic ring.[162] The DTG curves of conventional polymer showed two step degradation first steps could be low molecular weight

polymer or oligomers. However, high content RAFT polymers displayed single step degradation which could indicates the formation of homogenous network.

A B

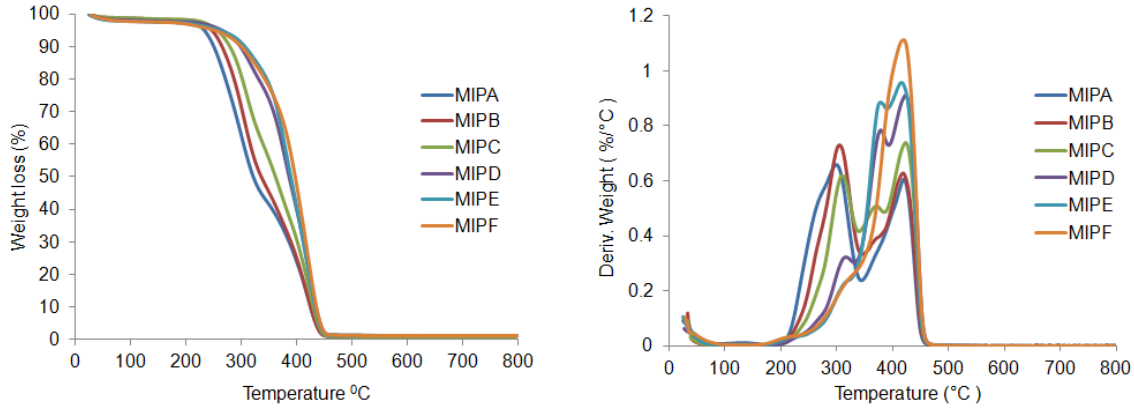

Figure 3.15 TGA curves of L-PA imprinted polymer (A) and DTG curves (B).

Table 3.4 Temperature at %Weight loss of imprinted and non imprinted polymers.

Polymer code	Onset (^{O}C)	Temperature at 'x'% mass loss		
		T_{25}(^{0}C)	T_{50}(^{0}C)	T_{75}(^{0}C)
MIPA	248	279	320	395
MIPB	263	294	336	399
MIPC	309	311	360	409
MIPD	339	345	384	416
MIPE	343	356	387	416
MIPF	347	357	396	420
NIPA	240	274	313	390
NIPB	261	294	336	395
NIPC	315	320	370	408
NIPD	325	345	378	412
NIPE	336	354	385	414
NIPF	345	354	390	416

3.2.7 Chromatography evaluation

The RAFT and conventional way prepared imprinted polymers were packed in to HPLC column (35mmX4.6mm) and evaluated using mobile phase (MeCN/ sodium acetate buffer, 0.01M, pH 4.8, 90/10, v/v) for their ability to resolve and retain the racemate corresponding to the template (D,L-PA). The resulting elution profiles were evaluated with respect to the retention of the two enantiomers, determined as the capacity factor (k′), the enantioselectivity, determined as the separation factor ($\alpha = k_L/k_D$), number of theoretical plates (N), and the resolution, determined as the resolution factors (R_s) (Figure 3.16, Table 3.5). The capacity factor, separation factor and

resolution increased at optimum ratio of RAFT to initiator (MIPD). At higher amount of RAFT/ABDV ratio (MIPF) display less selectivity and enantioselectivity towards target molecule because the MIPF has narrow pore size and high swelling ratio which makes difficult to the target molecule to access binding sites easily. Another possible reason could be the polymer compressed under the chromatographic condition due to the different morphologies compared to other polymers. Table 3.5 compares the chromatographic performance between MIPA (without RAFT agent) and with increasing amount of RAFT (MIPC, MIPD, MIPF); calculations were made assuming that the peaks have Gaussian distribution.[106] The results from Table 3.5 summarizes that at optimum ratio of RAFT/ABDV polymer (MIPD) has higher plate number and high resolution factor so by controlling the concentration of RAFT/ABDV one can improve the column efficiency and resolution. These results are very good agreement with pore analysis and swelling study.

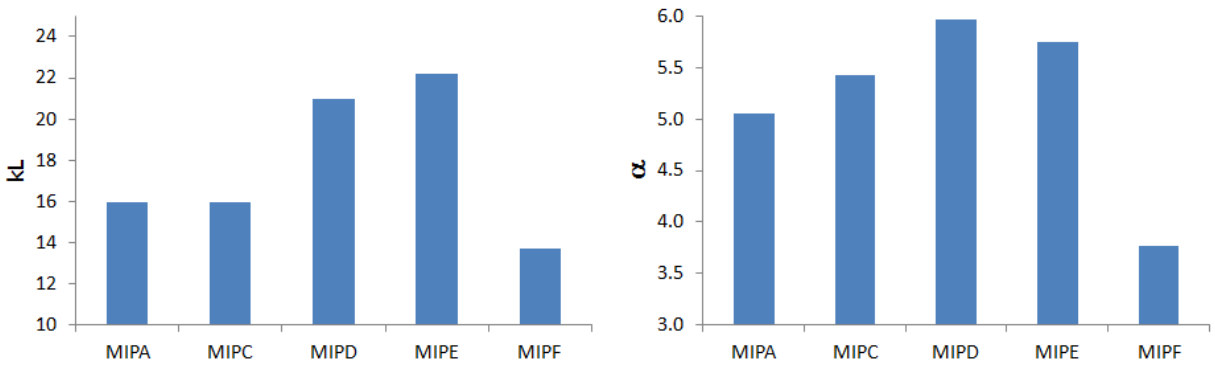

Figure 3.16 The graph shows Capacity factor (kL) and separation factor (α) for L-PA. Mobile phase: MeCN-0.01M sodium acetate buffer, pH 4.8 (9:1); 0.5mM racemate D- and L-PA enantiomer; injected voume 10µL, flow rate 0.5mL/min. DAD= 260nm, column 35mm X 4.6 mm.

Table 3.5 Comparison of chromatographic performance between conventional MIPs and RAFT MIPs.

Polymer Code	Resolution factor	Column efficiency(N)		HETP(h)	
	Rs	N_D	N_L	h_D	h_L
MIPA	1.07	19.66	10.95	0.18	0.32
MIPC	1.15	48.45	13.88	0.07	0.25
MIPD	1.54	102.99	17.57	0.03	0.19
MIPE	1.31	38.54	13.96	0.09	0.25
MIPF	1.19	86.23	15.78	0.04	0.22

Where, R_s= resolution factor, N_D= column efficiency for D-PA, N_L column efficiency for L-PA, h= height equivalent to theoretical plate

From this experiment, choose the best RAFT polymer (MIPD) and studied with different loading of racemate and compared with conventional polymer. 0.5mM, 1mM, 5mM, 10mM, 20mM, 50mM and 100mM concentration of racemate injected into MIPA and MIPD. From Figure 3.17 as can be seen the clear difference between the two polymers, until 50mM RAFT polymer having the shoulder peak which indicates that still it has the capability of discrimination between the two enantiomers. Both columns showed the nonlinear chromatography with constant overloading of low abundant high energies binding sites.

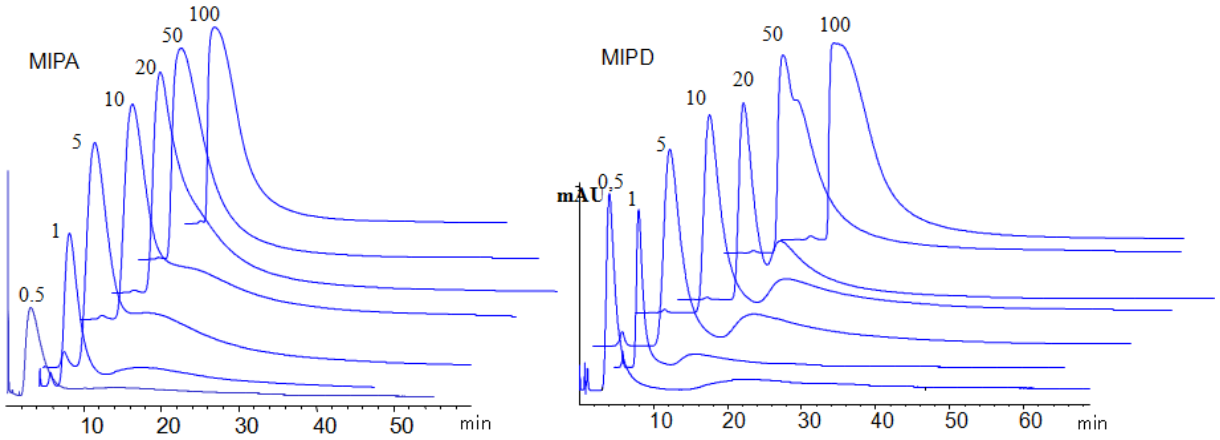

Figure 3.17 Elution profiles obtained for different concentration of racemic mixtures (D, L-PA) on MIPA and MIPD using as mobile phase: MeCN-0.01M sodium acetate buffer, pH 4.8 (9:1) at flow rate of 0.5mL/min, DAD = 260 nm and column size = 35 mm X 4.6 mm.

3.2.8 Determination of binding capacity of the MIPs

Equilibrium binding experiments were performed to study the template rebinding properties of the MIPs/NIPs in pure acetonitrile. Thus, quantifying the equilibrium free concentration (C_{free}) of solute by HPLC, the bound amount q could be determined and plots of q versus C_{free} giving the binding curves of template L-PA and of its optical antipode D-PA for the different imprinted polymer complements.

Figure 3.18 shows that the MIPs prepared via RAFT bound more template than their corresponding NIPs, suggesting the presence of selective binding sites in MIPs. Besides, the MIP prepared without RAFT showed less equilibrium loading capacity than the RAFT MIP in a wide range of polymer concentrations. The isotherms were subsequently fitted to mono-Langmuir, bi-Langmuir, and Freundlich isotherm model resulting in the isotherm parameters given in Table 3.6 to Table 3.8. The fisher values in Figure 3.19 reflect which of the model provides the best fit to a particular isotherm, a higher number indicating a better fit.

The binding features of D, L-PA to both the imprinted (MIPA, MIPD) and non-imprinted (NIPA, NIPD) RAFT polymers were accurately modelled using the Freundlich (FI) isotherm by plotting the experimental binding data in log format:[30,31]

$\log q = \log a + m \log C$ (1)

Where q is the bound concentration of D, L-PA and C is the free concentration in solution respectively, a is the binding capacity and m is the so called heterogeneity index. Latter ranges from 1 to 0 increasing with decreasing heterogeneity of the materials. The affinity distribution (AD) can be calculated using Eq. (2) and the experimentally derived FI fitting parameters (a and m):[32,163,164]

$N(K) = 2.303am(1 - m^2)e^{-2.303 \log K}$ (2)

The ADs calculated with this equation are valid within a range of binding affinities (K_{min} and K_{max}) that can be calculated from the experimental maximum and minimum free analyte concentrations (C_{min} and C_{max}) and the relationships

$K_1 = K_{min} = 1/C_{max}$ and $K_2 = K_{max} = 1/C_{min}$.

the apparent number of binding sites, N, and the apparent weighted average affinity, K , calculated using Eq. 3 and Eq.4:[32,163,164]

$N = a\,(1 - m^2)\,(K_1^{-m} - K_2^{-m})$ (3)

$$K = \left(\frac{m}{m-1}\right)\frac{K_1^{1-m} - K_2^{1-m}}{K_1^{-m} - K_2^{-m}} \quad (4)$$

Langmuir and Bilangmuir Fitting:

$q^* = q_s bC/(1+bC)$ (5)

$q^* = q_{s1} b_1 C/(1+b_1 C) + q_{s2} b_2 C/(1+b_2 C)$ (6)

Where q* is the concentration in the stationary phase at equilibrium with concentration C, and C is the concentration in the mobile phase. The Langmuir models (eqs. 5-6) assume that one (eq.5) or two (eq.6) distinguishable classes of sites are present on the surface, each with saturation

capacity q_s and association constant b. The dissociation constant K_d was calculated as the inverse of b.

Based on FI binding parameters (Table 3.6) revealed an increase in both the number of binding sites(N_t) and binding capacity(a) in imprinted polymers prepared via RAFT method (N_t=51.08 ± 2.26 µmol/g, a=36.81 µmolg^{-1} (mol^{-1})^m) over corresponding imprinted polymer networks prepared via conventional method (N_t=35.76 ± 2.03µmol/g, a=27.43µmolg^{-1} (mol^{-1})^m). The imprinted polymer networks prepared by RAFT method showed 30% increase in the number of binding sites and 25% increase in binding capacity over the imprinted polymer networks prepared by conventional method for L-PA. The heterogeneous index of imprinted polymers network via RAFT method is higher than the imprinted polymer networks via conventional method. Higher the heterogeneous index number indicates more homogenous network formation. This result agrees with delayed propagation phase in RAFT method which makes more homogeneous and uniform crosslink networks. This finding are agrees with some reported literatures such as Titirici etal reported the MIPs prepared via CRPs exhibited improved binding properties such as faster binding kinetics[94], higher binding capacities and larger binding association constants,[51,61,106,138] while in some other cases, the binding properties of the MIPs prepared via CRPs appeared very similar to those of the MIPs prepared via conventional approaches.[165] In the present study, we found out that RAFT MIPs display improved binding capacity and apparent maximum number of binding sites *(N_t)* than the conventional MIP.

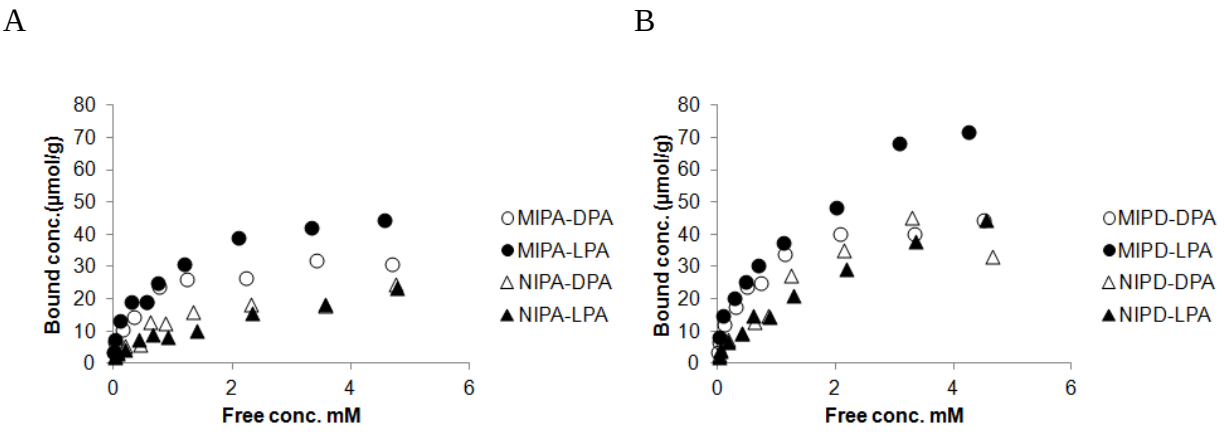

Figure 3.18 Adsorption isotherms of D/L-PA on MIPA (A) and MIPD (B) with corresponding non imprinted polymer, as solutions in pure acetonitrile.

Table 3.6 Freundlich isotherms fitting parameters obtained by nonlinear regression of data shown in Figure 3.18 as described in the experimental section.

Polymer		Affinity constant $Ka(mM^{-1})$	Total number of binding sites, Nt ($\mu molg^{-1}$)	Heterogeneity parameter, m	Binding capacity, a ($\mu molg^{-1}$ $(M^{-1})^{m}$)	Correlation coefficient r^2	F-value
MIPA	D-PA	6.3 ± 0.25	25.56 ± 1.36	0.298	21.5	0.945	407
	L-PA	5.56 ± 0.24	35.76 ± 2.03	0.354	27.43	0.980	942
MIPD	D-PA	5.74 ± 0.32	35.67 ± 2.11	0.340	28.05	0.964	520
	L-PA	2.88 ± 0.11	51.08 ± 2.26	0.476	36.81	0.987	1208
NIPA	D-PA	3.35 ± 0.51	9.90 ± 0.85	0.522	9.82	0.979	ND
	L-PA	4.51 ± 0.42	11.93 ± 0.91	0.414	12.3	0.934	ND
NIPD	D-PA	1.50 ± 0.12	26.47 ± 1.3	0.620	17.67	0.995	ND
	L-PA	2.88 ± 0.21	29.72 ± 1	0.494	20.16	0.862	ND

ND= not determined

Table 3.7 Mono-Langmuir Isotherm fitting parameters obtained by nonlinear regression of data shown in Figure 3.18 as described in the experimental section.

Polymer code		K_d (mM)	q_s (µmol/g)	r^2	F-value
MIPD	LPA	1.40 ± 0.36	93 ± 10	0.959	328
	DPA	0.55 ± 0.08	48 ± 2	0.981	799
MIPA	LPA	0.61 ± 0.14	49 ± 4	0.957	341
	DPA	0.36 ± 0.06	33 ± 2	0.973	624

Table 3.8 Bi-Langmuir Isotherm fitting parameters obtained by nonlinear regression of data shown in Figure 3.18 as described in the experimental section.

Polymer code		K_d1 (mM)	q_s1 (µmol/g)	K_d2 (mM)	q_s2 (µmol/g)	r^2	**F-value**
MIPD	LPA	0.026±0.025	15±4	5.21±2.79	131±35	0.993	746
	DPA	0.014±0.023	6.0 ± 4	0.82±0.25	44±3	0.993	821
MIPA	LPA	0.023±0.02	11.7 ±3.7	1.79±0.74	47±4.0	0.992	683
	DPA	0.005±0.02	4.4 ±3.6	0.57±0.2	30±3.0	0.988	532

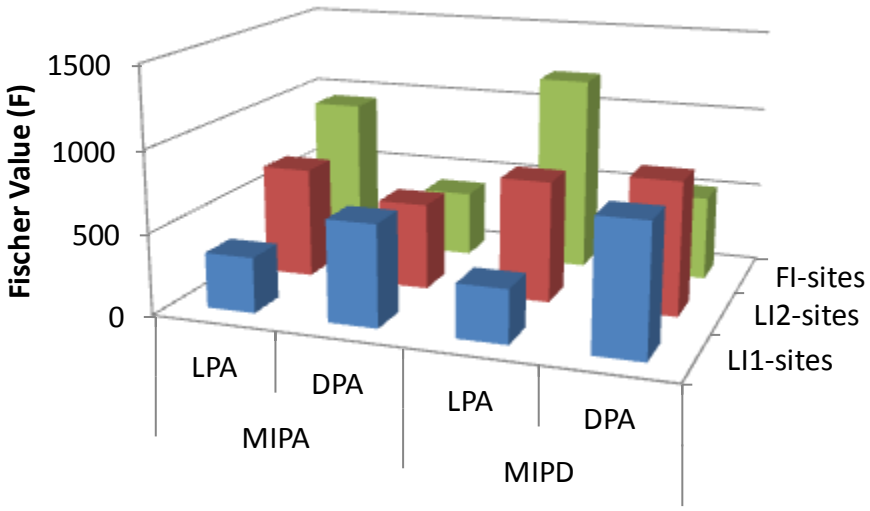

Figure 3.19 Fischer values obtained by fitting the L/D-PA binding curves in Figure 14 to mono-Langmuir (LI 1 site), bi-Langmuir (LI 2 sites) or Freundlich isotherm models (FI) (see Tables 3.6 to Table 3.8).

3.3 Conclusions

RAFT mediated living radical polymerization was introduced into the preparation of molecularly imprinted networks for the separation of L/D-PA enantiomers. This approach provides high binding capacity and selectivity towards target molecules. A smaller pore size was obtained

when the ratio of RAFT agent was increased in this study. However at high RAFT to initiator ratio gives less capacity and selectivity to the template due to higher swelling ratio where binding sites were not stable. The results of our research demonstrated that optimum RAFT to initiator ratio was important factors for the separation and column efficiency. The present work not only broadens the application area of RAFT in the molecular imprinting field, but also shows that the appropriate choice of RAFT agent to initiator ratio is crucial for the generation of MIPs with desired properties which is of significant importance for the rational use of CRPs in the synthesis of MIPs with improved binding properties.

4 Thin film MIP composite beads

4.1 Introduction

In recent decades, surface initiated(SIP) controlled radical polymerization (CRP) technique is a great interest to generate a polymer thin films on different surfaces.[82] By using these techniques one can control the functionality, density and thickness of polymer films with molecular precision. CRP can be used for quasi-living polymerization to prepare block copolymers of defined architectures to impart various advanced functions. Only a few reports are describing the surface initiated controlled radical polymerizations of crosslinked polymers commonly refer to molecularly imprinted films. MIPs are made with high level of cross linker because it is a necessity for preserving the integrity of the imprinted recognition sites.[93-95,97,106,166-168] In general, the use of grafting techniques for preparing MIP beads allows the bead morphology to be set independently from the formation of the MIP.[89] Hence, materials exhibiting similar bead size and porous properties can be prepared using widely different monomers and solvents. In addition to the above mentioned structural control, the added value of CRP comes from the degenerative nature of the chain growth leading to shorter more uniform primary chains and potentially a more regular homogenous network. The latter may positively impact the fidelity and reduce the binding site heterogeneity commonly observed for molecularly imprinted networks (see in section 2.5.6). Indeed, Byrne et al. recently demonstrated an enhanced uptake capacity for MIPs prepared by iniferter controlled radical polymerization.[51,53]

Moreover, SIP, CRP and template synthesis are widely employed for synthesizing well dispersed multifunctional nanoparticles (e.g. for drug delivery, imaging, diagnostics) and also imprinted nanoparticles[97,169] Walt *et al.* used atom transfer radical polymerization (ATRP) to graft thick polymer layers on porous silica.[170] Etching away the silica template hollow spheres remained with a relatively thick shell with thickness larger than 175 nm. Arnold and Yang reported on thin walled coaxial nanotubes prepared by ATRP from initiator modified silica/silicone core shell nanowires[171], while Wang et al. applied a similar approach to produce molecular imprinted nanotube membranes for separation and sensing [172,167] or TNT [173] which can otherwise be difficult to access by alternative approaches such as precipitation polymerization and miniemulsion polymerization.

Recently, the group of Sellergren reported on "grafting from" techniques for the synthesis of MIP composite materials with improved static and dynamic binding properties.[80,81,89,92,93] Sulitzky *et al* first reported the thin film MIP composites beads with improved mass transfer characteristics using immobilized azoinitiator on silica surface.[89] Controlled grafting of thin film MIP was achieved by use of immobilized dithiocarbamate initiators.[92,93] The living character of this polymerization was used for layer by layer grafting of different MIPs onto wide pore silica.[93] A few years ago Titirici et al investigated the use of soluble chain transfer agents (RAFT agents) as another means of achieving SIP and CRP.[94] The materials could be prepared in short time and exhibited superior mass transfer properties compared to the traditional imprinted bulk monoliths or materials prepared without the polymerization control through RAFT agents.

Nevertheless several drawbacks of the previously described grafting protocols became obvious. Due to the fact that the film thickness is controlled by interrupting the polymerization at given times the monomer conversion is low leading to significant batch to batch variations with respect to structure and performance. Moreover unreacted monomer is difficult to recover leading to low overall yields and loss of reagents. To address these problems I have focused on methods for grafting to reach full monomer conversion and methods relying on thermal homolysis of the initiator. In this chapter, the grafting of thin film molecularly imprinted polymers on porous silica support either using immobilized azoinitiator alone or an R-immobilized RAFT agent[123] with soluble azo-initiator (Figure 4.1) is presented. Evaluation was performed by characterising the pore structure, morphology and template recognition of the polymers. Some parts of this chapter have been published as a article.[81]

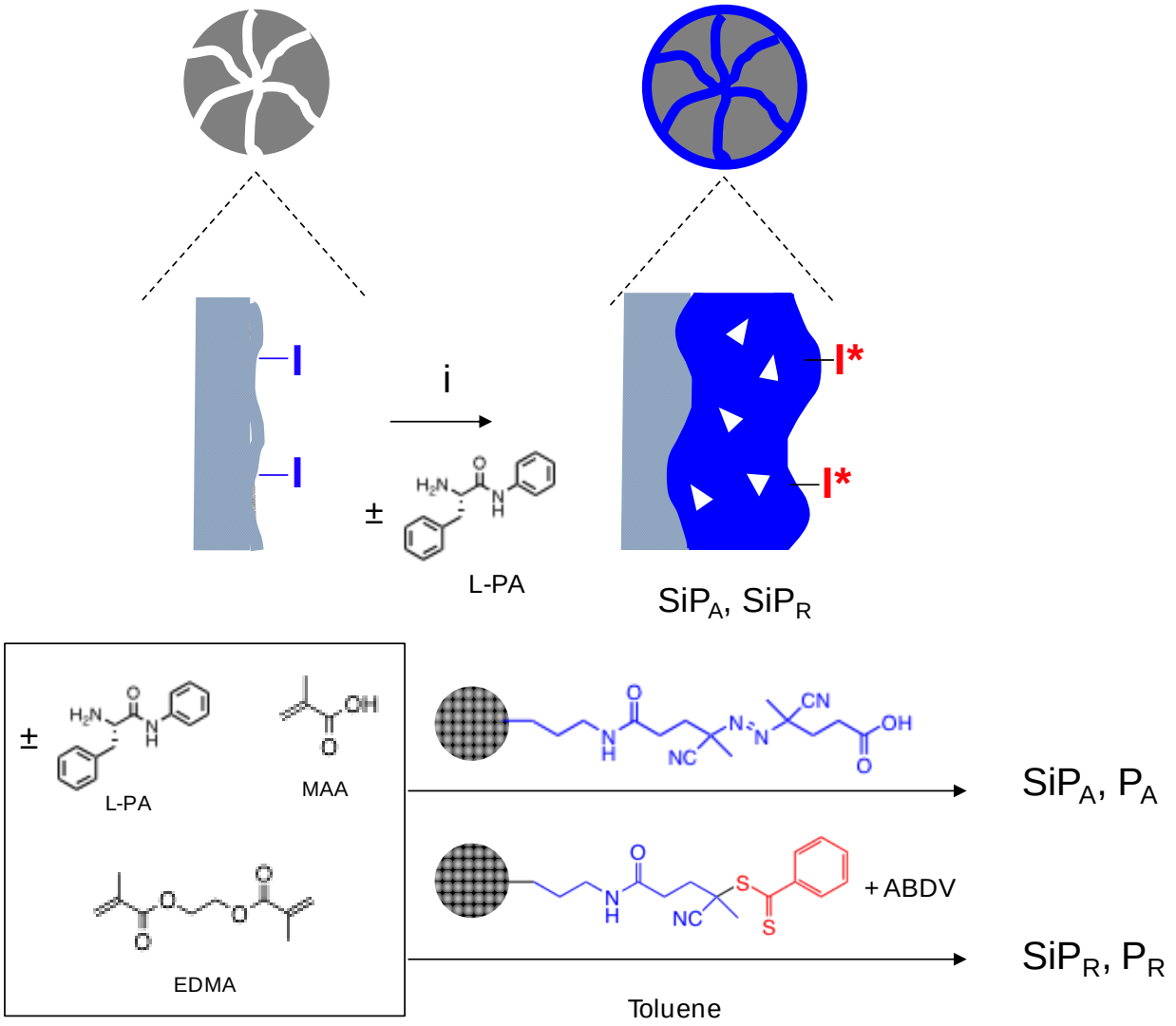

Figure 4.1 Grafting of L-phenylalanine anilide (L-PA) imprinted polymer films from an porous silica support modified with azoinitiator (A), or RAFT agent (R). The grafting was performed using a common prepolymerization mixture to reach near full conversions under five different dilution (0-20mL) for Azo-system and using different RAFT/initiator ratio in RAFT system.

4.2 Results and discussion (IIA)

4.2.1 Grafting of molecularly imprinted polymers via azo initiator modified silica support

The "grafting from" technique for producing L-phenylalanine anilide (L-PA) imprinted composites was investigated using two previously reported initiator systems as depicted in Figure 4.1. The first system (A) is based on conventional azoinitiators immobilized to silica decomposable by either thermolysis or photolysis,[87] whereas the second (R) relies on chain transfer agents (RAFT) immobilized to the silica surface via the R-group.[123] In the latter case, surface grafting requires a source of primary radicals generated in the solution phase. In order to compare the relative merits of these techniques therefore grafted imprinted copolymers of methacrylic acid and ethyleneglycol dimethacrylate under similar conditions following the protocols outlined in Figure 4.1 i.e. in a 1:5 molar ratio in presence of 5 mol% of L-phenylalanine anilide as chiral template and toluene as solvent. The common support was mesoporous silica (Si100) with a high surface area (S=380 m^2/g) allowing support modifications to be conveniently monitored by conventional techniques e.g. IR spectroscopy, elemental analysis, gravimetric techniques and nitrogen sorption analysis. The use of a chiral template allowed achiral nonspecific binding to be easily deconvoluted from enantioselective binding caused by imprinting.

4.2.2 Silica surface activation

First, the silica surface was activated by rehydroxylation, because there is loss of silanol groups during the calcinations process subsequent to the silica synthesis. This was accomplished through treatment with hydrochloric acid (17% aq.sol), which converted the siloxane bonds into silanol groups according to Scheme 2. The amount of silanol groups per unit of surface can be determined by TGA or by the methyl lithium method.[174,175] However, this value can be considered as a physicochemical constant, independent of the silica type, thus it was assumed that fully hydroxylated silica contains around 8 $\mu mol/m^2$ of silanol groups.[176]

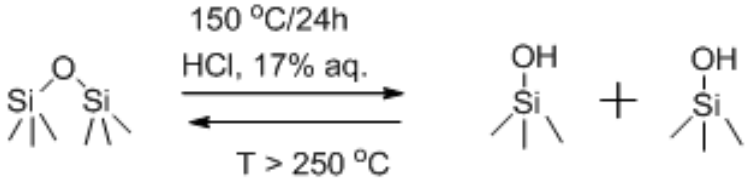

Scheme 2 Rehydroxylation of siloxane groups.

4.2.3 Functionalisation of silica surface with APS

After rehydroxylation, the silica surface was modified using aminopropyltriethoxysilane (APS). The reactions were performed according to well established literature procedures [84,177]. The silane coverage for a complete modification of the silica surface is expected to range from 3.5 to 4.0 μmol/m^2.[178] Therefore, the amount of APS was calculated according to the number of silanol groups on the silica surface (8 μmol/m^2) and the specific surface area of silica sample. The reaction was performed under inert conditions and with an excess APS (i.e. 2 equivalents), in order to obtain the maximum coverage of amino groups. The silanol groups on the silica surface were converted into amino functional groups via the condensation reactions shown in Scheme 3.

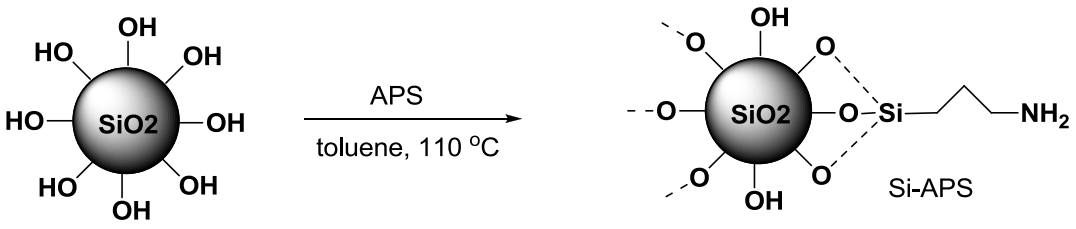

Scheme 3 Functionalisation of silica surface with APS.

The surface densities of the introduced ligands depended strongly on the reaction conditions and on reagent stoichiometry. These densities were determined from elemental analysis data (Table 4.1). Due to sterical hindrance between the introduced chains, not all the surface hydroxyl groups

were available for reaction with the silane molecule. The unreacted silanol group were end-capped in a subsequent step in order to prevent them from interfering in later reactions.

4.2.4 End capped amino modified silica

Prior to Azoinitiator immobilization, all remaining free silanol groups were end-capped with hexamethyldisilazane (HMDS), well-known as a methylating and deactivating reagent. HMDS reacts readily with hydrophilic silanols, yielding very stable methylsilyl groups according to the reaction shown in Scheme 4. Through this procedure, one ensured that all the initiator precursors reacted only with the functional groups at the surface. In addition, after the polymerization process in the silica pores, the silanol group could not interfere in the chromatographic separation and recognition processes.

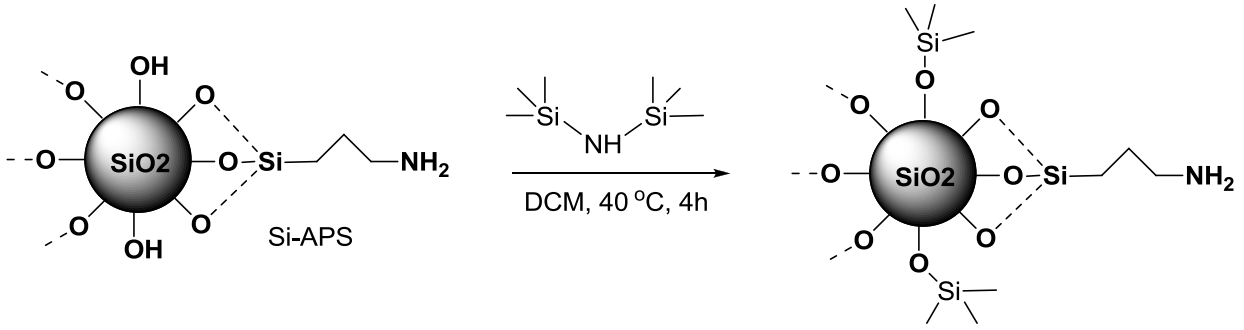

Scheme 4 Consecutive synthesis of amino silica and end-capping of remaining silanol groups.

4.2.5 Surface attachment of free radical initiator - 4,4' azobis (4-cyanopentanoic acid)

A modified amino silica support was used for the coupling of azo initiator. This reaction was performed according to literatures protocol (Scheme 5).[89,179] The azo modified silica support was used for grafting of thin film MIP.

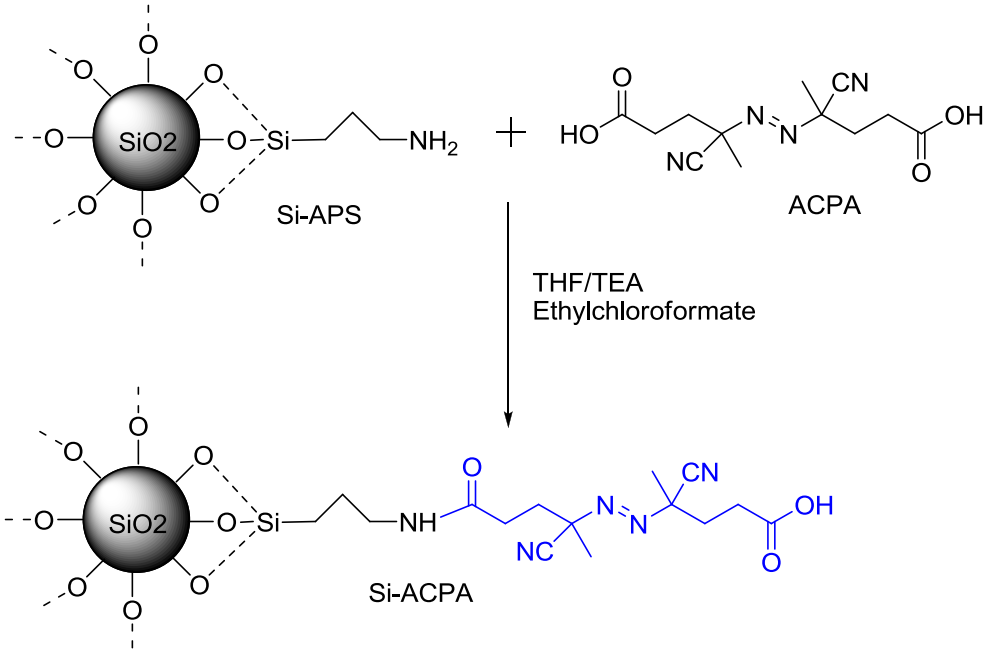

Scheme 5 Covalent immobilization of Azo- initiator on silica surface.

4.2.6 Characterization of the resulting intermediates

The products resulting from the previously described reactions were characterised using elemental microanalysis, Thermogravimetry analysis and FTIR spectroscopy. From elemental microanalysis data, more precisely from the change in carbon and nitrogen contents in each step, we could estimate the amount of immobilized ligand on the silica surface. The data is presented in Table 4.1. The area density (D_S) of immobilized ligand was calculated based on the change in carbon (ΔC) or nitrogen (ΔN) content versus the preceding step, e.g. for ΔN:

$$D_s = \frac{m_N}{M_N \times S} \qquad (1)$$

Where:

$$m_N = \frac{\Delta N\%}{100 - \frac{\Delta N\% \times M_w}{M_N}}$$

M_w=molecular weight of the coupled ligand,

M_N=weight of nitrogen per mole of coupled ligand,

S= surface area of the silica support ($380 m^2/g$).

The coverage (C) was calculated as equation 2, assuming a maximum silanol group density of $8 \mu mol/m^2$

C=100xD/8 (2)

The average distance d_L (nm) between the coupled ligands assuming a random ligand distribution was calculated as equation 3

$$d_L = \sqrt{\frac{10^{18}}{D \times 10^{-6} \times N}} \qquad (3)$$

where N is the Avogadros number

The yield of coupling in each step was calculated based on results obtained from elemental microanalysis. A maximum half of the silanol groups reacted with 3- aminopropyl triethoxysilane (APS) in the first silanisation step. The subsequent step was the attachment of the initiator azobis (cyanopentanoic acid) ACPA (Scheme 5). On the basis of the increase in nitrogen content, a maximum area density of 1.5 μmol/m2 coupled initiator was calculated. This corresponded to *ca.* 36% conversion of the surface amino groups and an overall conversion of silanol groups of *ca.* 18%.

Table 4.1 Characterisation of azoinitiator modified silica supports used for grafting.

Modified support	%C	%N	Area density ($\mu mol/m^2$)	Coverage (%)	Distance (nm)
Si-APS	3.79	1.34	2.9	36	0.8
Si-ACPA	11.76	3.93	1.5	18	1.1

Infrared spectra of the silica supports usually show a broad and intense band at 1000-1100 cm^{-1} corresponding to the stretching of the siloxane bonds (Si-O-Si) and a narrow and weak to medium intensity band at 810 cm^{-1} corresponding to the Si-O stretch of the silanol bonds.

Although the fingerprint region (910 to 1300 cm^{-1}) is covered by the broad band at 1100 cm^{-1} it is still possible to observe the ACPA coupling by comparing the spectra of bare silica (SiO_2), rehydroxylated silica (Si-OH), amino modified silica (Si-NH_2),and immobilized initiator (Si-ACPA) as shown in Figure 4.2. After the amino modification the broad band between 3700-3200 cm^{-1} for free or hydrogen-bonded hydroxyl groups (-OH stretch) decreases in intensity but is still visible because the bands for the NH stretch, of aliphatic primary amines, appear in the same region. The additional weak band at 1560 cm^{-1} can be attributed to the NH bend and the weak band around 2930 cm^{-1} to the CH_2 stretch from the alkyl chain present in the aminopropyl silane. In the spectra of the silica containing the immobilized initiator we observed a new band at 1725 cm^{-1} assigned to C=O stretch from carboxyl acid and 1650 cm^{-1}, 1560 cm^{-1} corresponding to the, C=O and N-H stretches of the amide bond formed by coupling ACPA to the amino modified silica and the intensity of the broad band between 3700-3200 cm^{-1} was slightly increased compared to amino modified silica, as expected for hydroxyl groups of the carboxylic acid.

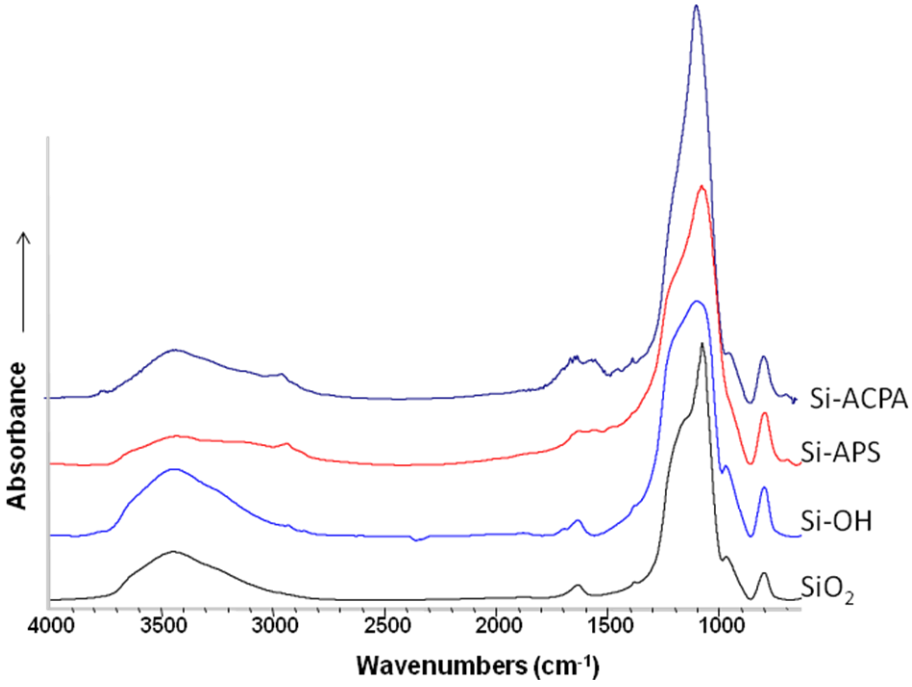

Figure 4.2 FT-IR spectra of Si-ACPA initiator and corresponding intermediate step such as bare silica SiO_2- before (SiO_2) and after rehydroxylation (Si-OH), and after modification with APTS (Si-NH2).

4.2.7 Composites prepared by grafting from techniques

Due to the limitations of the kinetically controlled grafting (poor reproducibility, low overall yields, nonstoichiometric monomer incorporation, film heterogeneity) protocols relying on quantitative monomer conversions are expected to offer general improvements.[81] An obvious approach is here to simply adjust the addition of monomer assuming it to be fully incorporated in the grafted film. A theoretical film thickness can then be calculated based on the assumption that the added monomer will form a liquid film covering the entire surface of the support. Therefore, imprinted copolymers of methacrylic acid and ethyleneglycol dimethacrylate were grafted from the supports under similar conditions following the protocols outlined in Figure 4.1. The quantity of monomer relative to the silica support was adjusted to result in films with approximately 1, 2 and 3nm average thickness followed by photoinitiated grafting at five different dilutions with inert solvent toluene (Figure 4.3).

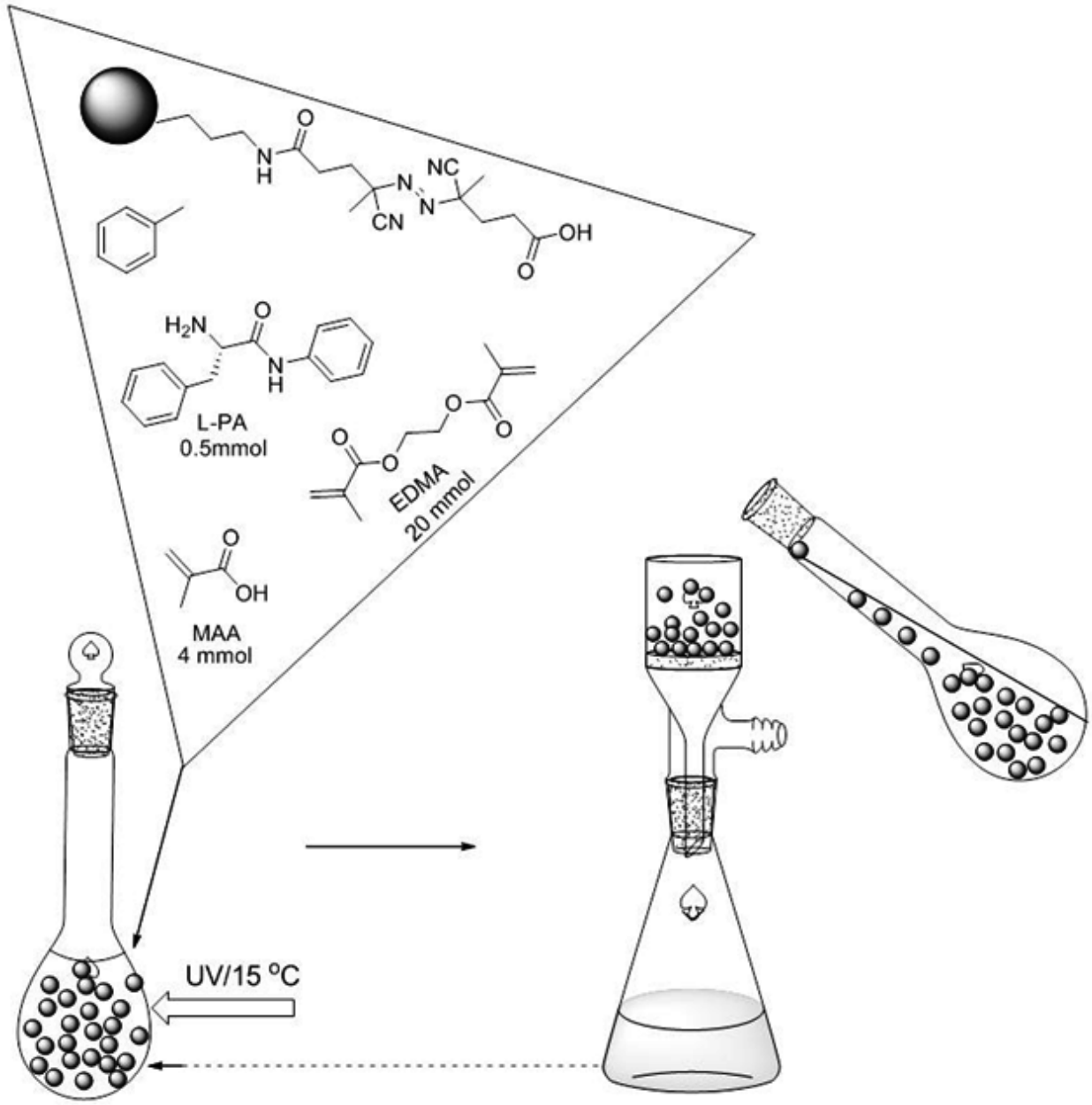

Figure 4.3 Protocol for grafting of imprinted polymer layers on support materials with recycling of monomer solution.

4.2.8 Characterization of grafted polymer layers

After polymerization, the particles were subjected to extensive extraction with acidified methanol, dried and subsequently characterised by elemental microanalysis, FT-IR, SEM, N_2 sorption and fluorescence microscopy

Table 4.2 Characteristics of molecularly imprinted polymer composites prepared by photoinitiated grafting to full monomer conversion from silica modified with azoinitiator.

Targeted Film thickness	Solvent mL	%C	%N	Mass loss (%)	S_A (m^2/g)	V_p (mL/g)	D_p (nm)	d (TGA) (nm)	d (%C) nm	Conversion (%)
d=1 nm	0	22.47	2.56	35.74	211	0.3	3.71	0.67	0.72	79
	5	22.89	2.4	36.26	336	0.5	4.12	0.69	0.75	82
	10	20.72	2.52	33.49	236	0.4	4.13	0.56	0.58	68
	15	21.37	2.49	33.86	239	0.4	4.14	0.58	0.63	70
	20	20.55	2.52	32.78	243	0.4	4.14	0.53	0.56	64
d=2 nm	0	28.56	2.15	45.29	44	0.06	3.70	1.23	1.3	76
	5	28.24	2.08	44.24	125	0.17	3.49	1.16	1.26	72
	10	26.94	2.16	43.67	180	0.21	3.70	1.12	1.13	70
	15	25.92	2.24	42.37	163	0.24	4.11	1.03	1.03	66
	20	24.61	2.33	39.81	174	0.27	4.11	0.88	0.91	57
d=3 nm	0	11.50	3.23	19.13	174	0.60	10.22	0.06	0	3
	5	31.03	1.72	50.84	130	0.14	3.69	1.70	1.6	75
	10	31.26	1.72	53.14	159	0.16	3.69	1.95	1.62	83
	15	28.91	1.82	48.55	206	0.19	3.68	1.49	1.34	68
	20	26.52	1.98	45.91	214	0.25	3.70	1.28	1.12	60

Where,

S_A = Specific surface area

V_p= Specific pore volume

D_p= Average pore diameter

The calculation of the film thickness *d* (nm) was performed assuming a homogeneous grafted layer as follows.

From elemental analysis: (%C)[94]

$$d = \frac{m_c \times M_w}{M_c \times \rho \times S} \times 10^3 \qquad (4)$$

$$m_c = \frac{\%C}{100 - \left(\frac{\%C \times M_w}{M_c}\right)} \qquad (5)$$

where m_c = weight of carbon of the grafted polymer per gram of bare silica support, M_w = weighted average molecular weight of the grafted polymer assuming stoichiometric incorporation of reactive monomers, M_C = weighted average molecular weight of the carbon fraction of the grafted polymer, ρ= weighted average density of monomers (g mL^{-1}) and S = specific surface area of the bare silica support (m^2g^{-1}).

The value used for the % C in these calculations took in account the incorporation of monomer and cross linker for grafted polymer layer.

From Thermogravimetric analysis (TGA) (% mass loss)[180]

$$d = \frac{dp}{2}\left\{1 - \sqrt{1 - \left[\frac{\%\, wt.loss}{(100 - \%wt.loss)VpX\rho}\right]}\right\} \qquad (6)$$

Where

dp= pore diameter of the composites

V_p= pore volume of the composites

ρ= density of the polymer

In these calculations percentage mass loss of azo initiator was not considered which means subtracted from the total composite mass loss.

As seen in Table 4.2 all parameters indicated successful formation of grafted films with an average thickness and density roughly proportional to the quantity of added monomer. Hence, the carbon content increased (Figure 4.4A) with added monomers but the carbon content was decreased with dilution. It indicates that the monomer conversion was decreased with dilution due to the slower polymer kinetics (Table 4.2) whereas the nitrogen content, given the lack of nitrogen in the grafted film, showed a decrease with added monomer (Figure 4.4B). The average thickness of the grafted MIP layer was calculated from elemental analysis data and thermogravimetry analysis, assuming a homogeneous grafted layer according to the equations (4) and (6). Estimates of film thickness based on gravimetric results correlated well with the nominal thickness although the former values were systematically ca 50% lower (Figure 4.6). An explanation is that chains also propagate and terminate in solution and remain nonattached to the support. Nonattached polymer could indeed be observed in the SEM images of the composites (Figure 4.8). Although no pronounced effect of dilution on the compositional parameters was seen a strong impact on the pore system parameters from nitrogen sorption was observed (Figure 4.7). The composites prepared under high dilution displayed somewhat lower graft densities and higher pore volumes but were similar with respect to the transmission FTIR spectra in Figure 4-9.

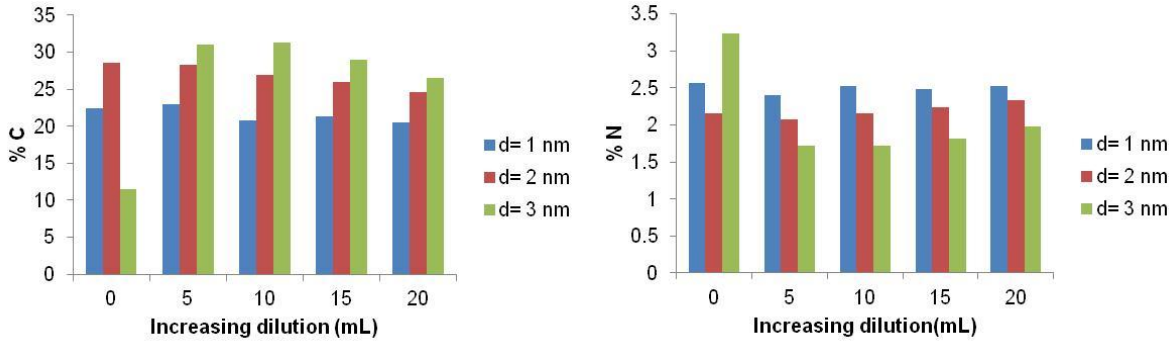

A B

Figure 4.4 Elemental composition of the imprinted composite beads tuned to 1 (blue bars), 2 (red bars) or 3 (green bars) nm film thickness, prepared under different dilutions with toluene.

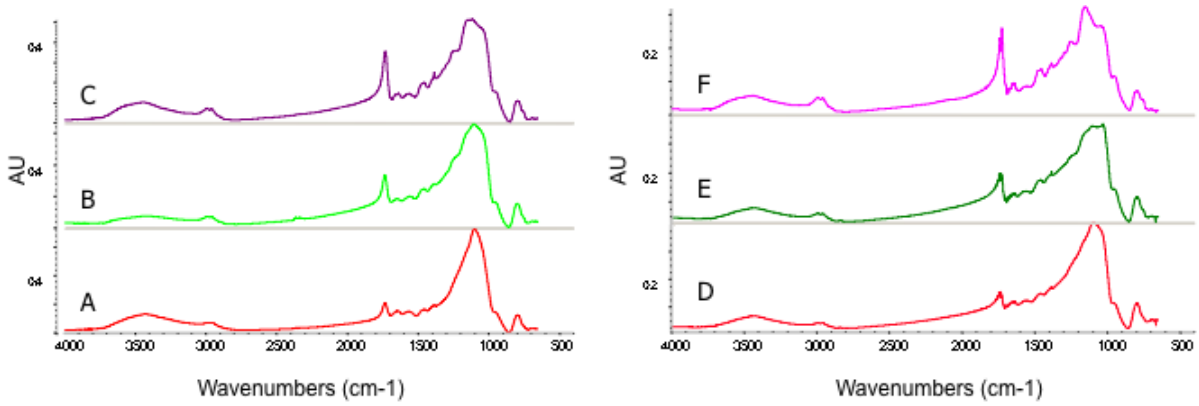

Figure 4.5 FT-IR transmission spectra (KBr) of imprinted composites prepared using azoinitiator modified silicas (A) $SiPA_{20}^{1}$, (B) $SiPA_{20}^{2}$, (C) $SiPA_{20}^{3}$, (D) $SiPA_{5}^{1}$, (E) $SiPA_{5}^{2}$ and (F) $SiPA_{5}^{3}$

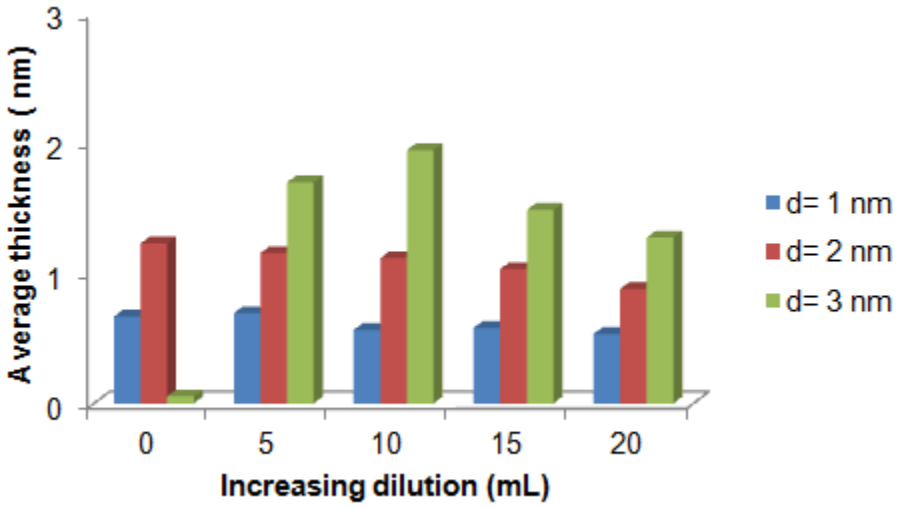

Figure 4.6 Thickness of grafted polymer films calculated based on the mass loss obtained by TGA. for composites with film thickness adjusted to 1, 2 or 3 nm thickness prepared under different dilutions with toluene.

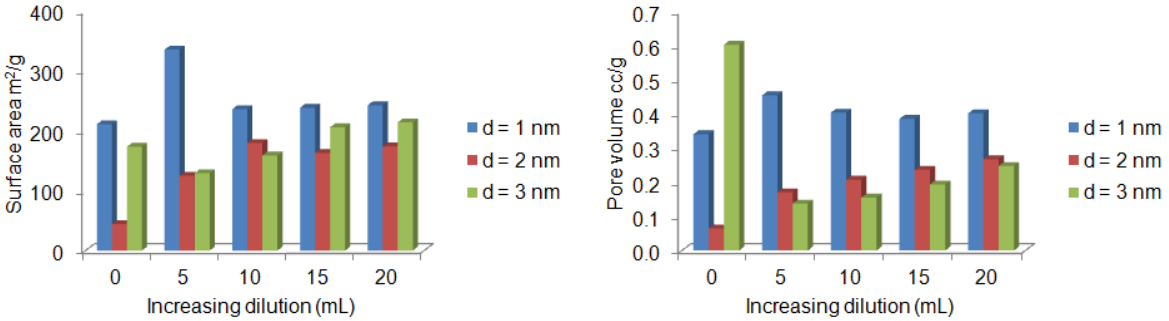

Figure 4.7 Pore system parameters from BET for the composites with films adjusted to 1 nm, 2 nm and 3 nm thickness prepared under different dilutions with toluene.

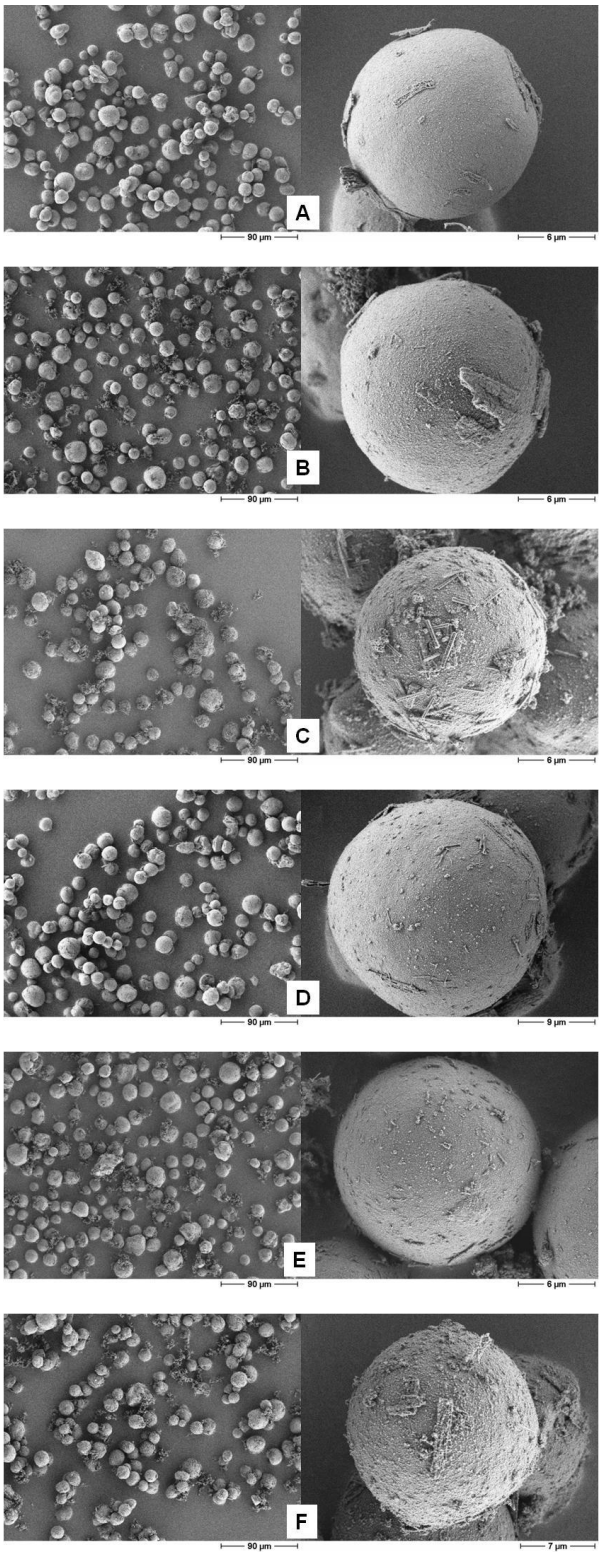

Figure 4.8 Scanning electron micrographs of imprinted composites (A) $SiPA_{10}^{1}$, (B) $SiPA_{10}^{2}$, (C) $SiPA_{10}^{3}$, (D) $SiPA_{20}^{1}$, (E) $SiPA_{20}^{2}$ and (F) $SiPA_{20}^{3}$

4.2.9 Characterisation of composite beads in chromatographic mode

The particles were slurry packed into HPLC columns and evaluated in a mobile phase with a high water content MeCN/ sodium acetate buffer, 0.01M, pH 4.8: 70/30 (v/v) for their ability to resolve and separate the enantiomers of the racemate of the template (L/D-PA). The resulting elution profiles were evaluated with respect to the retention of the two enantiomers, determined as the retention factor (k) and the enantioselectivity, determined as the separation factor (α=kL/kD). The chromatographic efficiency and separation factors obtained using the composite particles prepared with three different film thicknesses such as 1 nm, 2 nm, 3nm and five different dilutions as 0mL, 5mL, 10mL, 15mL, 20mL. These three systems with different dilution compared**.** For respective data obtained upon analysis of the films see in Table 4.3.

Table 4.3 Characterisation of the materials in chromatographic mode using sodium acetate buffer/acetonitrile as mobile phase (30/70, v/v).

Targeted Film thickness	Porogen mL	Capacity factor (k_L)			Separation factor(α)		
		0,05mM	0,5mM	5mM	0,05mM	0,5mM	5mM
d=1 nm	0	0.55	0.41	0.34	1.35	1.18	1.04
	5	0.6	1.15	0.66	0.89	1.59	1.12
	10	1.63	0.73	0.52	2.36	1.29	1.06
	15	3	1.44	0.96	2.37	1.33	1.07
	20	3.09	1.51	1.04	2.23	1.29	1.06
d=2 nm	0	0.012	-0.05	-0.04	-0.51	1.4	0.77
	5	0.4	0.21	0.11	1.83	1.28	1.05
	10	1.85	0.55	0.19	7.4	2.77	1.59
	15	33.16	4.38	1.4	14.23	2.68	1.31
	20	8.06	4.43	1.7	3.28	2.25	1.19
d= 3nm	0	-0.08	-0.07	-0.06	0.94	0.99	0.98
	5	0.67	0.36	0.21	1.75	1.21	1.06
	10	>20	3.02	0.7	>20	3.13	1.32
	15	>20	3.27	0.83	>20	3.13	1.36
	20	>20	12.48	2.61	>20	4.71	1.57

A B

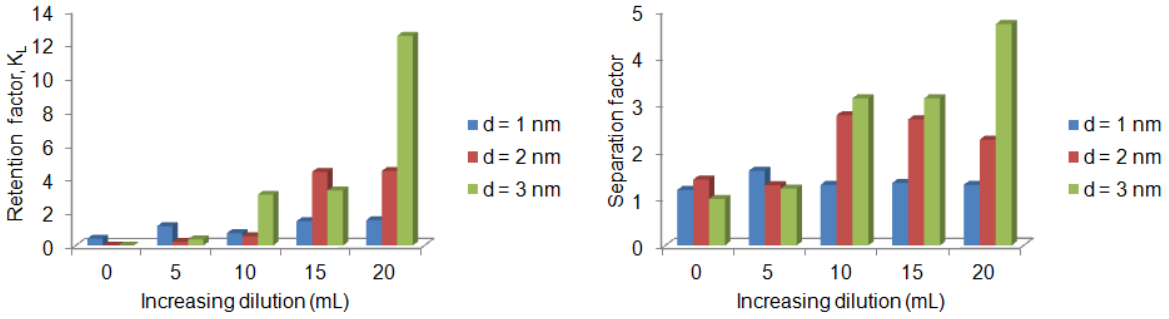

Figure 4.9 Plot of retention factors (k) for L-PA (A) or enantiomer separation factors (B) for composites with films adjusted to 1, 2 or 3 nm thickness prepared under different dilutions with toluene. Mobile phase: MeCN/ acetate buffer pH 4.8:70/30 (v/v).

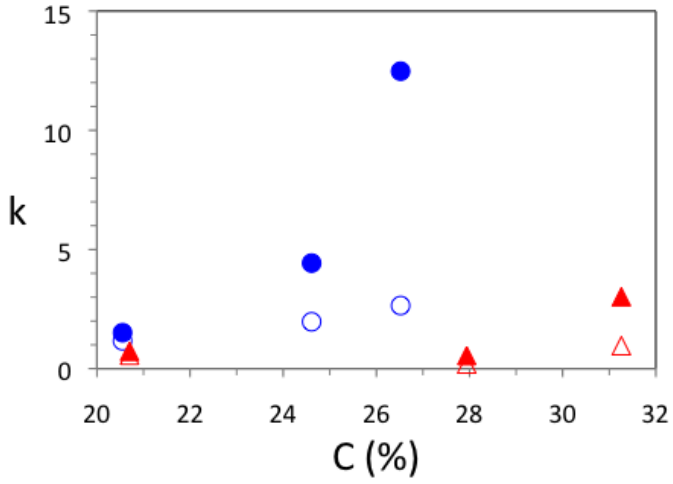

Figure 4.10 Plot of retention factors (k) for L-PA (solid symbols) and D-PA (open symbols) versus carbon content (%C) for $SiPA_{20}$ (blue circles) and the $SiPA_5$ (red triangles) series composites. Mobile phase: MeCN/ acetate buffer pH 4.8:70/30 (v/v).

Figure 4.9 summaries the results from Table 4.3 for 0.5mM loading of target molecule with the respective analogue. The dilution did however strongly influence the chromatographic properties of the composites.

Figure 4.10 shows the retention factor versus graft density for the composites reported in Table 4.2. Composites prepared from concentrated monomer solution feature much lower retention

factors and enantioselectivities compared to the composites prepared in the dilute system, this in spite of the higher carbon content of the former. A low dilution corresponds to a high monomer and subsequent radical concentration, an increased rate of propagation, and potential film in-homogeneities due to diffusion limited reactions. This may also cause unwanted macrogelation and blocking of pores – an indication for this trend is the low pore volume and surface area obtained for the thicker films prepared from more concentrated monomer solutions (Table 4.2). At higher dilutions on the other hand the rate of propagation will be lower but this will in turn give the monomers more time to diffuse into the pore system of the beads. The qualities of the resulting films are likely to be higher. Counteracting this effect is the dilution effect on the monomer – template complex stability. A more dilute system will promote dissociation of the complex but given that the solvent promotes complex formation this effect may be negligible. In this particular case the favorable factors seem to outweigh the latter. The typical chromatographs are shown in Figure 4.11.

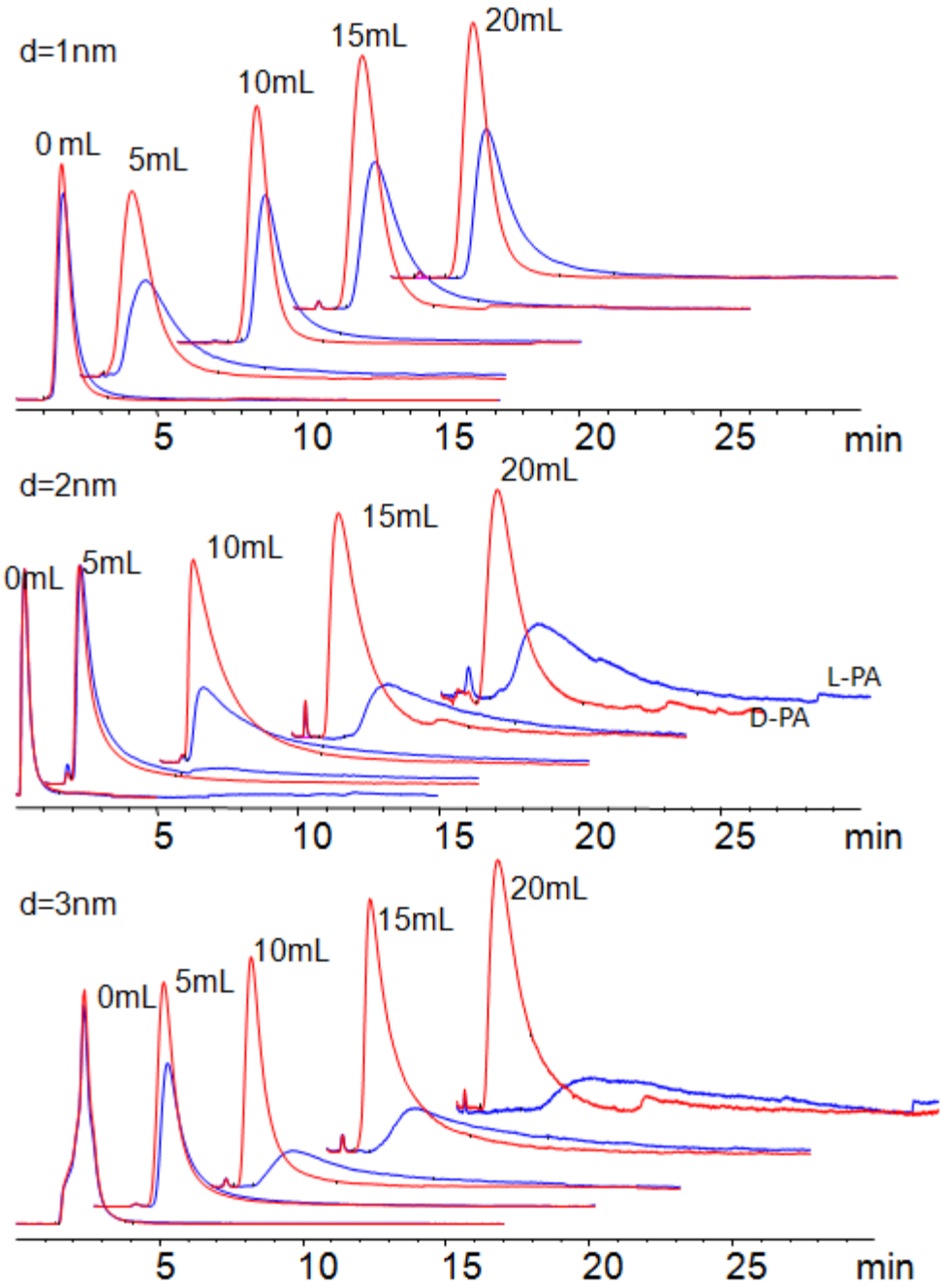

Figure 4.11 Chromatogramms obtained by separate injection of(10µL of 0.5mM) D-PA (red traces) and L-PA (blue traces) on columns (35mm X 4.6 mm) packed with the indicated materials. Mobile phase: MeCN/sodium acetate buffer 0.01M pH 4.8: 70/30 (v/v).

4.2.10 Fluorescence labeling

The enhanced binding site accessibility anticipated for the composite prepared under more dilute conditions was further confirmed from labeling experiments (Scheme 6).

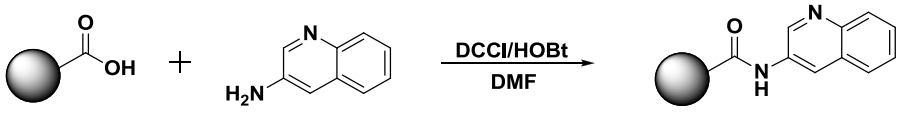

Scheme 6 Labelling of COOH groups with 3-aminoquinoline

Table 4.4 Coupling of Fluorescent Label for high dilution system (20mL) composites

Film thickness	%C Before 3-AQ	%C After 3-AQ	%N Before 3-AQ	%N After 3-AQ	Load %C mmol/g	Load %N mmol/g	Coupling yield (%)
d=1nm	20.55	21.96	2.52	2.56	0.099	0.0143	47
d=3nm	26.52	28.15	1.98	2.25	0.16	0.097	43

These experiments rely on covalent coupling of a fluorescent probe 3-aminoquinoline (3-AQ) to the functional carboxylic acid groups of the polymers. Thereafter, materials were characterized in qualitative terms from fluorescence microscope images and quantitative terms based on the increase in carbon and nitrogen content upon coupling. Higher film thickness composites exhibited a stronger and more uniform fluorescence intensity compared to the lower film thickness composite materials (Figure 4.12). As seen in Table 4.4, for thickwalled composite (d=3nm) 0.16 mmol/g of the carboxylic acid were converted whereas the degree of conversion was lower for the thin walled materials (d=1nm, 0.09 mmol/g). Possibly the latter is due to collaps of the pore structure under the reaction conditions used to perform the labeling.

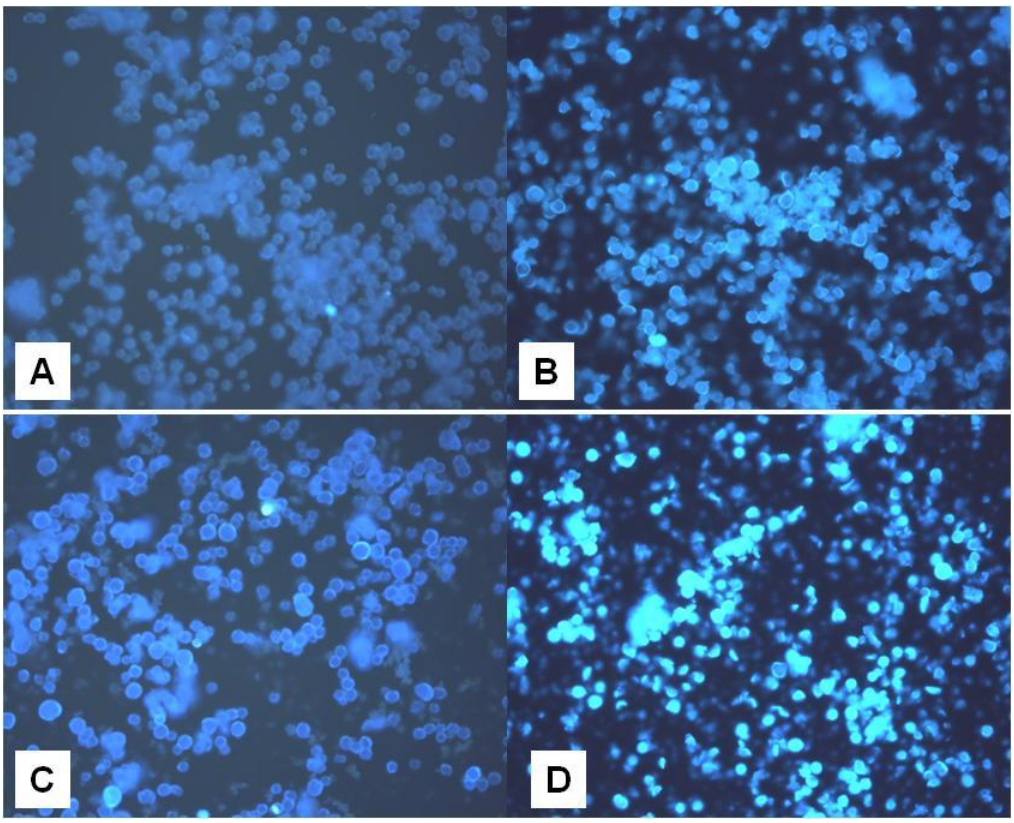

Figure 4.12 Fluorescence micrographs (20 X magnification) of (A) SiPA201 ,(C) SiPA203 before coupling with 3-aminoquinoline and (B) SiPA201 ,(D) SiPA203 after coupling with 3-aminoquinoline.

4.2.11 Grafting of molecularly imprinted polymers via RAFT modified silica support

In recent years the use of surface initiated controlled radical polymerization (CRP) has proven to be the most versatile approach for producing a wide range of polymer chains on solid surface.[82,181] By using this technique, one can manipulate the structure of the resultant polymer through changes in grafting density, composition, molar mass and functionality. In general surface initiated CRP can be achieved by stable free-radical polymerization, e.g. nitroxide-mediated processes (NMP), metal catalyzed atom transfer radical polymerization (ATRP) and degenerative transfer, e.g. Reversible Addition-Fragmentation chain Transfer (RAFT). Recently, significant interest has been shown in the use of surface initiated CRP for the preparation of MIP composites[106] (see section 2.6). The presented work explores the use of surface initiated RAFT polymerization technique to functionalize silica gel with molecularly imprinted polymer films.

The RAFT agents were directly immobilized on the surface of silica gel and polymerized inside the pore. The resulting thin film MIP composite beads were used as stationary phase in HPLC.

4.2.12 Synthesis and characterization of RAFT modified silica particles

Prior to the first modification step, the silica surface was rehydroxylated according to standard procedures described previously (see above section 4.2.), resulting in a maximum density of free silanol groups of *ca*. 8µmol/m². The yield of coupling in each step was calculated based on results obtained from elemental microanalysis (Table 4.5). At maximum half of the silanol groups reacted with (3-aminopropyl) triethoxysilane (APS) in the first silanization step. The subsequent step was the coupling of 4-cyanopentanoic acid dithiobenzoate as CTA by ethylachloroformate catalyzed (Scheme 7). On the basis of the increase in carbon content, a maximum converage of 7.6% coupled CTA for Si100 support and 27% for the support Si500 was calculated. The distance between two ligands was 1.7 for Si100 support and 0.9 nm for Si500 which is likely higher than the first step. This indicates that the coupling reaction was successfully formed.

Table 4.5 Characterisation of the RAFT modified silica supports used for grafting.

Modified support[a]	%C	%N	%S	Area density[b] (µmol/m^2)	TGA (% mass loss)	Area density[c] (µmol/m^2)	Coverage[d] (%)	Distance[d] (nm)
Si100-APS	3.96	1.38	-	1.25	8	1.23	16	1.2
Si100-RAFT	6.83	1.36	1.01	0.61	14	0.72	7.6	1.7
Si500-APS	1.80	0.80	-	5.82	3	3.84	73	0.5
Si500-RAFT	3.28	0.76	0.56	2.17	7	3.32	27	0.9

a) The immobilizations were performed in two steps by consecutive coupling of 3-aminopropyltriethoxy silane (APS) and 4-cyanopentanoic acid dithiobenzoate (RAFT agent) on Si100 silica beads and the

modified supports analyzed by elemental analysis and thermal gravimetric analysis (TGA). The Si100 silica beads (15µm average particle size) were mesoporous with a surface area (S_A) of 320m^2/g(After treatment with 17% HCl); an average pore diameter (D_p) of 11.6 nm and an pore volume (V_p) of 1.28mL/g whereas the Si500 beads (30µm average particle size) displayed a surface area (S_A) of 45m^2/g; an average pore diameter (D_p) of 48nm and an pore volume (V_p) of 0.81mL/g.

b) The area density (D) was calculated from the increase in carbon after the corresponding coupling as described in section 4.2.6.

c) The area density (D) was calculated from the mass loss as described in 7.4.1

d) The coverage (C) and the average distance d_L (nm) between the coupled ligands were calculated as described in 4.2.6

Each step of coupling was monitored by elemental analysis as well as TGA. The percentage mass loss and percentage of carbon increased with each step respectively. The area density of coupled ligand was calculated by two methods. The obtained results are in good agreement (Table 4.5).

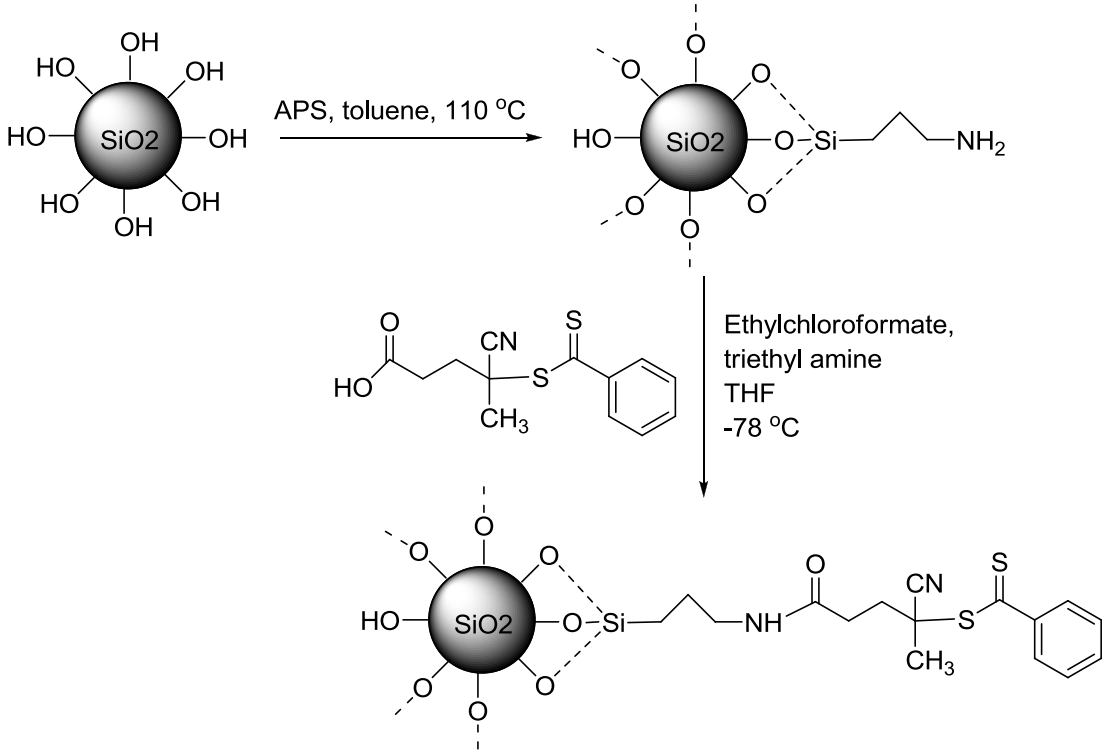

Scheme 7 Immobilization of RAFT agent on silica surface.

4.2.13 Polymer Grafting and composite characterization

Addition of a propagating radical to the dithioester will generate a tertiary carbon centered radical identical to the one resulting from photolysis of the azomodified silica. Hence external addition of soluble initiator is here required. Adjusting the quantity of soluble initiator in relation to the immobilized RAFT agent offers a simple way of controlling the kinetics of the grafting.

Thermally initiated grafting was therefore performed on two different RAFT modified silica supports from a dilute prepolymerization mixture (vide supra), tuned to generate thicker films with 3-4nm average thickness, in presence of different amounts of ABDV corresponding to the molar ratios of RAFT/ABDV given in Table 4.6.

Table 4.6 Characteristics of molecularly imprinted polymer composites prepared by thermally initiated grafting to high monomer conversion from silica modified with RAFT agent.

Composite[a]	Support	RAFT/ ABDV	%C	%N	Mass loss (%)	S_A[b] (m^2/g)[b]	D_p[b] (nm)[b]	V_p[b] (mL/g)[b]	Conversion[c] (%) [c]
SiPR	Si100-RAFT	0.5	32.1	0.85	56	207	4.1	0.25	70
$SiPR_E$	Si100-RAFT	2.0	31.7	0.81	56	260	3.7	0.33	70
$SiPR^{500}$	Si500-RAFT	0.3	11.0	0.72	17	68	32	0.39	60
$SiPR_E^{500}$	Si500-RAFT	1.4	10.6	0.74	19	72	32	0.35	73
$SiPR_{EE}^{500}$	Si500-RAFT	14	12.7	0.99	20	57	24	0.31	74

a) The composites were prepared by thermally initiated grafting to high monomer conversion from different silica supports modified with RAFT agent using different ratios of RAFT agent to azoinitiator (ABDV).

b) The BET specific surface area (S_A), specific pore volume (V_p) and average pore diameter (d_p) were calculated from the nitrogen adsorption isotherms as described in the experimental part.

c) Monomers converted into grafted polymer (%) calculated based on thermogravimetry assuming a contribution to the mass loss from the initiator modified silica's as specified in Table 4.5.

The presence of the RAFT dithioester groups post grafting was indicated by the characteristic pinkish color (Figure 4.13) which was of similar intensity as prior to grafting.

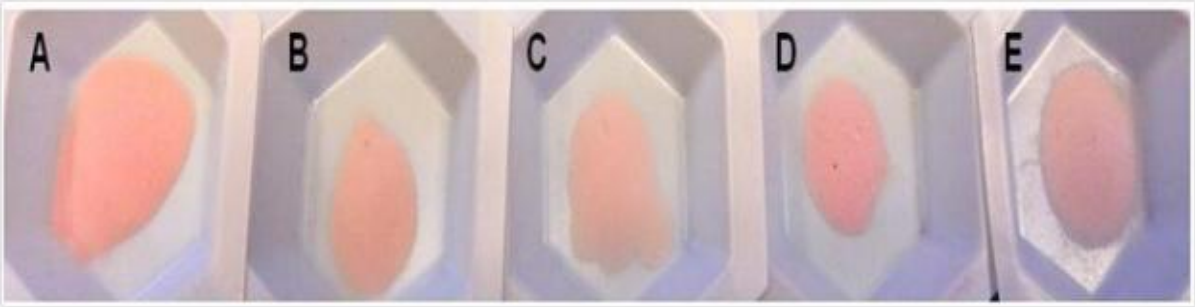

Figure 4.13 Picture of imprinted composite RAFT (A) Si-500 RAFT agent (B) $SiPR^{500}$ (C) $SiPR_E^{500}$ (D) SiPR (E) PR (after etching).

Scanning electron micrographs (Figure 4.14) indicate the successful formation of the graft polymer inside the pores. No agglomeration is observed also in the case of smaller particles; neverthless polymer chains are grown on the surface. This might be the propagating chains terminated at high radical concentration and other reason was diffusion limitation of monomers at smaller particles. This is not the case for bigger size particles even at high concentration of radical initiator. In case of the bigger sized particles the pores are easily accessible and diffusible to monomers.

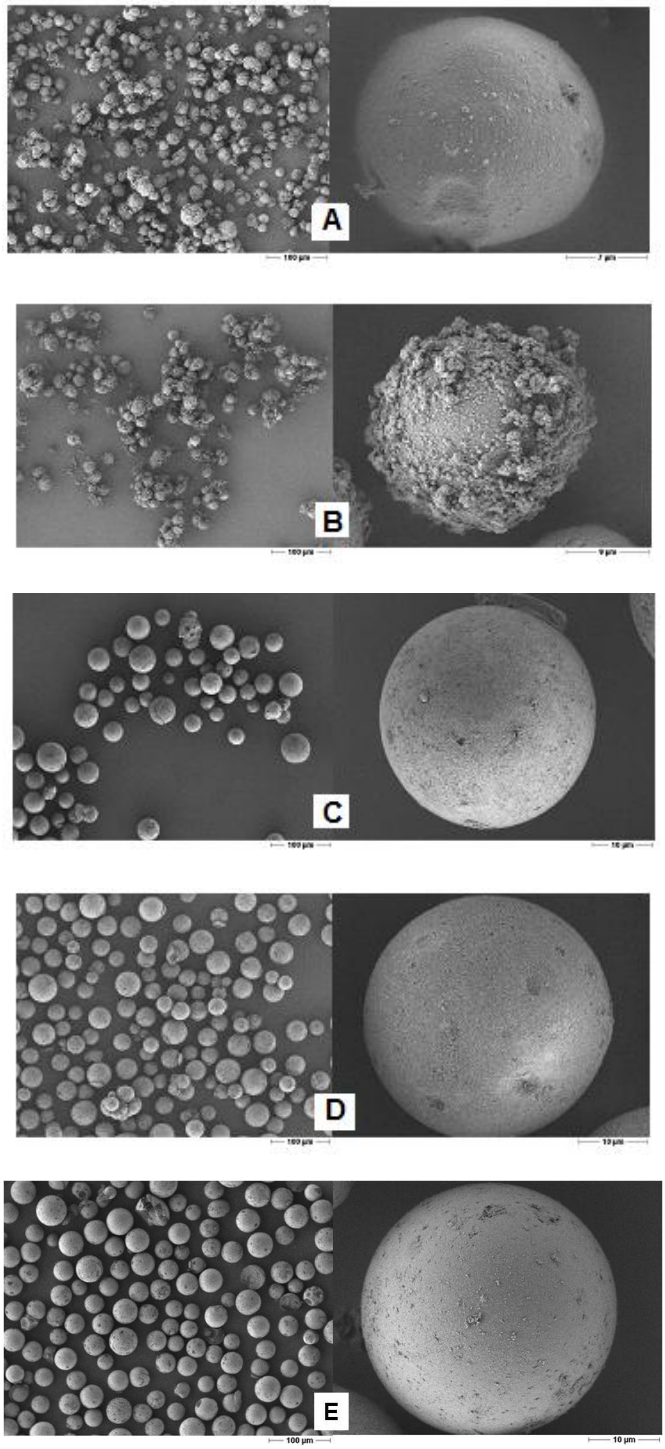

Figure 4.14 Scanning electron micrographs of imprinted composites (A) SiPR, (B) $SiPR_E$, (C) $SiPR^{500}$ and (D) $SiPR_E^{500}$ (E) $SiPR_{EE}^{500}$ at two magnifications.

Additional evidence for the grafted polymer films was obtained by nitrogen sorption analysis and % mass loss by TGA. Nitrogen sorption isotherms display type IV hysteresis loop Figure 4.15 which means that the composites still exhibits the mesoporous morphology. The average pore diameters of silica samples were evaluated using the BJH theory. Figure 4.15 shows the pore size distribution of the amino silica gel and MIP-Silica. The presence of homogeneously grafted MIP films is obvious from the similar widths of the pore size distribution of the RAFT silica gel and MIP-Silica.

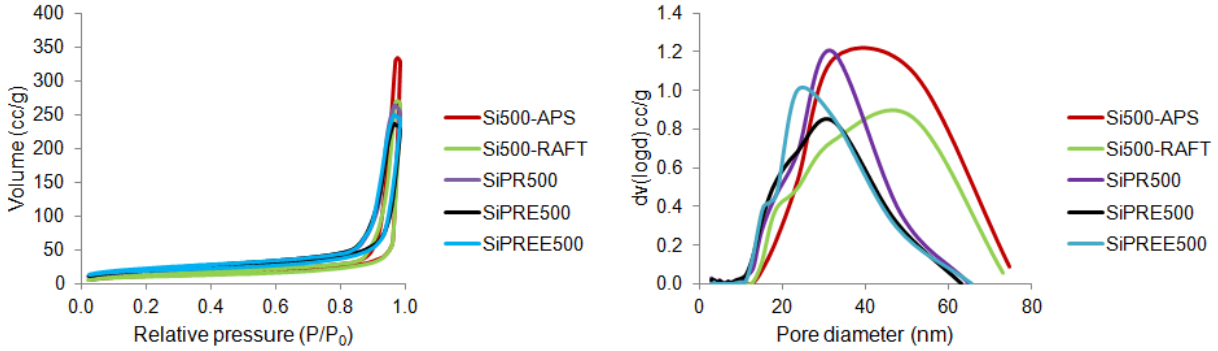

Figure 4.15 Nitrogen sorption isotherm (A), and pore size distribution (B) of respective imprinted RAFT composites beads.

4.2.14 Chromatographic evaluation

The resultant composite beads were packed in to stainless steel columns and investigated by liquid chromatography for their ability to retain L-PA and its optical antipode D-PA using MeCN as mobile phase. As can seen from Figure 4.16, at lower concentration of RAFT/ABDV ratio display the inferior retentivity and enantioselectivity in both kinds of silica support due to the higher concentration of radical initiator makes polymerization kinetics faster and possibly propagate chains terminates, potential polymer film inhomogeneity. This observation is much similar to above discussed for lower dilution effect. In contrast, higher RAFT/ABDV ratio exhibits high selectivity and enantioselectivity in both supports. This is due the slower polymerization kintetics where monomer has an enough time to diffuse and to propagate the

chains and to make more uniform polymer networks. This is likely high dilution effect (vide supra) All the composites display a trend of decreasing retention and enantioselectivity with increasing sample load in agreement with previous reports. This is the result of nonlinear chromatography with constant overloading of low-abundant high energy binding sites.

In view of the similar graft conversions (Table 4.6), the reaction appears to have run to similar overall conversions, also for the elevated RAFT/ABDV ratios where propagation is expected to be significantly slower. It was then striking to observe the pronounced influence this parameter had on the retentivity and enantioselectivity of the composites (Figure 4.16). With increasing RAFT/ABDV ratio a strong increase in both retentivity and enantioselectivity was observed for both the mesoporous (Si100) and macroporous (Si500) supports. Obviously the RAFT control has a positive influence on the quality of the imprinted films in this case.

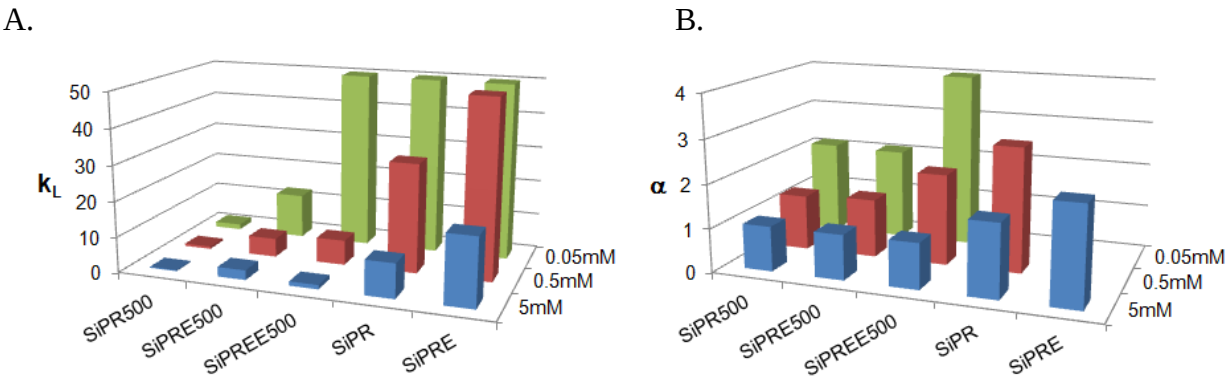

Figure 4.16 Plot of retention factors (k) for L-PA (A) and associated separation factors (α) (B) at three different sample loads for L-PA imprinted composites prepared by grafting from different RAFT modified supports. Mobile phase: MeCN.

4.3 Conclusion and outlook

In this study we compared two different techniques to graft imprinted polymers with respect to the robustness, synthetic accessibility, versatility and composite performance. Particularly interesting was the pronounced effect of monomer dilution and the RAFT/initiator ratio on the quality of the imprinted films, in terms of chromatographic retentivity and enantioselectivity.

How can these effects be rationally explained? A low dilution corresponds to a high monomer and subsequent radical concentration, an increased rate of propagation, and potential film inhomogeneities due to diffusion limited reactions. This may also cause unwanted macrogelation. At higher dilutions on the other hand the rate of propagation will be slower but this will in turn give the monomers more time to diffuse into the pore system of the beads. The quality of the resulting films is likely to be higher. Counteracting this effect is the dilution effect on the monomer – template complex stability. A more dilute system will promote dissociation of the complex but given that the solvent promotes complex formation this effect may become less important. In this particular case the favorable factors seem to outweigh the latter.

The effect of the RAFT/initiator ratio can be explained in similar terms. Referring to the previous report by Byrne et al. one can expect that an increase in the RAFT/initiator ratio will lead to a decrease in the average kinetic chain length and the dispersity of those chains.[51] This can be envisaged to result in a more homogenous distribution of crosslinks which combined with the slower propagation per se will in turn increase the accessibility and possibly produce a more uniform distribution of imprinted sites. This effect has previously been observed for imprinted amorphous network polymers (see in chapter 3), but has not been demonstrated for grafted systems. As for the dilution effects discussed above, the slower propagation will also result in a more evenly grafted film covering the entire inner surface of the particles. Significant improvements were achieved by allowing the grafting to proceed to high conversions and by introducing immobilized RAFT agents. The latter offers a fully reproducible procedure for grafting, which can be applied to both photo and thermal initiator homolysis and to different monomers and solvents ranging from nonaqueous styrene/divinylbenzene to aqueous acrylamide based systems.

5 Template synthesis of thin walled materials

5.1 Introduction

The aim of this chapter was to produce thinwalled beads with high binding capacity, uniform binding sites with better accessibility compared to previously described composite MIPs. The concepts of template synthesis allow the design of nanoscale porous materials with different morphologies[128,182,183](See in section 2.7). Templated synthesis materials involve either an organic polymer may serving as a shape template for the synthesis of an inorganic porous network or alternatively an inorganic material serving as template for the synthesis of organic materials of defined morphology.[128,184] In the latter, porous silica has been used as a sacrificial template for the synthesis of mesoporous organic polymer networks.[132] Templating at a molecular level is referred to as molecular imprinting where the shape and functionality of individual molecules are molded into a network polymer.[185,3] This approach has been used to generate porous materials exhibiting receptor-like affinity for a large variety of template structures.[185,1,186] One recurring problem in the development of a new molecularly imprinted polymer (MIP) is the incompatibility between conditions that are optimal to generate the templated binding sites at a molecular level with those leading to the desirable format or morphology at the nano- or microscopic level, *i.e.* particle and pore sizes, surface areas and swelling properties.[80]

In order to circumvent these problems imprinting techniques relying on either grafting or so called "hierarchical imprinting" have been developed (see in section 2.7).[27,89,94,132,187] For instance, the "grafting from" technique has been used by several research groups to graft imprinted polymer layers on various substrates.[127,167] Recently, we assessed the relative merits of the different grafting techniques for producing imprinted thin film composite materials.[81] This led to the conclusion that azoinitiated polymerizations that were allowed to proceed to high conversion under dilute conditions or in presence of an excess of chain transfer agents (RAFT) resulted in films with an enhanced homogeneity and template binding affinity. Hierarchical imprinting on the other hand takes advantage of the morphology control offered by template synthesis. Imprinted polymer beads obtained from hierarchical imprinting exhibits a molecular recognition property combined with a predefined and unique morphology. Porous silica is used

as a mold in order to control the particle size, shape and porosity of the resulting imprinted polymer.[132] The template can either be immobilized to the walls of the mold or the template can be simply dissolved in the monomer mixture.

In this work the combination of the two approaches to generate a novel class of porous materials. Grafting a thin film onto a disposable support and subsequently removing the support we anticipated would leave behind a porous material with thin walls (Figure 5.1). The wall thickness will impact the stability of the framework leading to either gellike material with a collapsed structure when the walls are thin or permanently porous morphologies when the walls are sufficiently thick. In the latter case the support removal will lead to an increase in surface area impacting the saturation capacity of the materials when used for adsorption under static conditions or in chromatography. If the grafting is performed by living CRP, multiple layers may be grafted exhibiting different composition, structure and function. After removing the support the innermost layer (the first grafted layer) would be exposed within walls which thus would contain two non-equivalent surfaces In order to test whether this approach could produce such effects we have started from an identical model system used in our previous investigations.[81] This refers to poly (MAA-co-EDMA) imprinted with an enantiomerically pure template (L-phenylalanine anilide (L-PA)). Imprinting effects are here straightforwardly assessed as the ability of the materials to discriminate between the template and its optical antipode as well as their affinity for the template. L-PA imprinted polymers were thus grafted from a common silica support using an immobilized azo initiator or by CRP from RAFT modified supports. Evaluation was performed by characterising the pore structure, morphology, pore wettability and template recognition of the polymers prior to and post silica removal. Some parts of this chapter have been published as article.[80]

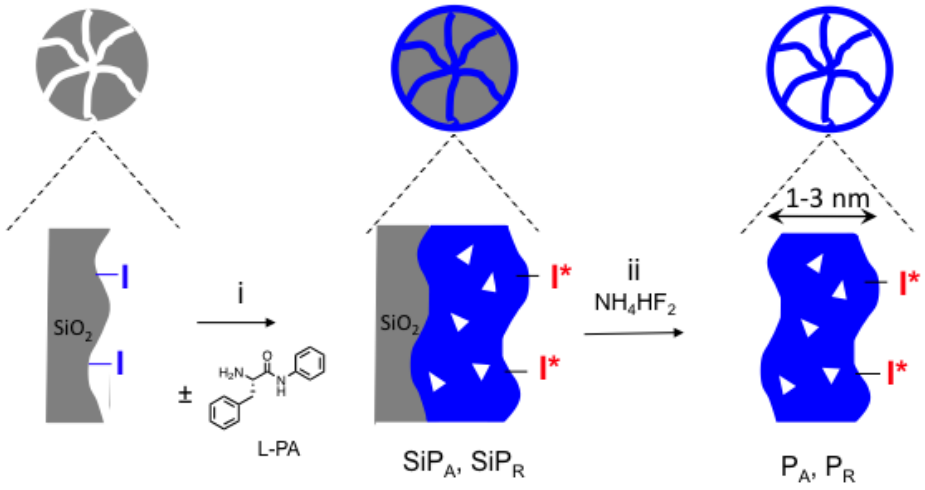

Figure 5.1 Generation of thinwalled beads from composite MIPs.[80]

5.2 Results and discussion (IIB)

5.2.1 Thin walled imprinted polymer beads generated from azoinitiator or RAFT composite MIPs.

The concept of combining the "grafting from" technique with templated synthesis of materials was investigated using two different SIP protocols that we described in our previous chapter. The first (A) starts from silica containing an immobilized azoinitiator (Si-ACPA) which can be decomposed by either thermolysis or photolysis,[87] whereas the second (R) relies on the use of a RAFT chain transfer agents immobilized to the silica surface via the R-group (Si-RAFT) (Figure 5.1).[123] Grafting of polymer from the latter requires an external source of primary radicals which is provided by addition of a soluble initiator. The azoinitiator and RAFT modified silicas were synthesised according to previously reported protocols resulting in surface coverages of initiators in accordance with our previous investigations.[81]

For comparison study of thinwalled materials and thin film composites we choose the best composites system (from chapter 4) based on HPLC performance such as 10mL, 15mL, and 20mL diluted system from azo modified. These systems showed the highest affinity for the template and an analogue. Therefore, we focused on these materials and generated polymers with nanometre thin walls as shown in Figure 5.1.

This procedure has been developed previously for hierarchical imprinting in order to generate surface confined binding sites for various target molecules.[132,187,188] Here the pore system is filled with the monomer mixture, polymerized and thereafter the silica is etched away by treatment with fluoride. This leaves behind a rigid polymer replica of the silica pore system with a narrow pore size distribution and high surface area similar to the original silica mold. In contrast to hierarchical imprinting, removal of the silica from the thin film composites would leave behind thin walled beads which integrity should depend on the thickness of the grafted films (Figure 5.2). Such uncollapsed beads would exhibit in theory twice the surface area of the original silica mold. The extent of silica removal was monitored using microelemental analysis, EDX, TGA and FT-IR spectroscopy. The percentage of carbon in the resulting polymers was very close to the theoretical value calculated considering the stoichiometry of the monomers used in the grafting step (59.2%C for MAA/EDMA). The results from the carbon analysis are given in Figure 5.2.

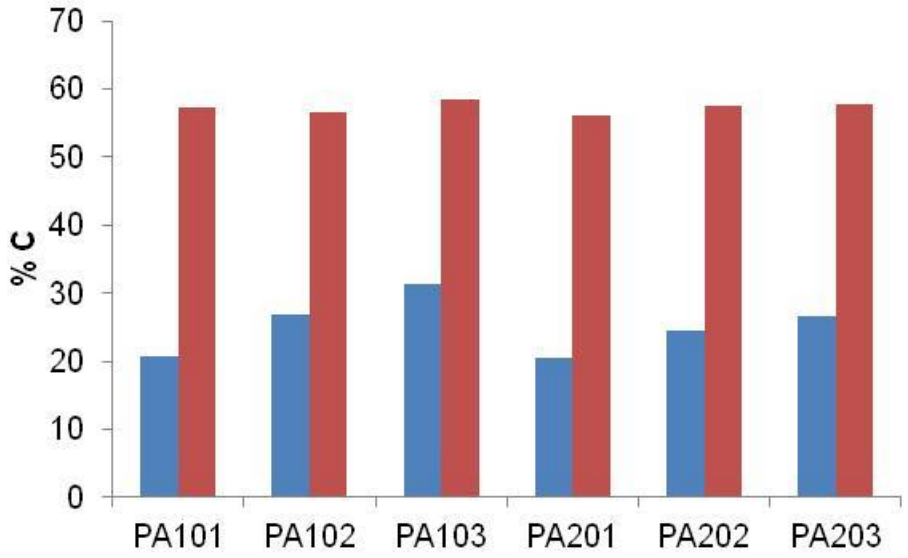

Figure 5.2 Carbon content of the composites (blue bars) and the corresponding polymers obtained after fluoride etching (red bars) listed in Table 5.1.

Table 5.1 Characteristics of molecularly imprinted polymer composites and corresponding thinwalled imprinted beads prepared by photoinitiated grafting from silica modified with azoinitiator.

Sample[a]	%C	%N	Mass loss (%)	d (nm)[b]	S_A (m^2/g) [c]	D_p (nm) [c]	V_p (mL/g) [c]
$SiPA_{10}^1$	20.7	2.52	33	1.4	236	4.1	0.40
$SiPA_{10}^2$	26.9	2.16	43	2.3	179	3.7	0.21
$SiPA_{10}^3$	31.3	1.72	53	3.1	159	3.7	0.16
$SiPA_{20}^1$	20.6	2.52	33	1.8	243	4.1	0.40
$SiPA_{20}^2$	24.6	2.33	40	2.4	174	4.1	0.27
$SiPA_{20}^3$	26.5	1.98	46	2.7	214	3.7	0.25
PA_{10}^1	57.4	0.33	97	--	21	3.9	0.04
PA_{10}^2	56.7	0.31	97	--	126	3.5	0.14
PA_{10}^3	58.5	0.19	97	--	364	5.3	0.49
PA_{20}^1	56.0	0.71	97	--	2.35	3.0	0.02
PA_{20}^2	57.6	0.48	97	--	15	3.5	0.04
PA_{20}^3	57.8	0.26	99	--	112	3.5	0.16
PA_{ref}	58.25	0.23	--	--	358	23	0.69

(a)The composites were prepared by photoinitiated grafting to full monomer conversion from silica modified with azoinitiator in a nondiluted (10ml) ($SiPA_{10}$) or diluted (20ml) ($SiPA_{20}$) system to 1, 2 or 3nm film thickness.(b)Film thickness estimated from the carbon content of the grafted film. (c)The BET specific surface area (S_A), specific pore volume (V_p) and average pore

diameter (D_p) were calculated from the nitrogen adsorption isotherms as described in the experimental part

In view of the nominal elemental composition based on the monomer ratio (60%C) it is clear from the values in Table 5.1 that the silica had been effectively removed from the polymers. The removal of the silica was further supported by the results from IR spectral analysis and TGA. The IR spectra showed dissapearence of the silica backbone bands at near 1100cm-1 and a spectrum which was essentially superimposable on the spectrum of a corresponding solution polymerized reference polymer. The intensity of the peak corresponding to the C=O group increased as compared to the one in the composite spectrum (see in Figure 5.3).The TGA showed mass losses of the etched samples of ca 95% of their weights which should correspond to the removal of ca 90% of the silica mold (Table 5.1and Figure 5.4).

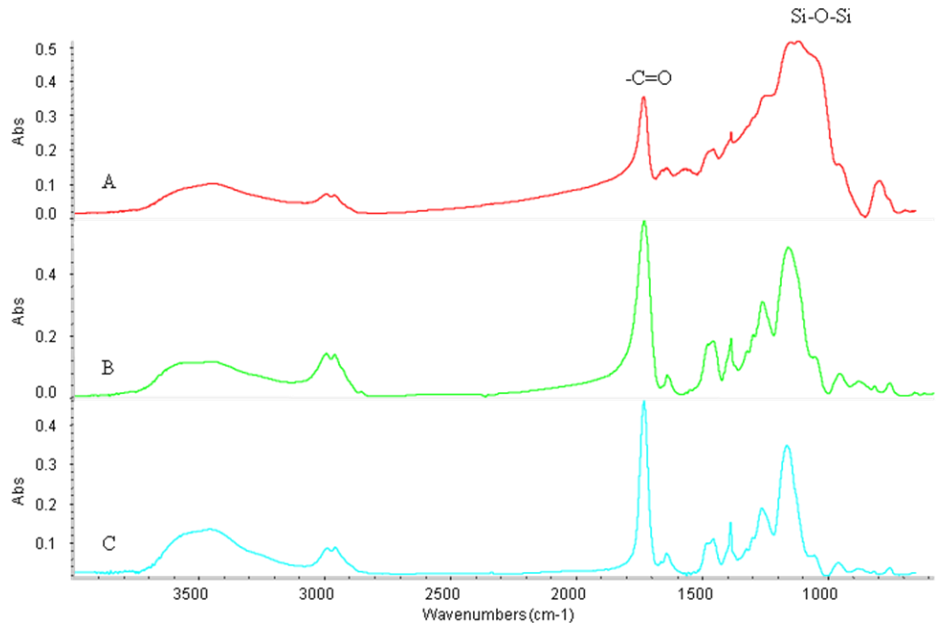

Figure 5.3 FT-IR of the composite $SiPA_{20}^{3}$ (A)and the corresponding thin-walled MIP PA_{20}^{3} (B) and bulk polymer(C).

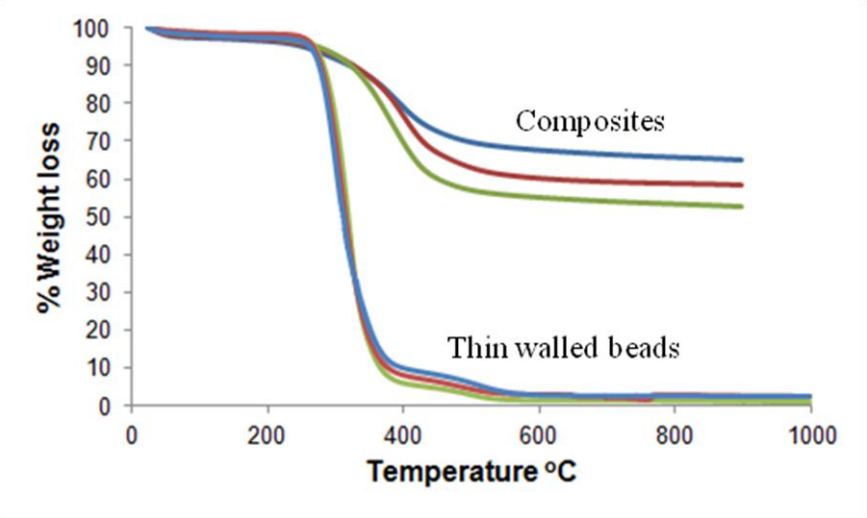

Figure 5.4 TGA of the composites $SiPA_{20}^{1}$ (blue),$SIPA_{20}^{2}$(red),$SiPA_{20}^{3}$(green) and the corresponding thin-walled imprinted polymers.

Scanning electron micrographs revealed spherical and non-agglomerated particles with a size around 5 µm, smaller than the original silica (Figure 5.5). The surface was not as smooth as for the composite particles being probably due to shrinking of the particles during the dissolution step, as was also reflected by the smaller particle sizes of the new polymers as compared to the composites.The beads resulting from the composites with the thinner films are on the average smaller than the silica beads used as a mold whereas the thicker film composites result in beads which seem to retain the size of the mold. In agreement with this observation, the close-up micrographs reveal pores on the surface of the latter beads, whereas the thinner walled beads exhibit a more compact and seemingly collapsed structure (See in Figure 5.6).

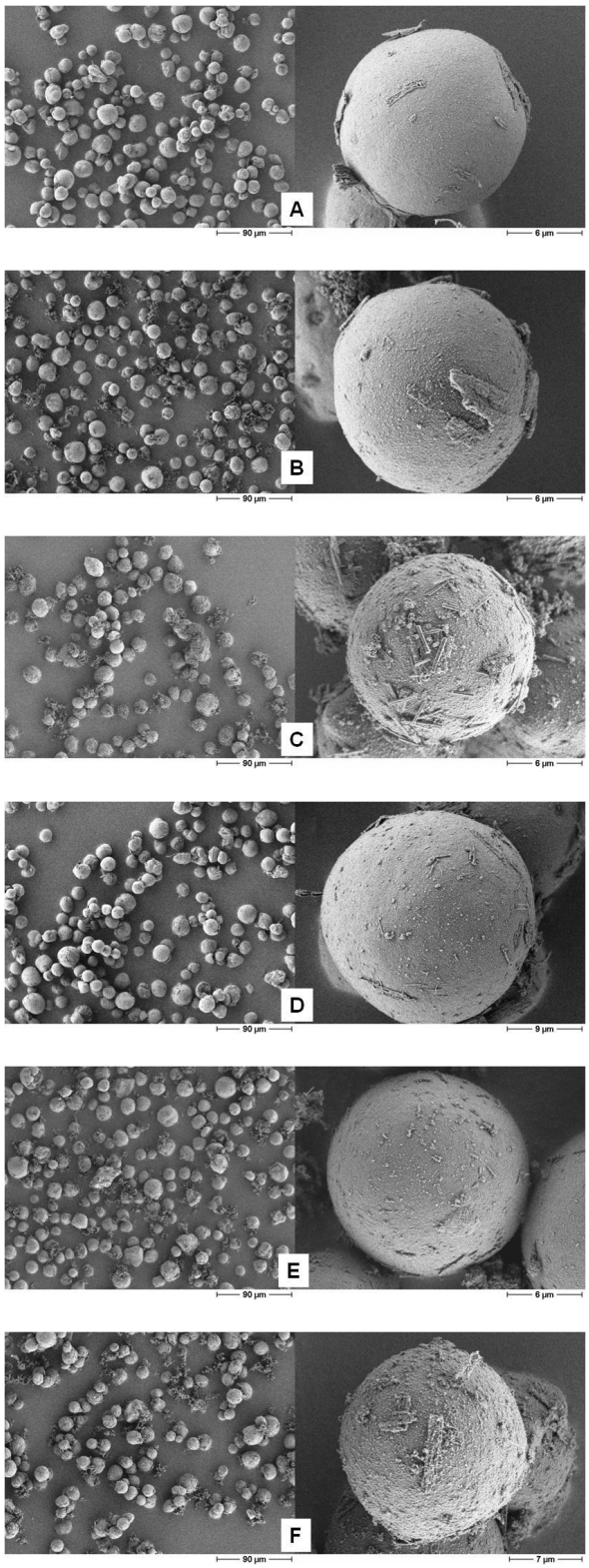

Figure 5.5 Scanning electron micrographs of imprinted composites beads (A) $SiPA_{10}^{1}$, (B) $SiPA_{10}^{2}$, (C) $SiPA_{10}^{3}$, (D) $SiPA_{20}^{1}$, (E) $SiPA_{20}^{2}$ and (F) $SiPA_{20}^{3}$

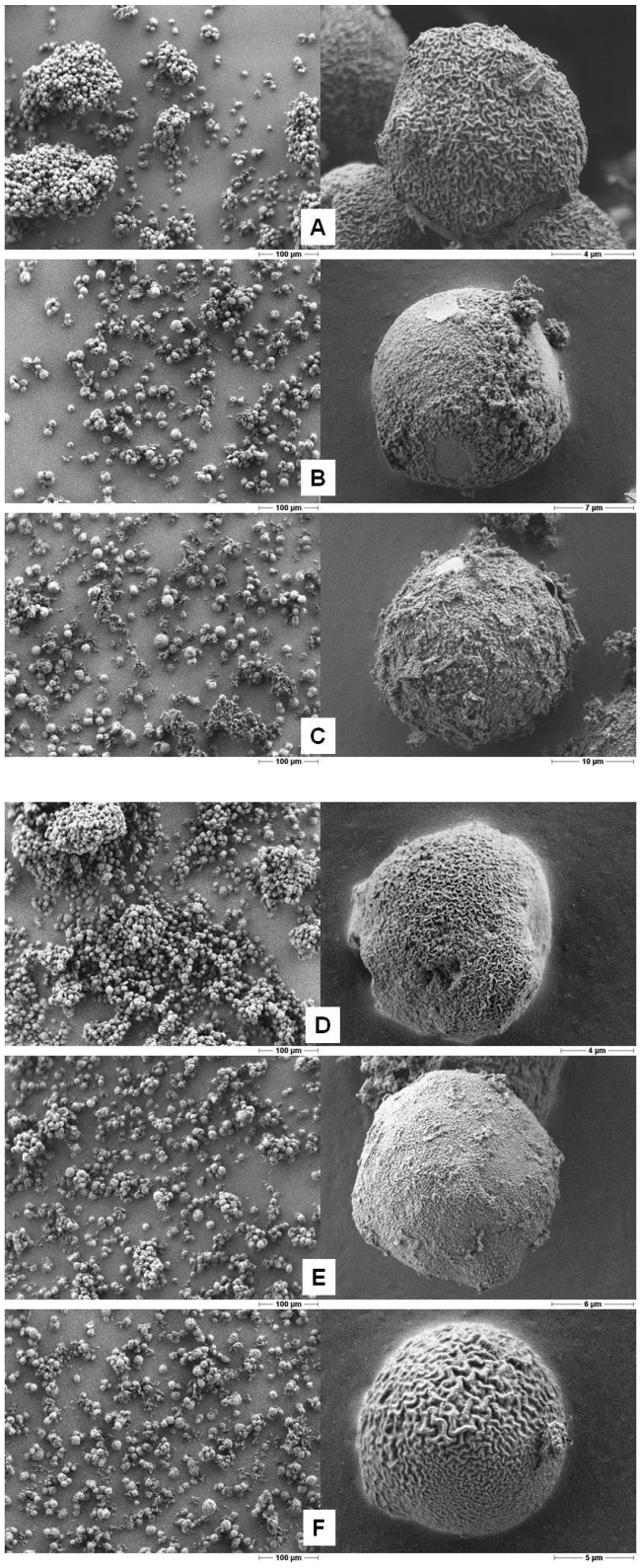

Figure 5.6 Scanning electron micrographs of the polymers resulting from etching of the composites – thinwalled imprinted polymer beads. (A) PA_{10}^{1}, (B) PA_{10}^{2}, (C) PA_{10}^{3}, (D) PA_{20}^{1}, (E) PA_{20}^{2} and (F) PA_{20}^{3}

Indeed the measured swelling factors reported in Figure 5.7 confirms that the thinner walled beads swell more than the thicker walled beads, resulting in swollen state diameters which approach the size of the silica mold.

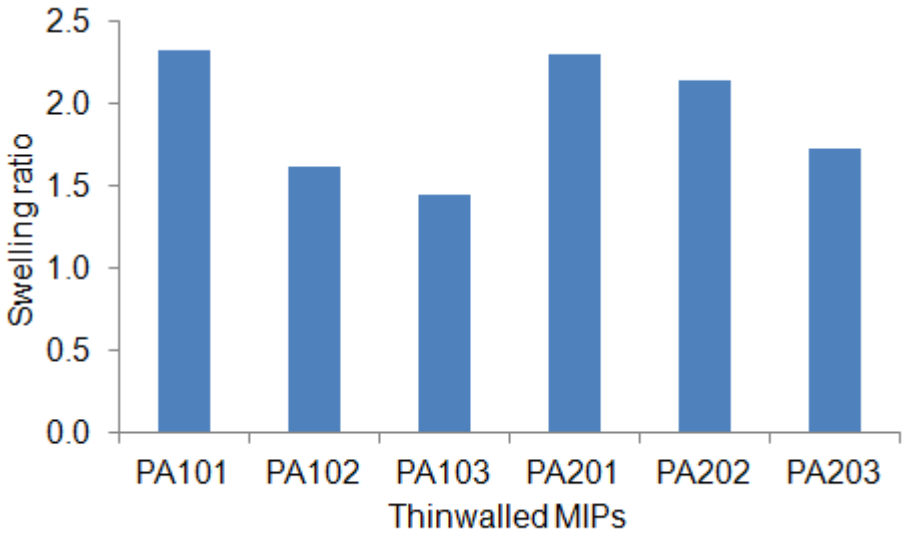

Figure 5.7 Volume swelling ratio of thinwalled beads in pure acetonitrile.

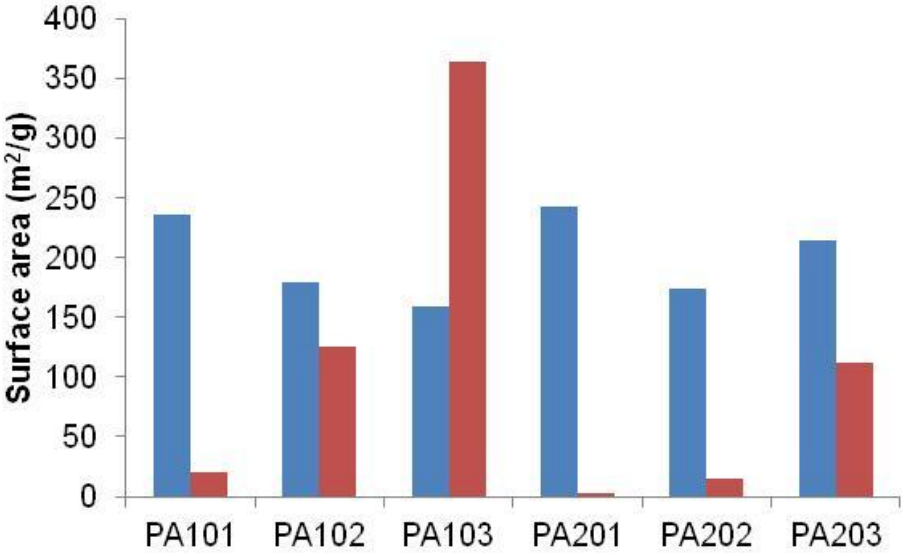

Figure 5.8 Surface area in the dry state of composites (blue bars) and corresponding polymers (red bars) resulting after fluoride catalyzed etching.

Thus, as anticipated above, the thicker walled beads appear to retain their porosity in the dry state which is also clearly revealed by the dry state surface area of the materials (Figure 5.8). The 2 nm and 3nm film composites prepared at intermediate dilution showing higher carbon contents clearly confirm that this is the case. The polymer beads resulting after etching of these composites feature much enhanced surface areas - the surface area of the 3nm bead even exceeding that of the corresponding composite. This was also confirmed by the lower swelling exhibited by this material.

This implies that the film thickness of the composite can be used as a parameter for tuning the volume changes of the beads. To the best of our knowledge this represents a new approach to engineer hard/soft properties of network polymers which does not involve the crosslinking level or distribution of crosslinks.

5.2.2 Characterization of Thin walled materials by chromatographic mode

In order to get an overview of the binding affinities, capacities and mass transfer properties of the various materials they were packed in small columns and investigated by liquid chromatography for their ability to retain L-PA and its optical antipode D-PA using MeCN as mobile phase. An initial comparison of the SiP_A series of composites revealed a strong influence of the monomer dilution and film thickness on the chromatographic retentivity and selectivity. Hence, increasing dilution and nominal film thickness led to a general improvement of the chromatographic properties manifested in an increased retention factor and separation factor. Figure 4.9 shows the corresponding results for the composites reported in Table 5.1.Composites prepared from concentrated monomer solution feature much lower retention factors and enantioselectivities compared to the composites prepared in the dilute system, this in spite of the higher carbon content of the former. We have attributed this to the faster polymerization occurring in the more concentrated system.[81] This rapidly leads to locally high viscosities and blocking of pores – hence the low chromatographic retention factors. This contrasts with grafting under more dilute conditions where monomers can diffuse more freely and access the inner pore

system of the material. The trend of increasing pore volume and surface area with increasing dilution offers support for this explanation (Figure 4.9).

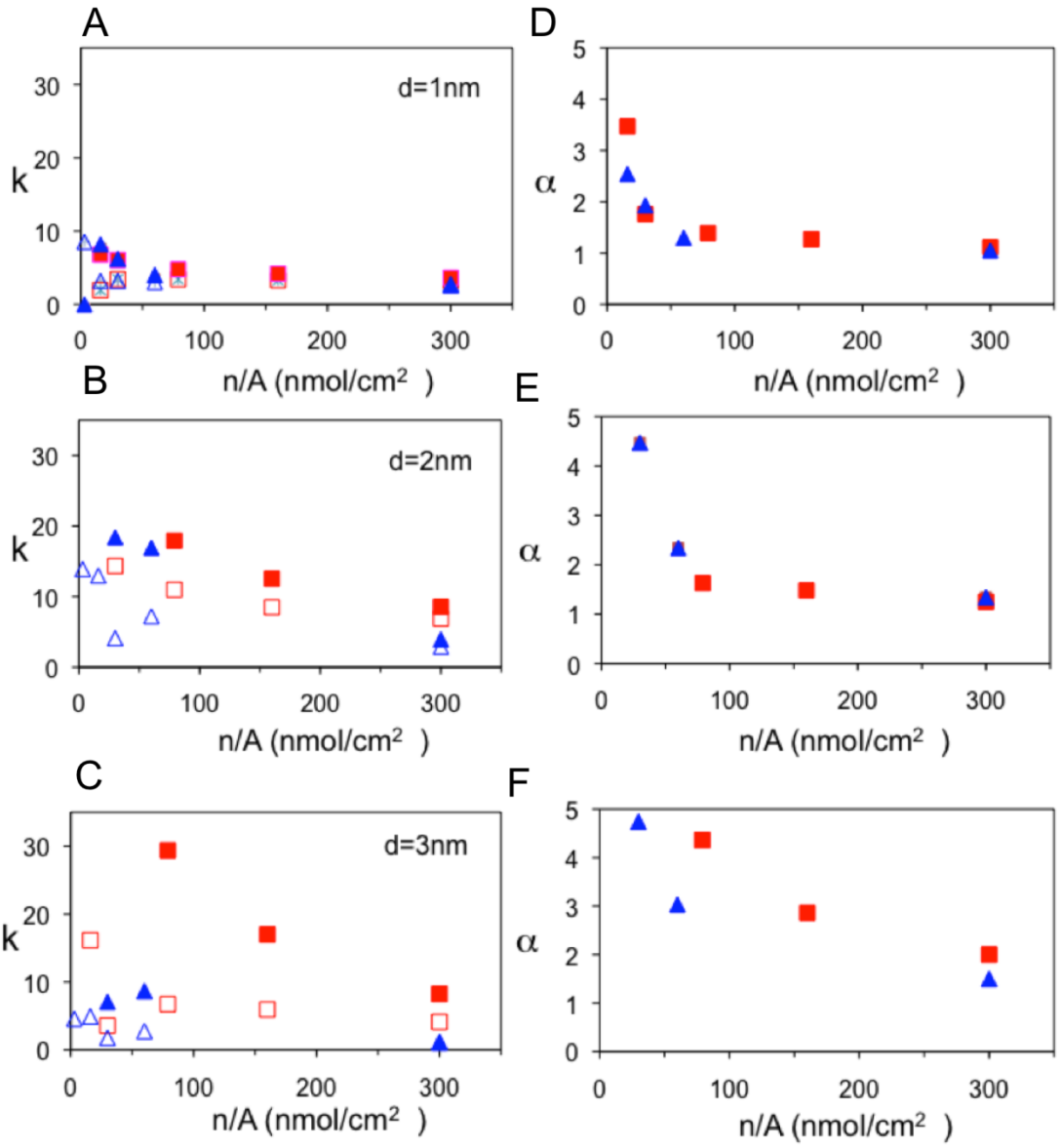

Figure 5.9 Plot of retention factors (k) (A-C) and enantiomer separation factors (D-F) versus sample load per column cross section area (n/A) for L-PA (filled symbols) and D-PA (open symbols) on columns packed with composite beads (blue triangles) and beads after etching (red squares) for $SiPA_{15}^{1}$ and PA_{15}^{1} (A and D); $SiPA_{15}^{2}$ and PA_{15}^{2} (B and E) and $SiPA_{15}^{3}$ and PA_{15}^{3} (C and F). Mobile phase: MeCN. The nominal film thickness (d) has been indicated.

Figure 5.9 shows a comparison of the sample load dependence of retentivity and enantioselectivity for the composites and thin walled materials prepared using 15mL toluene as

diluents. All columns display a trend of decreasing retention and enantioselectivity with sample load in agreement with previous reports. This is the result of nonlinear chromatography with constant overloading of low-abundent high energy binding sites. Whereas the shape of the curves for the 1nm film composites and thin walled polymers are nearly superimposable, the thicker film materials behave differently. Removal of the silica support here give rise to beads displaying much enhanced retentivity and in the case of the 3nm films also enhanced enantioselectivity. In principle this behavior could have a simple explanation. Removal of the silica support could result in a denser MIP presenting a higher functional capacity and density of imprinted sites. However, this effect should also be noticeable for the thin film materials. The result is more likely related to the enhanced binding site accessibility resulting from silica removal – an effect which should be more marked for the thicker films, where accessibility is poor from the start. Removal of silica opens up a new pore system providing new diffusional paths for the solutes to reach the MIP sites. The improved mass transfer properties are reflected in the number of theoretical plates and peak asymmetry (Figure 5.10 and Figure 5.11). It is clear from the more than 2x higher plate numbers and the lower peak asymmetry factors that the thin walled beads feature significantly higher column efficiency.

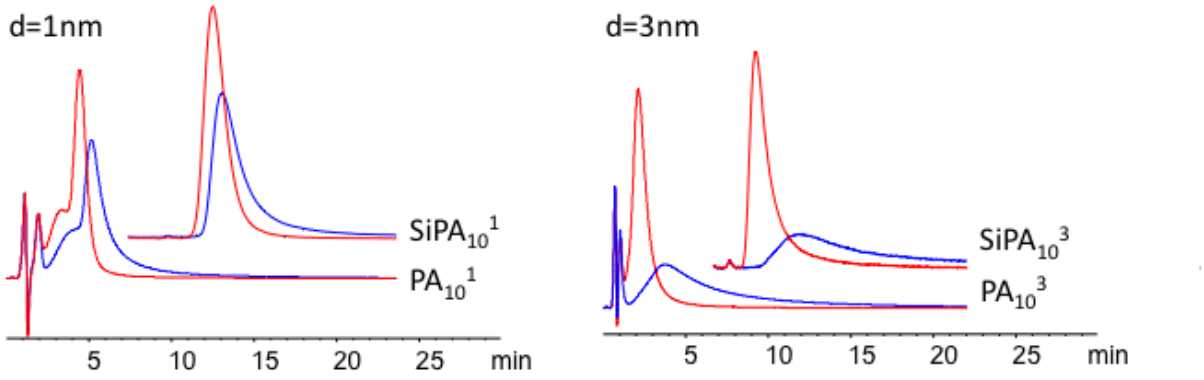

Figure 5.10 Chromatogramms obtained by separate injection of D-PA (red traces) and L-PA (blue traces) on columns packed with the indicated materials. The sample load per column cross section area was 30nmol/cm2. Mobile phase: MeCN/sodium acetate buffer 0.01M pH 4.8: 70/30 (v/v).

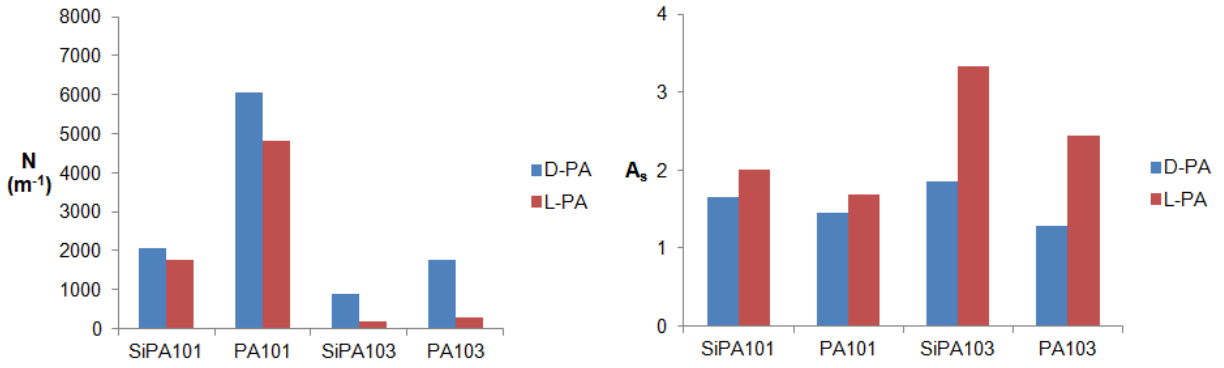

A B

Figure 5.11 Number of theoretical plates (A) and peak asymmetry factors (B) at comparable sample loads (30nmol/cm2) on columns packed with the indicated materials. Mobile phase: MeCN/sodium acetate buffer (0.01M), pH 4.8: 70/30 (v/v).

5.2.3 Thinwalled imprinted polymer beads generated from RAFT modified support

To introduce livingness in the polymer matrix, we decided to modify the two different kind of silica support (Si100 and Si500) by immobilizing CTA on aminomodified silica support by catalyzing the ethylchloroformate. After successful grafting of MIP layer on support by surface initiated graft polymerization techniques. The resulting MIP composites were tested latter exposed to etching solvent ammonium hydrogen difluoride for 24h and leaves behind the thinwalled beads which having the leaving properties. These RAFT thinwalled beads were characterized thoroughly using standard techniques such as FTIR, Microelemental analysis, TGA, SEM, N2 sorption analysis and evaluated in LC mode as well as batch rebinding studied. The successful removal of silica was confirmed by the complementary techniques as can see in the Table 5.2. These results are very much similar to the azomodified thinwalled beads. Here also one can see that the percentage of carbon were increased and well comparable to solution polymer or bulk polymer composition. Thermogravimetry also confirms that the percentage mass loss were almost 98% which mean more than 95% of silica was successfully removed. These results are good agreement with azomodified thinwalled beads. Scanning electron microscopy also revealed that there is no agglomeration between the particles during the polymerization and after etching showed the smaller beads compared to original silica which are shown in the Figure 5.14 and Figure 5.15. The surface was not as smooth as for the composite particles being

probably due to shrinking of the particles during the dissolution step, as was also reflected by the smaller particle sizes of the new polymers as compared to the composites. From BET results concluded that these thinwalled beads are shriking means no porosity. This was the fact due to the harss condition were used in dissolvation process. Lack of porosity in dry state confirmed that these beads were acted like gels (Table 5.2).

Table 5.2 Characteristics of molecularly imprinted polymer composites prepared by thermally initiated grafting to full monomer conversion from silica modified with RAFT agent.

Samples[a]	RAFT/ABDV	%C	%N	%S	Mass loss (%)	S_A (m^2/g) [b]	D_p (nm) [b]	V_p (mL/g) [b]
SiPR [c]	0.5	32.1	0.85		56	207	4.1	0.25
$SiPR_E$ [c]	2.0	31.7	0.81		56	260	3.7	0.33
SiR^{500} [d]	0.3	11.0	0.72		17	68	32	0.39
$SiPR_E^{500}$ [d]	1.4	10.6	0.74		19	72	32	0.35
$SiPR_E^{500}$ [d]	14	12.7	0.99	0.29	20	57	23.7	0.31
PR	0.5	58.23	0.58		98	2.17	3.75	0.004
PR_E	2.0	58.61	0.37		98	6.35	3.75	0.008
PR^{500}	0.3	ND	ND		98	1.9	3.57	0.007
PR_E^{500}	1.4	ND	ND		98	ND	ND	ND
PR_{FE}^{500}	14	58.17	1.22	0.99	96	6	13	0.007
PR_{ref}	1	58.72	0.25	0.01	-	321	6.1	0.43
PR_{ref}^{NIP}	1	58.66	0.22	0.03	-	354	7.6	0.51

a) The composites (SiPR) were prepared by thermally initiated grafting to full monomer conversion from (c) Si-RAFT or (d) Si_{500}-RAFT using different ratios of RAFT agent to azoinitiator (ABDV). These were etched with fluoride to yield thin walled polymers PR.

b) The BET specific surface area (S_A), specific pore volume (V_p) and average pore diameter (D_p) were calculated from the nitrogen adsorption isotherms as described in the experimental part.

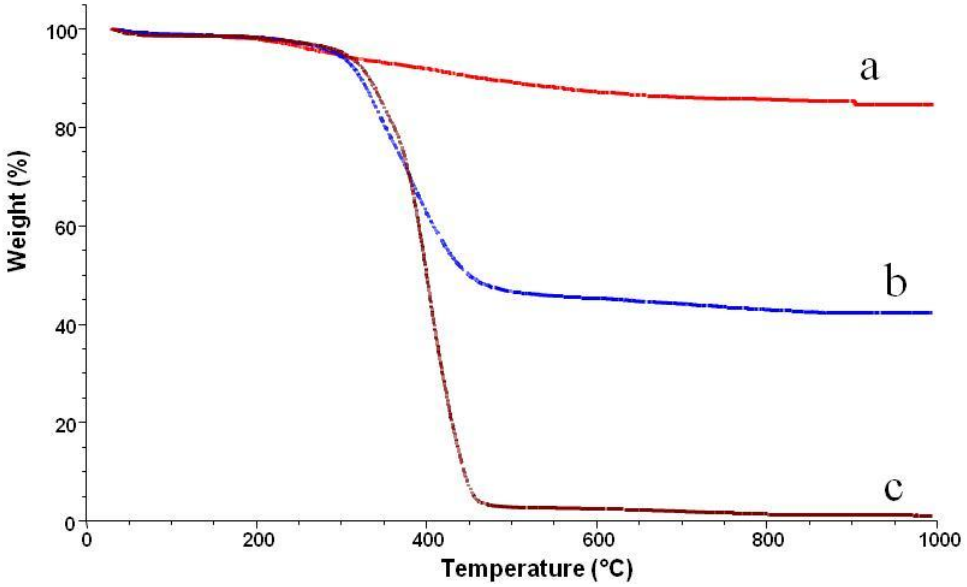

Figure 5.12 TGA curves of Si100RAFT-agent (a), L-PA imprinted composite SiPRE (b), and the thin-walled imprinted polymer PRE (c).

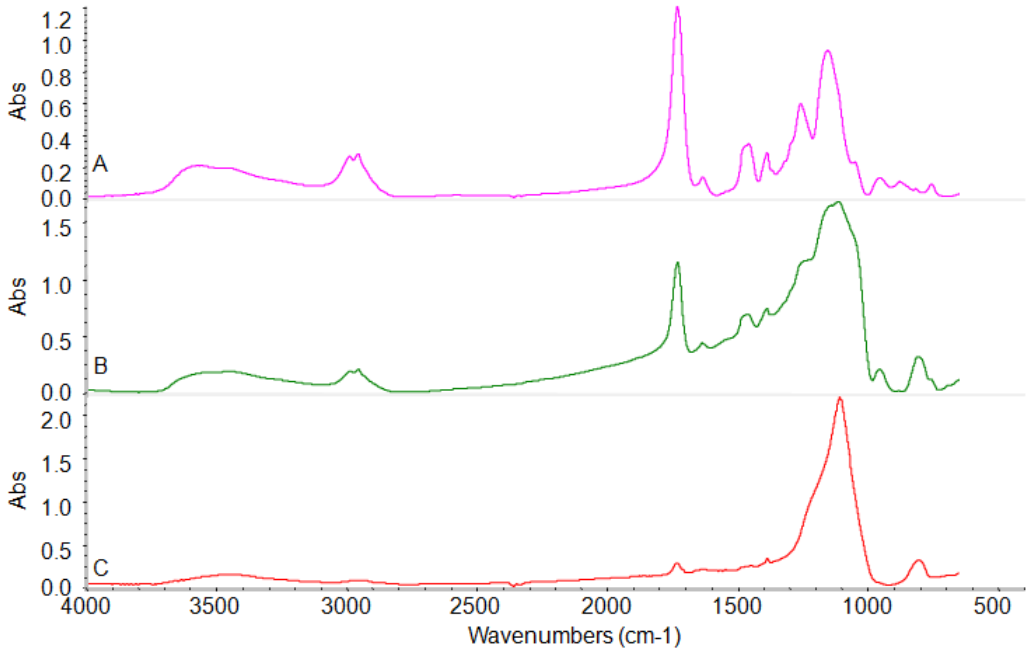

Figure 5.13 FTIR of the thinwalled PR_E (A), composite $SiPR_E$(B), and RAFT agent si100RAFT (c).

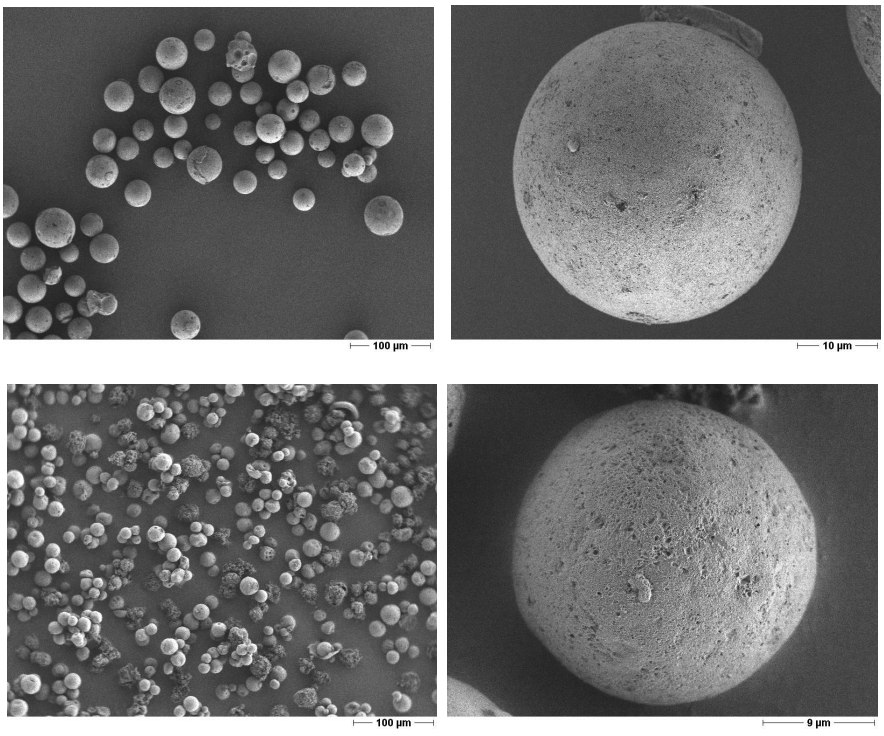

Figure 5.14 Scanning electron microscopy of composites and corresponding thinwalled bead of PR^{500} in two magnification.

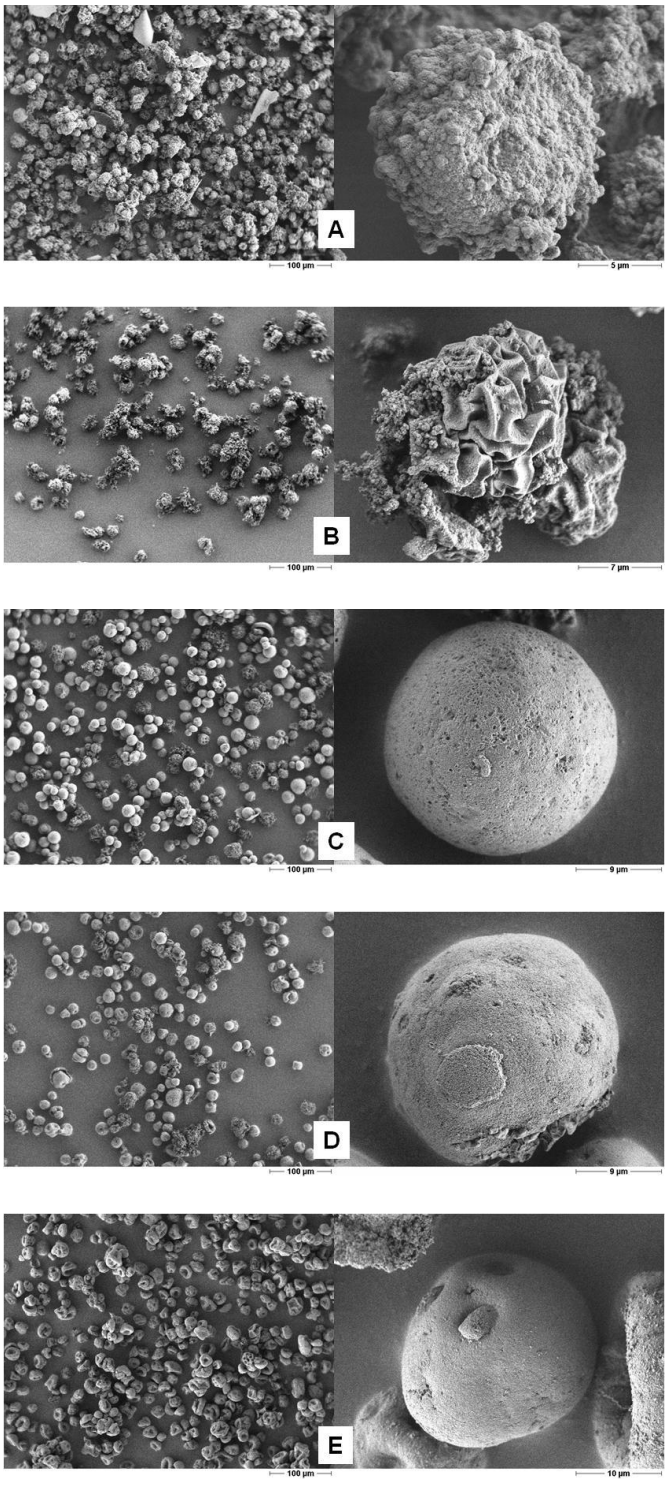

Figure 5.15 Scanning electron micrographs of the polymers resulting from etching of the composites (A) PR, (B) PR_E, (C) PR^{500}, (D) $PR_E{}^{500}$ and (E) $PR_{EE}{}^{500}$ at two magnifications.

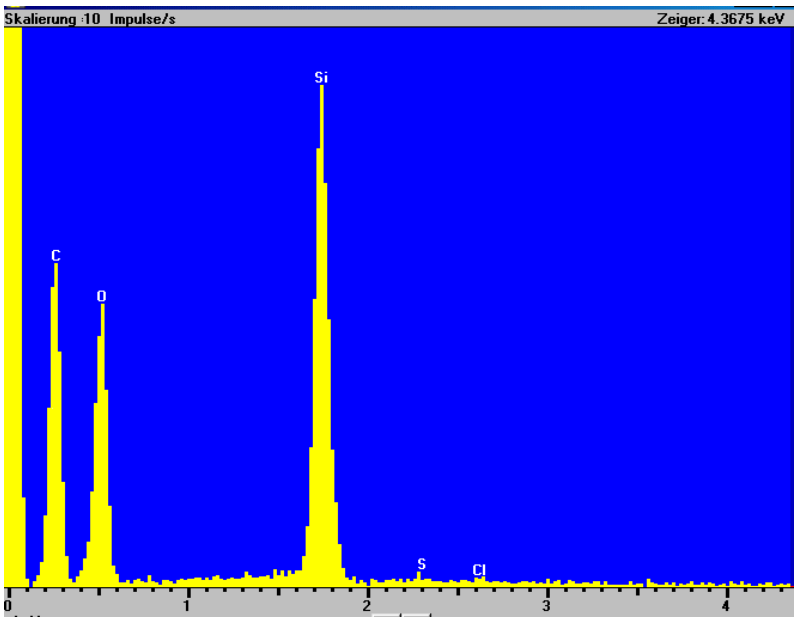

A

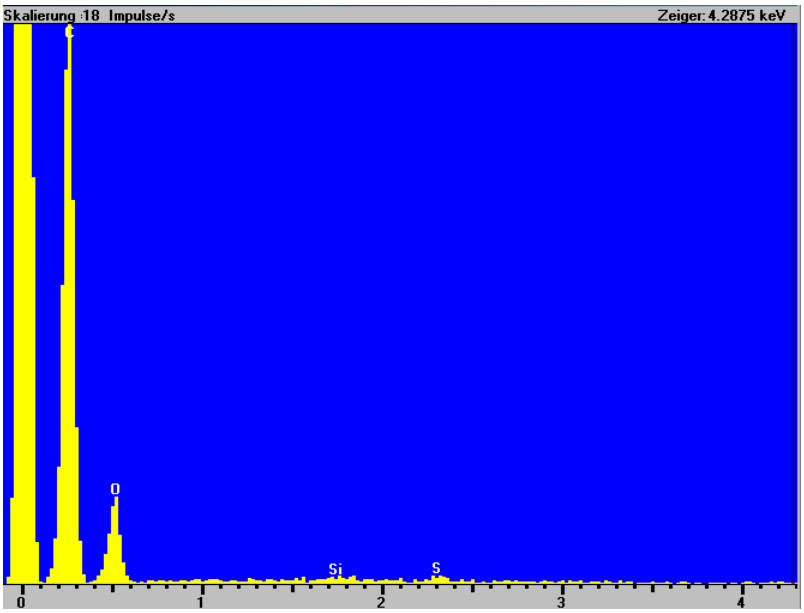

B

Figure 5.16 SEM-EDX spectrum of SiPR^{500} composite (A), and corresponding thinwalled material, PR^{500} (B).

EDX spectrum shows the presence of sulfur in composite and generated thin wall. The Silica (Si) peak was disappeared in thinwalled and increased the peak intensity of carbon which indicates the successful removal of silica.

5.2.4 Evaluation of RAFT thinwalled beads in liquid chromatography mode

All thin walled beads were packed in a small column (20 x 2 mm) and tested in pure acetonitrile with four different sample loads. The capacity and separation factor were calculated as above mentioned. From Figure 5.17, it clearly display that the influence of chain transfer agent on the capacity and separation factor. The high RAFT/ABDV ratio displays the enhanced enantioselectivity in both kinds of silica supports, which indicates the positive influence of a chain transfer agent.[81] Another one interesting things observed when template concentration was decreased the retentivity and selectivity were increased it means most of the binding sites are available at low concentration. The typical chromatograms were shown in Figure 5.18, where 0.1mM solutions of D/L-PA enantiomers were injected separately.

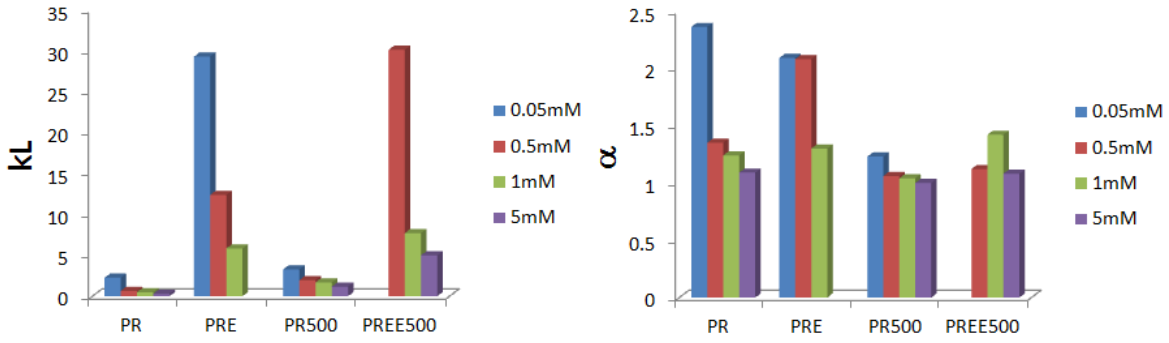

Figure 5.17 Plot of retention factors (k) for L-PA (A) and associated separation factors (α) (B) at four different sample loads for L-PA imprinted TW material prepared by grafting from different RAFT modified supports. The RAFT/ABDV ratio and type of silica support has been indicated in above table. Mobile phase; MeCN.

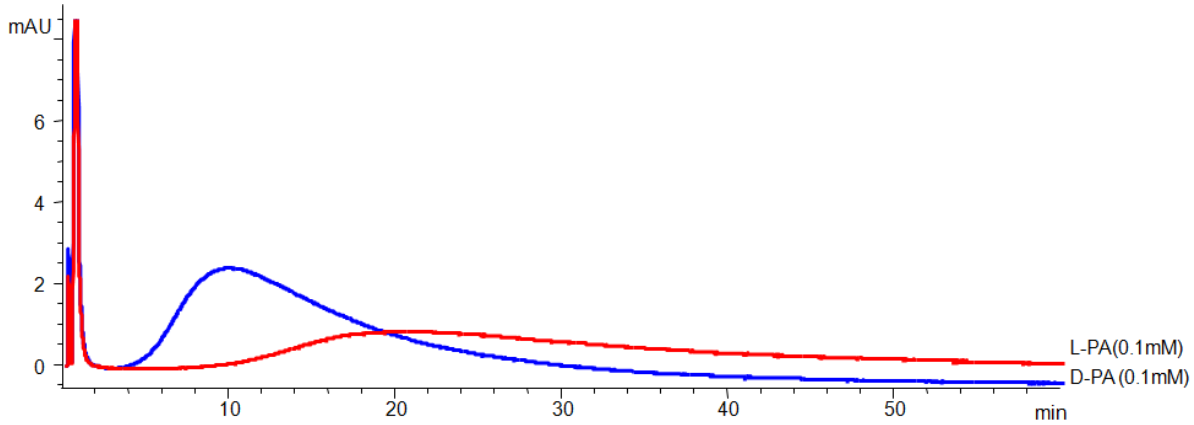

Figure 5.18 Elution profiles of D,L-PA injected (10 mL of a 0.1 mM solution) separately into columns (20X2mm) packed with the indicated L-PA imprinted RE100- TW material. The RAFT/ABDV ratio is 2. Mobile phase: MeCN.

The PR_E^{100} was further tested in pure sodium acetate buffer with different volume of acetonitrile as mobile phase and injected three different sample loads of two enantiomers separately and calculated the retentivity and selectivity factor (Figure 5.19). As can see in the Figure 5.19 only at 15% and 20% of volume of acetonitre could break the nonspecific interaction otherwise both enantiomers were fully retained non specifically, so here we shown only the selectivity factor for 85:15 and 80:20 sodium acetate buffer: MeCN mobile phase. The selectivity factor was not changed so much for both cases. The same observation was found in corresponding composites but the retentivity was less (Figure 5.20). This means after removing the silica leaves behind the soft and hydrophilic material which was further confirmed by Engelhardt test.

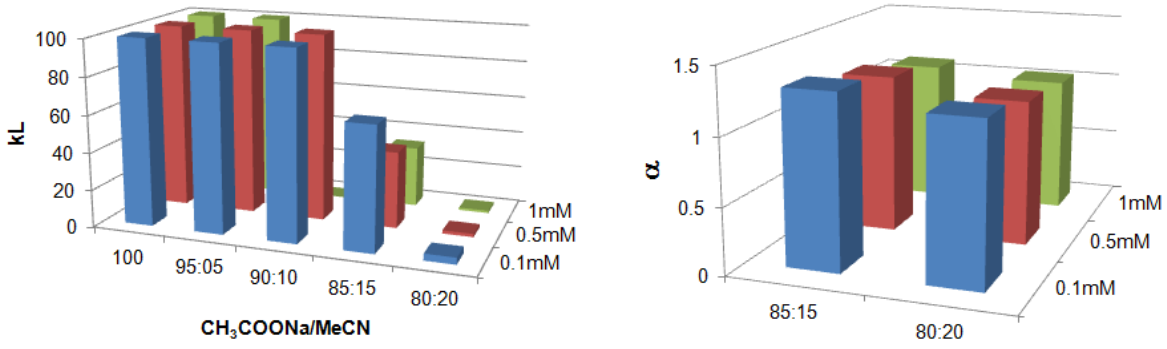

Figure 5.19 Plot of retention factors (k) for L-PA (A) and associated separation factors (α) (B) at three different sample loads for L-PA imprinted PR_E^{100} TW material. The RAFT/ABDV ratio is 2. Mobile phase: Sodium acetate buffer (pH 5) with increasing amount of acetonitrile.

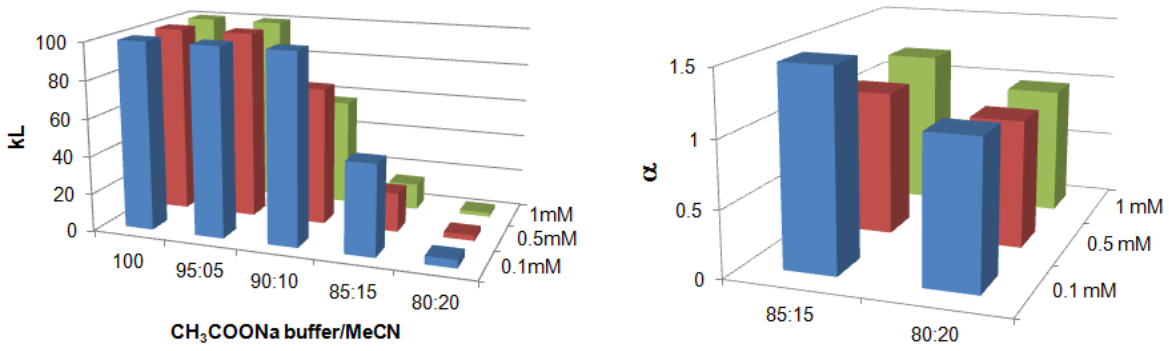

Figure 5.20 Plot of retention factors (k) for L-PA (A) and associated separation factors (α) (B) at three different sample loads for L-PA imprinted $SiPR_E^{100}$ composite material. The RAFT/ABDV ratio is 2. Mobile phase: Sodium acetate buffer (pH 5) with increasing amount of acetonitrile.

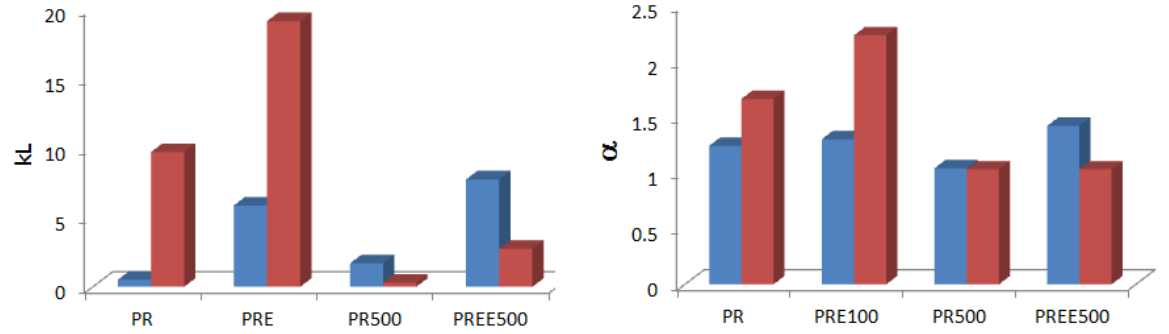

Figure 5.21 Retention factors (k) for L-PA (A) and enantiomer separation factors (B) obtained in the chromatographic mode at comparable sample loads (300 nmol/cm2) on columns packed with the indicated composite beads(red bar) or polymer beads(blue bar). Mobile phase; MeCN.

Figure 5.21 shows retention factors and enantiomer separation factors for two different support and corresponding thin walled beads obtained from chromatograpy. The wide pore silica beads behave different than the smaller beads where the smaller polymer beads shows less retention and separation factors than the original composites. This results support the scanning electron microscopy pictures where one can see the morphology of these beads. The polymer beads shrinks a lot more than 50% of the original composites but the polymer beads generated from wide pore silica display its original size of the mold. In this case the smaller size polymer beads may not be accessible to the target molecule because of the less time interaction between the solute and stationary phase vice versa to the bigger polymer beads were easily accessible to the target molecules. These smaller polymer beads were further used for equilibrium binding

isotherm study where they display higher capacity and enantionselectivity towards target molecules compared to composites. This is described in below section.

5.2.5 Saturation binding experiments

Insights into the relative binding energies and abundance of imprinted sites were obtained by equilibrium partitioning experiments using acetonitrile as solvent. Thus, quantifying the equilibrium free concentration of solute (C_{free}) by HPLC, the bound amount q could be determined and plots of q versus C_{free} giving the binding curves of the template L-PA and of its optical antipode D-PA for the different imprinted polymer complements. In addition to the beaded polymers conventional crushed MIP monoliths (PAref and PRref), prepared by solution polymerization of an identical monomer composition, and was included as controls.

As seen in Figure 5.22 the shape of the isotherms depended strongly on whether the polymers had been prepared by RAFT mediated grafting or not. The non-RAFT composites and resulting thin walled polymers featured a clear saturation behavior whereas the shape of the isotherms obtained using the RAFT materials appeared discontinuous and slightly sigmoidal in the low concentration regime and a much higher final saturation capacity (Figure 5.25). The isotherms were subsequently fitted to mono-Langmuir, bi-Langmuir and Freundlich isotherm models[30] resulting in the isotherm parameters given in Table 5.3, Table 5.4 , and Table 5.5. The Fisher values in Figure 5.24 reflect which of the models provides the best fit to a particular isotherm, a higher number indicating a better fit.

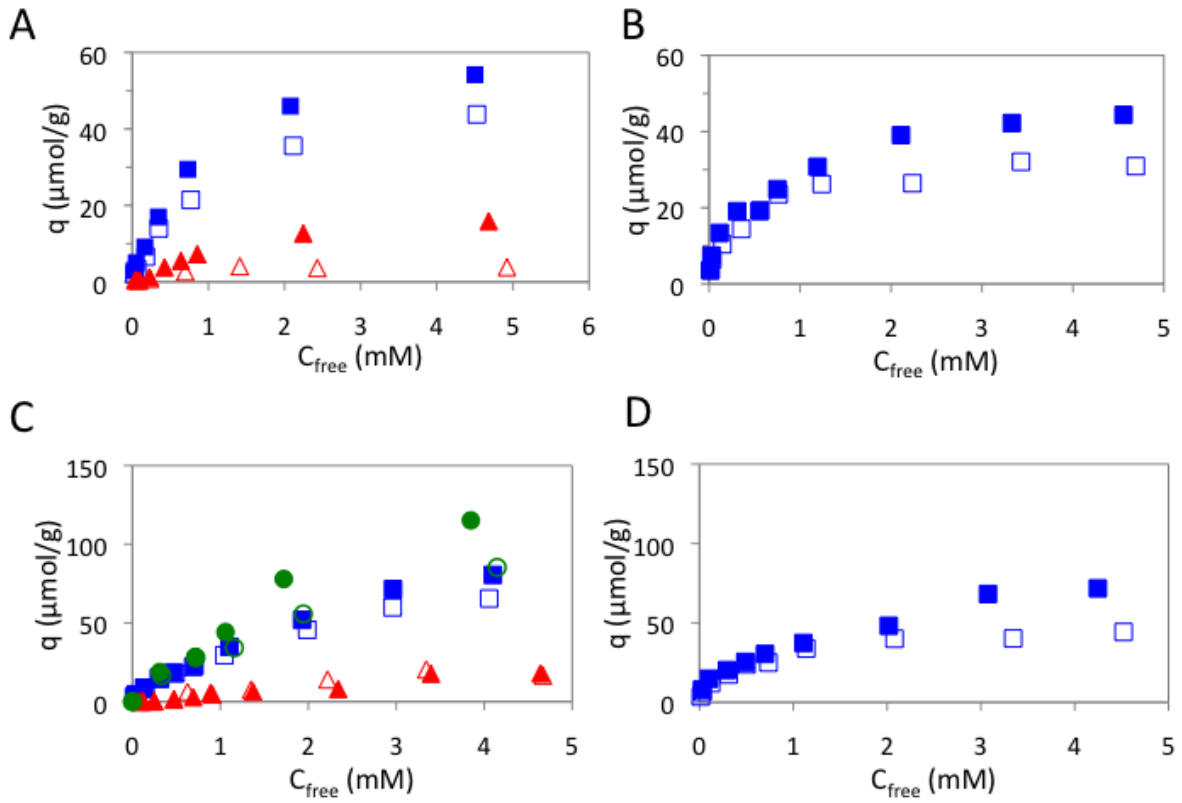

Figure 5.22 Equilibrium binding isotherms of D- (open symbols) and L-PA (solid symbols) (A) for composite beads SiPA203 (red triangles) and the resulting beads after etching PA203 (blue squares); (B) a bulk reference polymer PA_{ref}; (C) composite beads SiPR (red triangles), the resulting beads after etching PR (blue squares) and PRE (green circles); (D) a bulk RAFT reference polymer $PR_{ref.}$ Solvent: MeCN.

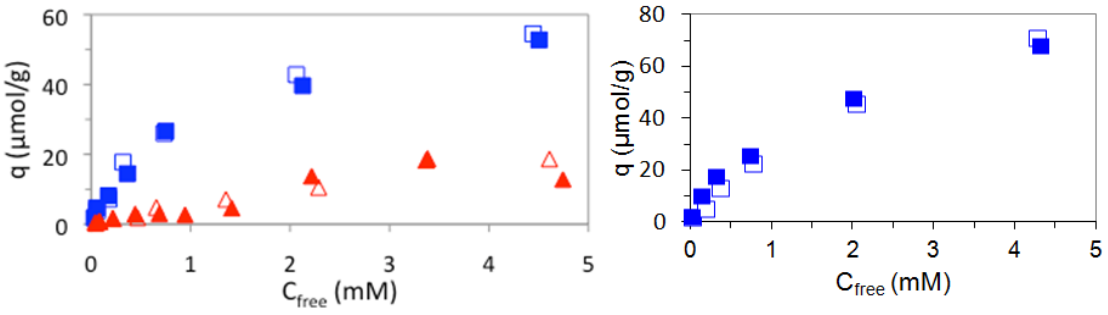

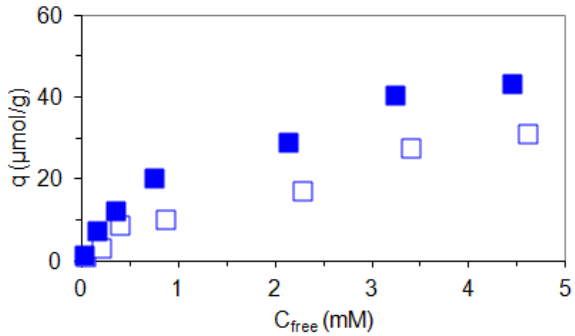

C.

Figure 5.23 Equilibrium binding isotherms of D- (open symbols) and L-PA (solid symbols) for (A) composite beads $SiPA_{20}^{2}$ (red triangles) and the resulting beads after etching PA_{20}^{2} (blue squares), (B) PA_{10}^{2} and (C) PA_{10}^{3}

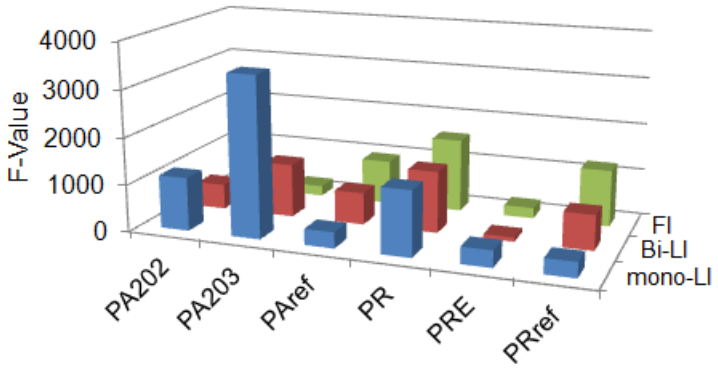

Figure 5.24 Fisher values obtained by fitting the L-PA binding curves in Figure 5.22 and Figure 5.23 to mono-Langmuir (mono-LI), bi-Langmuir (bi-LI) or Freundlich isotherm models (FI) (see Table 5.3 to Table 5.5)

Table 5.3 Mono-Langmuir Isotherm fitting parameters obtained by nonlinear regression of data shown in Figure 5.22 and Figure 5.23 as described in the experimental section.

Polymer code		K_d (mM)	q_s (μmol/g)	r^2	F-value
PR	LPA	3.60 ± 0.53	153 ± 13	0.993	1382
	DPA	2.46 ± 0.31	106 ± 7	0.993	1425
PR_E	LPA	4.57 ± 1.44	256 ± 52	0.986	356
	DPA	3.78 ± 0.71	162 ± 18	0.993	820
PR_{ref}	LPA	1.40 ± 0.36	93 ± 10	0.959	328
	DPA	0.55 ± 0.08	48 ± 2	0.981	799
$PA_{20}{}^2$	LPA	1.21 ± 0.15	65 ± 3	0.994	1135
	DPA	1.12 ± 0.14	67 ± 3	0.993	1042
$PA_{20}{}^3$	LPA	0.92 ± 0.06	66 ± 2	0.997	3415
	DPA	1.13 ± 0.08	55 ± 2	0.998	3820
PA_{ref}	LPA	0.61 ± 0.14	49 ± 4	0.957	341
	DPA	0.36 ± 0.06	33 ± 2	0.973	624
$SiPA_{20}{}^3$	LPA	2.06 ± 0.28	23 ± 2	0.991	897
	DPA	0.58 ±0.24	4.7 ± 0.6	0.921	116
$SiPA_{20}{}^2$	LPA	5.0 ± 4.6	34 ± 20	0.820	46
	DPA	42 ± 65	64 ± 93	0.986	565
$PA_{10}{}^3$	LPA	1.35 ± 0.31	55 ± 5	0.981	458
	DPA	4.24 ± 2.0	59 ± 15	0.966	227
$PA_{10}{}^2$	LPA	1.86 ± 0.32	95 ± 7	0.991	732
	DPA	4.09 ± 0.39	139 ± 8	0.999	3942

Table 5.4 Bi-Langmuir Isotherm fitting parameters obtained by nonlinear regression of data shown in Figure 5.22 and Figure 5.23 as described in the experimental section.

Polymer code		K_d1 (mM)	q_s1 (µmol/g)	K_d2 (mM)	q_s2 (µmol/g)	$\mathbf{r^2}$	F-value
PR	LPA	0.005±0.02	3.6 ± 1.8	5.04 ± 1.11	175 ± 20	0.997	1306
	DPA	0.07±0.12	5.8 ± 4.7	4.06 ± 1.4	122 ± 16	0.998	1157
PR_E	LPA	4.57±4.6	112±77	4.57±0.06	143 ±23	0.986	88
	DPA	0.14±0.85	6.0 ± 21	6.15±7.12	197±93	0.996	408
PR_{ref}	LPA	0.026±0.025	15±4	5.21±2.79	131±35	0.993	746
	DPA	0.014±0.023	6.0 ± 4	0.82±0.25	44±3	0.993	821
$PA_{20}{}^2$	LPA	2.5×10^{13}	6.6×10^{13}	0.81±0.27	48±11	0.993	535
	DPA	8.5×10^{8}	1.5×10^{9}	0.89±0.35	56±17	0.990	356
$PA_{20}{}^3$	LPA	0.92±0.19	31 ± 2	0.92 ± 0.05	35 ± 0.93	0.997	1138
	DPA	0.37±0.10	0.55 ± 2	1.2 ± 0.2	55 ± 1.9	0.998	1594
PA_{ref}	LPA	0.023±0.02	11.7 ±3.7	1.79±0.74	47±4.0	0.992	683
	DPA	0.005±0.02	4.4 ±3.6	0.57±0.2	30±3.0	0.988	532
$SiPA_{20}{}^3$	LPA	2.06	6.4	2.06	17	0.990	320
	DPA	0.58	1.3	0.58	3.4	0.870	35
$SiPA_{20}{}^2$	LPA	5.0	12	5.0	22	0.770	18
	DPA	9.1	24	9.1	35	0.960	116
$PA_{10}{}^3$	LPA	0.31 ± 0.43	19 ± 19	13 ± 43	101 ± 201	0.987	344
	DPA	0.21 ± 0.59	95 ± 1448	6.8 ± 10	550 ± 7791	0.972	140
$PA_{10}{}^2$	LPA	0.22 ± 0.25	116 ± 24	5.1 ± 3.6	116 ± 24	0.997	1215
	DPA	2.60 ± 1.46	8.6 ± inf	1.8 ± inf	82 ± 49	0.998	1400

Table 5.5 Freundlich Isotherm fitting parameters obtained by nonlinear regression of data shown in Figure 5.22 and Figure 5.23 as described in the experimental section.

Polymer code		K_a (mM^{-1})	N_t ($\mu mol\ g^{-1}$)	*m*	*a* (mmol/g (mol^{-1})m	r^2	F-value
PR	LPA	2.54	44.18	0.67 ± 0.03	32 ± 0.96	0.994	1567
	DPA	2.45	40.73	0.61 ± 0.02	29 ± 0.77	0.994	1595
PR_E	LPA	0.816	47.80	0.72 ± 0.07	45 ± 4	0.978	225
	DPA	0.789	39.82	0.65 ± 0.03	34 ± 1	0.995	1162
PR_{ref}	LPA	3.1	51.25	0.476 ± 0.02	37 ±1	0.987	1208
	DPA	5.74	35.67	0.340 ± 0.02	28 ± 1	0.964	520
$PA_{20}{}^2$	LPA	2.6	37.47	0.5 ± 0.04	26±1	0.980	362
	DPA	2.7	38.85	0.49 ± 0.05	27±2	0.966	205
$PA_{20}{}^3$	LPA	3.1	41	0.46 ± 0.05	29 ± 2	0.96	215
	DPA	2.7	32	0.49 ± 0.05	22 ± 2	0.97	276
PA_{ref}	LPA	5.56	35.76	0.354 ± 0.02	27 ± 0.8	0.980	942
	DPA	6.3	25.56	0.298 ± 0.03	21 ± 0.9	0.945	407
$SiPA_{20}{}^3$	LPA	1.5	10	0.590	6.81± 0.5	0.974	183
	DPA	2.77	3.26	0.370	2.51± 0.3	0.81	38
$SiPA_{20}{}^2$	LPA	1.48	7.61	0.740	5.4± 1.3	0.79	39
	DPA	1.40	6.6	0.810	5.79± 1.3	0.96	273
$PA_{10}{}^3$	LPA	2.966	31.08	0.5± 0.03	21 ± 0.94	0.988	386
	DPA	1.89	16.26	0.65± 0.07	11 ± 0.97	0.979	366
$PA_{10}{}^2$	LPA	2.41	43.75	0.55± 0.03	30.6 ± 1.0	0.994	1115
	DPA	1.89	36.28	0.69± 0.03	27 ± 0.94	0.996	1108

N_t=total number of binding sites; K_a=affinity constant.

Binding site homogeneity: The composite materials prepared by RAFT polymerization (PR, PR_E and PR_{ref}) are either poorly fitted by all models, or are best fitted by the FI model (PR_{ref}) and they are giving the sigmoidal isotherm shapes. The non-RAFT beads behave differently. The bulk reference polymer (PAref) is best fitted with Freundlich isotherm model. It shows a typical MIP binding curve indicating a heterogeneous binding site distribution. In contrast to this, the composite and corresponding thinwalled beads PA_{20}^2 (Figure 5.23A) and PA_{20}^3 (Figure 5.22A) are best fitted to mono-Langmuir model with a smooth saturation behaviour and a high F-value. It indicates a homogeneous binding site distribution. In search for an explanation for this behaviour two effects should be considered. As invoked in the previous section, silica removal will open up new pores leading to enhanced access to the imprinted sites from both sides of the wall. Hence, this will remove the influence of the silica-polymer interface as a source of hetereogeneity (different microenvironments, chain stiffness, silica surface interactions etc). Secondly, the increased dilution results in a slower rate of propagation giving the monomers time to diffuse into the pores prior to reaction. This per se should result in more homogenously grafted films.

Which of these two effects is dominating appears by considering the results of two additional materials – the precursor composite to PA_{20}^3 ($SiPA_{20}^3$) and the thin walled materials prepared from more concentrated monomer solutions (PA_{10}^2 and PA_{10}^3). In contrast to the materials prepared from more dilute monomer solutions ($PA_{20}^2$and PA_{20}^3) the binding curves corresponding to $PA_{10}^2$and PA_{10}^3 are more shallow and are better fitted with the biLangmuir or Freundlich isotherm models. Studying the influence of wall thickness, the binding sites in the thicker walled beads appear for both dilutions more uniform (Figure 5.22A, Figure 5.23C) displaying a pronounced enantioselectivity. On the other hand, the thinner walled beads showed no enantioselectivity in the static binding test. This agrees with our previous finding of a critical thickness for enantiomeric discrimination.

Collectively, these results offer sufficient evidence to explain the origin of the enhanced homogeneity displayed by PA_{20}^2 and especially PA_{20}^3. As seen in Figure 5.22A and in Figure 5.23, also the isotherm corresponding to $SiPA_{20}^3$ is best fitted by a mono-Langmuir isotherm model. The fact that the silica precursor displays a uniform site distribution implies that monomer dilution is the decisive parameter controlling the film homogeneity. Hence a careful

tuning of dilution can remove the main source of binding site heterogeneity in MIPs, leading to a material displaying a perfectly uniform distribution of binding sites. This is in agreement with the chromatographic test results shown in Figure 5.9 and stresses the importance of this key parameter for the formation of discriminative sites.

Binding capacity: The saturation capacities of all thin walled materials clearly exceeded those of the corresponding composites. This is obviously a consequence of removing the silica which contributes weight only and should not contribute to binding especially when its surface is covered with a homogenous polymer film. However the capacity increase, especially for the RAFT grafted composites, is higher than this theoretical value (for the RAFT materials: expected ca 2.7x, found ca 4x) and hence they also exceeded those of the bulk reference materials PA_{ref} and PR_{ref} (Figure 5.25). Particularly noteworthy is the capacity shown by the MIP prepared by RAFT polymerization using a high RAFT/initiator ratio. This attains a Q-value of nearly 120µmol/g, which is close to the nominal capacity of the material i.e. the capacity for a MIP where every template molecule has given rise to an accessible binding site. The enantioselective contribution to binding here amounts to nearly 30µmol/g.

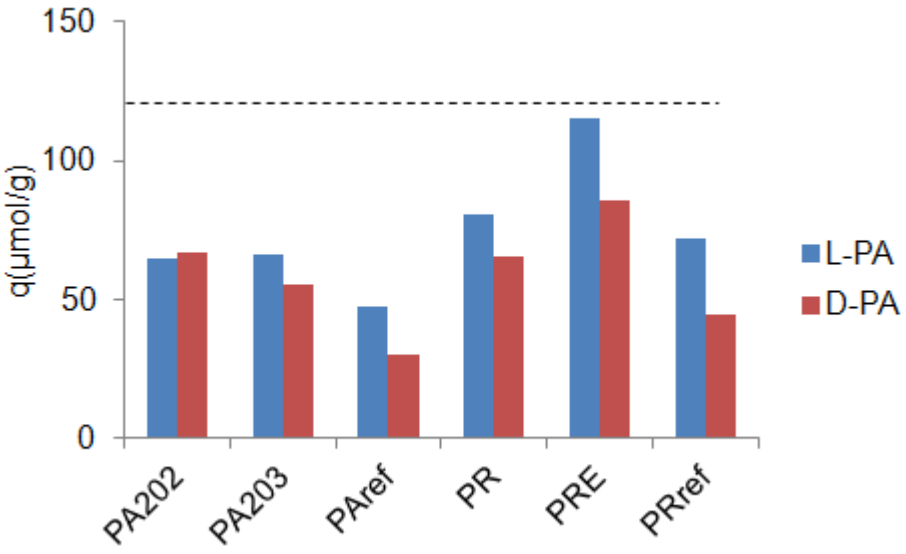

Figure 5.25 Adsorption saturation capacities (q) for D-PA (red bars), L-PA (blue bars) obtained for the materials in Tables 5-3 to table 5-5 estimated from mono-Langmuir curve fitting (PA_{20}^{2}, PA_{20}^{3}), bi-Langmuir curve fitting (PAref) or estimated as the q-value at the highest concentration of L-PA (PR, PR_E and PR_{ref}). The dashed line represents the theoretical saturation capacity assuming a quantitative yield of imprinted sites.

5.2.6 Kinetic binding experiment

To better understand the binding events that take place in thinwalled polymers adsorption kinetics experiments were performed on PA_{10}^2. MIPs prepared via conventional monolith procedure have very slow association-dissociation kinetics due to a heterogeneous population of binding sites and a poor mass transfer. In the TW-polymers the binding events take place in very thin walls, and as concluded from batch rebinding experiments the binding sites in these materials were homogeneous. Therefore, a fast adsorption kinetic should be expected for such materials.[27]

Kinetic experiments were performed by adding 0.05-1mM solution of the template L-PA to a known amount of TW polymer. After the addition of the solute, the binding events were recorded by measuring the concentration in the supernatant solution using an Agilent 1200 series instrument after 1h, 5h, 10h, 24h, and 96h. The concentration was monitored till it remained constant, meaning that no more templates was bound in the binding sites. The polymer adsorption kinetics was very fast. It appeared that after 1h the most of the binding sites are saturated for all concentration and it remains constant until 96h. The results obtained are shown in Figure 5.26. The results obtained from the kinetics experiments were in good agreement with the results obtained from batch rebinding.

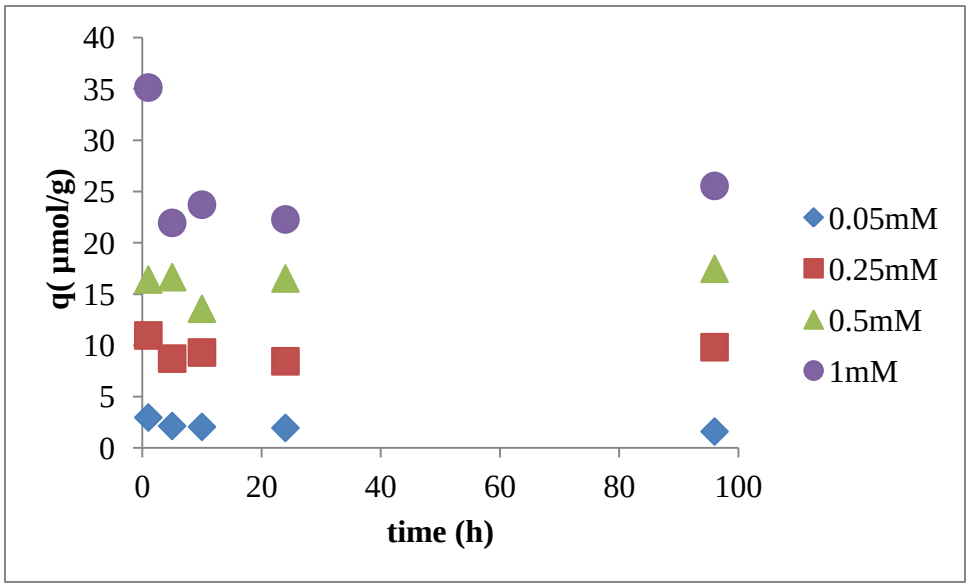

Figure 5.26 Kinetics of the binding data for PA_{10}^2 shown in Figure 5.23B

5.2.7 Engelhardt test: Surface acidity and hydrophobicity

In view of the higher capacity and selectivity of the thin walled MIPs compared to the bulk monoliths and the composites, it is tempting to interpret this result as being due to an increase in surface area after silica etching. This would allow access to the imprinted film from a pore newly created by the silica removal in addition to the original pore defined by the silica mesopore system. One question that arise concerns the nature of the interfaces post silica removal. After grafting of the polymer films capped end groups should reside near the pore walls and could serve as reactive groups for continued grafting. What about the new pore wall? The silica polymer interface is covalently anchored and therefore the fluoride etching should create new endgroups on the emerging wall.

Table 5.6 Properties of stationary phases and columns used in the Engelhardt test.

Columns	Dimensions L x I.D. (mm x mm)	Particle size (µm)	S_A (m^2/g)	V_p (ml/g)	D_p (nm)
C18	150 x 4.6	5	400	--	10
SiPR	35 x 4.6	15	206.9	0.249	4.1
$SiPR_E$	35 x 4.6	15	260	0.329	3.68
$SiPR_{EE}^{500}$	35 x 4.6	20-45	57	0.309	23.7
$SiPA_{10}^{3}$	20 x 2	15	158	0.16	3.7
PA_{10}^{3}	20 x 2	15	364	0.49	5.25
PR	20 x 2	15	2.2	0.004	3.75
PR_E	20 x 2	15	6.35	0.008	3.75
PR_{EE}^{500}	20 x 2	20-45	1.55	0.007	3.57
PR_{ref}	20 x 2	25-50	354	0.51	7.63
PR_{ref}^{H}	20 x 2	25-50	--	--	--

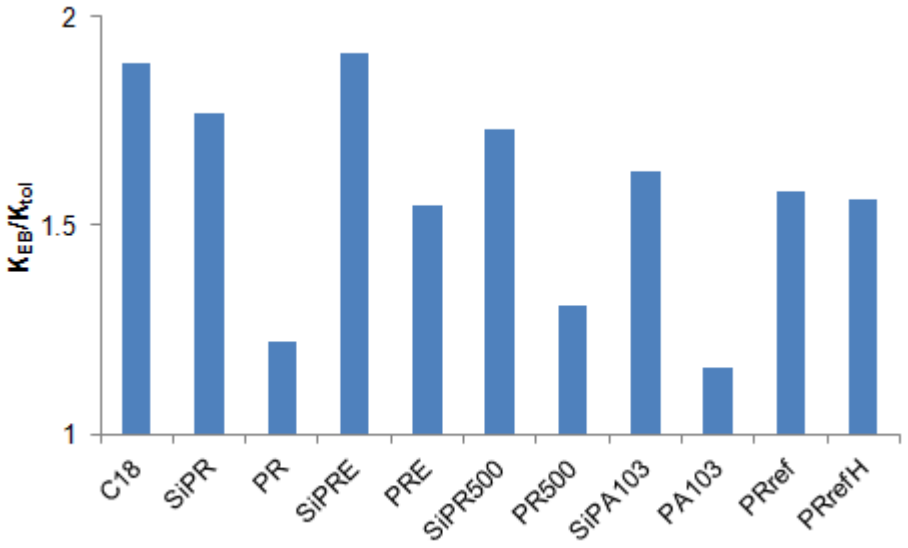

Figure 5.27 Hydrophobicity index, estimated as the ratio of retention factors of ethylbenzene to toluene, of columns packed with the indicated materials. Mobile phase: MeOH/H20: 55/45 (v/v).

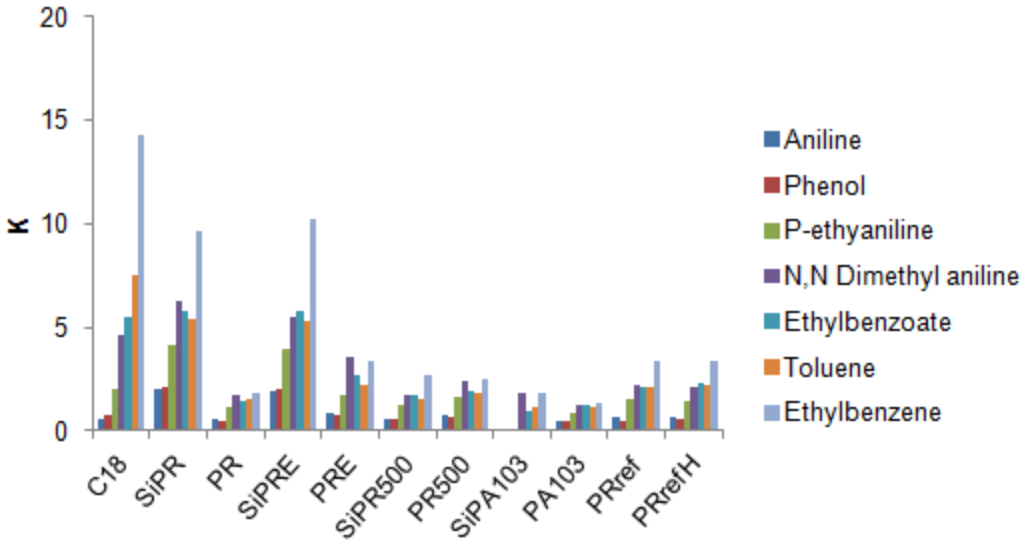

Figure 5.28 Retention factors (k) on columns packed with the indicated materials, for compounds used to probe surface acidic groups and hydrophobicity.

In order to demonstrate with other means that the resulting pore walls are different we turned to the so called Engelhardt test. This is commonly used in chromatography for characterising reversed phase columns with respect to their surface hydrophobicity.[189] The assumption is here that the RAFT grafted composites will leave behind a more hydrophobic surface due to the

capping of chains by dithioester groups as schematically drawn in Figure 5.1. We therefore characterized the packed columns (Table 5.6) with respect to retention and separation of a test mixture of solutes with different basicity and hydrophobicity (See experimental section 7.4.14). This would be informative of the abundance of accessible COOH groups as well as the general hydropobicity of the materials. First it became obvious that all the MIPs retained the basic test solutes more than the reversed phase reference column – this agrees with the presence of COOH groups in the backbone (Figure 5.28). Figure 5.27 otherwise confirms the view discussed above whereas the RAFT composites exhibit a rather similar hydrophobicity as the C18 column, this character disappears upon the HF treatment. Obviously this may be the result of a chemical hydrophilization induced by the strong hydrolytic treatment but the absence of this effect when the treatment was performed on a bulk MIP prepared by RAFT (PR_{ref} versus PR_{ref}^{H}) shows that it has another origin. More likely here is that the enhanced hydrophilicity is due to the newly created pore system after silica removal which, in view of the lower abundance of dithioester moieties is more hydrophilic (Scheme 8).

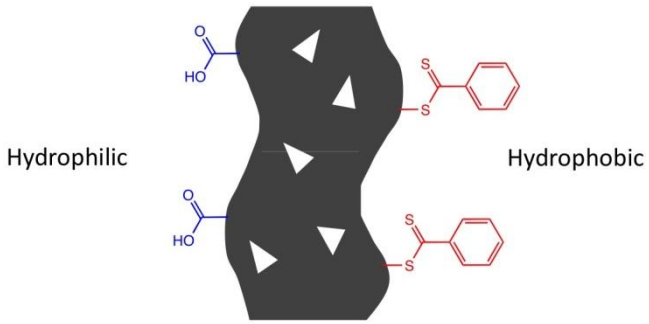

Scheme 8

The stability of the dithioester RAFT group under the fluoride etching conditions is indicated by the retention of the characterstic pink color Figure 5.29 and Figure 5.30. Further for more evidence of stability of RAFT under fluoride etching was confirmed by ^{13}C-NMR (Figure 5.31). In ^{13}C-NMR spectrum of HF treated RAFT agent, the peaks corresponding to carbon atoms are in good agreement with non treated RAFT agent.

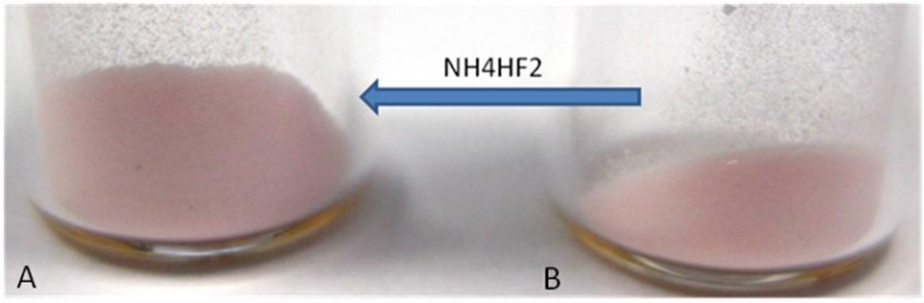

Figure 5.29 Photographs of imprinted composites prepared by RAFT mediated grafting corresponding to SiPRE (B) and PRE(A) after removal of silica by etching.

Figure 5.30 Photograph of a solution of RAFT agent in DMSO-d6, after treatment with aqueous HF solution (NH4HF2, 3M) (A) and before treatment (B).

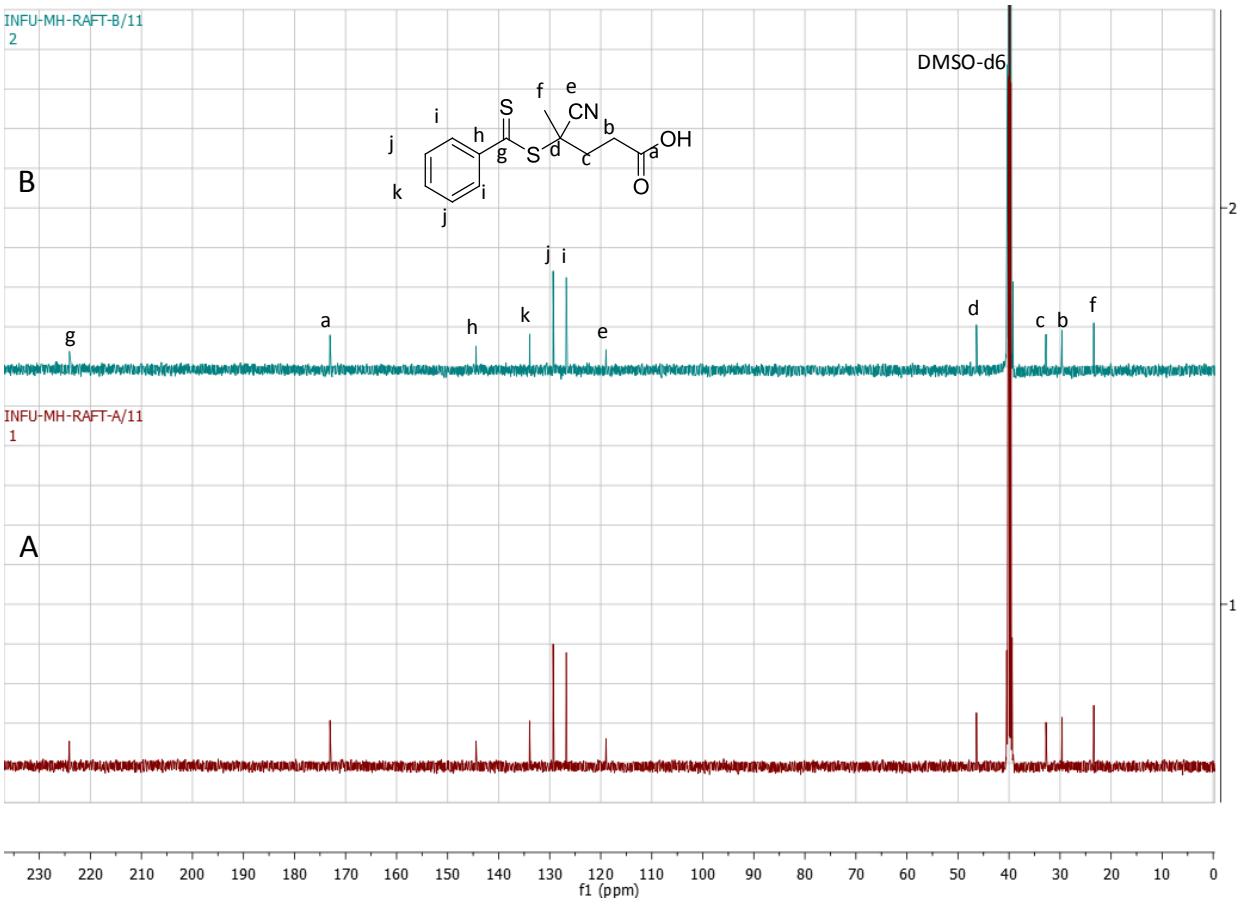

Figure 5.31 ^{13}C-NMR of RAFT agent dissolved in DMSO-d6, after treatment with aqueous HF solution (A), and before treatment (B).

5.3 Conclusions and Outlook

Thin molecularly imprinted polymer (MIP) films were grafted from porous silica using immobilized azoinitiators or RAFT chain transfer agents. Removing the silica supports from the above composites by etching, led to nanometer thin walled beads with structure, morphology and recognition properties strongly depending on the film thickness of the original composite. The resulting polymer beads prepared using immobilized azoinitiators showed a perfectly uniform distribution of binding sites whereas those prepared by controlled grafting showed a record high saturation capacity. The method combining templated synthesis, surface initiated polymerization

and controlled polymerization techniques hence, successfully address the main deficiencies of previous imprinting techniques in terms of imprinting efficiency, binding capacity and a binding site heterogeneity.

This approach may be extended to develop new kind of materials, where one can tune the surface properties. Surface initiated controlled radical polymerization offers the grafting of multiple layers with different composition, structures and functions on different support materials. After removing the support, the innermost layer would be exposed to give a material with non equivalent surfaces (Scheme 8). For example, first poly (HEMA) as hydrophilic layer grafted on porous silica support and consecutively constructed a second layer with poly (styrene) as a hydrophobic. After the silica removal, a porous material with walls containing one hydrophobic and one hydrophilic surface would be obtained. This could be used to enhance the efficiency in liquid-liquid extractions where the hydrophobic pores would be filled with organic phase and the hydrophilic pores with the aqueous phase.[27] Based on support material morphology one can design and synthesis thin walled materials with high surface area. The living properties of the grafting allow an improved control of the surface properties of the two pore systems. This suggests a new concept for the engineering of nanostructured materials for dedicated separations, catalysis or transport.

6 Results and discussion (IIC): Layer by layer grafting of thinfilm MIP via SIRAFT

Few years ago the group of Sellergren showed that functionally imprinted composite materials can be prepared by grafting of MIPs from azo-initiator[89,94] or benzyl-N,N-diethyldithiocarbamate iniferter[92] modified porous silica supports. They demonstrated the living properties of the latter system by consecutive grafting of two polymer layer imprinted with two different templates or one imprinted and one non imprinted layer in any order.[93] Later these composites were evaluated as a stationary phase in HPLC and selectively they showed the switching phenomenal properties towards target molecules. The authors did not show the layered nature of the composites by removing the underlying silica support. Moreover iniferter based supports have been used for layer by layer grafting of imprinted polymers. For example Mayes group prepared a multi layer molecularly imprinted core shell nanoparticles for propranolol, naproxen and morphine using iniferter modified support.[97]

To expand on the topic focused on methods for polymers were grafted from a common silica support using an R-immobilized RAFT agent[80,123] with soluble azo-initiator further the living character of this polymerization was used for consecutive grafting of three polymer layer imprinted with two different templates and one non imprinted layer in any order. Later these composites were treated with aqueous ammonium hydrogen difluoride to remove the silica support (Figure 6.1). Evaluation was performed by characterising the pore structure, morphology and template recognition of the polymers.

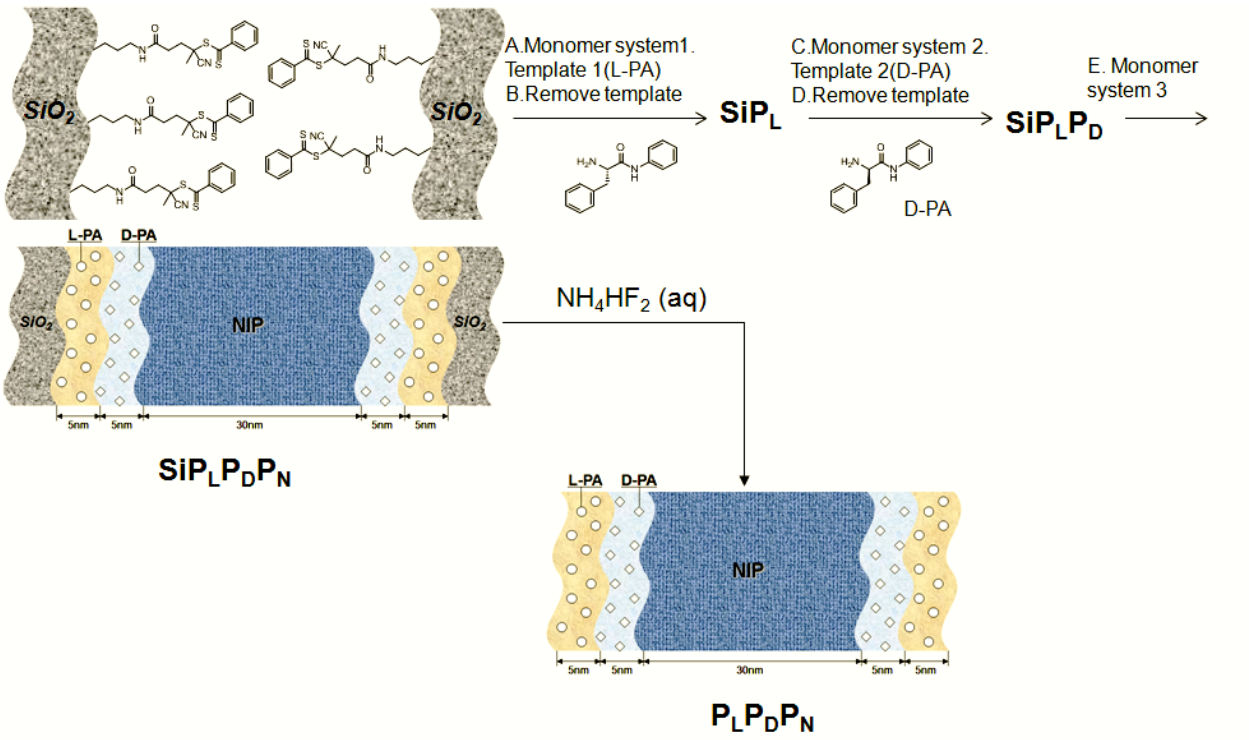

Figure 6.1 Schematic representation of layer by layer grafting procedure

6.1 Synthesis and characterization of RAFT modified support

The present work demonstrates that RAFT-modified support materials can be used to prepare molecularly imprinted composites exhibiting a switching molecular recognition property. The RAFT agent were coupled to readily available silica-based supports; this was followed by grafting of copolymers of methacrylic acid (MAA) and ethyleneglycol dimethacrylate (EDMA) using D- or L-phenylalanine aniline [D(L)-PA] as template and toluene as solvent (Figure 6.1 and Table 6.2). The success of the grafting was confirmed by the standard characterization technique (Table 6.3). As can see the percentage mass loss was increased with consecutive grafting as well %C increases with respective grafted layers. The film thickness was calculated using TGA. After successful consecutive grafting of three layers with two imprinted layers and one nonimprinted layers the silica support was dissolved in HF solution and confirm the complete removal of silica by TGA and elemental analysis.

RAFT modified silica was synthesized by ethyl chloroformate catalyzed coupling of 4- cyno pentanoic acid dithiobenzoate to amino modified silica to reach a final coverage of 19% for the

support. As shown in Table 6.1 this resulted in a surface coverage of initiators in accordance with previous investigations.[80] The coupling reaction was monitored by TGA (Figure 6.2) and Elemental analysis. TGA curves diplays the 2% mass loss in between 50-900 ^{o}C for starting material while after coupling the mass loss percentage was increased to 3.9% which means the area density was 1.54 µmol/m^2 of RAFT agent was covered the silica surface that is 19% surface coverage from total (8 µmol/m^2) The area density and surface coverage values were calculated using TGA and elemental analysis and they are in good agreement. The values shown in the bracket was calculated by mass loss from TGA (See in experimental section).

Table 6.1 Characterization of the RAFT modified silica supports used for grafting.

Si-500 support	%wt loss (100-900^{0}C)	Elemental comp.			Area density (Ds) µmol/m^2	Coverage %
		%C	%N	%S		
Si500APS	2	0.55	0.28		1.72 (2.53)	22 (32)
Si500RAFT	3.9	1.18	0.29	0.35	0.91 (1.54)	11 (19)

6.1.1 Layer by layer grafting and characterisation

The composites were consecutively prepared by surface initiated RAFT polymerization using ratio of RAFT agent to azoinitiator (ABDV) is 2. The first (layer1), the second (layer2), and the third (layer3) grafted layers were produced in presence or absence (non imprinted polymer layer, NIP) of added template (L or D-PA) Table 6.2. The third layer composite ($SiP_LP_DP_N$) etched with fluoride to yield new kind of material $P_LP_DP_N$ (Figure 6.1).

Table 6.2 Polymer feed composition with respect to nominal film thickness.

composite Si-500-RAFT	Nominal film thickness value indicated in bracket (nm)			Silica Support	Template (LPA/DPA) mg	Monomer (MAA) µL	Crosslinker (EDMA) µL	RAFT/ABDV	Toluene mL
	Layer1	Layer2	Layer3						
SiP_L	L-PA (5)	--	--	1g	7.7	22	244	2	20
SiP_LP_D	--	D-PA (5)	--	600mg	4.65	13.2	146	2	12
$SiP_LP_DP_N$	--	--	NIP (15)	400mg	--	20	229	2	8

The consecutive grafted layer thickness was estimated using TGA. The nominal thickness and average thickness values were in good agreement. From Table 6.3 one can see the percentage of carbon goes on increasing with thickness as well as the percentage mass loss. These results suggest that the consecutive grafted layer was successfully constructed. The scanning electron micrographs (SEMs) shown in Figure 6.4 revealed that the grafting of the first two layers resulted in perfectly spherical beads indistinguishable from the starting silica support. However, the final grafting, performed in order to block any chiral recognition sites, resulted in a rough surface texture indicating an excessive pore filling. Nitrogen sorption isotherms are informative of homogeneity of the grafted polymer films. The isotherms for all composites were type IV exhibiting a hysteresis profile which indicates mesoporosity. Desorption branch was used to calculate the pore size distribution of the composites where the average pore size and pore volume slightly decreases continuously with the grafting content. The pore size distribution was shown in the Figure 6.3.

Table 6.3 Characteristics of Layer-by-Layer molecularly imprinted polymer composites prepared by SI RAFT polymerization.

Composites[a]	RAFT/ABDV	Mass loss (%)	Total film Thickness[b] d(nm)	% C	%N	% S	S_A[c] m^2/g	D_p[c] nm	V_p[c] Cc/g
SiP_L	2	19	5(4.6)	10.61	0.33	0.28	72.33	32.4	0.281
SiP_LP_D	2	30	10(9.4)	17.38	0.30	0.19	41.2	18.6	0.119
$SiP_LP_DP_N$	2	55	25(23)	28.65	0.26	0.15	46.8	22.8	0.06
$P_LP_DP_N$	--	98	--	56.56	2.21	0.19	115	3.5	0.22

a) *The composites were consecutively prepared by surface initiated RAFT polymerization using different ratios of RAFT agent to azoinitiator (ABDV). The first (SiP_L), the second (SiP_LP_D), and the third ($SiP_LP_DP_N$) grafted layers were produced in presence or absence (non imprinted polymer layer, NIP) of added template (L or D-PA). The third layer composite ($SiP_LP_DP_N$) etched with fluoride to yield new kind of thinwalled material $P_LP_DP_N$.*

b) *Film thickness estimated from the % mass loss of the grafted layers film as described in the experimental part.*

c) *The BET specific surface area (S_A), specific pore volume (V_p) and average pore diameter (D_p) were calculated from the nitrogen adsorption isotherms as described in the experimental part.*

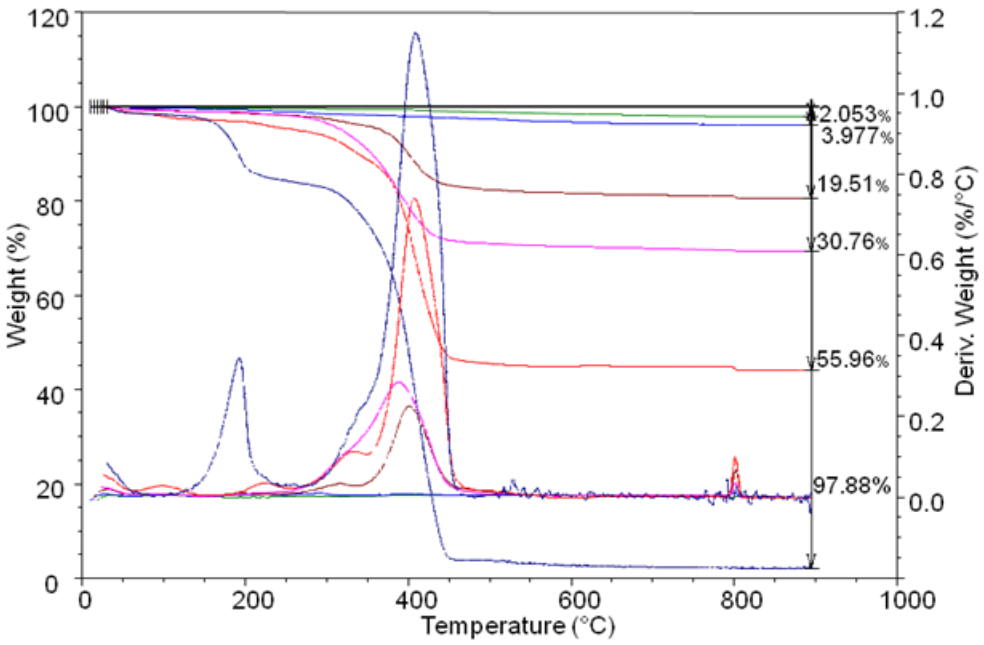

Figure 6.2 TGA curves of (a) aminosilica (b)RAFT modified silica (c) SiP_L(Layer1), (d) SiP_LP_D (Layer2), (e) $SiP_LP_DP_N$ (Layer3), (f) $P_LP_DP_N$, after removal of silica by etching.

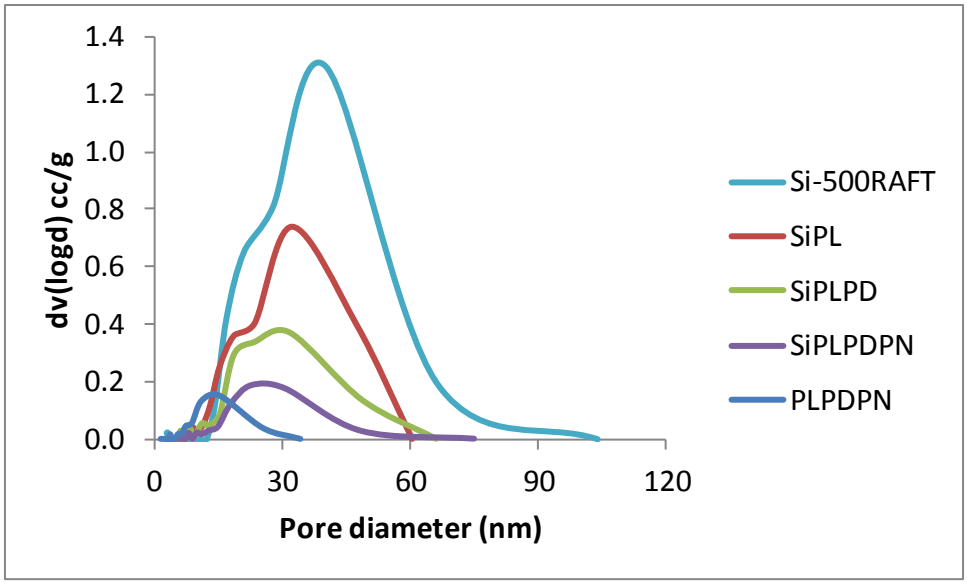

Figure 6.3 Pore size distribution of consecutive grafted layer and RAFT modified silica support.

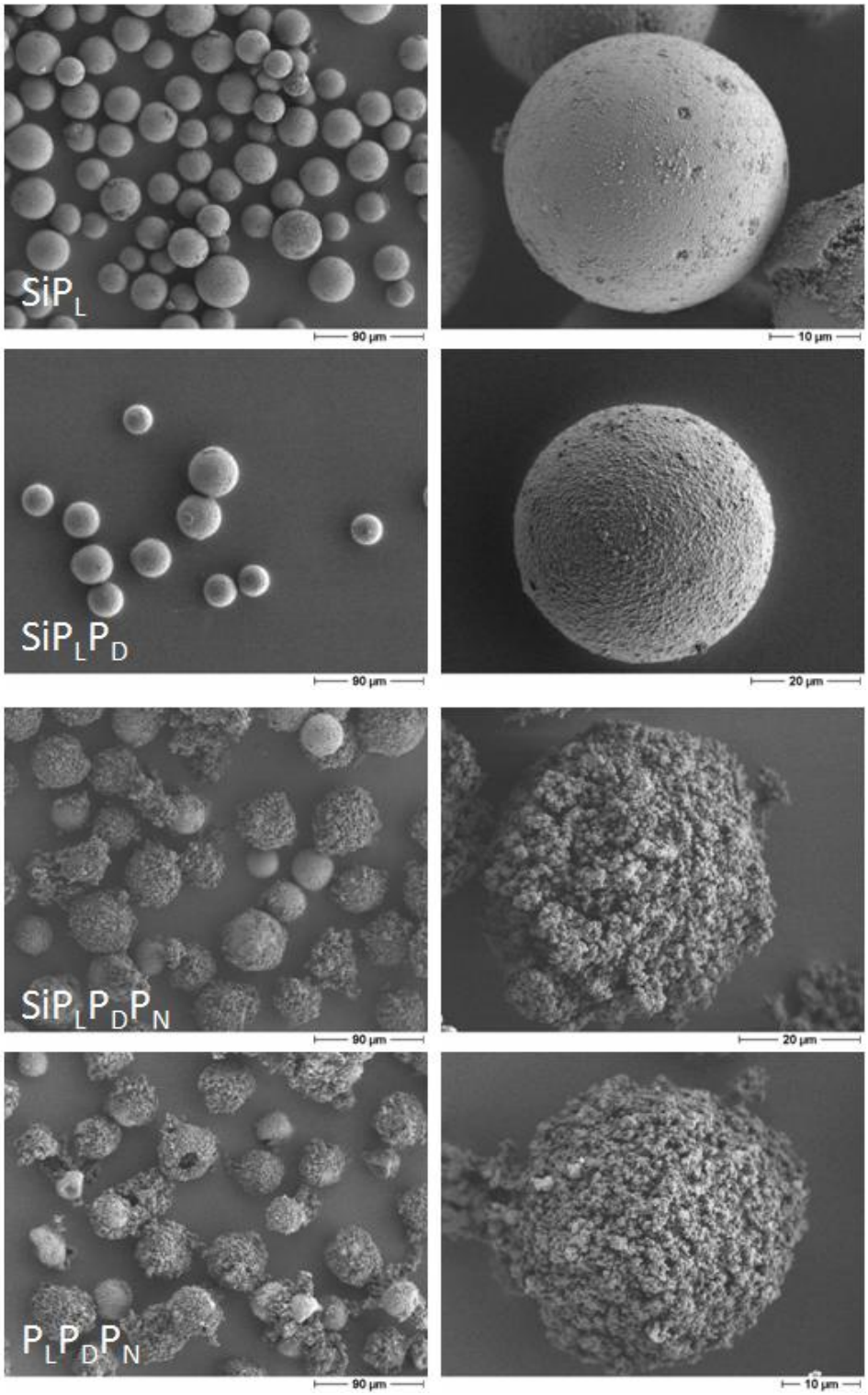

Figure 6.4 Scanning electron micrographs of imprinted polymer composite prepared by RAFT mediated consecutive grafting corresponding to SiP_L(Layer1), SiP_LP_D(Layer2), $SiP_LP_DP_N$(Layer3), and $P_LP_DP_N$ after removal of silica by etching.

6.1.2 Chromatographic Evaluation

The obtained composites beads were packed in to small stainless steel HPLC columns and investigated by liquid chromatography for their ability to retain L-PA and its optical antipode D-PA using pure MeCN and MeCN/sodium acetate buffer pH4.8 (70/30,v/v) as mobile phase. The resulting elution profiles were evaluated with respect to the retention of the two enantiomers, determined as the capacity factor (k′), the enantioselectivity, determined as the separation factor (α= kL/kD). The typical elution profile for 1 mM analyte concentrations were shown in Figure 6.6.

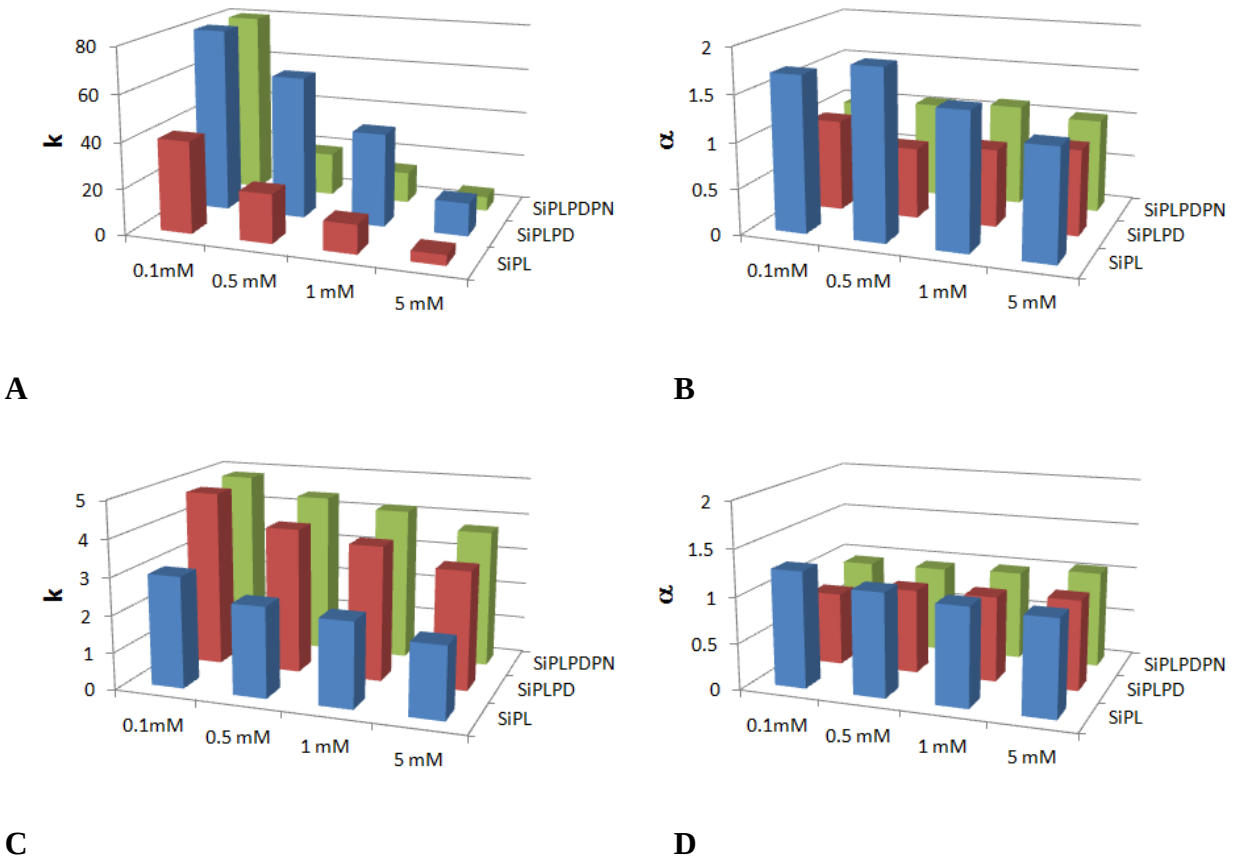

Figure 6.5 Retention factors (kL) for L-PA (A,C) and enantiomer separation factors (α) (B,D) obtained in the chromatographic mode after separate injection of stock solutions of D- and L-PA at four different sample loads for corresponding imprinted composites beads prepared by consecutive grafting from RAFT modified support. Mobile phase: for (A,B); pure acetonitrile, for (C,D);MeCN/Sodium acetate buffer pH 4.8(70/30,v/v).

From Figure 6.5 (A, B) indicated material were packed in to HPLC columns and tested in pure acetonitrile. The composite imprinted with L-PA selectively retain L-PA more than the optical antipode D-PA. In case of D-PA imprinted polymer selectively retain D-PA more than the L-PA it indicates that the enantioselectivity is reversed after consecutive grafting of second layer. This is not the case for third layer where pores were completely filled with prepolymerization mixture without template. This material was also tested in chromatography. As expected, this resulted in an effective cancellation of chiral discrimination ability of the composites. This can be explained as due to the more abudance of carboxyl group on the walls of composites it makes to bind the both analyte non specifically and most of the specific cavity was blocked with non imprinted polymer. All columns display a trend of decreasing in retention factor and enantioselectivity with increasing concentration of sample load in the agreement with previous reports. This is the result of nonlinear chromatography with constant overloading of low abundant high energy binding sites.[80] In case of more aqueous environment mobile phase MeCN/CH_3COONa buffer pH4.8 same trend has been observed but the retentively was somehow decreased as compared to organic mobile phase (Figure 6.5, (C, D)). In aqueous environment the selectivity was increased for second and third layer due the more abundance of carboxyl groups available on walls but the enantioselectivity was not changed significantly.

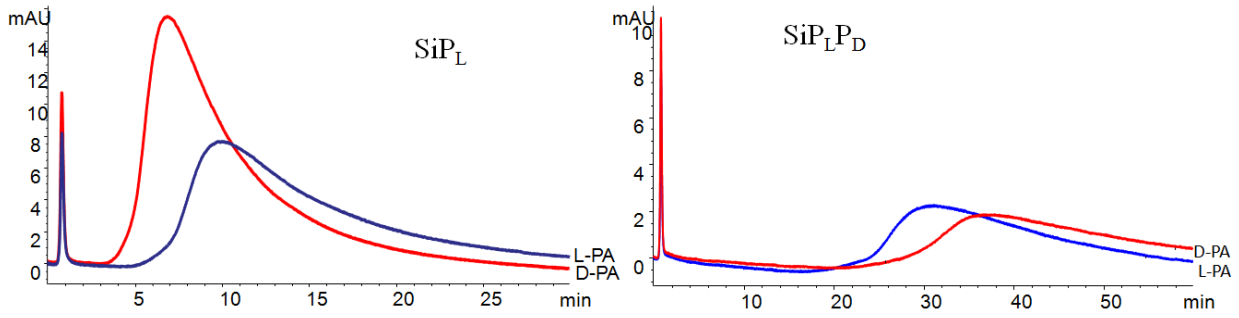

Figure 6.6 Elution profiles of D(red), L(blue)-PA injected (10µL of 1mM solution) separately on columns (35mm x 4.6 mm) packed with indicated material. Mobile phase; pure MeCN, flow rate 0.5mL/min, DAD=260 nm.

After characterization of the consecutive grafted thin film composites the silica support of the pore filled material ($SiP_LP_DP_N$) was removed by fluoride catalyzed etching.to result in polymer beads ($P_LP_DP_N$). This procedure has been developed previously for generating the thinwalled

beads.[80] Here the polymer films was grown inside the silica pore system by azo modified silica support or RAFT modified silica support after the polymerization the silica is etched away by treat with fluoride. This leaves behind a thinwalled beads which size is strongly depending on nominal thickness of grafted films. In contrast to thinwalled beads, removal of the silica from consecutive grafted layers would leaves behind the new kind of material as shown in Figure 6.1. After the etching step the resulting polymeric material was characterized by standard technique as in Table 6.3. It is clear from results of elemental analysis and TGA mass loss curve that the silica had been effectively removed from the third layer. Figure 6.4 shows that the scanning electron micrographs of the composites beads as well as the particles resulting from silica etching. A closer study leads to the following general observation. Whereas the composite particle was spherical and size of the bead was 20µm but polymer also looks grown out side of the pores, the etched particles size was 10µm which is retained the original shape of the composite precursor. Interestingly $P_LP_DP_N$ features much narrower pores 15 nm average pore diameter and higher surface area than the composites. Assuming that this pore system represents a perfect inverse replication of the original silica mold it is reasonable that these walls are thinner than the original diameter of the pore system.

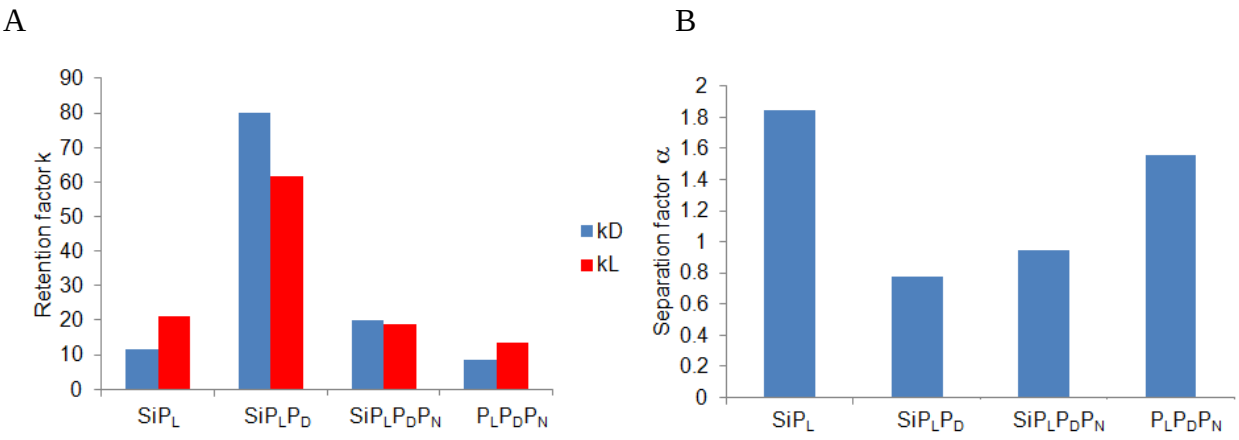

Figure 6.7 Retention factors (k) for L-PA(kL) and D-PA (kD) (A) and enantiomer separation factors (α) (B) at 30 nmol/cm^2 sample loads for corresponding imprinted composites beads and thinwalled material after removal of third layer. Mobile phase: pure Acetonitrile.

The resultant bead from etched one was packed in to stainless steel column under negative pressure using vacuum membrane pump and investigated by liquid chromatography for their

ability to retain L-PA and its optical antipode D-PA using MeCN as mobile phase. Figure 6.7, shows the chromatographic properties of the materials after 1-3 successive grafting of imprinted or non imprinted polymer layers. The first layer was prepared with a thickness of 5 nm in presence of LPA exhibited pronounced L- selectivity as manifested in a separaton factor of 1.8. The reciprocity of this approach was demonstrated by grafting a layer in the presence of D-PA which as expected resulted in the opposite enantioselcectivity.

The living properties of the RAFT were then assessed by the grafting of a second layer targeted toward the optical antipode of the template used in the first layer and third layer was grafted with non imprinted layer. Thus grafting of a DPA imprinted layer on the LPA imprinted layer resulted in reversal of enantioselectvity (Figure 6.7). It is interesting to note that this occurs despite the same average thickness of the first layer compared to second This could be the results of blocking of the sites of the first layer by the second graft of better access to the second layer or combination of the both effects.[93] The non imprinted third layer was slightly selective towards the DPA but decreased the selectivity and separation factor compared to second layer, it suggest that the second layer binding sites were minor accessible to DPA. For getting back to the first layer access it is necessary to remove the silica from consecutively grafted three layered composites. After removing the silica the new type of beads packed in to the column and assessed by HPLC in acetonitrile mobile phase. The HPLC results clearly suggest that the newly generated beads were selectively bound to LPA over DPA (Figure 6.7). It indicates that the blocked binding sites were opened or accessible to the target molecule.

6.2 Conclusions

New approaches toward fabrication of nanostructured molecularly imprinted thin films were grafted on solid silica support via surface initiated RAFT polymerization. The first layer was grafted with thickness of 5 nm of poly (MAA-co-EDMA) in presence of L-PA as template or target molecule. The living properties of the first layer system used by consecutive grafting of two polymer layer imprinted with antipode of first layer target molecule and one non imprinted layer. The successful grafting was confirmed by the elemental analysis and thermogravimetric analysis. Layer thicknesses were calculated using themogravimetric analysis (TGA) which is well accordance with nominal thicknesses. The successes of grafting were reflected in the

separation of the two enantiomers obtained using the composite materials as chromatographic stationary phases. Later the silica was removed from the composites by etching, led to new kind of beads exhibits mesoporous morphology and enantionselectivity towards first layer target molecule L-PA. The previously covered L-selective sites had been uncovered. This concept of construction of surface imprinted layer by layer films can be easily extended to the other bioactive molecules.

7 Experimental Section

7.1 Investigation of influence of RAFT agent on performance of L-PA MIPs

7.1.1 Odourless RAFT agent synthesis

The synthesis of odourless RAFT agent (α-Cyanobenzyl Dithibenzoate) is reported in the literature[77] and consists of two different steps: synthesis of α-bromobenzene acetonitrile followed by Grignard reaction.

7.1.1.1 Synthesis of α-bromobenzene acetonitrile

Phenylacetonitrile (1.0 g, 8.53 x 10^{-3} mol), N-bromosuccinimide (1,6 g, 8.53 x 10^{-3} mol) and benzoylperoxide (0.01 g, 4.13 x 10^{-5} mol), were refluxed in dry carbon tetrachloride (10.0 mL) for 6hours. The product was cooled and filtered and the solvent was removed under vacuum. The product was purified through a silica column (hexane: diethyl ether, 70:30). The product was obtained as yellow oil (40 %).

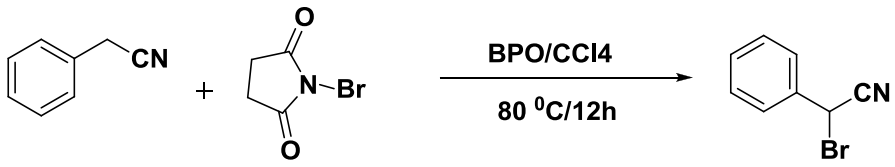

Scheme 9 Synthesis of α-bromobenzene acetonitrile

C8H6BrN; ^{1}H NMR ($CDCl_3$) δ (PPM): 5.50 (s, 1H, C(CN)*H*(C6H5)), 7.43-7.46 (m, 3H,Ar*H*), 7.55-7.58(m, 2H, Ar*H*).

C8H6BrN; **^{13}C** NMR ($CDCl_3$) δ (PPM): 27.4, 116.4, 127.8, 128.9, 129.5, 129.8, 130.4

7.1.1.2 Synthesis of α-Cyanobenzyl Dithibenzoate

Phenylmagnesium bromide (3M solution in ethyl ether), was diluted to 20ml with anhydrous THF. Carbon disulfide (1.2 g) was added dropwise to this mixture, and the mixture was stirred for 0.5h at room temperature. To the dark red solution was added drop wise 3g of alpha-bromobenzene acetonitrile, and the mixture was stirred for another 3h. Water was added to the mixture, and organic product was extracted with diethyl ether (3X 50ml), dried with magnesium sulfate overnight, and filtered. After the removal of the solvent and column chromatography (3:1 mixture of hexane and ethyl ether), pure product was obtained as a red, odourless solid (70% yield).

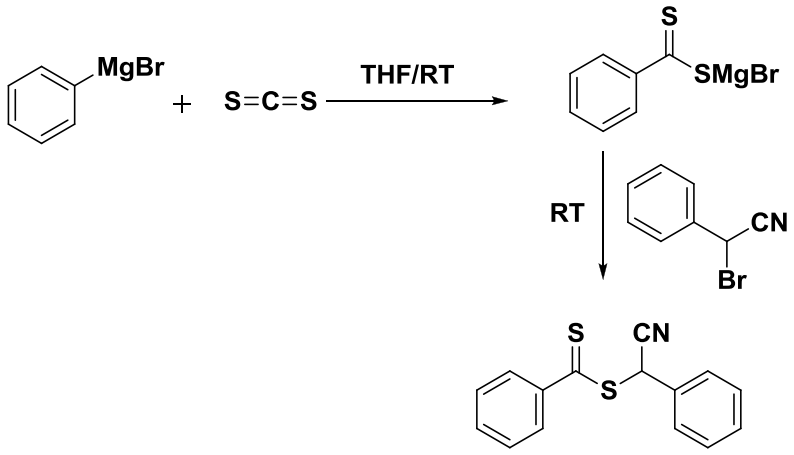

Scheme 10 Synthesis of α-Cyanobenzyl Dithibenzoate

^{1}HNMR (CDCl3) δ(PPM): 6.06 (s,1H,C(S)SC(CN)H), 7.40-7.47 (m,5H,ArH), 7.55-7.61 (m,3H,ArH), 7.98-8.00 (d,2H,ArH)

^{13}C-NMR ($CDCl_3$); 43.33, 116.59, 117.08, 127.42, 128.08, 128.47,129.04, 129.78, 130.77, 133.83, 143.44, 222.71

7.1.2 Template Synthesis

The synthesis of L/D-phenylalanine anilide is reported in the literature [27]and consists of two different steps: synthesis of *BOC*-L/D-phenylalanine anilide followed by deprotection.

7.1.2.1 Synthesis of BOC-L/D-Phenylalanine anilide

BOC-L-phenylalanineanilide was prepared by condensation of *BOC*-L-phenylalanine and aniline in DMF using DCC and HOBt as condensation agents. 0.05 mol (4.5 mL) of freshly distilled aniline were added under stirring to a solution of 0.06 mol (15.7 g) *BOC*-L/D-Phe-OH, 0.06 mol (8.1 g) HOBt and 0.08 mol (16.5 g) DCC in 200 mL dry DMF. After stirring for a few hours, the mixture was filtered, the filtrate dried over $MgSO_4$ and filtered. The filtrate was then reduced to dryness under reduced pressure. The solid residue was dissolved in DCM and washed with 300 mL each of 1M $NaHCO_3$, 0.5 M HCl and water. The product obtained after evaporation of DCM was recrystallised from ethanol.

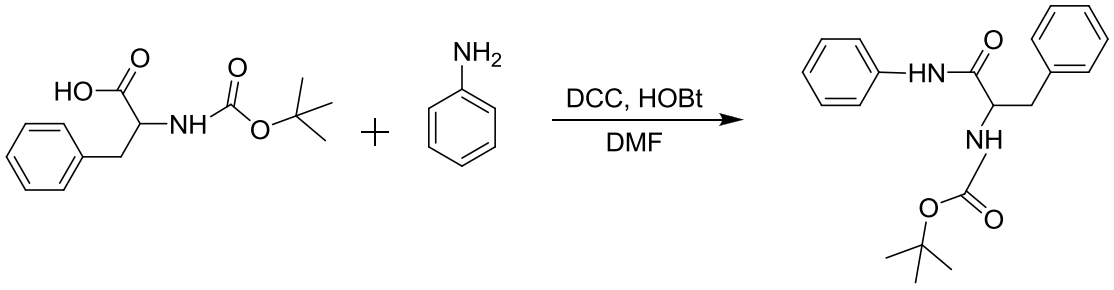

Scheme 11 Synthesis of BOC-L/D phenylalanine aniline

7.1.2.2 Synthesis of L/D-Phenylalanine anylide

BOC-protecting group was removed by treatment with trifluoroacetic acid. To a solution of 0.03 mol *BOC*-L/D-phenylalanine anilide in 30 mL DCM were added 30 mL TFA under cooling with an ice/salt mixture. The mixture was stirred for 2h and reduced to dryness under reduced pressure. The solid residue was dissolved in 100 mL toluene and the same amount of 1M HCl

was added. After stirring for a short time, the phases were separated and the toluene phase was washed again with 1M HCl. The combined aqueous phases were basified with 5M NaOH and extracted with DCM. After drying over $MgSO_4$, filtration and evaporation of the solvent, the residue is recrystallised from tert butylmethyl ether.

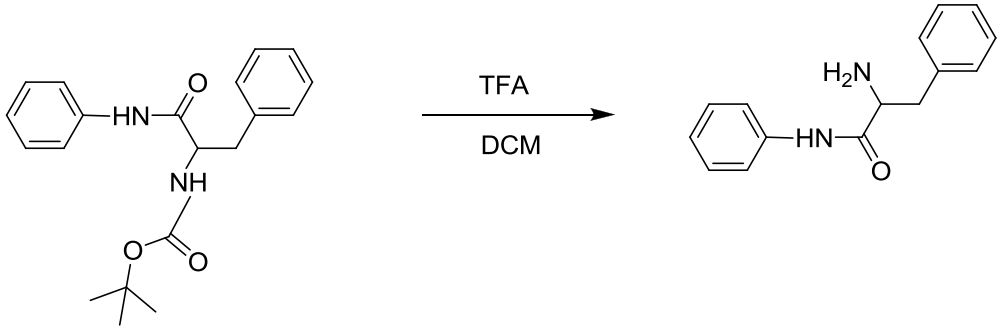

Scheme 12 Synthesis of L/D- Phenylalanine anilide.

Elemental Analysis: %C= 75.06; %H=6.71; %N=11.6

^{1}H-NMR ($CDCl_3$): δ=1.4 (s, 2H, -NH_2), δ=2.76 (m, 1H, -CH_2^{β}), δ=3.3 (m, 1H, -CH_2^{β}), δ=3.7 (m, 1H, -C*H*) δ=7.05 (m, 2H, m- NH-C_6H_5); δ=7.3 (m, 5H, -C_6H_5), δ= 7.5(m, 3H, o- and p- in NH-C_6H_5), δ=9.37(s, 1H, N*H*)

7.1.3 General Polymerization Procedure

The standard polymerization procedure is as fallows. To 0.34mL (4 mmol) MAA, 120mg (0.5 mmol) L-phenylalanine anilide (L-PA), 3.8 ml (20mmol) EDMA in 5.7 ml toluene as porogen, 62.1mg (0.25 mmol) ABDV as initiator and different concentration of (α-Cyanobenzyl Dithibenzoate) RAFT agent was added in a 20mL glass scintillation vial. The mixture was transferred to a 50ml glass polymerization tube. This was degassed with nitrogen for 10 minutes and flame sealed. The thermally initiated polymerization was done at 50 ^{o}C for 24h and further curing was carried out at 70 ^{0}C for 24h in an oil bath. After 48h the tubes were crushed and the polymers ground in a mortar, followed by soxhlet extraction in methanol and formic acid

mixture in ratio 80:20 for 24h and 24h in methanol. The polymers were dried overnight under vacuum at 40 ^{0}C and sieved to a 25-50 µm particle size fraction.

The Non Imprinted polymers were prepared exactly similar procedures but in absence of template.

7.2 Thin film composite beads and generated thinwalled beads

7.2.1 Silica Surface Activation

300 mL (115mL HCL+ 185mL H2O) of 17 % HCl were poured into a 500 mL three-necked round bottom flask, using a funnel. The round bottom flask was equipped with a condenser and an overhead stirrer. The calcined silica (20 g) was added in small portions while stirring. The flask was placed in an oil-bath (electronic-thermometer; 150°C; heater: 200°C) and the suspension was subsequently refluxed for 24h. The silica was filtered through a glass filter funnel and washed twice with 150 mL aliquots methanol. Finally, the silica was dried in a vacuum oven at 80°C for 4h and at 150°C for 12h.

7.2.2 Silanisation of silica surface with Aminopropyl triethoxysilane

In a three-necked 250 mL round bottom flask equipped with an overhead stirrer, a condenser and a dropping funnel, 20g of previously rehydroxilised silica were suspended in 270 mL dry toluene and the flask was connected to a N_2 stream. Then, 17 g (76.8 mmol) of amino propyltriethoxysilane were added drop-wise to the suspension and the mixture was refluxed with stirring for 24h. The modified silica was filtered, washed with 100 mL toluene and 200 mL MeOH and dried in a vacuum oven at 60°C.

Surface density of APS modified silica (Ds = 1.2 µmol/m^2). This is calculated based on percentage mass loss by Thermogravimetry.

7.2.3 End-Capping using Hexamethyldisilazane (HMDS)

In 250 mL three-necked round bottom flasks equipped with a condenser, an overhead stirrer and a dropping funnel, 5 g of the silanised silica gels obtained in the previous step were suspended in 60 mL DCM. 1 mL of HMDS in 20 mL dry DCM was added drop-wise to the suspension under N_2 flow and the whole mixture was stirred at room temperature under nitrogen for 24h and then refluxed for a further 3h The products were filtered through glass funnels, washed with 50 mL MeOH to remove traces of unreacted HMDS and dried in a vacuum oven at 40°C for 24h.

7.2.4 Azo-initiator immobilization

The silica supports were modified with azoinitiator in two steps as previously reported.[81] Silanization of rehydroxylated silica with APS was followed by condensation of the initiator ACPA with the surface amino groups to give the initiator modified supports listed in Table 4-1. In 250 mL three-necked round-bottom flasks equipped with a condenser, an overhead stirrer and a dropping funnel, 6g batches of rehydroxylated silica were suspended in 80 mL dry toluene. The whole system was flushed with N_2. According to the number of silanol groups on the silica surface (8 μmol/m^2) the appropriate amounts of APS was added to the mixture and refluxed overnight at 110°C. The products were filtered through glass funnels and washed with 2x 50 mL of toluene and 2x 50 mL of MeOH. The products were dried in a vacuum oven at 40°C for 24h. The products were characterised using elemental microanalysis, FT-IR spectroscopy and TGA and the amount of coupled ligands was estimated.

The silica gel used for this experiment had a 2.9 μmol/m^2 surface coverage of amino groups, meaning that ~ 30 % of the initial silanol groups had been converted into amino groups. The amino groups were reacted with the diacid azo-initiator (ACPA) in order to obtain one material with high initiator coverage, used for the RAFT polymerization, and another one with lower initiator coverage, useful for the conventional grafting in order to minimise solution polymerization. Based on our previous experience, 100% conversion of the amino groups into initiator groups will lead to a complete pore blockage in the resulting composites and a low

efficiency in HPLC. Therefore, the reaction conditions were designed to favour a maximum 50% conversion of the existing amino groups for the highest initiator coverage. Thus, for the high density SiACPA (1.5 μmol/m^2), to a 500 mL three-necked round bottom flask, equipped with a dropping funnel, on overhead stirrer and a ethanol thermometer, were introduced 250 mL dry THF. The mixture was then cooled at - 78°C using a liquid-nitrogen-ethanol bath. Under continuous N_2 flow, 5.04 g (18 mmol) azo-initiator (ACPA), 1.95 g (18 mmol) ethylchloroformate and 1.82g (18 mmol) triethylamine were added. After stirring for 30 min at -78°C, 25 g of amino-modified silica were added to the mixture and the suspension was stirred for 3h at -78°C and then for 4 h at -10°C. The product was filtered, washed with THF and MeOH and dried under vacuum at room temperature.

7.2.5 Immobilization of RAFT agent

In a three-necked round bottom flask (250 mL), equipped with a dropping funnel, an overhead stirrer and an ethanol thermometer, was introduced 200 mL dry THF and the flask purged with nitrogen. For Si100-APS: 1.60g (5.74 mmol) 4-cyanopentanoic acid dithiobenzoate, 0.62g (5.75 mmol) ethylchloroformate and 0.58g(5.75 mmol) triethylamine and for Si500-APS: 1.395g 4-cyanopentanoic acid dithiobenzoate, 543mg ethylchloroformate and 506 mg triethylamine were consecutively added. The mixture was then cooled at -78°C using a liquid-nitrogen-ethanol bath. After stirring for 30 min, amino modified silica (Si100-APS: 15g; Si500-APS: 25g) was added to the mixture and the suspension was stirred for 3h at -78°C and then for 4 h at -10°C. The product was then filtered, washed with THF and MeOH and dried under vacuum at room temperature. The surface density of RAFT agent calculated based on percentage mass loss by Thermogravimetry (TGA) was 0.72μmol/m^2 (Si100-RAFT) and 3.32μmol/m^2 (Si500-RAFT).

7.2.6 Grafting of polymer from azo-modified silica

The grafting was performed in specially designed tubes containing 1g of azo-modified silica particles suspended in a mixture containing L-PA (8.0mg (d=1nm), 14.0mg (d=2 nm) or 18.9mg

(d=3nm)), MAA (23.0mg (d=1nm), 41.0mg (d=2nm) or 54.1mg (d=3nm)) and EDMA (264.5mg, (d=1nm) 472.2mg (d=2nm) or 623.1mg (d=3nm)) diluted with different volumes (0, 5, 10, 15, 20 mL) of dry toluene. After purging the mixture with nitrogen, polymerization was initiated by UV-irradiation at 15°C for 24h. After polymerization, the suspended particles were filtered through a sintered glass funnel and extensively washed with methanol/formic acid/water 80/15/5 (v/v/v) and pure methanol. The composites were finally dried in vacuum oven at 40°C for 12h.

7.2.7 Grafting of polymer from RAFT-modified silica

RAFT modified silica particles (Si-RAFT) (1g) were suspended in a prepolymerization mixture containing L-PA (28.9mg, 0.12mmol), MAA (0.081mL, 0.96mmol) and EDMA (0.905mL, 4.8mmol) dissolved in 20 mL of dry toluene. The polymerization mixture was subjected to three freeze-thaw cycles under nitrogen whereafter the initiator ABDV (115 mg, (SiPR) and 29mg, ($SiPR_E$)) was added. This corresponds to a ratio of RAFT/initiator of 0.5 (SiPR) and 2 ($SiPR_E$). Polymerization was initiated at 50°C for 24h. After polymerization the particles were filtered through a sintered glass funnel and washed with methanol/formic acid/water, 80:15:5(v/v/v) and pure methanol and then the polymer was dried under vacuum at 40°C overnight.

$SiPR^{500}$, $SiPR_E^{500}$ and $SiPR_{EE}^{500}$ were prepared in a similar manner but the prepolymerization mixtured contained L-PA (5.2mg, 0.022mmol), MAA (0.015mL, 0.173mmol) and EDMA (0.163 mL, 0.865mmol) and the RAFT/initiator ratio was adjusted to 0.3, 1.4 and 14 respectively.

7.2.8 Coupling of the fluorescence label

The obtained polymers (50 mg), 1-hydroxybenzotriazole (HOBt) (8 mg, 1.08 mmol) and 1,3-dicyclohexylcarbodiimide (DCC) (12.3 mg, 2.53 mmol) were mixed in dry DCM (10 mL) and stirred for 0.5h before a solution of 3-aminoquinoline (3-AQ) (8.5 mg, 1.22 mmol) in 0.5 mL

DCM was added dropwise. The solution was stirred for several hours and the modified polymer was washed with 50 mL DMF and with 50 mL MeOH and dried under vacuum at 40°C.

7.2.9 Generation of thinwalled MIPs

Portions (1g) of the composite materials were suspended in 10 mL of 3M NH_4HF_2 (aq.) in Teflon flasks. The suspensions were shaken at room temperature for 2 days and then filtered through glass funnel. The resulting polymer was washed with water to remove unreacted NH_4HF_2 and dried in vacuum oven at 40 ^oC for 24h.

7.2.10 Dithoester RAFT group survival test

200 mg of soluble RAFT agent was dispersed in 2mL of 3M NH_4HF_2 (aq.) solution in eppendorf tube. The suspension was kept shaking for 24h and then filtered through glass funnel followed by washed with water and dried under vacuum at laboratory temperature and characterized by NMR.

7.3 Layer by layer grafting of thinfilm MIP via SIRAFT

End capped Amino modified silica was purchased from Fuji Japan and directly used for RAFT agent immobilization as described section 7.2.5.

7.3.1 Immobilization of RAFT agent

In a three-necked round bottom flask (500 mL), equipped with a dropping funnel, an overhead stirrer and an ethanol thermometer, was introduced 250 mL dry THF and the flask purged with nitrogen. 795.15mg (2.85 mmol) 4-cyanopentanoic acid dithiobenzoate, 274µL (309.28mg, 2.85 mmol) ethylchloroformate and 397µL (288.4mg, 2.85 mmol) triethylamine were consecutively

added. The mixture was then cooled at -78°C using a liquid-nitrogen-ethanol bath. After stirring for 30 min, 25g of aminomodified silica was added to the mixture and the suspension was stirred for 3h at -78°C and then for 4 h at -10°C. The product was then filtered, washed with THF and MeOH and dried under vacuum at room temperature. The surface density of RAFT agent calculated based on % mass loss by Thermogravimetry (TGA) was 1.54 μmol/m^2.

7.3.2 Grafting of Layer by layer MIP films via RAFT-modified silica

Layer1-LPA (SiP_L): Si500-RAFT particles (1g) were suspended in a prepolymerization mixture containing L-PA (7.7mg, 0.032mmol), MAA (0.022mL, 0.26mmol) and EDMA (0.244 mL, 1.3 mmol) dissolved in 20 mL of dry toluene. The polymerization mixture was subjected to three freeze-thaw cycles under nitrogen where after the initiator ABDV (8.7mg), was added. This corresponds to a ratio of RAFT/initiator of 2. Polymerization was initiated at 50°C for 24h. After polymerization the particles were filtered through a sintered glass funnel and washed with methanol/formic acid/water, 80:15:5(v/v/v) and pure methanol and then the polymer was dried under vacuum at 40°C overnight.

Layer2-DPA (SiP_LP_D): This was prepared in a similar manner but the prepolymerization mixture contained D-PA (4.65mg), MAA (13.2 μL) and EDMA (146 μL) for 600mg of (layer 1)Si500 RAFT composite and the RAFT/initiator ratio was adjusted to 2.

Layer3-Nonimprinted ($P_LP_DP_N$): This was also prepared in a similar manner but the prepolymerization mixture contained without template MAA (20 μL) and EDMA (229 μL) for 400mg of (layer 2) Si500 RAFT composite and the RAFT/initiator ratio was adjusted to 2.

7.3.3 Silica removal

This experiment was performed as described in above section 7.2.9. Portions (1g) of the composite materials were suspended in 10 mL of 3M NH_4HF_2 (aq.) in Teflon flasks. The suspensions were shaken at room temperature for 2 days and then filtered through glass funnel.

The resulting polymer was washed with water to remove unreacted NH_4HF_2 and dried in vacuum oven at 40 ^oC for 24h.

7.4 Characterization techniques

7.4.1 Thermogravimetric analysis

Thermogravimetric analysis (TGA) was carried out using a TGAQ50 (TA instruments, Eschborn, Germany). The sample (~ 10-15 mg) was placed in a platinum pan, which is suspended in a sensitive balance together with the reference pan. The sample was then heated, in a furnace, with at a rate of 10 or 20°C/min, under N_2 atmosphere.

This analysis is a thermal method that involves the measurement of weight loss as a function of temperature or time. TGA can be used to quantify the mass change in a polymer associated with transitions or degradation processes [190]. Furthermore, information on the extent of residual silica in composite materials can be obtained.

The film thickness of grafted polymer layer was calculated using following equation[180]

From % mass loss (TGA)

$$d = \frac{Dp}{2}\left[1 - \sqrt{1 - \left(\frac{\%\text{wt. loss}}{(100 - \%\text{wt. loss})\rho . Vp.}\right)}\right] \qquad \text{Eq. 7.1}$$

Where, D_p = pore diameter of the composite (nm), V_p = pore volume of the composite (mL/g),

ρ = weighted average density of monomers (g mL^{-1})

The area density (Ds) of the immobilized ligand and grafted amount of polymer was calculated based on % weight loss of content versus the preceding step monitored by thermogravimetric analysis.[191]

$$Grafting\ amount\ (\mu mol g^{-1}) = \frac{\left[\frac{\%W100-900}{100-\%W100-900}\right] X\ 100 - \%Wsilica}{Mw\ X\ 100}\ X\ 10^6 \qquad \text{Eq. 7.2}$$

$$Ds\ (\mu mol m^{-2}) = \frac{\left[\frac{\%W100-900}{100-\%W100-900}\right] X\ 100 - \%Wsilica}{S\ X\ Mw\ X\ 100}\ X\ 10^6 \qquad \text{Eq. 7.3}$$

Where

$\%W_{100\text{-}900}$ = % mass loss of modified silica between 100 ^{0}C and 900 ^{0}C

$\%W_{silica}$ = % mass loss of starting silica

Mw = Molecular weight of coupled ligand

S = surface area of the silica support (Si100=320 m^2/g, Si500=45 m^2/g)

7.4.2 Differential scanning colorimeter (DSC)

Reaction kinetics was measured by DSC using a DSC-Q200 TA- instrument. Approximately 8 mg (8 µL) of the reaction mixture was placed in hermetically sealed aluminum sample pan and the DSC cell was purged with ultra high purity nitrogen for 5 min before the DSC was equilibrated at the reaction temperature. During the isothermal DSC scanning, a nitrogen flow rate of 50 ml/min was maintained to prevent intervention by oxygen. Dynamic scanning was also carried out using 10 ^{0}C/min heating rate. The DSC measures the heat flow (dH/dt) from the smaple relative to the reference pan. The heat flow evolving from the exothermic reaction was measured as a function of time. The double bond conversion could be calculated by using fallowing equation(X1, X2).[49]

$$X1 = \Delta Ht/\Delta H_0 \qquad \text{Eq. 7.4}$$

$$X2 = \Delta H_{dy}/\Delta H_0 \qquad \text{Eq. 7.5}$$

Where ΔHt is the reaction heat released up to time t, ΔH_{dy} is the reaction heat generated during dynamic scan and ΔH_0 is the theoretical enthalpy of the methacrylate double bond (13.1 kcal/mol).

7.4.3 Thermoporometry

Thermoporometry is a technique to measure the porosity of the materials in swollen state by using Differential scanning colorimeter. [151,152] The DSC measurements were performed on DSC Q200 apparatus (TA Instruments) in nitrogen atmosphere. Samples of about 1–2 mg immersed in the 2-5µL of solvent were put in hermetic aluminum pans. The samples were quenched at -60 ^{0}C at 5 ^{o}C/min scanning rate and measured their melting behaviour of solvent.

7.4.3.1 Pore diameter[151]

From DSC curves $\Delta T = T - T_0$ was calculated, T_0 being the melting point of the pure acetonitrile = -46± 0.3 ^{0}C. Linear regression yields the following numerical expression for acetonitrile. The ΔT valued substituted in fallowing equation and calculated the radius of the pore.

$$Rp\ (Å) = -309/\Delta T + 13. \qquad \text{Eq. 7.6}$$

The value 13Å represents the thickness of the solvent layer remaining adsorbed on the internal pore surface (non-freezable solvent)

7.4.3.2 Pore volume measurement[152]

Total pore volume V_p (e.g., cm^3pore per gram porous solid) is another important parameter for characterizing porous materials. A simple calculation of V_p can be obtained from a single thermoporometry heating experiment using.

$$Vp = \frac{\Delta Hpore}{\Delta Htot} \frac{Cliq}{\text{Csolid } \rho\text{liq}} \qquad \text{Eq. 7.7}$$

where a known mass of liquid C_{liq}, of density ρ_{liq}, is added to a known mass of porous solid C_{solid}. The pore melt area, ΔHpore, and combined pore and excess melt peak areas, ΔH_{total}, are determined from the DSC melt endotherms, and their ratio is related to the fraction of liquid contained in the pores. The expression assumes a temperature-independent heat of fusion ΔH and liquid density, as well as a sufficient separation of the pore and excess melt peaks to independently integrate their areas. It is also assumed that all of the liquid has frozen during the initial quench cooling step and melts during heating, i.e., the contribution of the thin liquid layer adjacent to pore walls, and other non-frozen liquid, is negligible

7.4.3.3 Surface area

Once you know the pore diameter and pore volume of the material it is easy to calculate the surface area of the materials using wheeler equation.[192]

Surface area $(SA) = 4000X\, Vp/Dp$ Eq. 7.8

Where, V_p = pore volume, D_p= pore diameter

7.4.4 Swelling tests

The Swelling properties of the polymers were studied as described elsewhere[1]. NMR tubes were filled during intermittent vibrations up to 1 cm with dry polymer particles and the solvent (1mL) added. The particles were allowed to equilibrate in the solvent for 24h, whereafter the volume of the swollen particles was measured. The volume swelling ration was calculated as:

$$Swelling\ ratio = \frac{bed\ volume\ \ of\ wet\ particles}{bed\ volume\ \ of\ dry\ particles}$$

Eq. 7.9

7.4.5 Infrared spectroscopy

The FT-IR spectra were recorded using a NEXUS FT-IR spectrometer (Thermo Electron Corporation, Dreieich, Germany). The samples were prepared by adding the solid (~ 2 mg, carefully dried) to KBr salt, this matrix was grinded and mixed with an agate mortar and pestle, and then pressed into a transparent disk or pellet at sufficiently high pressure.

Fourier transform infrared (FT-IR) spectroscopy is one of the most common spectroscopic techniques used in organic and inorganic chemistry and generalized tables of the positions and relative intensities of absorption bands can be found in the *CRC Handbook of Chemistry and Physics*[193] and a number of other publications.

7.4.6 Solution NMR

NMR spectra were recorded on a Bruker 500 spectrometer using $CDCl_3$ and DMSO as solvent.

7.4.7 Elemental analysis

Carbon, hydrogen, nitrogen and sulphur contents were determined at the Department of Organic Chemistry, Johannes Gutenberg University of Mainz using a Heraeus CHN-rapid analyser (Hanau, Germany).

This technique involves the catalytic combustion of the sample, with selective adsorption of the evolved gasses. The relative weight percentages of the elements (e.g. C, O, H, N and S) may thus be obtained.

The microanalysis of carbon and nitrogen provides reliable information on the initiator coupling yields when working with the higher surface area materials. Elemental analysis also provides information on the efficiency of the silica removal process and the polymerization step. Thus, agreement between theoretical C, H and N contents based on the monomer ratios in the pre-polymerization mixture and the measured values indicated that the monomers were randomly incorporated in the material.

The characterization of the synthesized silica supports using elemental analysis is based on the change in percentage of an element, *X*, between two consecutive steps of a reaction. The *loading* is expressed in mmol of ligand, *L*, per gram of bare silica, *Si*, and can be calculated[129]

$$loading = \frac{m_X}{M_X} \cdot 10^3 \qquad \text{Eq. 7.10}$$

where M_X is the weight of the element per mol of ligand

$$m_X = \frac{\%X}{100 - \%X \cdot \frac{MW_L}{M_X}} \qquad \text{Eq. 7.11}$$

where %*X* is the content in percentage of one of the elements present in the modified silica.

Finally, if the surface area of the support, a_s (m^2/g), is known, the loading can be converted to surface density, D_S, and expressed in µmol of ligand per m^2 of silica

$$D_S = \frac{loading}{a_s} \cdot 10^3 \qquad \text{Eq. 7.12}$$

Film thickness estimation

The calculation of the film thickness *d* (nm) was performed assuming a homogeneous grafted layer as follows.[27]

From elemental analysis:

$$d = \frac{m_c \times M_w}{M_c \times \rho \times S} \times 10^3 \qquad \text{Eq. 7.13}$$

$$m_c = \frac{\%C}{100 - \left(\frac{\%C \times M_w}{M_c}\right)} \qquad \text{Eq. 7.14}$$

where m_c = weight of carbon of the grafted polymer per gram of bare silica support, M_w = weighted average molecular weight of the grafted polymer assuming stoichiometric incorporation of reactive monomers, M_C = weighted average molecular weight of the carbon fraction of the grafted polymer, ρ = weighted average density of monomers (g mL^{-1}) and S = specific surface area of the bare silica support (m^2g^{-1}).

7.4.8 Optical microscopy

The optical microscopy was performed using a LEICA DMR fluorescence microscope HC (Leica, Bensheim, Germany). Standard optical microscopy was used to gain rapid information on the particle size distribution as well as the quality of the particles obtained after polymerization and etching.

7.4.9 Scanning electron microscopy

SEM was provided at the Department of Biochemical and Chemical Engineering, TU Dortmund. The SEM pictures were recorded on a Hitachi H-S4500 FEG in secondary electron mode with an acceleration voltage of 1 kV. The samples were deposited on holders with carbon foil.Scanning electron microscopy (SEM) gives information on the morphology and surface texture of the materials, and in this work in particular it also provided information on the effectiveness of the replication from silica to templated polymer.

7.4.10 Energy Dispersive X-ray analysis

EDX is a technique often implemented in scanning electron micrographs. This was performed using a SEM Hitachi S 4500 at the Fachbereich, Technische Chemie, Universität Dortmund. It is an inelastic emission process and the mechanism of signal generation is the decay of excited states by photons. Each atom emits X-ray photons with specific/characteristic energy and the technique is used for qualitative analysis.

7.4.11 Nitrogen adsorption

Nitrogen adsorption measurements were performed on a Quantachrome Nova4000e (Quantachrome Corporation, Boynton Beach, FL) automatic adsorption instrument. Before measurements, the equivalent weight of 10 to 20 m^2 of sample were placed in a glass cell, and degassed under vacuum over night at different temperatures depending on the nature of the sample (e.g. bare silica at 80°C, polymers at 40°C, and initiator modified silica at room temperature).[129]

The characterization parameters extrapolated from the resultant physisorption isotherm are specific surface area (S_A), pore volume (V_p), pore diameter (D_p).

According to the IUPAC classification [194], porous materials are divided into:

- macroporous (D_p > 50 nm)
- mesoporous (2< D_p < 50 nm)
- microporous (D_p < 2 nm)

The composite MIPs and corresponding thinwalled beads showed isotherms of the *Type IV* which are characterized for their hysteresis loop, associated with capillary condensation taking place in mesopores. The initial part of this isotherm is attributed to monolayer-multilayer adsorption and in this region was applied the Brunauer-Emmett-Teller (BET) method to determine the the surface area.[195,196] The range of linearity required for the BET plot is restricted to a limited part of the isotherm – usually not outside of the relative pressure (p/p_0) range of 0.05-0.30. The determination of the specific pore volume, according to Gurvich [197], is as follows: at a high relative pressure ratio of p/p_0>0.95 the isotherm specific for mesoporous materials shows a plateau, indicating complete filling of the mesopores with adsorbate liquid. The amount of adsorbed nitrogen at the relative pressure 0.95 < p/p_0 < 1 is converted into the volume of liquid nitrogen using the normal liquid density. The pore volume distribution according to Barrett, Joyner and Halenda (BJH)[198] was calculated from the desorption branch of the nitrogen adsorption isotherm at 77K in the relative pressure range between 0.3 < p/p_0 < 0.99. The calculation starts at the highest p/p_0 value where saturation is obtained and the isotherm is parallel to the relative pressure abscissa.[129]

7.4.12 Chromatography

7.4.12.1 Evaluation of binding affinity and selectivity in the chromatographic mode

The chromatographic evaluation of the molecularly imprinted polymers (MIPs) beads was performed on a Hewlett-Packard HP 1100 instrument (Agilant Technologies, Waldbronn, Germany) equipped with a UV-DAD detector and an autosampler. The materials were slurry packed into stainless steel columns (33x4.6mm or 20x2mm) using MeOH/H_2O 80:20 (v/v) as

dispersing solvent. The composites prior to etching were packed at a maximum pressure of 200 bars using an air-driven fluid pump (Haskel DSTV-122) whereas the thin walled beads were packed under negative pressure using a vacuum pump. The flow rate was adjusted between 0.2mL/min to 1mL/min in order to achieve a similar linear velocity for all columns. 10µL aliquots of 1 mM solutions of pure enantiomers or racemate were injected unless otherwise mentioned. The elution was monitored at 260nm. The retention factors (k_L and k_D) and the separation factor (α) were calculated using the following formulae:

$$\text{Retention factor } (k_{L)} = (t_L - t_O)/t_O$$

$$\text{Retention factor } (k_{D)} = (t_D - t_O)/t_O \qquad \text{Eq. 7.15}$$

$$\text{Separation factor } (\alpha) = k_L/k_D \qquad \text{Eq. 7.16}$$

where t_L is the retention time of the L-enantiomer, t_D is the retention time of the D-enantiomer and t_O is the retention time of the void marker, acetone.

When the analyte travels through the column, the peak width increases proportionally to the time spend in the column. The increase in peak width is expressed by the theoretical plate height[27]

$$H=(\sigma_L)^2/L \qquad \text{Eq. 7.17}$$

Where:

σ_L = standard deviation of a Gaussian peak in units of length,

$(\sigma_L)^2$ = variance of the peak in units of length

L = length of the analytical column.

Instead of the theoretical plate hight H, the theoretical plate number N is often used. Both parameters are related as follows:

$$H=L/N \qquad \text{Eq. 7.18}$$

$$N= 5.54 (t_r /w_{t\,0.5})^2 \qquad \text{Eq. 7.19}$$

Where:

t_r = the retention time;

$w_{t\,0.5}$ = peak width at half height.

For bulk polymers which showed non Gaussian peak so the following formula was used for calculating the plate numbers.[106]

$$N=16 (t_r /W_b)^2 \qquad \text{Eq. 7.20}$$

Column efficiency: $N_D = 16\left(\frac{t_D}{W_{b^D}}\right)^2$; $N_L = 16\left(\frac{t_L}{W_{b^L}}\right)^2$ Eq. 7.21

Height equivalent of a theoretical plate: $H_L = \left(\frac{L_L}{N_L}\right)$; $H_D = \left(\frac{L_D}{N_D}\right)$ Eq. 7.22

Resolution: $R_s = \frac{2(t_L - t_D)}{(W_{b^L} + W_{b^D})}$ Eq. 7.23

Where N_D and N_L = column efficiency for D-PA and L-PA,

$W_b{}^D$ and $W_b{}^L$ is the width at the baseline of a peak D-PA and L-PA,

L_D and L_L is the length of the column of a D-PA and L-PA

For a given column, the number of theoretical plates is a measure of its separation efficiency. The higher the plate numbers higher the separation efficiency and the narrower the peaks.

7.4.13 Binding experiments

7.4.13.1 Evaluation of binding affinity and selectivity in the static mode

The L-PA imprinted composites or bulk RAFT polymers and corresponding thin-walled materials (5mg) were weighed into 2mL rubbersealed vials. Solutions of D- or L- PA in acetonitrile (0.5 mL) made up to concentrations within the range (C= 0.05- 5 mM) were added. After 24 h incubation at room temperature the supernatants were sampled (30 µL) and the aliquots diluted in 270 µL of water and transferred to HPLC vials for measurement of unbound solute concentration by reversed phase HPLC. The HPLC system consisted of an Agilent HPLC 1100 series instrument (Agilent) equipped with a UV-DAD detector and an autosampler. The column was a reversed phase (C18) column (Phenomenex Luna C-18, 250 x 4.6 mm), the mobile phase: MeOH/H_2O: 62/38 (0.2% TFA) and the detection performed by UV absorbance at 260 nm. The resulting peak areas were used to calculate the amount of bound analyte on the polymer (in µmol/g of polymer). Each data point is based on the average of two replicate measurements. Non-linear fitting of theoretical isotherms to experimental data was performed using Sigma plot or Microcal™ Origin 5.0, and best fits were evaluated with the Fisher test where a higher F-value indicates a better fit.[31] The adsorption isotherm models evaluated were Langmuir (Eq. 7.24), Bi-Langmuir (Eq. 7.25) and Freundlich (Eq. 7.26) where q* is the concentration in the stationary phase at equilibrium with concentration C, and C is the concentration in the mobile phase.

$$q^* = q_s bC/(1+bC) \qquad \text{Eq. 7.24}$$

$$q^* = q_{s1} b_1 C/(1+b_1 C) + q_{s2} b_2 C/(1+b_2 C) \qquad \text{Eq. 7.25}$$

$$q^* = aC^m \qquad \text{Eq. 7.26}$$

The Langmuir models assume that one (eq.7.24) or two (eq.7.25) distinguishable classes of sites are present on the surface, each with saturation capacity q_s and association constant b. The dissociation constant K_d was calculated as the inverse of b. The Freundlich isotherm (eq. 7.26), on the other hand, assumes sites with a Gaussian distribution of binding strengths. Here the width of the Gaussian distribution describes the degree of heterogeneity, through the index m. This parameter ranges from 1 (homogeneous samples) to 0 (heterogeneous samples). Moreover, with the use of *a* and *m* it is possible to characterize the affinity distribution of the polymer by calculating the average affinity constant, *K* (Eq.7.27), and the average number of binding sites, *N* (Eq.7.28), as described in.[33]

$$K = \left(\frac{m}{m-1}\right)\frac{K_1^{1-m} - K_2^{1-m}}{K_1^{-m} - K_2^{-m}} \qquad \text{Eq. 7.27}$$

$$N = a\left(1-m^2\right)\left(K_1^{-m} - K_2^{-m}\right) \qquad \text{Eq. 7.28}$$

7.4.13.2 Kinetic Experiments

The L-PA imprinted thin-walled materials (5mg) were weighed into 2mL rubbersealed vials. Solutions of L- PA in acetonitrile (0.5 mL) made up to concentrations within the range (C= 0.05-5 mM) were added. After 1 h, 5 h, 10 h, 24h and 96 h incubation at room temperature the supernatants were sampled (30 µL) and the aliquots diluted in 270 µL of water and transferred to HPLC vials for measurement of unbound solute concentration by reversed phase HPLC. The HPLC system consisted of an Agilent HPLC 1100 series instrument (Agilent) equipped with a UV-DAD detector and an autosampler. The column was a reversed phase (C18) column (Phenomenex Luna C-18, 250 x 4.6 mm), the mobile phase: MeOH/H_2O: 62/38 (0.2% TFA) and the detection performed by UV absorbance at 260 nm. The resulting peak areas were used to calculate the amount of bound analyte on the polymer (in µmol/g of polymer). Each data point is based on the average of two replicate measurements.

7.4.14 Engelhardt test of hydrophobicity and acidity

The Engelhard test [189] was applied to composites and corresponding thinwalled materials as well as a bulk polymer prepared in presence of RAFT.[80] The materials were packed in stainless steel

columns(33mmX4.6 or 20mm X 2mm) and a commercially available C18 column (Phenomenex Luna C-18, 250 x 4.6 mm) was used as a reference. The Engelhard test was performed at room temperature, the mobile phase was MeOH/H_20 (55/45) and the flow rate was adjusted to achieve a similar linear velocity for all columns i.e. 1.0ml/min for the C18, 0.5ml/min for SiPR, $SiPR_E$, $SiPR_{EE}^{500}$ and 0.2mL/min for SiPA , PA_{10}^3, PR, PR_E, PR_{EE} and $PR_{ref.}$ Thiourea was used as a void marker, the detector was set at 254 nm and the test compounds were Aniline (1mg/mL), Phenol (2mg/mL), p-ethylaniline (2mg/mL), N,N-dimethylaniline (0.4mg/mL), Ethylbenzoate (2mg/mL), Toluene (10mg/mL), Ethylbenzene (10mg/mL).

The chromatographic information that can be obtained through the retention behaviour of the different test compounds regards various properties of the columns, like hydrophobicity, polarity and hydrogen binding. The retention factors (k) of each test compound are calculated using above equation. The column hydrophobicity is measured by the separation factor, (α) estimated as the ratio of retention factors of ethylbenzene to toluene ($k_{ethylbenzene}$ / $k_{toluene}$), and also called hydrophobic selectivity.[80]

7.4.15 Inverse size exclusion chromatography (ISEC)

The RAFT bulk and non RAFT bulk polymer particles were packed into stainless steel column (33mm X 4.6 mm) as mentioned above protocol. The measurements were performed using an Agilent 1200 HPLC system containing a binary pump, an autosampler and a variable wavelength detector. THF was used as mobile phase at a flow rate of 0.2 ml/min. The wavelength of detection was 254 nm. Polystyrene standards with a molecular weight ranging from 162 to 11,100,000 Da were from Polymer Standards Service, Mainz, Germany, and dissolved in THF at concentration of 1 mg/ml. Acetone or smallest probe of polystyrene was used as void marker. The pore analysis based on the inverse size exclusion measurements was carried out by means of the PSS Porocheck Software. The pore size distributions were calculated as average on the volume. [158]

8 CHEMICALS

1-Hydroxybenzotriazole	**Across, Geel, Belgium**
3-Aminoquinoline	**Fluka, Deisenhofen, Germany**
4,4´-azo bis (cyanopentanoic acid)	**Fluka, Deisenhofen, Germany**
4-Cyano-4-(phenylcarbonothioylthio) pentanoic acid	**Strem Chemicals, Germany**
Acetone (for synthesis)	**Merck KGaA, Darmstadt, Germany**
Aminopropyltriethoxysilane	**Aldrich, Steinheim, Germany**
Ammonium hydrogen difluoride	**Across, Geel, Belgium**
Aniline	**Aldrich, Steinheim, Germany**
Azo-bis-dimethylvaleronitrile	**Wako Chemicals, Neuss, Germany**
α-bromobenzene acetonitrile	**Own synthesis**
Benzene	**Merck KGaA, Darmstadt, Germany**
Benzoic acid	**Across, Geel, Belgium**
Benzoyal peroxide	**Aldrich, Steinheim, Germany**
BOC-D-Phe-OH	**Bachem, Heidelberg, Germany**
BOC-Phe-OH	**Aldrich, Steinheim, Germany**
α-cyanobenzyldithibenzoate	**Own synthesis**
Carbon disulfide	**Aldrich, Steinheim, Germany**
Carbontetrachloride	**Aldrich, Steinheim, Germany**
Choroform(dueterated)	**Aldrich, Steinheim, Germany**
Dicyclohexyl carbodiimide	**Aldrich, Steinheim, Germany**
Dichloromethane (dry)	**Fluka, Deisenhofen, Germany**
Dimethylsulphoxide (p.a.)	**Merck KGaA, Darmstadt, Germany**

Dimethylformamide (dry)	**Fluka, Deisenhofen, Germany**
D/L-phenylalanine anilide	**own synthesis**
Ethanol (dry)	**Fluka, Deisenhofen, Germany**
Ethanol(p.a.)	**Merck KGaA, Darmstadt, Germany**
Ethyl chloroformate	**Aldrich, Steinheim, Germany**
Ethylbenzene	**Acros, Geel, Belgium**
Ethylbenzoate	**Acros, Geel, Belgium**
Ethyleneglycol dimethacrylate	**Aldrich, Steinheim, Germany**
Hexamethyldisilazane	**Merck KGaA, Darmstadt, Germany**
Hydrochloric Acid (conc.)	**Merck KGaA, Darmstadt, Germany**
Magnesium sulphate	**Across, Geel, Belgium**
Methacrylic Acid	**Aldrich, Steinheim, Germany**
Methanol (p.a.)	**Merck KGaA, Darmstadt, Germany**
N-bromosuccinimide	**Aldrich, Steinheim, Germany**
N, N-Dimethylaniline	**Merck KGaA, Darmstadt, Germany**
Neutral alumina	**Across, Geel, Belgium**
p-Ethylaniline	**Acros, Geel, Belgium**
Phenol	**Merck KGaA, Darmstadt, Germany**
Phenylacetonitrile	**Aldrich, Steinheim, Germany**
Phenyl magnesium bromide (3M solution in ethylether)	**Aldrich, Steinheim, Germany**
Si-100	**Merck KGaA, Darmstadt, Germany**
Si-500	**Fuji chemicals Japan**
Si-500-aminomodified	**Fuji chemical japan**
Sodium hydrogen carbonate	**Merck KGaA, Darmstadt, Germany**

Sodium hydroxide	**Merck KGaA, Darmstadt, Germany**
Succinic anhydride	**Merck KGaA, Darmstadt, Germany**
Tetrahydrofuran (dry)	**Fluka, Deisenhofen, Germany**
Tetrahydrofurane(p.a)	**Merck KGaA, Darmstadt, Germany**
Toluene (dry)	**Fluka, Deisenhofen, Germany**
Triethylamine	**Aldrich, Steinheim, Germany**
Trifluoroacetic acid	**Aldrich, Steinheim, Germany**

Solvents

From Merck KGaA, Darmstadt, Germany:

Acetone (for synthesis)

Acetonitrile (HPLC grade)

Chloroform (p.a)

Dichloromethane (dry)

Diethyl ether (p.a.)

Dimethylsulphoxide (p.a.)

Dimethylformamide (dry)

Ethanol (dry)

Ethanol (p.a.)

Hexane (p.a.)

Methanol (HPLC grade)

Methanol (p.a.)

Tetrahydrofurane(p.a)

Toluene (dry)

Tetrahydrofuran (dry)

Water (HPLC grade)

Ethyleneglycol dimethacrylate was purified by extraction with 10% NaOH, washing with brine, drying over magnesium sulphate and subsequent distillation under reduced pressure. Methacrylic acid was distilled under reduced pressure prior to use. All other reagents were used as received.

PSS Polymer Standards services GmbH Germany

Polystyrene standards	Mn	Mw	D=Mw/Mn
Psp1	162	162	1
Ps17041	269	309	1.15
Ps24094	735	795	1.08
Ps12034	1500	1560	1.06
Ps6126	3260	3460	1.06
Ps1126	5270	5610	1.06
Ps24076	10000	10300	1.03
Ps21116	26600	27500	1.04
Ps9068	97,400	101,000	1.03
Ps28060	288,800	301,600	1.04
Ps30077	1,010,000	1,070,000	1.06
Ps22087	9,250,000	11,100,000	1.20

9 REFERENCES

(1) *Molecularly imprinted polymers. Man made mimics of antibodies and their applications in analytical chemistry.*; Sellergren, B., Ed.; Elsevier Science B.V.: Amsterdam, 2001; Vol. 23.
(2) Philp, D.; Stoddart, J. F. *Angew. Chem., Int. Ed.* **1996**, *35*, 1154-1196.
(3) Alexander, C.; Andersson, H. S.; Andersson, L. I.; Ansell, R. J.; Kirsch, N.; Nicholls, I. A.; O'Mahony, J.; Whitcombe, M. J. *J. Mol. Recognit.* **2006**, *19*, 106-180.
(4) Sellergren, B. *Angew. Chem., Int. Ed.* **2000**, *39*, 1031-1037.
(5) Haupt, K.; Mosbach, K. *Chem. Rev.* **2000**, *100*, 2495-2504.
(6) *Molecularly Imprinted Polymers*; Haupt, K.; Linares, A.; Bompart, M.; Bui, B., Eds.; Springer Berlin Heidelberg, 2011; Vol. 325.
(7) Hoshino, Y.; Urakami, T.; Kodama, T.; Koide, H.; Oku, N.; Okahata, Y.; Shea, K. J. *Small* **2009**, *5*, 1562-1568.
(8) Wulff, G.; Sarhan, A. *Angew. Chem., Int. Ed.* **1972**, *11*, 341.
(9) Wulff, G. *Angew. Chem., Int. Ed.* **1995**, *34*, 1812-32.
(10) Shea, K. J.; Dougherty, T. K. *J. Am. Chem. Soc.* **1986**, *108*, 1091-1093.
(11) Mayes, a. G.; Whitcombe, M. J. *Adv. Drug Deliv. Rev.* **2005**, *57*, 1742-78.
(12) Arshady, R.; Mosbach, K. *Macromol. Chem.* **1981**, *182*, 687.
(13) Sellergren, B.; Shea, K. J. *J. Chromatogr.* **1993**, *635*, 31-49.
(14) Andresson Lars; Sellergren Borje; Mosbach klaus *Tetra. Lett.* **1984**, *25*, 5211-5214.
(15) Sellergren, B.; Shea, K. J. *J. Chromatogr., A* **1993**, *654*, 17-28.
(16) Sellergren, B. *J. Chromatogr., A* **2001**, *906*, 227-252.
(17) Sellergren, B.; Shea, K. J. *J. Chromatogr., A* **1995**, *690*, 29-39.
(18) Zander A; Findlay P; Thomas R.; B., S. *Anal. Chem.* **1998**, *70*, 3304-3314.
(19) Sellergren, B.; Lepisto, M.; Mosbach, K. *J. Am. Chem. Soc.* **1988**, *110*, 5853-5860.
(20) Chen, Y.; Kele, M.; Sajonz, P.; Sellergren, B.; Guiochon, G. *Anal. Chem.* **1999**, *71*, 928-938.
(21) Sajonz, P.; Kele, M.; Zhong, G.; Sellergren, B.; Guiochon, G. *J. Chromatogr. A* **1998**, *810*, 1-17.
(22) Sellergren, B.; Andresson Lars *J. Org. Chem.* **1990**, *55*, 3381-3383.
(23) Whitcombe, M. J.; Rodriguez, M. E.; Villar, P.; Vulfson, E. N. *J. Am. Chem. Soc.* **1995**, *117*, 7105-7111.
(24) Moad, G.; Solomon, D. H. *The Chemistry of Free Radical Polymerization*; Elsevier Science Ltd, **1995**.
(25) Otsu, T.; Matsumoto, A.; DiMari, S.; Funke, W.; Haralson, M.; Hunkeler, D.; Joos-Müller, B.; Matsumoto, A.; Okay, O.; Otsu, T.; Powers, A.; Prokop, A.; Wang, T.; Whitesell, R.; Springer Berlin / Heidelberg: 1998; Vol. 136, p 75-137.
(26) Odian, G. *Principle of polymerization*; John wiley and Sons,Inc., Hoboken, New Jersey, 2004; Vol. Fourth Edition.
(27) Titirici, M. M., *Dissertation* Universität Dortmund, 2005.
(28) Vlatakist, G.; Andersson, L. I.; Mullert, R.; Mosbach, K. *Nature* **1993**, *361*, 645.

(29) Sellergren, B.; Maeda, R. A. B. a. M., Ed.; American Chemical Society, Washington: 1998.
(30) Shimizu, K. D. In *Molecularly Imprinted Materials: Science and Technology*; Ramstrom, Y. A., Ed.; Marcel Dekker, NewYork: 2005, p 419-434.
(31) Chen, Y.; Kele, M.; Quinones, I.; Sellergren, B.; Guiochon, G. *J. Chromatogr., A* **2001**, *927*, 1-17.
(32) Umpleby, R. J.; Baxter, S. C.; Rampey, A. M.; Rushton, G. T.; Chen, Y.; Shimizu, K. D. *J. Chromatogr. B* **2004**, *804*, 141-149.
(33) Rampey, A. M.; Umpleby, R. J.; Rushton, G. T.; Iseman, J. C.; Shah, R. N.; Shimizu, K. D. *Anal. Chem.* **2004**, *76*, 1123-1133.
(34) Shimizu, K. D. *Mat.Res.Soc.Symp.Proc.* **2002**, *723*, 1-7.
(35) Kim, H.; Spivak, D. A. *J. Am. Chem. Soc.* **2003**, *125*, 11269-11275.
(36) Wulff, G.; Schonfeld, R. *Adv. Mater.* **1998**, *10*, 957-959.
(37) Hall, A. J.; Manesiotis, P.; Emgenbroich, M.; Quaglia, M.; De Lorenzi, E.; Sellergren, B. *J. Org. Chem.* **2005**, *70*, 1732-1736.
(38) Umpleby II, R. J.; Rushton, G. T.; Shah, R. N.; Rampey, A. M.; Bradshaw, J. C.; Berch, J. K.; Shimizu, K. D. *Macromolecules* **2001**, *34*, 8446-8452.
(39) Patel, A.; Fouace, S.; Steinke, J. H. G. *Chem. Comm.* **2003**, 88-89.
(40) Zimmerman, S. C.; Wendland, M. S.; Rakow, N. A. *Nature* **2002**, *418*, 399-404.
(41) Zimmerman, S. C.; Zharov, I.; Wendland, M. S.; Rakow, N. A.; Suslick, K. S. *J. Am. Chem. Soc.* **2003**, *125*, 13504-13518.
(42) Hoshino, Y.; Koide, H.; Furuya, K.; Haberaecker, W. W.; Lee, S.-h.; Kodama, T. *PNAS* **2011**, *109*, 33-38.
(43) Hoshino, Y.; Iii, W. W. H.; Kodama, T.; Zeng, Z.; Okahata, Y.; Shea, K. J. *J. Am. Chem. Soc.* **2010**, *132*, 13648-13650.
(44) Hoshino, Y.; Kodama, T.; Okahata, Y.; Shea, K. J. *J. Am. Chem. Soc.***2008**, *130*, 15242-15243.
(45) Lee, S.-H.; Hoshino, Y.; Randall, A.; Zeng, Z.; Baldi, P.; Doong, R.-a.; Shea, K. J. *J. Am. Chem. Soc.* **2012**, *134*, 15765-15772.
(46) Zeng, Z.; Hoshino, Y.; Rodriguez, A.; Yoo, H.; Shea, K. J. *ACS Nano* **2009**, *4*, 199-204.
(47) Szwarc, M.; Levy, M.; Milkovich, R. *J. Am. Chem. Soc.* **1956**, *78*, 2656-2657.
(48) Szwarc, M. *Nature* **1956**, *178*, 1168-1169.
(49) Yu, Q.; Zhang, J.; Cheng, M.; Zhu, S. *Macromol. Chem. Phy.* **2006**, *207*, 287-294.
(50) Boonpangrak, S.; Whitcombe, M. J.; Prachayasittikul, V.; Mosbach, K.; Ye, L. *Biosens. Bioelectron.* **2006**, *22*, 349-354.
(51) Vaughan, A. D.; Sizemore, S. P.; Byrne, M. E. *Polymer* **2007**, *48*, 74-81.
(52) Vaughan, A. D.; Zhang, J. B.; Byrne, M. E. *AIChE J.* **2010**, *56*, 268-279.
(53) Salian, V. D.; Vaughan, A. D.; Byrne, M. E. *J. Mol. Recognit.* **2012**, *25*, 361-369.
(54) Bompart, M.; Haupt, K. *Aust. J. Chem.* **2009**, *62*, 751-761.
(55) Otsu, T.; Yoshida, M.; Tazaki, T. *Die Makromol. Chemie, Rap. Comm.* **1982**, *3*, 133-140.
(56) Otsu, T. *J. Polym. Sci. Part A: Polym. Chem.* **2000**, *38*, 2121-2136.
(57) Peppas, N. A.; Ward, J. H. *Adv. Drug Deliv. Rev.* **2004**, *56*, 1587-1597.

(58) D. H. Solomon, E. R., P. Cacioli, ; *Eurpean Patent 135280A2*, Ed. 1985; Vol. *U.S.Patent 4581429* , **1985**
(59) E. Rizzardo *Chem.Aust.,* **1987**, *54*, 32.
(60) Hawker, C. J.; Bosman, A. W.; Harth, E. *Chem. Rev.* **2001**, *101*, 3661-3688.
(61) Boonpangrak, S.; Whitcombe, M. J.; Prachayasittikul, V.; Mosbach, K.; Ye, L. *Biosen. Bioelectr.* **2006**, *22*, 349-354.
(62) Wang, J.-S.; Matyjaszewski, K. *Macromolecules* **1995**, *28*, 7901-7910.
(63) Patten, T. E.; Matyjaszewski, K. *Adv. Mater.* **1998**, *10*, 901-915.
(64) Matyjaszewski, K.; Patten, T. E.; Xia, J. *J. Am. Chem. Soc.***1997**, *119*, 674-680.
(65) Kato, M.; Kamigaito, M.; Sawamoto, M.; Higashimura, T. *Macromolecules* **1995**, *28*, 1721-1723.
(66) Kharasch, M. S.; Reinmuth, O.; Urry, W. H. *J. Am. Chem. Soc.* **1947**, *69*, 1105-1110.
(67) Kharasch, M. S.; Jensen, E. V.; Urry, W. H. *J. Am. Chem. Soc.***1947**, *69*, 1100-1105.
(68) Kharasch, M. S.; Jensen, E. V.; Urry, W. H. *Science* **1945**, *102*, 128-128.
(69) Matyjaszewski, K.; Xia, J. *Chem. Rev.* **2001**, *101*, 2921-2990.
(70) Goto, A.; Ohno, K.; Fukuda, T. *Macromolecules* **1998**, *31*, 2809-2814.
(71) Zu, B.; Zhang, Y.; Guo, X.; Zhang, H. *J. Polym. Sci., Part A: Polym. Chem.* **2010**, *48*, 532-541.
(72) Sasaki, S.; Ooya, T.; Takeuchi, T. *Polym. Chem.* **2010**, *1*, 1684-1688.
(73) Mayadunne, R. T. A.; Rizzardo, E.; Chiefari, J.; Chong, Y. K.; Moad, G.; Thang, S. H. *Macromolecules* **1999**, *32*, 6977-6980.
(74) Chiefari, J.; Chong, Y. K.; Ercole, F.; Krstina, J.; Jeffery, J.; Le, T. P. T.; Mayadunne, R. T. A.; Meijs, G. F.; Moad, C. L.; Moad, G.; Rizzardo, E.; Thang, S. H. *Macromolecules* **1998**, *31*, 5559-5562.
(75) Moad, G.; Rizzardo, E.; Thang, S. H. *Aust. J. Chem.* **2005**, *58*, 379-410.
(76) Li, C.; Benicewicz, B. C. *J. Polym. Sci. Part A: Polym. Chem.* **2005**, *43*, 1535-1543.
(77) Gregory, A. M.; Thurecht, K. J.; Howdle, S. M. *Macromolecules* **2008**, *41*, 1215-1222.
(78) Liu, H.; Zhuang, X.; Turson, M.; Zhang, M.; Dong, X. *J. Sep. Sci.* **2008**, *31*, 1694-1701.
(79) Pan, G.; Zu, B.; Guo, X.; Zhang, Y.; Li, C.; Zhang, H. *Polymer* **2009**, *50*, 2819-2825.
(80) Halhalli, M. R.; Schillinger, E.; Aureliano, C. S. A.; Sellergren, B. *Chem. Mater.* **2012**, *24*, 2909-2919.
(81) Halhalli, M. R.; Aureliano, C. S. A.; Schillinger, E.; Sulitzky, C.; Titirici, M. M.; Sellergren, B. *Polym. Chem.* **2012**, *3*, 1033-1042.
(82) Barbey, R.; Lavanant, L.; Paripovic, D.; SchuÃàwer, N.; Sugnaux, C.; Tugulu, S.; Klok, H.-A. *Chemical Reviews* **2009**, *109*, 5437-5527.
(83) Olof Norrlow; Glad, M.; Mosbach, K. *J. Chromatogr.* **1984**, *299*, 29-41.
(84) Wulff, G. n.; Oberkobusch, D.; MinÃ¡rik, M. *Reactive Polymers, Ion Exchangers, Sorbents* **1985**, *3*, 261-275.
(85) Hirayama, K.; Burow, M.; Morikawa, Y.; Minoura, N. *Chem. Lett.* **1998**, 731-732.

(86) Radhakrishnan, B.; Ranjan, R.; Brittain, W. J. *Soft Matter* **2006**, *2*, 386-396.
(87) Prucker, O.; Rühe, J. *Macromolecules* **1998**, *31*, 602-613.
(88) Prucker, O.; Rühe, J. *Macromolecules* **1998**, *31*, 592-601.
(89) Sulitzky, C.; Rückert, B.; Hall, A. J.; Lanza, F.; Unger, K.; Sellergren, B. *Macromolecules* **2002**, *35*, 79-91.
(90) Quaglia, M.; Lorenzi, E. D.; Sulitzky, C.; Massolini, G.; Sellergren, B. *Analyst* **2001**, *126*, 1495-1498.
(91) Wang, H.; Dong, X.; Yang, M. *TrAC Trends in Anal. Chem.* **2012**, *31*, 96-108.
(92) Rückert, B.; Hall, A. J.; Sellergren, B. *J. Mat. Chem.* **2002**, *12*, 2275-2280.
(93) Sellergren, B.; Ruckert, B.; Hall, A. J. *Adv. Mater.* **2002**, *14(17)*, 1204-1208.
(94) Titirici, M.-M.; Sellergren, B. *Chem. Mater.* **2006**, *18*, 1773-1779.
(95) Tamayo, F. G.; Titirici, M. M.; Martin-esteban, A.; Sellergren, B. *Anal. Chim. Acta* **2005**, *542*, 38-46.
(96) Baggiani, C.; Baravalle, P.; Anfossi, L.; Tozzi, C. *Anal. Chim. Acta* **2005**, *542*, 125-134.
(97) Pe´rez-Moral, N.; Mayes, A. G. *Macromol. Rapid Commun.* **2007**, *28*, 2170-2175.
(98) Rong, F.; Feng, X.; Li, P.; Yuan, C.; Fu, D. *Chin. Sci. Bull.* **2006**, *51*, 2566-2571.
(99) Bao-Li;, L.; Min;, Z.; Ping;, J.; Xiang-Chao*, D. *Acta chimica sinica* **2007**, *65*, 955-961.
(100) Baggiani, C.; Baravalle, P.; Giraudi, G.; Tozzi, C. *J. Chromatogr., A* **2007**, *1141*, 158-164.
(101) Su, S.; Zhang, M.; Li, B.; Zhang, H.; Dong, X. *Talanta* **2008**, *76*, 1141-1146.
(102) Qin, L.; He, X.-w.; Zhang, W.; Li, W.-y.; Zhang, Y.-k. *J. Chromatogr., A* **2009**, *1216*, 807-814.
(103) Barahona, F.; Turiel, E.; Cormack, P. A. G.; Martín-Esteban, A. *J. Polym. Sci. Part A: Polym. Chem.*, *48*, 1058-1066.
(104) Gallego-Gallegos, M.; Garrido, M. a. L.; Olivas, R. M. o.; Baravalle, P.; Baggiani, C.; CÃ¡mara, C. *J. Chromatogr., A 1217*, 3400-3407.
(105) Xu, W.; Su, S.; Jiang, P.; Wang, H.; Dong, X.; Zhang, M. *J. Chromatogr., A* **2012**, *1217*, 7198-7207.
(106) Wei, X.; Husson, S. M. *Ind. & Eng. Chem. Res.* **2007**, *46*, 2117-2124.
(107) Wei, X.; Li, X.; Husson, S. M. *Biomacromolecules* **2005**, *6*, 1113-1121.
(108) Gai, Q.-Q.; Qu, F.; Liu, Z.-J.; Dai, R.-J.; Zhang, Y.-K. *J. Chromatogr., A 1217*, 5035-5042.
(109) Xu, J.; Gao, Y.; Li, H. *J. Nanosci. Nanotechnol.* **2012**, *11*, 1217-1224.
(110) Pan, G.; Zhang, Y.; Ma, Y.; Li, C.; Zhang, H. *Angew. Chem., Int. Ed.* **2011**, *50*, 11731-11734.
(111) Pan, G.; Ma, Y.; Zhang, Y.; Guo, X.; Li, C.; Zhang, H. *Soft Matter* **2011**, *7*, 8428-8439.
(112) Ma, Y.; Zhang, Y.; Zhao, M.; Guo, X.; Zhang, H. *Chem. Commun.* **2012**, *48*, 6217-6219.
(113) Zhang, H.; Pan, G.; Zhang, Y. In *Faming Zhuanli Shenqing*; Nankai University Peop.Rep.China: 2011 (Patent No. CN102059104A)
(114) Li, Y.; Zhou, W.-H.; Yang, H.-H.; Wang, X.-R. *Talanta* **2009**, *79*, 141-145.
(115) Li, Y.; Li, X.; Dong, C.; Li, Y.; Jin, P.; Qi, J. *Biosens. Bioelectron.* **2009**, *25*, 306-312.

(116) Hu, X.; Fan, Y.; Zhang, Y.; Dai, G.; Cai, Q.; Cao, Y.; Guo, C. *Anal. Chim. Acta* **2012**, *731*, 40-48.
(117) Xu, S.; Li, J.; Chen, L. *J. Mater. Chem.* **2011**, *21*, 4346-4351.
(118) *Hand book of RAFT polymerization*; ISBN 978-3-527-31924-4 - Wiley-VCH, Weinheim, 2008; Vol. 12.
(119) Marina Baum ; Brittain, W. J. *Macromolecules* **2002**, *35*, 610-615.
(120) Tsujii, Y.; Ejaz, M.; Sato, K.; Goto, A.; Fukuda, T. *Macromolecules* **2001**, *34*, 8872-8878.
(121) Yoshikawa, C.; Goto, A.; Tsujii, Y.; Fukuda, T.; Yamamoto, K.; Kishida, A. *Macromolecules* **2005**, *38*, 4604-4610.
(122) Rowe-konopacki, M. D.; Boyes, S. G. *Macromolecules* **2007**, *40*, 879-888.
(123) Li, C.; Han, J.; Ryu, C. Y.; Benicewicz, B. C. *Macromolecules* **2006**, *39*, 3175-3183.
(124) Wang, H. Y.; Kobayashi, T.; Fujii, N. *J. Chem. Techn. Biotec.* **1997**, *70*, 355-362.
(125) Ulbricht, M.; Richau, K.; Kamusewitz, H. *Colliod Surf. A: Phy. and Eng. Asp.* **1998**, *138*, 353-366.
(126) Ulbricht, M. *Reactive and Functional Polymers* **1996**, *31*, 165-177.
(127) Piletsky, S. A.; Matuschewski, H.; Schedler, U.; Wilpert, A.; Piletska, E. V.; Thiele, T. A.; Ulbricht, M. *Macromolecules* **2000**, *33*, 3092-3098.
(128) Thomas, A.; Goettmann, F.; Antonietti, M. *Chem. Mater.* **2008**, *20*, 738-755.
(129) Aureliano, C. S. A., *Dissertation* Technical University of Dortmund, **2010**.
(130) Yilmaz, E.; Haupt, K.; Mosbach, K. *Angew. Chem., Int. Ed.* **2000**, *39*, 2115-2118.
(131) Yilmaz, E.; Ramström, O.; Möller, P.; Sanchez, D.; Mosbach, K. *J. Mater. Chem.* **2002**, *12*, 1577-1581.
(132) Titirici, M. M.; Hall, A. J.; Sellergren, B. *Chem. Mater.* **2002**, *14*, 21-23.
(133) Aileen R. Wang, S. Z. *Polym. Eng. Sci.* **2005**, 720-727.
(134) Kannurpatti, A. R.; Anderson, K. J.; Anseth, J. A. Y. W.; Bowman, C. N. *J. Polym. Sci.:PartB:Polym. phy.* **1997**, *35*, 2297-2307.
(135) Oxelbark, J.; Legido-quigley, C.; Aureliano, C. S. A.; Titirici, M.-m.; Schillinger, E.; Courtois, J.; Irgum, K.; Dambies, L.; Cormack, P. A. G.; Sherrington, D. C.; Lorenzi, E. D. *J. Chromatogr., A* **2007**, *1160*, 215-226.
(136) Gonzato, C.; Courty, M.; Pasetto, P.; Haupt, K. *Adv. Funct. Mater.* **2012**, *21*, 3947-3953.
(137) Turson, M.; Zhuang, X. L.; Liu, H. N.; Jiang, P.; Dong, X. C. *Chin. Chem. Lett.* **2009**, *20*, 1136-1140.
(138) Pan, G.; Zu, B.; Guo, X.; Zhang, Y.; Li, C.; Zhang, H. *Polymer* **2009**, *50*, 2819-2825.
(139) Xu, S.; Li, J.; Chen, L. *Talanta* **2011**, *85*, 282-289.
(140) Liu, H.; Zhuang, X.; Turson, M.; Zhang, M.; Dong, X. *J. Sep. Sci.* **2008**, *31*, 1694-701.
(141) Zu, B.; Zhang, Y.; Guo, X.; Zhang, H. *J. Polym. Sci. Part A: Polym. Chem.* **2010**, *48*, 532-541.
(142) Wood, M. R.; Duncalf, A. D. J.; Findlay, B. P.; Rannard, B. S. P. *Polymer* **2007**, 772-778.
(143) Salian, V. D.; Byrne, M. E. *Macromol. Mater. Eng.* **2012**, Early view (DOI:10.1002/mame.201200191)

(144) Sellergren B. *Internal laboratory report Unpublished*.
(145) Sibrian-Vazquez, M.; Spivak, D. A. *J. Polym. Sci. Part A: Polym. Chem.* **2004**, *42*, 3668-3675.
(146) Sellergren, B.; Shea, K. J. *J Chromatogr.* **1993**, *635*, 31-49.
(147) Liu, Q.; Zhang, P.; Qing, A.; Lan, Y.; Lu, M. *Polymer* **2006**, *47*, 2330-2336.
(148) Yu, Q.; Xu, S.; Zhang, H.; Ding, Y.; Zhu, S. *Polymer* **2009**, *50*, 3488-3494.
(149) Seo, M.; Hillmyer, M. A. *Science* **2012**, *336*, 1422-1425.
(150) Weber, J.; BergstroÌˆm, L. *Macromolecules* **2009**, *42*, 8234-8240.
(151) Wulff, M. *Thermochimica Acta* **2004**, *419*, 291-294.
(152) Landry, M. R. *Thermochimica Acta* **2005**, *433*, 27-50.
(153) Lubbad, S. H.; Buchmeiser, M. R. *J. Sep. Sci.* **2009**, *32*, 2521-2529.
(154) Li, Y.; Tolley, H. D.; Lee, M. L. *Anal. Chem.* **2009**, *81*, 4406-4413.
(155) Thommes, M.; Skudas, R.; Unger, K. K.; Lubda, D. *J. Chromatogr., A* **2008**, *1191*, 57-66.
(156) Jandera, P. *J. Sep. Sci.* **2008**, *31*, 2521-2540.
(157) Eeltink, S.; Jandera, P.; Schoenmakers, P. J. *J. Chromatogr., A* **2008**, *1182*, 161-168.
(158) Lubda, D.; Lindner, W.; Quaglia, M.; Hohenesche, F. V.; Unger, K. K. *J Chromatogr A* **2005**, *1083*, 14-22.
(159) F.Lanza, M. R., A.J. Hall, C.Dauwe,B.Sellergren *Mater. Res. Soc. Sym. Pro.* **2002**, *723*.
(160) Al-bokari, M.; Guiochon, G. *J Chromatogr A* **2002**, *975*, 275-284.
(161) Ousalem, M.; Zhu, X. X.; Hradil, J. *J Chromatogr A* **2000**, *903*, 13-19.
(162) Lynne Katsikas; Milena Avramovic; Ruben Dario betancourt cortes; Milos Milovanovic; Melina T.Kalagasidis-Krusic; G.Popovic, I. *J. Ser. Chem. Soc.* **2008**, *73*, 915-921.
(163) Rampey, A. M.; Umpleby, R. J.; Rushton, G. T.; Iseman, J. C.; Shah, R. N.; Shimizu, K. D. *Anal. Chem.* **2004**, *76*, 1123-1133.
(164) Urraca, J. L.; Marazuela, M. D.; Merino, E. R.; Orellana, G.; Moreno-bondi, M. C. *J. Chromatogr. A* **2006**, *1116*, 127-134.
(165) Natalia, P.-M.; Mayes, A. G. *Macromol. Rapid Commun.* **2007**, *28*, 2170-2175.
(166) Wang, H. Y.; Kobayashi, T.; Fujii, N. *J. Chem. Technol. Biotechnol.* **1997**, *70*, 355-362.
(167) Wang, H.-J.; Zhou, W.-H.; Yin, X.-F.; Zhuang, Z.-X.; Yang, H.-H.; Wang, X.-R. *J. Am. Chem. Soc.* **2006**, *128*, 15954-15955.
(168) Lu, C.-H.; Zhou, W.-H.; Han, B.; Yang, H.-H.; Chen, X.; Wang, X.-R. *Anal. Chem.***2007**, *79*, 5457-61.
(169) Peng, Y.; Xie, Y.; Luo, J.; Nie, L.; Chen, Y.; Chen, L.; Du, S.; Zhang, Z. *Anal. Chim. Acta* **2010**, *674*, 190-200.
(170) Mandal, T. K.; Fleming, M. S.; Walt, D. S. *Chem. Mater.* **2000**, *12*, 3481-3487.
(171) Mulvihill, M. J.; Rupert, B. L.; He, R.; Hochbaum, A.; Arnold, J.; Yang, P. *J. Am. Chem. Soc.* **2005**, *127*, 16040-16041.
(172) Li, Y.; Yang, H.-H.; You, Q.-H.; Zhuang, Z.-X.; Wang, X.-R. *Anal. Chem.* **2006**, *78*, 317-320.
(173) Gao, D.; Zhang, Z.; Wu, M.; Xie, C.; Guan, G.; Wang, D. *J. Am. Chem. Soc.* **2007**, *129*, 7859-66.

(174) Unger, K. K. *Porous silica, its properties and use as support in column liquid chromatography.*; Elsevier Scientific Publishing Co.: New York, 1979.
(175) Lagaly, G. In *Berichte der Bunsengesellschaft für physikalische Chemie*; Wiley-VCH Verlag GmbH & Co. KGaA, Weinheim: 1980; Vol. 84, p 111-111.
(176) E.F. Vansant, P. V. D. V.; Vrancken, K. C. In *Studies in Surface Science and Catalysis*; Elsevier: 1995; Vol. Volume 93, p 79-91.
(177) NorrlÃ¶w, O.; Glad, M.; Mosbach, K. *J. Chromatogr. A* **1984**, *299*, 29-41.
(178) Björklund, M.; Hearn, M. T. W. *J. Chromatogr. A* **1996**, *728*, 149-169.
(179) Carlier, E.; Guyot, A.; Revillon, A. *Reactive Polymers* **1992**, *16*, 115-124.
(180) Nematollahzadeh, A., *Dissertation* Teharan University, **2011**.
(181) Edmondson, S.; Osborne, V. L.; Huck, W. T. S. *Chem. Soc. Rev.* **2004**, *33*, 14-22.
(182) Jaroniec, M.; Schüth, F. *Chem. Mater.* **2008**, *20*, 599-600.
(183) Johnson, S. A.; Ollivier, P. J.; Mallouk, T. E. *Science* **1999**, *283*, 963-965.
(184) Hentze, H.-P.; Antonietti, M. *Current Opinion in Solid State and Materials Science* **2001**, *5*, 343-353.
(185) Hall, A. J.; Emgenbroich, M.; Sellergren, B. In *Templates in Chemistry II*; Schalley, C. A., Vögtle, F., Dötz, K. H., Eds.; Springer Verlag: 2005; Vol. 249, p 317-349.
(186) *Molecularly imprinted polymers*; Piletsky, S. A.; Nicholls, I. A.; Turner, A. P. F., Eds.; Landes Biosciences (http://www.eurekah.com), 2004.
(187) Titirici, M. M.; Hall, A. J.; Sellergren, B. *Chem. Mater.* **2003**, *15*, 822-824.
(188) Titirici, M. M.; Sellergren, B. *Anal. and Bioanal. Chem.* **2004**, *378*, 1913 - 1921.
(189) Engelhardt, H.; Jungheim, M. *Chromatogr.* **1990**, *29*, 59-68.
(190) Stuart, B. H. *Polymer Analysis*; John Wiley & Sons: Chichester, 2002.
(191) Bartholome, C. l.; Beyou, E.; Bourgeat-Lami, E.; Chaumont, P.; Zydowicz, N. *Polymer* **2005**, *46*, 8502-8510.
(192) Wheeler, A., *Catalysis*. Vol. 2. 1955, New York Reinhold Pub. Corp., 1995.
(193) *CRC Handbook of Chemistry and Physics. 75th ed.*; CRC Press Inc.: Boca Raton, Fl, 1994-1995.
(194) Sing, K. S. W.; Everett, D. H.; Haul, R. A. W.; Moscou, L.; Pierotti, R. A.; Rouquerol, J.; Siemieniewska, T. *Pure and Applied Chemistry* **1985**, *57*, 603-619.
(195) Brunauer, S.; Emmett, P. H.; Teller, E. *J. Am. Chem. Soc.* **1938**, *60*, 309-319.
(196) Gregg, S. J.; Sing, K. S. W. *Adsorption Surface Area and Porosity*; Academic Press: London, 1982.
(197) Gurvich, L. *J. Phy. Chem. Soc. Rus.* **1915**, *47*, 805.
(198) Barrett, E. P.; Joyner, L. G.; Halenda, P. P. *J. Am. Chem. Soc.***1951**, *73*, 373-380.

APPENDIX

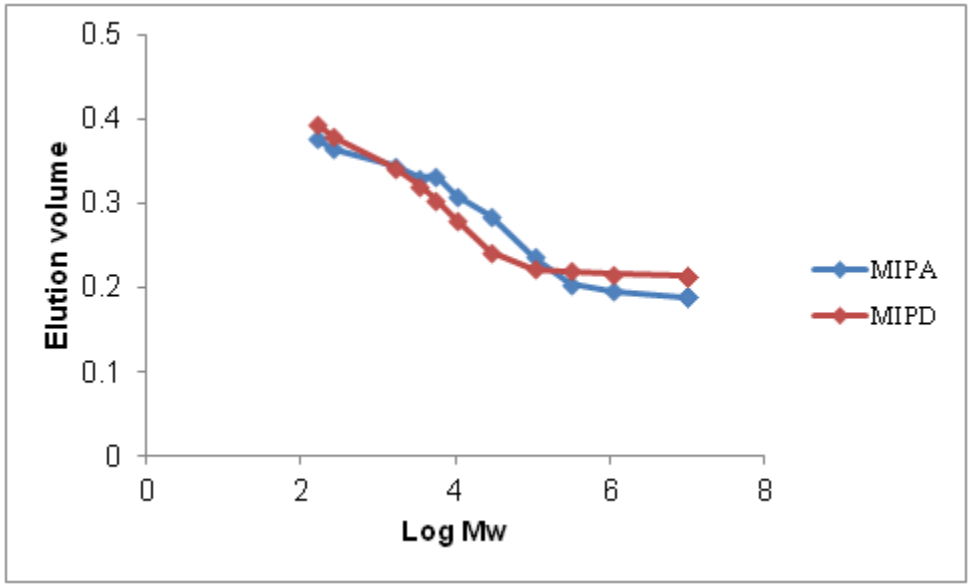

Figure 1. . SEC calibration curves for MIPA and MIPD column using polystyrene standards. Mobile phase: THF, UV detection at 254 nm

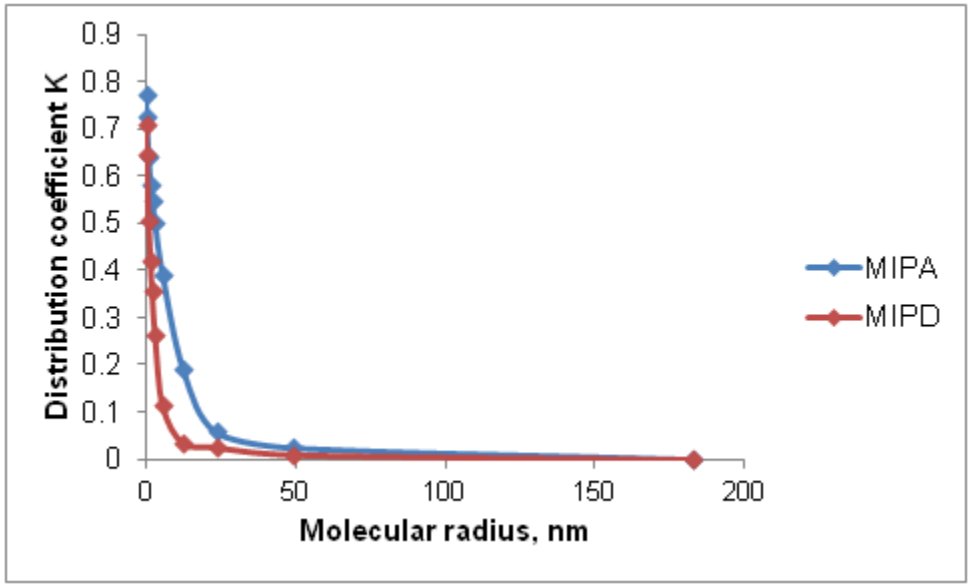

Figure 2. distribution coefficient plotted against molecular radius of polystyrene standards

CURRICULUM VITAE

Mr. Mahadeo R. Halhalli
M.Sc. (Polymer Chemistry)
INFU, Faculty of Chemistry,
Technical University of Dortmund,
Otto Hahn Strasse 6,
44221 Dortmund,Germany
Tel: +49-231-7554093
Mobile: +49-152-11239186
FAX: +49-231-7554234
Email: M.Halhalli@infu.uni-dortmund.de
mahadeo.halhalli@gmail.com

Educational Qualification

Qualification	College/University/Board	Year
M.Sc. Polymer Chemistry	PGTC, Solapur, Shivaji University, Kolhapur, India	2003-2005
B.Sc. Chemistry	CBK, Akkalkot, Shivaji University, Kolhapur, India	2000-2003

Additional Qualification

B.Ed. (General Science) from Shivaji University, Kolhapur in May 2006.

Research Experience

1. **INFU, Faculty of Chemistry,Technical University of Dortmund, Germany**

   - PhD Thesis (2009-2012) "*Functional porous polymer beads nanostructured by imprinting, layer by layer grafting, and templated synthesis*." Funded by EU-project NEMOPUR Marie Curie ITN
   - Project: "Synthesis and characterization of micro and nanobeads for antibody capture"(September 2012 - present)

- ❖ Co-supervised two master thesis and one bachelor thesis

2. **National Chemical Laboratory Pune, India**

   Worked as Senior Project Assistant on project entitled "*Polymer alloys based on new family of graft copolymer compatibilizers*" from July 2007 to January 2009.

3. **GE India Technology Centre Bangalore, India**

   Worked as Research Assistant on Project entitled *"Thermoplastic Elastomers based on Polyesters"* from 3rd July 2006 to 2nd July 2007

4. **Department of chemistry, Solapur Univesity, India**

   M.Sc. Project "Synthesis of Polyesters from Bisphenol-A" (2004-2005)

Publications

1. Thin walled imprinted polymer beads featuring both uniform and accessible binding sites
   Mahadeo R. Halhalli, Eric Schillinger, Carla S.A. Aureliano and Borje Sellergren
   Chemistry of Materials 2012, 24(15), 2909-2919
2. An improved grafting technique for producing imprinted thin film composite beads
   Mahadeo R. Halhalli, Carla S.A. Aureliano, Eric Schillinger, Claudia Sulitzky, M. Magdalena Titirici and Borje Sellergren
   ***Polymer Chemistry*, 2012, 3, 1033-1042**
3. Cover and uncover: chiral switching exploiting templating and layer by layer grafting.

   Mahadeo R. Halhalli**,** and Borje Sellergren *(Chem.Comm. to be submitted)*
4. Improved binding properties of imprinted polymers via RAFT bulk polymerization

   Mahadeo R. Halhalli**,** and Borje Sellergren *(manuscript under preparation)*
5. Novel poly(amide-hydrazide)s and copoly(amide-hydrazide)s from bis-(4 aminobenzyl) hydrazide and aromatic diacid chlorides: Synthesis and characterization
   M. Medhi**,** A. S. Patil, M. R. Halhalli, A. Choubey, P. P. Wadgaonkar and N. N. Maldar

Journal of Applied Polymer Science, 2010, 116(4), 2441-2450

6. Synthesis and characterization of New Polyimides Containing Pendent Pentadecyl Chains.
   Nilakshi Sadavarte, Mahadeo R. Halhalli, C.V. Avadhani and Prakash P. Wadgaonkar
   European Polymer Journal 2009, 45(2), 582-589

7. Polyimides Based on Aromatic Diisocyanates Containing Pendent Flexible Alkoxy Chains and Aromatic Dianhydrides: synthesis, Characterization and Their Liquid-Crystal Aligning Property
   Anjana Sarkar**,** Mahadeo R. Halhalli**,** Arun D. Kulkarni and Prakash P. Wadgaonkar
   Journal of Applied Polymer Science, 2009, 112(1), 461-472

Oral Communication

1. Halhalli M.R., Schillinger E., Sellergren B.,(2012)
   Addressing the heterogeneity and capacity issues of MIPs: Thin walled imprinted polymer beads. 7th International conference on Molecularly Imprinted Polymers-Science and technology, MIP2012 Paris, 27th-30th August 2012, France
2. Halhalli M.R., Sellergren B. (2011)
   Molecularly Imprinted Polymers via RAFT polymerization. 1st IRMED Summer School on MIPs, May 2011, La Vieille Perrotine,lle d'Oleron, France
3. Halhalli M.R., Sellergren B. (2011)
   Templated synthesis of materials featuring a dual pore system, 4th Graduate student symposium on Molecular Imprinting, 28-30 September 2011, Imperial College London, UK
4. Halhalli M.R., Sellergren B. (2011)
   Templated synthesis of materials featuring a dual pore system" 6th NEMOPUR meeting, September 2011, Imperial College London, UK
5. Halhalli M.R., Sellergren B. (2010)
   "Novel Formats in Molecular Imprinting". 5th NEMOPUR meeting April 2010, Lonza, Visp, Switzerland
6. Halhalli M.R., Sellergren B. (2010)

"Investigation of the influence of RAFT agent on the performance and properties of L-Phenylalanine anilide imprinted polymers". 6th International conference on MIP 2010, August 8th -12th, New Orleans, USA

7. Halhalli M.R., Sellergren B. (2010)
   "New Formats of molecularly imprinted polymers for peptide purification" 4th NEMOPUR midterm meeting September 2010, Imperial College London, UK
8. Halhalli M.R. (2010)
   "Porous organic polymers in pharmaceutical purification", Master students course work, Polymers in separation tools, November 2010, TU Dortmund, Germany
9. Halhalli M.R. (2010)
   "Polymer Characterization", Master students course work, Polymers in separation tools, December 2010, TU Dortmund, Germany
10. Halhalli M.R., Sellergren B. (2009)
    "A polishing phase for peptide purification" 2nd NEMOPUR meeting April 2009, TU Dortmund, Germany
11. Halhalli M.R., Sellergren B. (2009)
    "Investigation of the influence of RAFT agent on bulk imprinted polymer." 3rd NEMOPUR meeting Oct.2009, GSK, Stevenage, UK
12. Medhi M., Halhalli M.R., Choubey A., Wadgaonkar P.P., and Maldar N.N. (2008)
    "Synthesis and Characterization of Novel Poly(amide-hydrazide)s", 2nd International Symposium on Advance materials and Polymers for Aerospace and Defense Application (SAMPADA-2008) December 8-12, University of Pune, India
13. Halhalli M.R, Shaikh A. (2007)
    "High Heat Elastomer with Good Chemical Resistance," JFWTC, Bangalore, India

Poster Communication

1. **7th International conference on Molecularly Imprinted Polymers-Science and technology, MIP2012 Paris, 27th-30th August 2012, France**

   i) Halhalli M.R.**,** Sellergren B. (2012)

   Improved binding properties of imprinted polymers via RAFT bulk polymerization.

   ii) Halhalli M.R., and Sellergren B. (2012)

   Layer-by- layer grafting of thin film imprinted polymer composite beads via surface initiated Reversible Addition Fragmentation chain transfer polymerization.

   iii) Halhalli M.R.**,** Mohammadi R, Urraca J, Kadhirvel P., Dirkmann M, Abdel Qadar A., Fritz E., Sulc R., and Sellergren B. (2012)

   A versatile method to prepare RAFT anchored thin film imprinted polymer micro and nanobeads.

   iv) Kadhirvel P., Azenha M.**,** Halhalli M.R.**,** Schillinger E., Sellergren B., Silva F. A. (2012)

   Development of molecularly imprinted thin film composite beads prepared by RAFT mediated "grafting from" for the enantiomeric separation of breast cancer drug, Aminoglutethimide

   v) Mohammadi R, Wei S, Halhalli M.R.**,** Lindemann P., Tenboll A., Chandrasekaran D., Wang Z., Berghaus M., Schillinger E., and Sellergren B. (2012)

   MIPs for antibody capture.

   vi) Abdel Qadar A., Modry A., Halhalli M.R.**,** Aureliano C.A., Urraca J., and Sellergren B. (2012)

   MIPs for extracting peptidic disease biomarkers in blood and other matrices.

2. **3rd Tag der Chemie, TU-Dortmund, Germany, February 5th, 2010, Germany.**

Halhalli M.R**.,** Schillinger E., Sellergren B. (2010):
"Investigation of the influence of Reversible Addition Fragmentation chain Transfer (RAFT) agent on conventional imprinted polymers",

3. **43rd IUPAC World Polymer Congress, MACRO 2010, Glasgow, UK**

Halhalli M.R, Schillinger E., Sellergren B. (2010)
"Investigation of the influence of Reversible Addition Fragmentation chain Transfer (RAFT) agent on the performance and properties of an L-phenylalanine anilide MIP",.

4. **6th International conference on MIP 2010, August 8th-12th, New Orleans, USA**

- Halhalli M.R., Schillinger E., Sellergren B. (2010)
  Investigation of the influence of Reversible Addition Fragmentation chain Transfer (RAFT) agent on the performance and properties of an L-phenylalanine anilide MIP.
- Halhalli M.R., Schillinger E., Sellergren B.(2010)
  Molecularly imprinted polymers via 'Grafting from' Comparison of thin film MIP composites with thin walled material formats

5. **National Science day, National Chemical Laboratory, Pune, India**
   - Biyani M, Mahanta A, Halhalli M.R**.**, Wadgaonkar P., Nisal A., Lele A., Chatterjee,G., Gaggar S.,(2009)
     Polycarbonate-g-Polystyrene Copolymer: Synthesis and Evaluation as Compatibilizer for PC-PS Blends,
   - Sadavarte N., Halhalli M.R**.,** Avadhani C.V., and Wadgaonkar P. (2008)
     Synthesis and Characterization of New Processable Polyimides Containing Pendant Pentadecyl Chain, National Science Day, National chemical Laboratory, Pune, India

6. ***Attendance:***
   - 3rd International conference on organic solvent nanofiltration, 13-15 September 2010 Imperial college London, UK
   - International Seminar on Frontiers in Polymer Science and Technology (POLY-2007) November 2007, Guwahatti, Assam, India

IT Credentials

- MS Office (Word, Power Point and Excel), ISIS draw, Chem Office, Origin, Sigma plot, TA universal analysis, PSS Porcheck.
- Literature search (SciFinder, Delphion, Scopus)

Awards

- ❖ Marie Curie Fellowship (Early Stage Researcher) (2009-2012)
- ❖ DAAD matching fund scholarship (September 2012)
- ❖ Senior Research Fellowship of Council of Scientific and Industrial Research (CSIR) Delhi, India (October 2008).
- ❖ Royal Society of Chemistry (RSC) publishing prize- MACRO-2010, UK

Personal Vitae

Name	Mr. Mahadeo Ramchandra Halhalli
Date of Birth	1st June 1983
Marital Status	Single
Nationality	Indian
Languages known	English, Hindi, Marathi, Kannada, German (Basic)
Present Address	Vogelpathsweg 26/10/04,
	44149 Dortmund, Germany
Permanent Address	At: Binjager, Post: Maindargi,
	Tal: Akkalkot, Dist: Solapur 413217,
	State: Maharashtra, INDIA